Studies on supramolecular assemblies, metal complexes of aromatic oxime derivatives for molecular and ions recognition

A Dissertation submitted to the Indian Institute of Technology Guwahati as partial fulfillment for the Degree

Doctor of Philosophy in Chemistry

Submitted by

Arup Tarai

(Roll No. 136122034)

Thesis Supervisor: Prof. Jubaraj B. Baruah

Department of Chemistry

Indian Institute of Technology Guwahati

Guwahati-781039, Assam, India

March 2018

Dedicated to My Family and friends…

Indian Institute of Technology Guwahati

Department of Chemistry

Declaration

I do hereby declare that this thesis entitled "***Studies on supramolecular assemblies, metal complexes of aromatic oxime derivatives for molecular and ions recognition***" is the outcome of research work carried out by me under the supervision of **Prof. Jubaraj B. Baruah**, at the Department of Chemistry, Indian Institute of Technology Guwahati, India.

In keeping with the general practice of reporting scientific observations, due acknowledgement has been made whenever work described here has been based on the findings of other investigators.

IIT Guwahati
March, 2018

Arup Tarai
Roll No. 136122034

Prof. Jubaraj B. Baruah
Department of Chemistry
Indian Institute of Technology Guwahati
Guwahati, 781039, Assam, India

Phone no. +91-361-258-2311(O)
Fax no. +91-361-269-0762
Email: juba@iitg.ernet.in

CERTIFICATE

This is to certify that the research work presented in this thesis entitled "***Studies on supramolecular assemblies, metal complexes of aromatic oxime derivatives for molecular and ions recognition***" is an authentic record of the results obtained from the research work carried out by **Mr. Arup Tarai** (**Roll No. 136122034**) under my supervision in the Department of Chemistry, Indian Institute of Technology Guwahati, India. This work is original and has not been submitted elsewhere for a degree or award.

IIT Guwahati
March 2018

Prof. Jubaraj B. Baruah
(Thesis Supervisor)

Acknowledgement

I would like to acknowledge many people who have contributed directly or indirectly help, support and encouragement during the course of my research work. I would like express my heartfelt thanks to all of them.

- First of all my deep sense of gratitude goes to my supervisor **Prof. Jubaraj B. Baruah** for his guidance during the course of my research. I have been enlightened by his wide knowledge and logical way of thinking. This thesis would not have been possible without his assistance. His encouragement has given me so much confidence. When I succeeded, he gave me great congratulation and encouragement. When I failed, he consoled, encouraged me. He is such a capable instructor and mentor that he can always help me to solve problems. His kindness, patience, positive direction lightened the way of my doctoral studies here. I especially thank him for spending numerous hours on my project, along with getting this thesis through its final stages.
- I am highly indebted to "**Indian Institute of Technology Guwahati**" for the doctoral fellowship.
- I would like to thank my doctoral committee members **Dr. Debasis Manna** (IIT Guwahati), **Dr. Chandan Kumar Jana** (IIT Guwahati) and **Dr. Subhas Chandra Pan** (IIT Guwahati) for their valuable suggestions during progress my research work.
- I would like to acknowledge CIF (IIT Guwahati) and Department of Chemistry (IIT Guwahati).
- Thanks to, **Dr. Babulal Das**, **Mr. Aniruddha Gogoi**, **Mr. Imdadul Islam**, **Mr. Diganta Kumar Hira**, **Mr. John Sangma Dangou**, **Mrs. Abhilasha M. Baruah**, **Mr. Dr. Kulakamal Senapati** and **Mr. Kh Kesho Singh** for their support at instrumental laboratory during the research work.
- I express my sincere thanks to my lab mates namely; **Dr. Bhaskar Nath**, **Dr. Bigyan Ranjan Jali**, **Dr. Jayanta Kumar Nath**, **Dr. Prithiviraj Khakhlary**, **Dr. Nithi Phukan, Dr. Krapa Shankar Kashyap**, **Mr. Munendra Pal Singh** and **Mr. Arnav Bhuyan** for their advice, well wishes, encouragement and constant support during the research period at IIT Guwahati.
- I am thankful to my friends, seniors and juniors namely; **Panda (Subhankar), Buddha**, **Raghu**, **Sabyasachi**, **Sayanta**, **Rana**, **Rajat, Sourav**, **Ganesh, Avishek, Subhra, Soumendra, Monaranjan, Gupta (Ravindra), Balaram, Amlan, Kalyan (IITKgp), Ardhendu, Prabir (Habu), Samir (Vanu), Ajit, Anju, Titli, Gourangi, Sumana, Ahalya, Shilaj Da, Satya Da, Keshab Da, Uday Da, Soumen Da,**

Somnath Da, Wajid Da, Akhtar Da, Pijus Da, Rumki Di, Nibedita Di, Karuna Di, Pinaki, Nilu, Bapan, and **Utsab** for providing a good, academic, friendly, peaceful and entertaining atmosphere outside from our lab.

- I would like to remember all of those who have guided or assisted me throughout the journey of my educational career and also throughout various aspects of my life. I am grateful to my parents (**Maa** and **Baba**) who have always supported all my decisions and have been a source of constant energy and inspiration to me. Thank you **Maa**, thank you **Baba** for being all the time with me and keeping so much faith on me. I would also like to thank my other family members; **Swarup** (My brother), **Koyel** (My wife), My grandfather and grandmother, My uncles and aunty, Shankar, Dipankar, Ayon, Moyna, for always encouraging me. Thank you **Swarup** and **Koyel** for your encouragement and support all the time.
- I want to thanks **Tarun** Sir, who have provided continuous encouragement and have been with me in my successes and failures.

Arup Tarai

Thesis Title:

"***Studies on supramolecular assemblies, metal complexes of aromatic oxime derivatives for molecular and ions recognition***"

List of Conferences/Symposiums

1. **Chemical Research Society of India, 20th CRSI-2016**, 3-5th February, 2016, Department of Chemistry, Guwahati University.
2. **Chemconvene-2017**, July 25, 2017, Department of Chemistry, Indian Institute of Technology Guwahati.
3. **Modern Trends in Inorganic Chemistry, MTIC-XVII, 2017, Pune** held at CSIR-NCL, Pune, IISER Pune, 11-14th December.
4. **Emerging Trends in Chemical Sciences, ETCS-2018**, 26-28th February, 2018, Department of Chemistry, Dibrugarh University.
5. **ACS ON Campus**, 2017, Oral presentation, Indian Institute of Technology Guwahati.

List of Publications

1. **A. Tarai**, J. B. Baruah. A Study on fluoride detection and assembling of hydroxyaromatic aldoximes caused by tetrabutylammonium fluoride. *CrystEngComm***,** 2015, **17**, 2301-2309.
2. **A. Tarai**, J. B. Baruah. Anion assisted conformationally guided self-assemblies of multi-component cocrystals of dioxime *CrystEngComm***,** 2016, **18**, 5482-5491.
3. **A. Tarai**, J. B. Baruah. Solution and solid state study on the recognition of hydroxyaromatic aldoximes by nitrogen containing compounds. *Cryst. Growth Des*., 2016, **16**, 126-135.
4. **A. Tarai**, J. B. Baruah. Study on divalent copper, nickel and zinc model complexes for fluoride ions detection. *RSC Adv*., 2015, **5**, 82144-82152.
5. **A. Tarai**, J. B. Baruah. Inclusion of 2,4-Dihydroxybenzaldehyde and 2,4-Dihydroxybenzaldoxime in Cadmium Coordination Polymer and Conversion of Guest Aldehyde to Oxime. *ChemistrySelect*, 2017, **2**, 11482-11486.

6. **A. Tarai**, J. B. Baruah. Oxime synthons in the salts and cocrystals of quinoline-4-carbaldoxime for non-covalent synthesis.
   *CrystEngComm***,** 2016, **18**, 298-308.
7. **A. Tarai**, J. B. Baruah. Quaternary and senary sub-assemblies in cocrystals and salts of quinoline-4-carbaldoxime with aromatic carboxylic acids.
   *CrystEngComm***,** 2016, **18**, 9095-9102.
8. **A. Tarai**, J. B. Baruah. Different self-assemblies, absorption and emission properties of picrate salts of aromatic amine or heterocycle linked oximes.
   New J. Chem., 2018, **42**, 4757-4765.

Doctoral Committee:

Prof. Jubaraj B. Baruah (Supervisor)

Dr. Debasis Manna (Chairman)

Dr. Chandan Kumar Jana (Member)

Dr. Subash Chandra Pan (Member)

Thesis Abstract

The thesis entitled "**Studies on supramolecular assemblies, metal complexes of aromatic oxime derivatives for molecular and ions recognition**" deals with various non-covalently linked self-assemblies of oxime derivatives to establish their molecular and ions recognition abilities. The content of the thesis is divided into six chapters.

Chapter 1: Introduction

Self-assemblies of oxime containing compounds are well studied, and necessary supramolecular features of oxime derivatives to form non-covalently linked self-assembly are brought forward in the introductory chapter. This chapter contains discussions on pharmaceutical applications, molecular or ion recognition properties, coordination chemistry and biological activities of oxime derivatives and their metal complexes.

Chapter 2 (Part A): Anion Assisted Supramolecular Assemblies of Oxime Derivatives and Recognition of Fluoride ion

In this chapter we have discussed the role of hydroxyl-group together with oxime functional group on the self-assemblies of hydroxyaromaticaldoximes. Additionally, we have discussed on the role of deprotonating oxime or hydroxy functional group of oxime derivatives by fluoride ions to form new supramolecular architecture. Also solution and solid state studies presented in this chapter have suggested that fluoride ion can be distinguished from other anions through characteristic changes in absorption and emission spectra.

Chapter 2 (Part B): Anion Assisted Conformationally Guided Dendrimer-like Self-assemblies of Multi-component Cocrystals of Dioxime

Oximes having ability to remain as syn-syn or syn-anti conformation provides wide scope to study such effects in self-assemblies. These effects are shown in different self-assemblies of salts and cocrystals as well as in the parent aromatic dialdoximes. This chapter contains discussions on anion assisted conformational guided self-assemblies of dioxime in different cocrystals and salts of different tetrabutylammonium salts. The effects of hydration, conformational changes, multicomponent cocrystal formation are discussed. Role of hydrogen bonding ability of anions, hydrations and intrinsic basicity of anions anchored as tetrabutylammonium salt are presented. FT-IR and Raman spectra of oxime are used to distinguish different conformers.

Chapter 3: Recognition of Aggregation Induced Emission Active Oxime Derivatives by Nitrogen Containing Compounds in Solid and Solution State

The third chapter contains results obtained on selective crystallization of different cocrystals and signal transductions caused by nitrogen containing compounds upon interactions with aromatic hydroxyaldoximes and their cocrystals shown in the scheme 1. These oxime derivatives showed aggregation induced emission enhancement in dimethylsulfoxide solution with different water fractions. The packing pattern of the cocrystals with 4,4'-bipyridine, hexamethylenetetramine, caffeine and theophylline are investigated to correlate and is suggested the role of C-H…π interactions and π-π interactions in emission of solid samples.

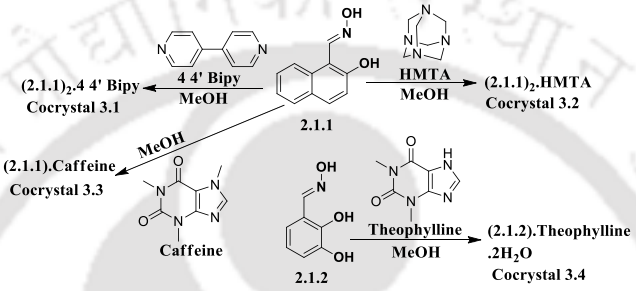

Scheme 1: Synthesis of different cocrystals of oxime derivatives

The differences in fluorescence emission found in solid and solution have suggested that the wide variations of emission properties in solid and solution phase. This also enabled to establish molecular recognition differently in solution and in solid state.

Chapter 4 (Part A): Transition Metal Complexes of Hydroxyaromaticaldoximes and Their Interactions with Fluoride ion

The self-assemblies of copper, nickel and zinc chelated metal complexes of hydroxyaromaticaldoximes are presented (Scheme 2). The roles of solvated molecules contributing to packing are discussed.

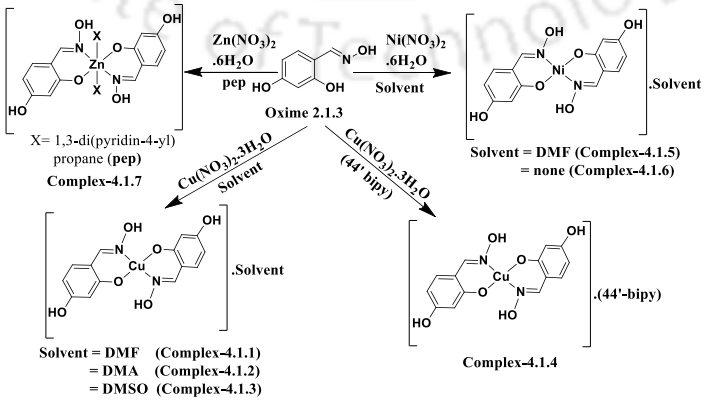

Scheme 2: Synthesis of transition metal complexes of 2,4-dihydroxybenzaldoxime.

Three different solvates from independent solvent of the copper complexes are discussed to suggest the directional properties of free hydroxyl group of the complex in guiding the respective self-assemblies of complexes**.** The role of free hydroxy functional group of these metal complexes on detection of fluoride ion in presence of other anions and the role of the metal ions in the complex to shift the emission patterns upon interactions with fluorides are presented. The advantage of using the zinc complex among copper and nickel complexes in the fluoride detection is demonstrated.

Chapter 4 (Part B): Inclusion of Aldehyde or Oxime in Cadmium Coordination Polymer and Conversion of Aldehyde to Oxime

The synthesis of different cadmium coordination polymers of 1,3-di(pyridin-4-yl)propane ligand encapsulating an oxime or aldehyde to understand possible reaction due to formation of inclusion complex is presented in this chapter. The association ability of the oxime with the parent cadmium complex is higher than aldehyde, facilitated conversion of aldehyde to oxime by the cadmium coordination polymer.

Chapter 5: Supramoleular Aspects of Quinoline-4-carbaldoxime with Aliphatic Dicarboxylic or Mineral or Aromatic Carboxylic Acids

The acid-oxime interactions are observed in quinoline-4-carbaldoxime cocrystals or crystalline salts with aliphatic dicarboxylic or mineral or aromatic carboxylic acids. Quinoline-4-carbaldoxime forms cocrystals with adipic acid, succinic acid, fumaric acid and 2-methylbenzoic acid whereas it formed salts with maleic acid, oxalic acid, nitric acid, hydrochloric acid, 2-hydroxybenzoic acid, 3-nitrobenzoic acid, 4-nitrobenzoic acid, 2,3-dihydroxybenzoic acid or 2,4-dihydroxybenzoic acid. Furthermore, in this chapter deprotonation, complementing hydrogen bond formation and competition between oxime-oxime, oxime-carboxylic acid, and carboxylic acid-carboxylic acid interactions are established to show that predesign synthesis is possible in systems having less competitive hydrogen bond factors to form different synthons.

Chapter 6: Self-assemblies, Absorption and Emission Properties of Picrate Salts of Aromatic Amine or Heterocycle Linked Oxime Derivatives

In this chapter we discussed on the self-assemblies, photo physical and thermal properties of picrate salts of aromatic amine or heterocycle linked oxime derivatives. Several oximes (scheme 3) are used for preparation of salts with different nitro-aromatic phenols. In this chapter the various aspects such as protonation at specific positions, the change of oxime-

oxime synthons on salt formation, charge transfer interactions are presented. The relevance of such interactions in solution is discussed.

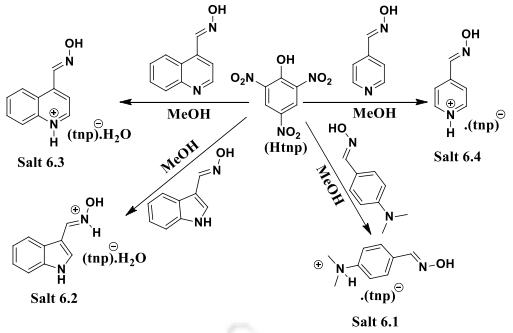

Scheme 3: Synthesis of different picrate salts of oxime derivatives with different protonation sites.

The extent of protonation of oxime derivatives by picric acid is found to be different in each case. Solid state UV-vis studies revels that picrate salt of indole-3-carbaldoxime has charge-transfer interactions between protonated oxime and picrate anion. Thermal properties observed in differential scanning calorimetry of the picrate salts are also described in this chapter. Furthermore, in this chapter it is shown that hydrogen bond donor-acceptor properties associated the heterocyclic amines makes different self-assemblies of salts that are having close structural relationship when independently considered. It is also shown that charge-transfer adducts of picric acids are observed only in specific cases.

The thesis is concluded with brief conclusions deliberating the major findings on different self-assemblies and the difference in solution properties from solid state properties. The major findings are attributed to the understanding on competitive hydrogen bond formation and conformational guidance to form specific types of architectures and to utilize them in molecular and ion recognitions. The synthon expansion and specificity in formation of charge transfer complexes are depicted. And also certain series of cocrystals and salts that are isostructural suggesting a step towards predesigned non-covalent synthesis. Certain spectra and crystallographic table for each compound is given at the end. The crystallographic information files are also included. And detail structural description, synthetic procedure and spectroscopic characterization of each oxime derivatives, cocrystals and salts are available in the experimental section which is included at the end of each chapter.

CONTENTS

ABBREVIATIONS

DNA: Deoxyribonucleic acid

RNA: Ribonucleic acid

AChE: acetylcholinesterase

DFP: Diisopropyl fluorophosphates

DCP: Diisopropyl chlorophosphates

DECP: Diethyl cyanophosphonate

BODIPY: Boron-dipyrromethene

TBAF: Tetrabutylammonium fluoride

TBAOH: Tetrabutylammonium hydroxide

TBAOAc: Tetrabutylammonium acetate

TBACl: Tetrabutylammonium chloride

HOCl: Hypochloric acid

μ_M: Micromolar

nM: Nanomolar

NLO: Nonlinear optical

DFT: Density functional theory

EPR: Electron paramagnetic resonance

NMR: Nuclear magnetic resonance

MS: Mass spectrometry

Å: Angstrom

K: Potassium

FRET: Forster resonance energy transfer

ICT: Internal charge transfer

CHEF: Chelation enhanced fluorescence

CH_3CN: Acetonitrile

THF: Tetrahydrofuran

EtOAc: Ethylacetate

MeOH: Methanol

EtOH: Ethanol

DMSO: Dimethyl sulfoxide

DMA: Dimethyl acetamide

DMF: Dimethyl formamide

H_2O: Water

HOMO: highest occupied molecular orbital

LUMO: lowest unoccupied molecular orbital

KBr: Potassium bromide

RT: room temperature (30 ℃)

U_{eff}: Magnetic moment

HF: Hydrofluoric acid

HCl: Hydrochloric acid

HNO_3: Nitric acid

IR: Infrared

UV-vis: ultraviolet-visible

AIE: Aggregation induced emission

PET: Photo-induced electron transfer

ESIPT: Excited state intramolecular proton transfer

DLS: Dynamic light scattering

FESEM: Field emission scanning electron microscope

DMG: Dimethylglyoxime

CP: Coordination polymer

ICT: Isothermal calorimetric titration

MOF: Metal-organic frameworks

44'-bipy: 4,4'-bipyridine

HMTA: Hexamethylenetetramine

TGA: Thermo-gravimetric analysis

TNP: 2, 4, 6-Trinitrophenol

Chapter 1

Introduction on supramolecular chemistry, molecular and ion recognition studied of oxime derivatives

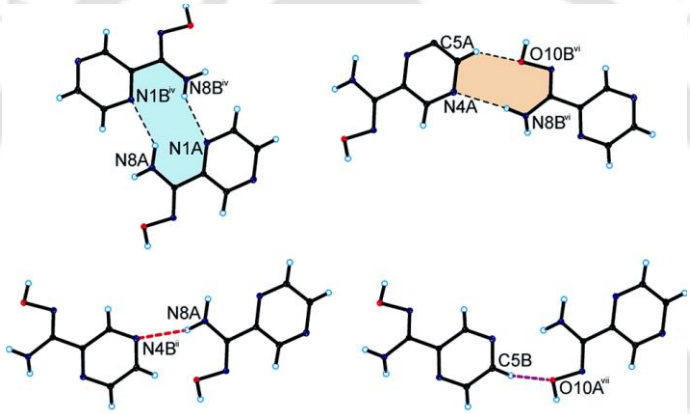

1.1: Introductory aspects on supramolecular chemistry

Supramolecular chemistry refers to chemistry beyond molecules and focuses on chemical systems that are made up of discrete numbers of assembled molecular sub-units or components and more precisely supramolecular chemistry is 'chemistry beyond the molecule' or 'the chemistry of the non-covalent bond'.[1] In 1987 Nobel Prize was awarded to Lehn, Cram and Pedersen for their outstanding work on molecular assemblies formed by weak interactions. Supramolecular chemistry deals with weak interactions whereas traditional chemistry focuses on the covalent, ionic and dative bonds. In supramolecular chemistry discrete molecules interact through varieties of weak interactions, such as Van der Waals forces,[2] hydrogen bonds,[3] π-π interactions,[4] cation-π interactions,[5] anion-π interactions,[6] C-H···π interactions,[7] etc. Important concepts derived from weak interactions have contributed to the topics like host-guest chemistry,[8] self-assemblies,[9] molecular recognitions[10] supramolecular architecture,[11] molecular machines[12] etc. Self-assemblies of many biological molecules such as nucleobases present in DNA or RNA[13] involve supramolecular interactions, which makes the subject indispensable. Molecular self-assemblies with supramolecular features are routinely used to generate materials with new optical,[14] magnetic[15] properties; chemical reactivities such as catalysis.[16] Supramolecular assemblies can be dislodged to easily different components; hence these assemblies are easily modified or reorganized to explore new properties. Alternatively, supramolecular chemistry may be also defined in terms of non-covalent interactions between 'host' and 'guest' molecules, where host molecule commonly refers to a relatively larger sized molecule or an aggregate such as an enzyme or synthetic cyclic and acyclic compound possessing sizeable central vacant space or cavity to accommodate guest molecule.[17] A guest may be a cationic or an anionic species, an ion pair or molecules with more complicated structure such as hormone, pheromone or neurotransmitter that are easily accommodated by a host. Though hydrogen bonds are the principal interactions in host-guest chemistry, the thermodynamic stability of host-guest complexes are enhanced by many other weak interactions such as chelate effect or macrocyclic effect.[18] Chelate or macrocyclic effect of cyclic hosts such as corands a sub-class of compounds of crown ether is provides more stable metal complexes as compared to the corresponding complexes formed by acyclic podands with similar binding sites. The non-covalent interactions in supramolecular chemistry are very weak as compared with covalent bonds of a compound.[19] For example, C-H bond energy is 430 KJ/mole and C-O bond energy is 340 KJ/mol. Whereas C-H···O interaction is less than 20 KJ/mol.

Certain covalent and non-covalent interactions (supramolecular interactions) are listed in **Table 1.1** for comparison. These energy values clearly suggest that the possibility of easy disruptions of supramolecular assemblies as compared to covalently linked systems.

Table 1.1 Strength of different supramolecular interactions and covalent bonds.

Non-covalent bonds (kJ/mol)		Covalent bonds (kJ/mol)	
Hydrogen bond	~4-120	C-C bond	360
Electrostatic interaction	~4.1-80	C-H bond	430
Van-der Waals interaction	~0.4-4	C=C bond	600
π-π interaction	~0-50	C=O bond	690
Cation-π interaction	~5-80		
Ion-dipole	~50-200		
Dipole-dipole	~5-50		
Ion-ion	~200-300		

1.2: Hydrogen bonds in supramolecular chemistry

Hydrogen bond is one of the major weak interaction in supramolecular chemistry which helps to construct various supramolecular assemblies.[20] Generally it is a dipole-dipole interaction in which a hydrogen atom attached to an electronegative atom (or electron withdrawing group) is attracted towards a more electronegative neighboring atom. Hydrogen bonds are typically represented as D-H···A, where D is the electronegative atom such as O or N to donate hydrogen to electronegative atom bearing a lone pair as an acceptor (A). A schematic representation of a hydrogen bond is shown in **Fig. 1.1a**, where D is hydrogen bond donor which donates hydrogen bond to acceptor A atom.

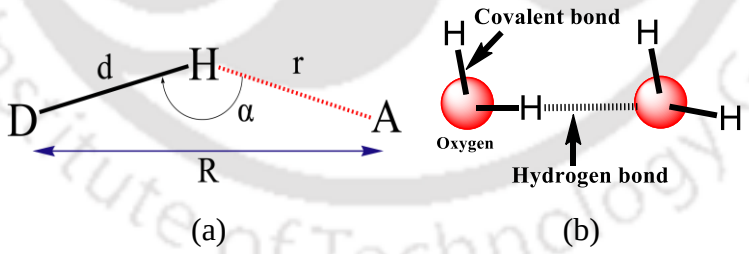

Figure 1.1: (a) Representation of hydrogen bond parameters and (b) Hydrogen bond between two water molecules.

In **Fig. 1.1a** the distance between donor and acceptor atom is represented by R, and the angle ∠DHA is represented by α. The separation distances between D···H and H···A are marked as d and r respectively. Based on the strengths of the hydrogen bonds they are classified in three different categories namely strong, moderate and weak hydrogen bond. A strong hydrogen bond has almost similar character to a covalent bond and formed between strong acid and good hydrogen bond acceptor with a linear geometry. But the moderate hydrogen bonds are

formed between neutral donor and neutral acceptor with slightly bending geometry. Different types of hydrogen bonds are listed in **Table 1.2** by their corresponding energy in kJmol^{-1}.There are also so large numbers of weak interactions involving C-H bonds such as C-H$\cdots\pi$ or interaction of C-H bonds with heavy atom (Br, S, Se etc) that have bond energy ranging from 2-10 kJ/mol.

Table 1.2: Hydrogen bond parameters in different types of hydrogen bonds.

Parameters	Strong	Moderate	Weak
Bond energy (kJmol^{-1})	60-120	16-60	<12
H$\cdots$A (r Å)	1.2-1.5	1.5-2.2	2.2-3.2
D$\cdots$A (R Å)	2.2-2.5	2.5-3.2	3.2-4.0
∠D-H$\cdots$A (α°)	175-180	130-180	90-150

A hydrogen atom attached to an electronegative atom of a functional group behaves as hydrogen bond donor. An electron rich atom within the same functional group or on a different functional group acts as hydrogen bond acceptor. These hydrogen bond donors and acceptors atom form intra and intermolecular hydrogen bond respectively depending on the orientations and locations. Hydrogen bonds formed between different functional groups such as carboxylic acids, phenols and amides are widely studied. These functional groups forming hydrogen bonds alone or together with another functional group in a molecule provide scope to construct different supramolecular assemblies.[21] Some common ways to form assemblies by amide, phenol and carboxylic acid are illustrated in **Fig. 1.2**. Based on the structures adopted due to the hydrogen bonds a self-assembly may be suggested to comprised of discrete, infinite chain, intramolecular and cyclic type hydrogen bonds or combinations of these hydrogen bonds.[22] Versatility in hydrogen bonded motifs necessitate their demarcation by descriptors. The concept of synthon to describe hydrogen bonded motifs present within non-covalent self-assemblies was introduced by Desiraju.[23] This has been used extensively describing hydrogen bonded assemblies. Synthons are widely used in supramolecular chemistry to describe the robust supramolecular assemblies in simplified manners. In supramolecular chemistry 'synthon' defines as the smallest intermolecular interacting units or non-covalently bonded two molecules in large size supramolecular assemblies. In general hydrogen bonded ring-like assemblies are most versatile supramolecular synthons which have been extensively used to describe supramolecular features in crystal engineering.

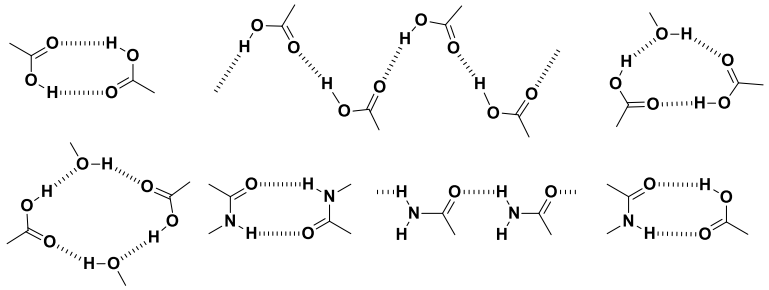

Figure 1.2: Different types of hydrogen bonded assemblies formed by carboxylic acid, phenol and amide functional groups.

Hydrogen bonded assemblies in biological systems are indispensable and hydrogen bonds among nucleobases pair of DNA or RNA or in proteins constitute the backbone of such examples. Nucleobases, such as adenine and thymine form a stable Watson-Crick base pair 'A-T' whereas similarly guanine and cytosine form similar base pair 'G-C' through hydrogen bonds (**Fig. 1.3**).[24]

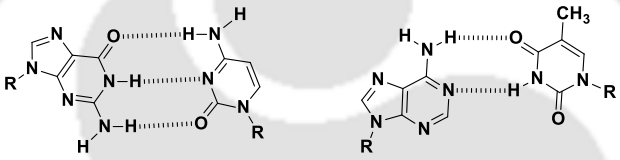

(a) (b)

Figure 1.3: Watson-Crick base pairs formed by hydrogen bonds between (a) adenine and thymine (A-T); (b) guanine and cytosine (G-C).

Depending on the number of hydrogen bonds formed by the same acceptor atom of a molecule; hydrogen bonds are classified into different categories like bifurcated and trifurcated hydrogen bonds. When one hydrogen atom interacts with two acceptor atoms it is called bifurcated[25] and when there are three acceptor atoms for single donor atom it is called trifurcated[26] hydrogen bonds. The bifurcated and trifurcated hydrogen bonds act as bridge in many supramolecular assemblies. Etter[27] introduced graph-set notation[28] to demarcate hydrogen bonded assemblies and she also formulated certain rules that may be prime factors to build pre-designed supramolecular assemblies. As per graph-set notation graph set designator 'G' is assigned into four different smallest building blocks, R for ring, D for discrete, C for chain and S for self or intramolecular hydrogen bonded systems. The number of donor and acceptor atoms present in the assemblies is designated by subscript and superscript respectively and total number of atoms involved in this graph set notation is put in the bracket (**Fig. 1.4a**).

Some examples of different types of hydrogen bonded assemblies with their graph set notations are given in **Fig. 1.4b**.

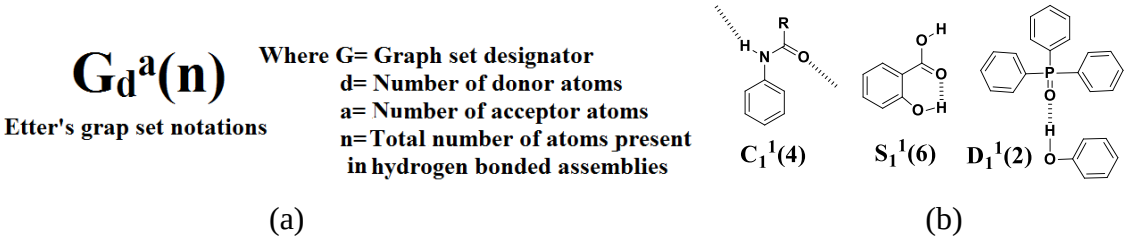

Figure 1.4: (a) Etter's graph set notations; (b) Some examples of hydrogen bonded assemblies with graph set notations.

Etter's rules are as follows:

(a) All good proton donors and acceptors are involved in hydrogen bonding interactions.

(b) Six-membered-ring intramolecular hydrogen bonds form in preference to intermolecular hydrogen bonds.

(c) The best proton donor and acceptor remaining after intramolecular hydrogen bond formation will form intermolecular hydrogen bonds.

In general, due to geometrical and energetics many functional groups have strong tendency to form cyclic hydrogen bonded synthons and some examples are illustrated in the Fig. **1.5**.

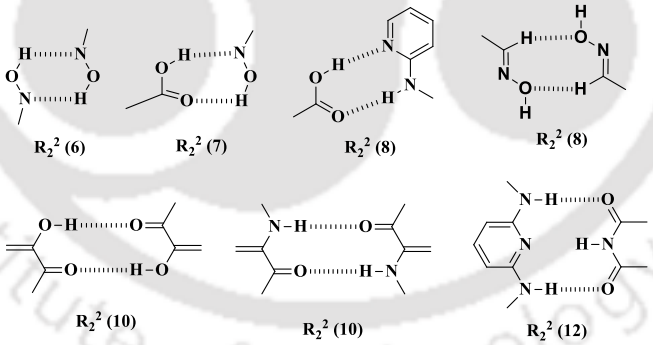

Figure 1.5: Examples of cyclic hydrogen bonded synthons and their corresponding graph-set notations.

1.3: Supramolecular assemblies formed by hydrogen bonds

Development of new and novel building blocks with the aid of hydrogen bonds as principal interactions assisted by other interactions is one of the challenges in supramolecular chemistry. Interplay among weak interactions and the directional nature of non-covalent interactions play major roles in deciding architectures of various supramolecular assemblies. Depending on the shape of host various network structures of supramolecular systems are

available.[29] Irrespective of the shape of the molecules, a hydrogen bonded system can be made by self-assembling or assemblies mediated by guest molecules or may be organized by combinations of two three different independent molecules. Self-assembly of four molecules of guanosine derivative **1.1** as shown in **Fig. 1.6** is such an example of hydrogen bonded quartet supramolecular assembly (**1.1a**).[30]

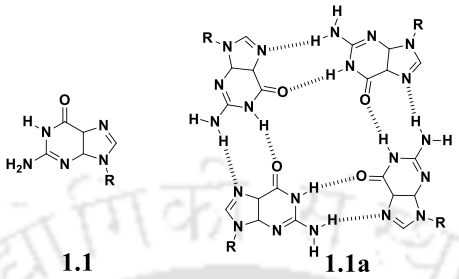

Figure 1.6: Guanosine derivative **1.1** and hydrogen bonded quartet **1.1a**.

The supramolecular assembly **1.1a** is formed by self-organization of hydrogen bonds. The carboxylic acid-adenine interactions can be stabilized in two different ways by V-shaped molecule **1.2** which has an active carboxylic acid group. The carboxylic acid acts as hydrogen bond acceptor or donor that helps to bind an nucleobase adenine molecule in two different ways.[31] Though both assemblies involve N-H···O and O-H···N hydrogen bonds but bind adenine molecule through two different sites to form two different supramolecular assemblies **1.2a** and **1.2b** as illustrated in **Fig. 1.7**.

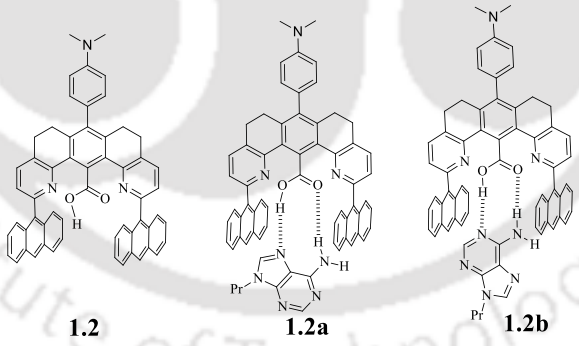

Figure 1.7: Structure of compound **1.2** and hydrogen bonded supramolecular assemblies **1.2a** and **1.2b** of **1.2**.

Indole containing a carboxylic acid group **1.3** at 3-position of the five-membered heterocycle form a 1:2 cocrystal with 5-nitroquinoline (**Fig. 1.8**). This cocrystal namely **1.3a** is formed by charge transfer interaction as well as by hydrogen bonds.[32]

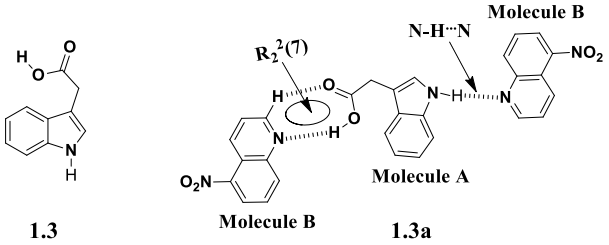

1.3 1.3a

Figure 1.8: Indole-3-carboxylic acid **1.3** and cocrystal of **1.3** molecule with 5-nitroquinoline (**1.3a)**.

These two examples show that the supramolecular assemblies can be modified to form supramolecular isomers or hydrogen bonded assemblies and some molecules can be hold multiple guests of same kind or other.

Above discussion ascertained different features of direction and energetic hydrogen bonds in different supramolecular assemblies. Hydrogen bonds play a major role in molecular and ion recognition in solid and solution state. As the present thesis is directed towards studied on supramolecular aspects and molecular or ion recognition of oximes and related compounds, the next portions of this chapter is on certain features of non-covalent self-assemblies and self-assemblies of various oxime related compounds.

1.4: Molecular recognition

The term molecular recognition means specific and selective interactions between two or more molecules through non-covalent interactions such as hydrogen bonding, metal coordination, hydrophobic forces, Van der Waals forces, π-π interactions and other non-covalent interactions.[33] Molecular recognition phenomenon is crucial in biological systems, and in modern chemical research where both inter or intramolecular phenomena are involved. Though topics such as "host-guest chemistry", "supramolecular chemistry", and "self-assembly" are limited to intermolecular processes, molecular recognition is constituent of each of them. In addition to *direct* interactions between host with guest or guest with guest or host with host, interactions of a substrate with solvents play a dominant indirect role in driving molecular recognition in solution.[34] Chemists have designed artificial supramolecular systems for molecular recognition. One of early example for molecular recognition is crown ether selectively binding with cations. Depending on the complex formations or host-guest binding capability molecular recognition sub-divided into two parts. One is static and other is dynamic molecular recognitions, schematically both recognitions are illustrated **Fig. 1.9**.[35] Static molecular recognition is the interactions between one key and one key hole, which mean formation of a 1:1 type complex between one host and one guest (**Fig. 1.9a**).

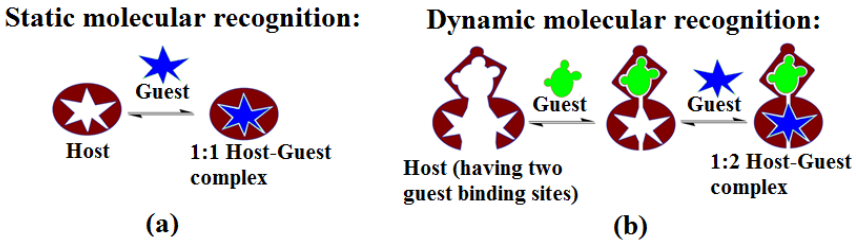

Figure 1.9: (a) Static and (b) dynamic type molecular recognition.

For static molecular recognition, it is necessary to create guest molecule specific binding sites in the host molecule. But in the case of dynamic molecular recognition the binding of the first guest to the first binding site of a host affects the association constant of a second guest located at a second binding site (**Fig. 1.9b**). In systems with positive allosteric effect the binding of the first guest increases the association constant of the second guest and vice-versa. Dynamic molecular recognition is important in biological systems because it provides the requisite mechanism to regulate binding of guest molecules. Such molecular recognition is also to design highly functional chemical sensors and molecular devices.[36]

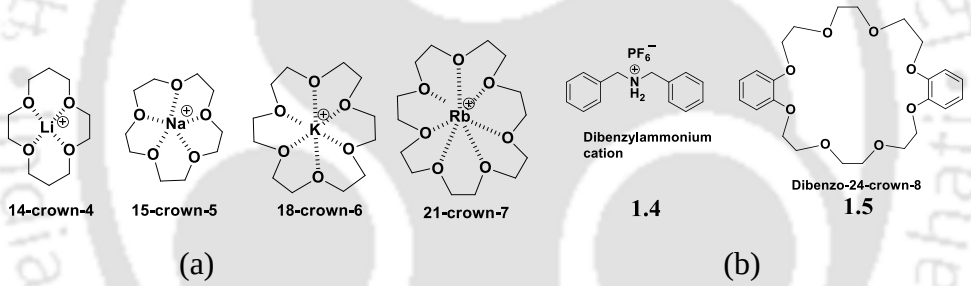

Figure 1.10: (a) Different crown ethers with their specific metal ions and (b) Example of molecular recognition by crown ether.

Artificial receptors have been designed for specific molecules to show molecular recognition properties. One early example of such a system was a crown ether which was capable of selectively binding to specific cations (**Fig. 1.10a**).[37] An example of static molecular recognition is shown in **Fig**. **1.10b**. In this example a dibenzylammonium cation **1.4** is recognised by crown ether **1.5** and the course of recognition process was studied through changes in photophysical properties due to complexation of ammonium cation with the crown ether (**Fig. 1.10b**).[38]

1.5: Weak interactions in anion bound non-covalent assemblies

Anions are important in our everyday life because they are regulating various processes in biological systems, bioinorganic chemistry, organic chemistry and mineralogy. They are present approximately 70 % in all enzymes sites and plays important role in manipulation and

storage of genetic information (as DNA and RNA are polyanions). Anions also control osmotic pressure, activate signal transduction pathways, maintain cell volume and produce electrical signals. In fact the transport of anions through phospholipid bilayers of a cell is mediated by variety of channels and anion transport proteins with mitochondrial anion transport systems are well established. Several X-ray crystal structures of enzymes and anionic substrates have revealed hydrogen bonds within them. Not only due to the impact of anions in biological system but also the supramolecular chemistry of anions is also of interest in the fields such as catalysis and environmental sciences.[39] Generally anions bind to receptors through hydrogen bonds or by electrostatic interactions or other non-covalent interactions as illustrated in **Fig. 1.11**. For anions recognition or sensing of an anion by specific receptors, anions must fit their structural framework within the host or bind to receptor molecule to change the photophysical properties of the receptor molecule. In general anions are larger in sizes than the most of metal cations. The fluoride anion, has an ionic radius of 1.33 Å, which is only slightly smaller than the relatively medium-sized metal cation K^+ (1.38 Å).[40] The cationic host conventionally holds an anion as counter-anion and the interaction between the host and guest in such case is electrostatic in nature. The synthesis of neutral anion receptors for selective anion binding is quite challenging. Several problems are encountered to design receptors for selective binding of anion. Many anions have relatively high free energies of solvation ($\Delta G_{solv}(F^-)$ = -465 kJ/mol; ΔG_{solv} (Cl^-) = -340 kJ/mol).[41] Hence to design of a receptor, requires the understanding on competing abilities of anion to bind to surrounding medium while binding to an anion. Secondly, some anions are spherical in shape having similar shape as that of metal ions; in such situations anions interfere the anion recognition process through self-assembling between anions. Thirdly, some anions are not stable at higher pH for example $H_2PO_4^-$ is stable at pH 3-5.5; HCO_3^- is stable between pH 6.5 to 10. So, their detection may be on the basis of interactions with a partially protonated receptor. However, difficulty arises when a receptor has possibility of interconversion between differently protonated species within a narrow pH window. To overcome these problems each of these aspects are required to be attended while designing anion selective receptors.

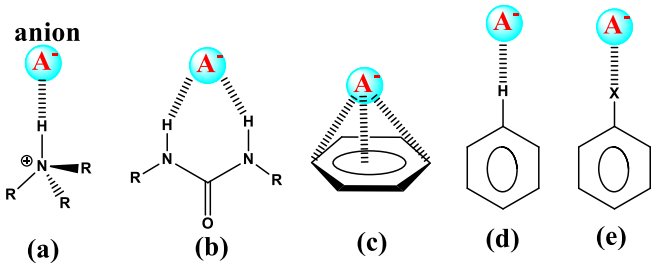

Figure 1.11: Anion binding with receptors by different types of noncovalent interactions; (a) Electrostatic N-H···anion interaction; (b) N-H···anion interaction; (c) Anion···π interaction; (d) C-H···anion interaction and (e) C-X···anion halogen bonds (X= F^-, Cl^-, Br^- and I^-).

As mentioned the most effective way to bind anions by neutral receptors involves utilization of the negative charge on anions. For this reason ammonium and quaternary ammonium ions are ideal receptors for binding anions. Various functional groups such as urea, thiourea, pyrrole, indole, amide etc. are extensively used as an anion sensors or anion receptors. Conventionally, anions are basic in nature, so it interacts with acidic proton. When the -NH protons of the above functional groups are deprotonated by anions like fluoride or acetate, they cause changes in photophysical properties. Several of papers dealt with anion sensors that have electron withdrawing group attached to urea, thiourea moiety.[42] Besides N-H···anion hydrogen bonds between receptors and anions, anion···π interactions occurs in solution as well as in solid-state. Anion···π interactions are commonly arise from anion with small sizes with high polarizing powers. Anion···π interactions are used to design of highly selective anion receptors.

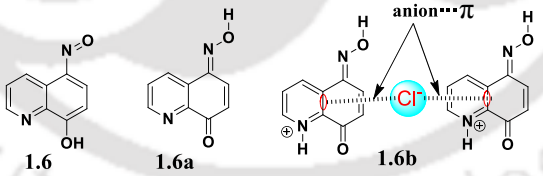

Figure 1.12: Keto and enol form of compound **1.6** and its anion···π interaction with Cl^- anion.

The importance of anion π-interactions are reflected in the salts of compound 5-(hydroxyimino)quinolin-8-one **1.6.** This compound having a nitrosyl substitutent 8-hydroxyquinoline unit exists in two different forms namely keto **1.6** or enol **1.6a** forms in solid-state depending on the neutral or salt of this compound. Compound **1.6** forms salts with mineral acids such as hydrochloric, perchloric, nitric or hydrobromic acid. Such salts form assemblies through interactions among the anions and receptor by different weak interactions.

One representative example of a salt shown in **Fig. 1.12** has a chloride ion interacting with cationic receptor **1.6b** through anion···π interaction.[43] On the other hand, weak σ interactions involving transfer of a fractional charge from anion to an arene where the anion is located above the periphery rather than the centre of arene are also known.[44]

1.6: Neutral host for anion binding

Urea, thiourea, pyrrole, indole and amide derivatives have been routinely used for the selective recognition and sensing of basic anion in polar organic media. Urea and thiourea derivatives can have symmetric and unsymmetric substitents and in solid state they can adopt varities of structures.[45] Commonly urea or thiourea adopts tape like structure for forming various supramolecular architectures.[46] Some of the urea based receptors are discussed details in different articles with special context to detect anions through signal transductions.[47] Some of the examples are listed in **Fig. 1.13.** One such example of urea derivative **1.7** has two nitro groups at para position with respect to urea functional unit shows significantly high acidity. Due to which the -NH proton of urea moiety can easily be deprotonated and the deprotonation influences the spectral response. Such response can be ion specific and are utilized to differentiate anions. The compound **1.7** selectively interacts with fluoride anion with high binding affinity ($K_a > 10^{-7}$ M^{-1}) in acetonitrile in comparison to other anions.[48]

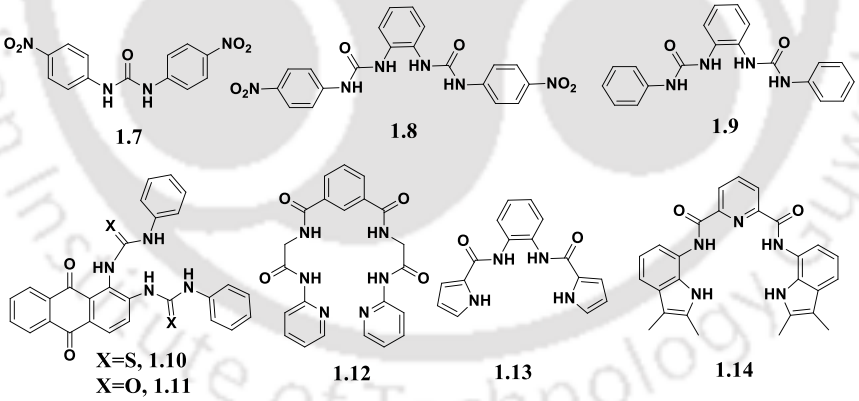

Figure 1.13: Some neutral receptors for anions binding studies having -NH binding sites.

Compounds **1.8** and **1.9** were identified by Gale and his co-worker as selective to interact with specific anions. Compound **1.8** binds with carboxylate anion more strongly as compared to compound **1.9**. In DMSO-H_2O (9.5:5, v/v) mixed solvent, compound **1.9** strongly binds with acetate (K_a= 3210 M^{-1}) anion over benzoate (K_a= 1399 M^{-1}) anion or dihydrogen phosphate (K_a= 666 M^{-1}). Whereas compound **1.8** binds with acetate ion with high affinity with binding constant K_a= 4018 M^{-1}, a value much higher as compared to binding constant with receptor **1.9**.[49]

Anthraquinone units attached as signaling unit to urea and thiourea, namely compounds **1.10** and **1.11**.[50] Among these two compounds the thiourea derivative **1.11** is useful for naked eye detection of fluoride at room as it changes color on interaction with fluoride ions at room temperature. Whereas urea based receptor showed similar colour changes at 60 °C on addition of fluoride. This difference arises due to the difference in the self-assemblies of urea and thiourea derivatives. Kondo and co-workers have reported amide based neutral receptor **1.12** for sensing of dihydrogen phosphate.[51] In mixed solvent DMSO-CH_3CN (0.5:9.5, v/v) compound **1.12** showed strong binding affinity with dihydrogen phosphate (K_a=1,000,000 M^{-1}) over the acetate ion (K_a=17,000 M^{-1}). Dihydrogen phosphate anion has hydrogen bond acceptor and donor sites to form stable complex with receptor **1.13**.[52] Receptor **1.13** has strong binding with dihydrogen phosphate (K_a=295M^{-1}) over acetate (K_a= 251M^{-1}) and benzoate (K_a=113M^{-1}). It is interesting to mention that -NH proton of pyrrole group is 100 times less acidic as compared to the -NH proton of indole functional group. Hence, indole based receptors are more effective in anion binding in comparison to pyrrole based receptors. An indole based receptor **1.14** shown in **Fig. 1.13** has the ability to interact with fluoride ions selectively in a DMSO-water solution. The solid state structural study has provided evidence of a twisted geometry of the host while bound to fluoride ion.[53] The foregoing examples show the varieties of interactions leading to formation of anion assisted assemblies which in turn affect color changes resulting in easy detection of selective anions. Though there are many anions assisted assemblies based on N-H or O-H containing compounds are also used in anion binding hosts for detection of basic anions. Hundal and co-workers have developed a tripodal catechol-based receptor **1.15** that showed high selectivity toward fluoride anion in DMSO with colour change from colourless to bright yellow.[54] This was attributed to deprotonation of the hydroxyl groups based on ^{1}H NMR studies and also form the fact on obtaining a similar optical response for the strong base TBAOH. Zhang et al. have developed chemosensor **1.16** for rapid and selective detection of CN^- in aqueous medium. Chemosensor **1.16** showed strong fluorescence enhancement upon addition of CN^- in DMSO/H_2O (9:1, v/v) with high detection limit 4×10^{-7} M.[55] **A** colorimetric fluorescent receptor **1.17** (**Fig. 1.14**) was reported by Chattopadhyay and co-workers for selective and sensitive detection of $H_2PO_4^-$ anion in aqueous medium. Compound **1.17** showed an optical change from yellow to green upon addition of $H_2PO_4^-$ anion.[56] A bifunctional fluorescent chemosensor **1.18** was reported by Chang et al. for the selective detection CN^- anion in MeOH solution through colorimetric as well as fluorometric changes.[57]

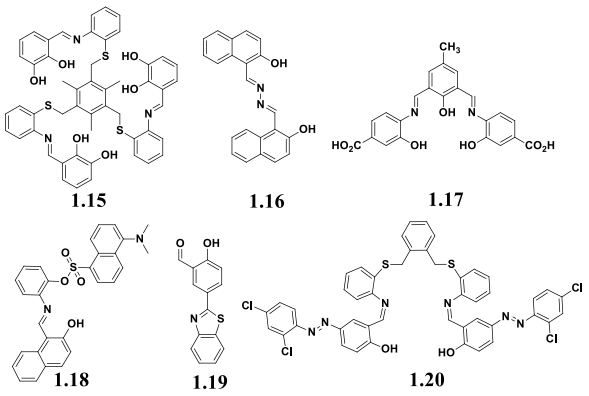

Figure 1.14: Some neutral receptors for anions binding studies having -OH binding sites.

Chemosensors **1.19** was reported by Yang and co-workers having a hydroxyl group free for the selective binding of fluoride anion. Spectroscopic studies indicated that an aldehyde group in conjugation with the **1.19** core at an adjacent position to the hydroxyl group would elevate the sensitivity towards fluoride immensely.[58] A new azo-azomethine receptor **1.20,** containing active phenolic sites, has been designed and synthesized for quantitative detection and colorimetric sensing of inorganic fluoride ion in aqueous media.[59] Compound **1.20** showed facile detection of fluoride ion present in aqueous media without any spectroscopic instrumentation with a detection limit 0.058 ppm through colorimetric.

These clearly establish that the anion binding abilities of molecules through hydrogen bond has a wide scope to prepare and understand new assemblies and unearthing novel properties. In this thesis we focus on supramolecular aspects of oximes and following section is on the existing literate on various features associated with oxime functional group containing compounds.

1.7: General feature of oxime functional group

Oxime derivatives are well studied in organic and inorganic chemistry because of their versatile applications in various fields.[60] Among various functional groups oxime is one of common functional group in organic and inorganic chemistry. Depending on the reactant, oxime derivatives are divided into different categories namely aldoxime (synthesised from aldehydes), ketoxime (synthesised from ketones) and amidoxime (synthesised from the amide). The general formula of oxime is $R_1R_2C{=}NOH$, where R_1 is one organic side chain and R_2 is hydrogen atom for aldoxime or it may be alkyl or aryl group for ketoxime.[61] But in the case of amidoxime, general formula is $R_1C(=NOH)NR_2R_3$.

Oxime molecules generally exist in two form syn and anti, depend on the position of the higher group and the -OH group. Aldoxime and ketoxime are found in both forms except aromatic aldoxime.

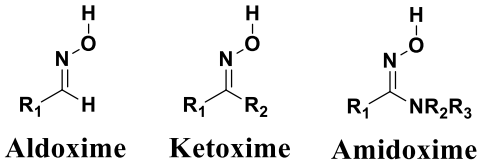

Figure 1.15: Structures of different oximes.

Synthesis of oximes is very simple, as they are formed upon reaction of aldehydes or ketones with hydroxylamine. There are several procedures available for industrial synthesis of oxime from commercially available substrates in solid or liquid state.[62]

1.8: Oxime molecules in biological systems

Oxime functional group is found in many natural products and biologically active compounds.[63] In 1956 Wilson and Ginsburg introduced pralidoxime **1.21**, commonly known as 2-PAM.[64] Pralidoxime (pyridinium aldoxime) is used to recover the activity of enzyme that are blocked by the organophosphate functional groups. Pralidoxime reacts with organophosphate and releases million times faster than the release caused by normal hydroxylamine. Several oxime containing molecules **(Fig. 1.16)** were discovered for organophosphates inhibiter. Such compounds include trimedoxime (**1.22**),[65] obidoxime (**1.23**)[66] and (1-2-hydroxyiminomethyl-1-pyridino-3-4-carbamoyl-1-pyridino-2-oxapropane dichloride) (**1.24**)[67] etc.

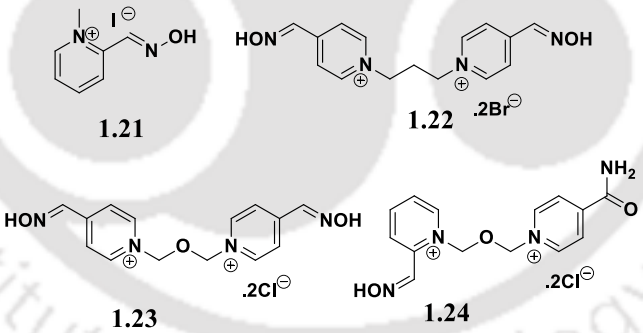

Figure 1.16: Some oximes which facilitate release of organophosphates from phosphate containing enzymes.

Compound **1.22** shows high solubility as well as high stability in comparision to the compound **1.21**, both these compounds are similar in reactivity towards releasing organophosphates. Whereas, compounds **1.23** and **1.24** are more effective antidote against organophosphate as compared to compounds **1.21** and **1.22**. There are other examples of oxime functional group containing molecules are used as antibiotic for treatments against bacterial infection. Cephalosporin is one of the oldest examples of oxime containing antibiotic drug. Cephalosporin belongs to a class of *beta*-lactam antibiotics, which are used

for the treatment of a wide range of bacterial infections, such as respiratory tract infections like tonsillitis or bronchitis and urinary tract infections. Depending on their antimicrobial activity, cephalosporins are classified into four different generations. First generation cephalosporins drug molecules (**Fig. 1.17**) are used for minor bacterial infections like skin or soft-tissue infections, whereas second generation cephalosporins drug molecule used as gram negative bacteria.

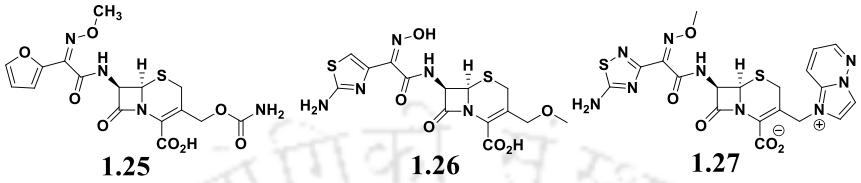

1.25 **1.26** **1.27**

Figure 1.17: Structures of different cephalosporins.

Cefuroxime (**1.25)**, is a second generation cephalosporin antibiotic drug molecule. It shows higher activity against *Haemophilus influenzae* and *Lyme disease* compared with the first generation cephalosporins.[68] A third generation cephalosporin antibiotic cefdaloxime (**1.26)** shows greater activity against gram-negative oranisms. Zwitterionic cephalosporins antibiotic drug cefozopran (**1.27**), is a better antibiotic drug against gram-positive organisms.[69a] Pyrazole substituted aryl oxime derivatives are also well known for regulating apoptosis and autophagy studies in A549 lung cancer cells.[69b]

1.9: Different supramolecular synthons of oxime based molecules

Major goal in supramolecular chemistry is to control the self-assemblies of molecules by interplay of weak interactions. Thus the ability of a functional group to form homomeric or heteromeric assembly is one prime concern to predict a supramolecular assembly. For such a purpose in addition to identify weak interactions, the synthons involved in a self-assembly becomes very important. Among different groups that form hydrogen bonded assemblies such as carboxylic acid, amide, phenol, alcohol etc, oxime is another group that has special interest. The interest in self-assembling ability of oxime group is due to the participation of nitrogen atom as well as the hydroxyl group independently or together in hydrogen bond formation. Due to different ways of hydrogen bond formation with slight energy differences, oxime group is no exception to show varieties of supramolecular assemblies resulting in polymorphs and self-assemblies to form inclusion complexes. Oxime groups act as hydrogen bond donor (via the -O-H) and as hydrogen bond acceptor via -C=N and the -O-H. Oxime form hydrogen bonded dimers, as well as oxime···oxime catemers via O-H···N=C and O-H···O-H hydrogen bonds in solid-state (**Fig. 1.18**).[70]

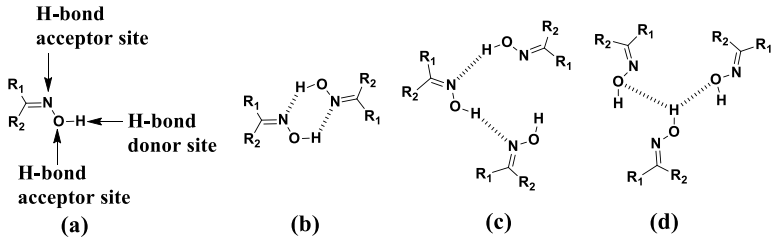

Figure 1.18: (a) Hydrogen bond donor and acceptor sites of an oxime; (b) Hydrogen bonded dimer and catemer formed by (c) O-H···N and (d) O-H···O hydrogen bond.

There are also other cyclic hydrogen bonded assemblies as shown in **Fig. 1.19a** that is relatively less in numbers.[71] Having such diversities there are advantages to study assemblies of oximes to tune structures by variation of the substituent. Such a factor along with ease to convert to various functional groups provides edge on utility of oxime self-assemblies over other hydrogen bond forming functional group such as carboxylic acid or amide.[72] Presence of another functional group such as -NH_2/-C≡N with oxime functional group in a molecule influences structures in solid-state. Such changes are brought about by the additional weak interactions, for example O-H···NH_2 and O-H···N≡C interactions shown in b and c of **Fig. 1.19**. Aakeröy and his coworkers described structural details of various oxime molecules and elucidated various oxime synthons.[73] They performed systematic structural and spectroscopic examination of the cocrystals formed between aldoximes R-C=N-OH (where R is H, Me, or CN) with N-heterocycles. Such studies have showed that the acidity of the oxime -OH hydrogen bond is a crucial factor to decide the efficacy of the supramolecular assembling.[74] Careful manipulation of the substituents of oximes also enhances solubility of oxime derivatives. Thus enhanced solubility facilitates supramolecular synthesis.

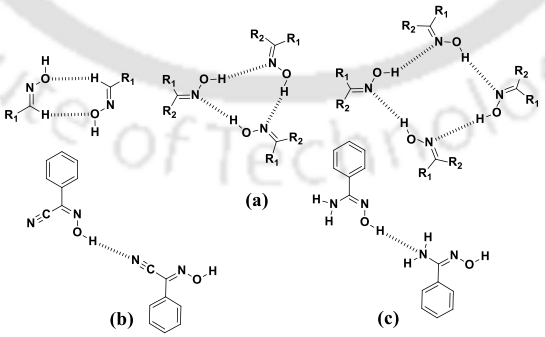

Figure 1.19: (a) Less commonly encountered hydrogen bonded cyclic assemblies of oximes. Hydrogen bonded chains formed through (b) O-H···N≡C and (c) O-H···NH_2 interactions.

Structure directing effect caused by hydrogen bonds in a competing situation between hydrogen and halogen bond donors is shown by Aakeröy and his co-workers in different cocrystals of 3,3'-azobipyridine and 4,4'-azobipyridine with aromatic oximes with halogen

atoms, carboxylic acids, phenolic -OH as substituents (**Fig. 1.20a**).[75] In these examples different competitive binding interactions are observed such as halogen-nitrogen bonds, carboxylic acid-nitrogen bonds, cyanide-oxime interactions. These interactions compete with oxime-oxime interactions

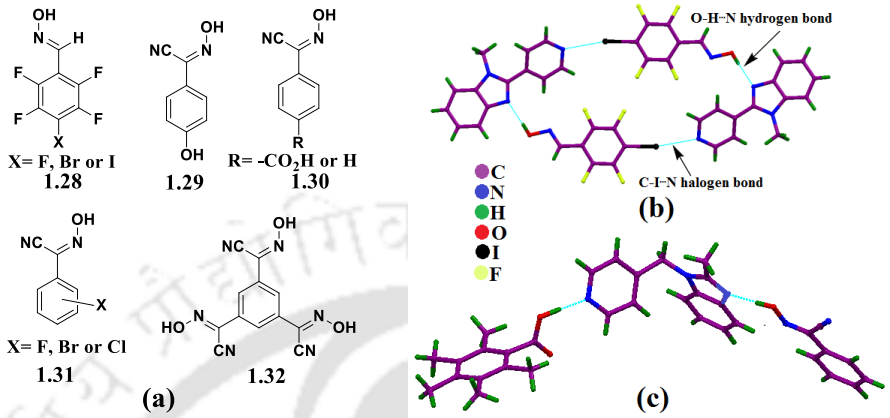

Figure 1.20: (a) Different types of oximes; (b) Hydrogen and halogen bonding interactions in cocrystal and (c) One ternary cocrystal of oxime.

Due to such competitive effects, halogen substituted phenylaldoxime **1.28** (X= F, Br or I) forms three different 1:1 cocrystals with 1-methyl-2-(pyridin-4-yl)-1H-benzo[d]imidazole.[76] Self-assemblies of these cocrystals have strong hydrogen bonds along with weak halogen bonds (**Fig. 1.20b**). Strong hydrogen bonds are between oxime -OH and nitrogen atom of 1-methyl-2-(pyridin-4-yl)-1H-benzo[d]imidazole. Whereas halogen bonds are between halogen atoms on the phenyl ring with nitrogen atom of 1-methyl-2-(pyridin-4-yl)-1H-benzo[d]imidazole.[76] Hydroxy and cyano-oxime functionalized oxime (Z)-N,4-dihydroxybenzimidoyl cyanide **1.29** has two hydrogen bond donor sites forms hydrogen bonds with hydroxy and cyano-oxime groups.[77] From the structural study of these cocrystals along with electrostatic potential surfaces calculation, it is established that hydroxyl group as a better hydrogen bond donor as compared to cyano-oxime. Ternary cocrystals were obtained from binary cocrystals of **1.30** by changing the substitution on to form various cocrystals.[78] Compound **1.31** effectively binds to five-membered or six-membered N-heterocyclic molecules to forms cocrystals.[79] Compound **1.31** forms a 2:3 cocrystal with 1, 2-di(4-pyridyl)ethane, the self-assembly of this cocrystal has a porous supramolecular three diemensional network structure.[79] In another example, α,α',α''-tris(hydroxyimino)-1,3,5-benzene-triacetonitrile oxime **1.32** which has a three-fold symmetry with three coplanar effective hydrogen bond forming moieties is a choice for porous organic networks.[80]

1.10: Oxime derivatives in molecular recognitions

The detection or removal of hazardous materials is important for environment as well as for human life. For specific detection and subsequent removal of hazardous materials, it requires specificity in binding by an analyte or in a sense molecular recognition can be a guiding factor to achieve them. One such potential example is selective interaction of oximes with poisonous nerve gas and phosphate containing insecticides. Nerve agents or phosphorous containing materials (**Fig. 1.21**) are some most dangerous materials for human or animal's life. Since these compounds rapidly affect human and animal life by blocking the action of acetylcholinesterase (AChE), causes a critical problem to central nervous system. This enzyme is responsible for the breakdown of the neurotransmitter acetylcholine. The blocked enzyme becomes free by reacting with oximes.

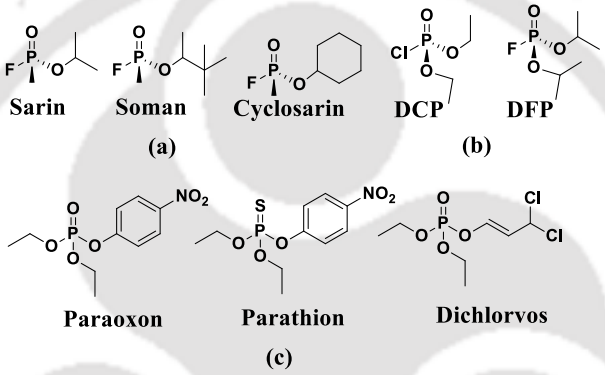

Figure 1.21: (a) Nerve agents and (b) Synthetic mimics of nerve agents used as less toxic and (c) some toxic pesticides.

Rapid and selective detection of nerve agents are essential for environment and human life. Several oximes are used to visualize the presence of nerve agents and related pesticides through changes in their fluorescence emissions or colours. The reactivity of an oxime without a pyridine unit attached to oxime towards nerve agents are better than a pyridinium oxime such as pralidoxime.[81] Some oxime derivatives used as sensor for nerve agents are listed in **Fig. 1.22a**. Anslyn and his co-workers have developed certain oxime based sensors containing a fluorophore for the selective detection of nerve agents.[82-83] Anslyn and co-workers showed that oximate are much better nucleophile than the hydrazine. They developed two simple chromogenic sensors **1.33a** and **1.33b** for such study.[82] Phosphorylation of oxime (**Fig. 1.22b**) by reacting with nerve agent in a solution causes a hypsochromic shift of approximately 50 nm in basic medium, this change was observed through naked eyes (**Fig. 1.22c**). The compound **1.34** is an oxime and coumarin based sensor, which is non-fluorescent in basic condition due to the photoinduced electron transfer mechanism operative in the system on pH change.[83]

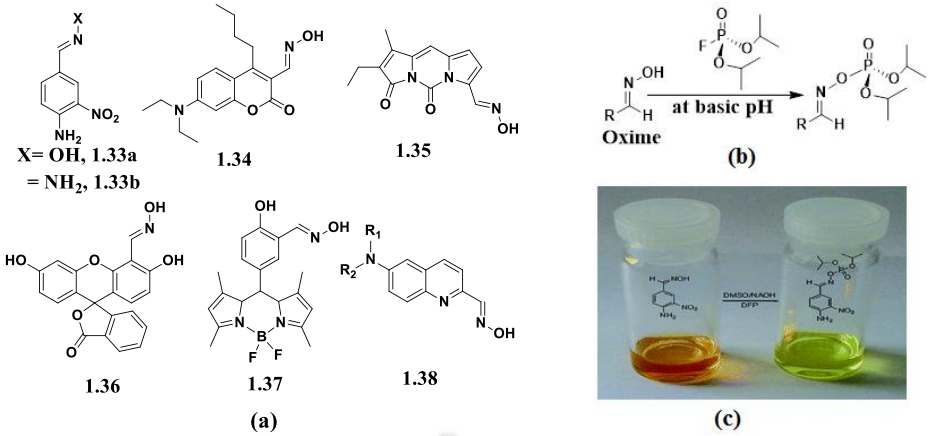

Figure 1.22: (a) Some oximes that detect nerve agents; (b) Reaction between oxime and nerve agents and (c) Naked eye detection of nerve agents by oxime molecule.

Fluorescence emission of the anionic form of the compound **1.34** gradually increases upon addition of diisopropyl fluorophosphates (DFP). Rebek and co-workers have developed some *ortho*-hydroxy aromatic oximes associated with fluorescence properties that were utilized to sense nerve agents.[84] Fluorescent arylisoxazole was formed by interaction of *ortho*-hydroxy aromatic oxime with nerve agents; due to formation of cyclized product there was sharp optical signal changes was found. *N,N*-Carbonyl-bridged dipyrrinone oxime **1.35** is a potential sensor for organophosphates. The deprotonated form of **1.35** shows a distinct crimson red colour by absorbing at 561 nm, which disappears upon addition of organophophates or pesticide. The toxic organophophates were detected by this oxime **1.35** through change of colour as well as changes in fluorescence emission properties.[85] The oxime **1.36** containing a dye moiety as fluorophore is useful in the detection of nerve agent diethyl chlorophosphate (DCP) with a detection limit of 10 nM in buffer solution.[86] This detection process occurs through cascade reactions by conversion of oxime to nitrile via an isoxazole intermediate. The transformation of **1.36** into fluoresceinyl oxime nitrile on reaction with nerve agent induces dramatic fluorescence enhancement, enabling one to detect by naked eye detection.

Churchill group developed a BODIPY-salicylaldehyde oxime **1.37** that showed high selectivity in binding with nerve agent diethyl cyanophosphonate (DECP) through fluorescence turn on mechanism.[87] Song and his co-workers developed 6-substituted amino-quinolinoxime **1.38** for visual detection of nerve agent.[88] Detection of nerve agent in this particular example passes through rapid phosphorylation-protonation reaction.

1.11: Oxime derivatives in detection of cations

Design of new chemosensors with high sensitivity for selective binding of metal ions is an attractive and challenging in research field. This is true for transition metal ions as they are of significance in environment pollution. Generally for selective binding of metal ion with a receptor, it should have some pre-organised metal binding sites. This criterion is easily fulfilled by designing functionalised receptors with different metal binding sites. Oxime functional group is more specific toward anion binding studies, as it has acidic proton, but recognitions of metal ions by oximes are rare. Compound (E)-7-(diethylamino)-2-oxo-2H-chromene-3-carbaldehyde oxime **1.39**, detects copper(II) ion under physiological conditions.[89] Compound **1.39** showed high selectivity toward copper(II) ions by forming a 2:1 copper(II) complex. Oxime based compound 2'-hydroxy-4-methoxy-5'-chlorochalcone oxime **1.40** (**Fig. 1.23**) reacts with palladium(II) to form a 1:2 palladium(II)-**1.40** chelate complex. This complex is extractable at pH 2.5 with iso-butanol. The compound is unable to detect palladium(II) in presence of other interfering ions such as Au^{3+}, $Cr^{3+}$and Zr^{4+}.[90] Phenylazobenzaldehyde oxime **1.41** is another oxime based molecular sensor that shows a weak and strong absorption band at 430 and 550 nm upon addition of Pd^{2+} metal ion.[91] A purple colored palladium(II)-complex of **1.41** is formed within 15 minutes remains stable for several days at room temperature or upon boiling.

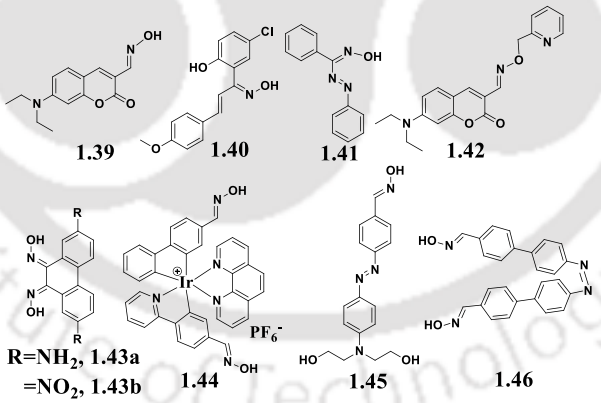

Figure 1.23: Examples of oximes used in detection of metal ions.

Oxime-ether based compound **1.42** is useful for fluorometric and colorimetric detection of palladium(II). This compound shows high selectivity and sensitivity to detect Pd^{2+} in aqueous and biological samples.[92]

Compound **1.42** shows strong green fluorescence emission at 505 nm in aqueous medium (**Fig. 1.24**). Addition of solution of palladium(II) to a solution of **1.42** decreases the green florescence consistently. In this process an intramolecular charge transfer process is induced by forming stable palladium complex. 2,7-disubstituted phenanthrene-based bis-oximes

1.43a and **1.43b** are explored for heavy metal cation binding study. The fluorescence properties associated with this oxime **1.43a** and **1.43b** are helpful to understand their sensing ability to discriminate Cr^{3+} and Fe^{3+} ions. Binding stoichiometry of these ligands depend on the nature of cations. For example, **1.43a** form Cr^{3+} complex with 1:2 molar ratio, whereas a 1:1 stoichiometry was observed for **1.43a**-Fe^{3+} complex.[93] Schmittel and co-workers synthesized an oxime based non-emissive iridium complex **1.44** for highly selective detection of Hg^{2+} and ClO^- ions. This non-emissive iridium complex **1.44** acts as a chemodosimeter responding to Hg^{2+} by dehydration reaction in acidic solution. In basic medium it is oxidized by ClO^-, resulting in large increase in emissions at distinct wavelengths depending on the ions under consideration.[94]

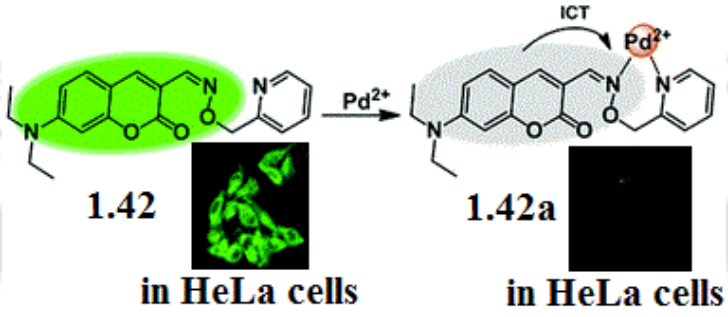

Figure 1.24: Detection of Pd^{2+} ion by compound **1.42**.

Dual sensing of $Hg^{2+}$and F^- ions is possible with compound **1.45** which **is** an aldoxime and azobenzene based compound. It showed excellent sensitivity and selectivity towards Hg^{2+} ions through catalytic dehydration reaction at pH = 5. On addition of Hg^{2+} ion to a solution of **1.45** a 70 nm red shift in absorption maximum was observed, thus colour change from pale yellow to dark violet makes an easy detection process. Similarly compound **1.45** showed high sensitivity and selectivity toward F^- ions in DMSO as solvent, In this case colour changes from pale yellow to dark red.[95] A biphenyl-azo conjugated aldoxime **1.46** is photo-responsive upon addition of $Hg^{2+}$and F^-. It shows highly selective binding toward $Hg^{2+}$and F^- over a wide range of metal ions or anions.

The detection process takes place through "turn-on" fluorogenic mode. The coordination of **1.46** with Hg^{2+} is reversible and it shows less interference from the other common metal ions.[96] These examples exemplify that the oxime based receptors can be designed based on the coordination ability of oximes and tuning the environment sensitive optical properties.

1.12: Oxime derivatives in detection of anions

Many examples of anion binding receptors are gifted by nature. Such anion binding receptors are in neutral or charged states, which based on hydrogen bonding interaction. Many fluorescent and colorimetric anion receptors or sensors are developed rapidly. Selective detection of anions using synthetic chemosensor has received attention during the past few decades. Among those, oxime based compounds have provided a broad ranges of templates for selective and sensitive binding of anions. Lin and his co-workers has developed an oxime based sensor **1.47 (Fig. 1.25a)** for selective and sensitive detection of hypochlorite anion.[97] Compound **1.47** showed a strong blue fluorescent emission at 439 nm when excited at 394 nm in phosphate buffer (0.1 M, pH 9.0) : DMF (1 : 4, v/v). But in the presence of hypochlorite it showed a red shift of about 70 nm. Due to formation of deoximation product with intra-molecular charge-transfer mechanism is operative in such system that causes fluorescence change (**Fig. 1.25b**). The compound **1.47** showed high selectivity for hypochlorite over other anions, cations and oxidants due to the distinct deoximation ability of oxychloride. Compound **1.47** is able to detect ClO^- anion at different pH (2.5 to 10.5).[97]

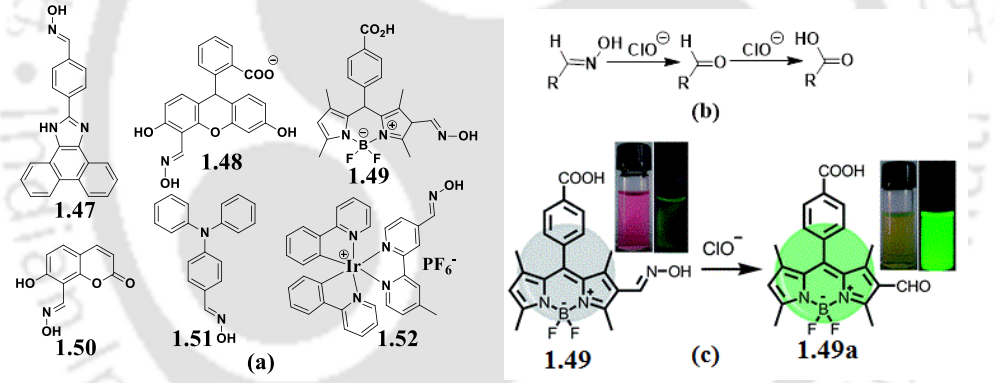

Figure 1.25: (a) Oxime based molecules for detection of hypochlorite anion; (b) Reaction between oxime and hypochlorite anion and (c) Naked eye detection of hypochlorite by oxime molecule.

A "turn-on" fluorescent and colorimetric probe **1.48** having fluorescein-oxime architecture is used for detection of hypochloric acid. The probe **1.48** displayed high sensitivity and extremely high selectivity for ClO^- anion with a 5 μM limit of detection. The deoximation reaction of **1.48** on addition of ClO^- showed a distinct fluorescent emission at 530 nm when excited at 454 nm.[98]

Another acid and oxime functionalized BODIPY-based sensor **1.49** is able to detect ClO^- in aqueous media through "turn-on" fluorescent mechanism (**Fig. 1.25c**).[99] It exhibits poor fluorescence in absence of ClO^- but it showed a new band at 525 nm when excited at 500 nm upon addition of HOCl under suitable conditions. Other potentially competing reactive

oxygen species or reactive nitrogen species did not affect the detection of HOCl. A fluorescent coumarin attached oxime based compound **1.50** exhibits a rapid, highly selective and sensitive response to HOCl.[100] The oxidation reaction of oxime **1.50** is accompanied by a 7-fold increase in the fluorescent quantum yield (from 0.03 to 0.21) and it has a detection limit 25 nM. Compound **1.51** showed strong blue fluorescence emission at 458 nm when excited at 339 nm in phosphate buffer.[101] Upon addition of HOCl, a dramatic fluorescent decrease was visually observed.[101] A phosphorescent chemosensor comprising of iridium(III) complex **1.52** containing oximated 2,2′-bipyridine unit was reported for selective and sensitive detection of ClO^- anion.[102] Complex **1.52** is weakly emissive due to isomerization of C=N-OH passes through a predominantly non-radiative decay path. But in presence of ClO^-, the emission of **1.52** is remarkably enhanced. During the course of reaction oximated 2,2′-bipyridine unit in **1.52** is converted to a carboxylic acid 4′-methyl-2,2′-bipyridine-4-carboxylic acid (**Fig. 1.25b**).

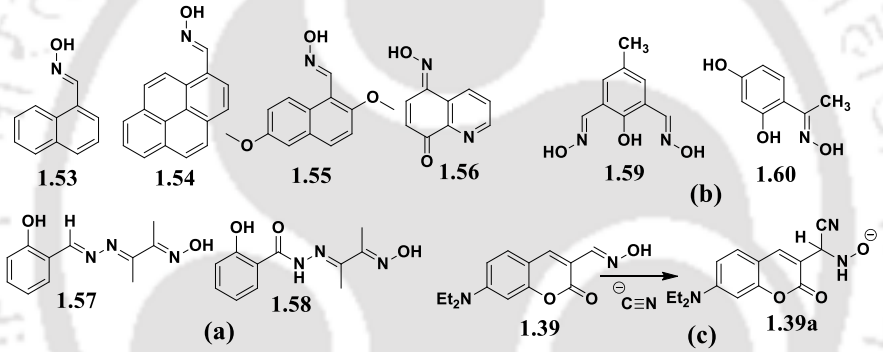

Figure 1.26: Oxime based molecules for detection of (a) fluoride; (b) arsenate and (c) cyanide anions.

Oxime based ligands **1.53-1.55** have shown selective colorimetric and fluorescent chemosensor for quantification of fluoride ions (**Fig. 1.26a**).[103] Fluoride ion is basic in nature which abstracts the oxime acidic proton to generate a phenoxide ion and HF_2^-. UV-Vis spectroscopic studies of sensors **1.53** to **1.54** in DMSO revealed a significant red-shift from 310 nm to 395 nm (**1.53**), 360 nm to 460 nm (**1.54**) in the presence of TBAF.

The compound **1.55** has a distinct advantage over the other two molecules **1.53** and **1.54** in sensing fluoride ions, as it is able to detect fluoride ions through both emission and absorption spectroscopy.[103] Oxime based compound 5-(hydroxyimino)quinolin-8-one (**1.56**) shows selective interaction with fluoride ions. Formation of supramolecular adducts between **1.56** and tetrabutylammonium fluoride in solution causes a drastic colour change to cause quenching of the fluorescence emission of **1.56**.[104] The compound **1.56** is also able to detect zinc ions in the presence of other competitive cations and anions by causing a selective

colour change or through distinguishable fluorescence emission changes. Phenolic oximes **1.57** and **1.58** linked via different aliphatic spacers[105] exhibit intense and instantaneous colour change upon addition of fluoride ion which are clearly discernible by naked eyes. The aliphatic spacers create a large different between the two sensing abilities of the **1.57** and **1.58** in detection of fluoride ion. Such differences cause remarkable change in optical, electrochemical properties in recognition study.[105]

Arsenate or arsenite are highly toxic anions, these can cause serious health problems with an increased risk of liver, bladder and lung cancer.[106] Compounds **1.59** and **1.60** (**Fig. 1.26b**) are used in selective and sensitive detection of arsenate or arsenite anions in water, which are present as pollutant.[107-108] These compounds are weakly fluorescent in aqueous medium. But in presence of arsenate or arsenite anions emission of **1.59** and **1.60** gradually increases with increase amount of arsenate or arsenite anions.

Among various anions cyanide ions are extremely toxic to living organisms and a trace amount of cyanide anions can caused death. Coumarinyloxime-based fluorescent probe **1.39 (Fig. 1.26c)** has ability to distinguish selective and sensitive manner cyanide from other anions. Sensor **1.39** has shown highly selective and sensitive response to the cyanide anion over other various anions with a submicromolar limit of fluorimetric detection.[109] These examples show that the selectivity of oxime toward anions depends on the structure of the oxime derivative or on the signal transduction unit of oxime derivatives. The ability to undergo deprotonation of oxime derivatives with a fluorophore or chromphore unit in presence of anions and the supramolecular feature of oxime derivatives makes it possible to detect and prevent many noxious properties associated with anions.

1.13: Coordination chemistry of oxime derivatives

The oximes show amphiprotic behavior due to acidic hydroxyl group and basic nitrogen atom present on them. Oximes have played a crucial role in the development of coordination chemistry.[110] In early examples of coordination chemistry of oximes, dimethylglyoxime was identified as a strong binding ligand to nickel(II) ion forming stable bis-dimethylglyoximato nickel(II) complex.[111] Oxime or oximato groups can bind to a metal ion in different ways[110]; some of the common binding modes of oxime or oximato groups with a metal ion are shown in **Fig. 1.27**.

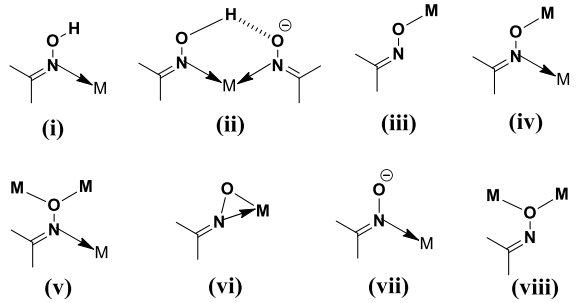

Figure 1.27: Coordination modes of oxime or oximato groups with metal ion.

Phenolic oximes (**1.61-1.63**) are used extensively in industry for metal extraction from waste streams, mainly for the extraction of copper.[112] They show remarkable selectivity for copper(II) over other metal ions present in solutions together with copper ions. The favorable selectivity for copper is due to the fitting of copper ion in the space formed by two hydrogen bonded ligands as **1.61a,** shown in **Fig. 1.28**. Another important feature of phenolic oximes is their ability to form polynuclear complexes as both the oximate and phenolate groups can bridge metals.

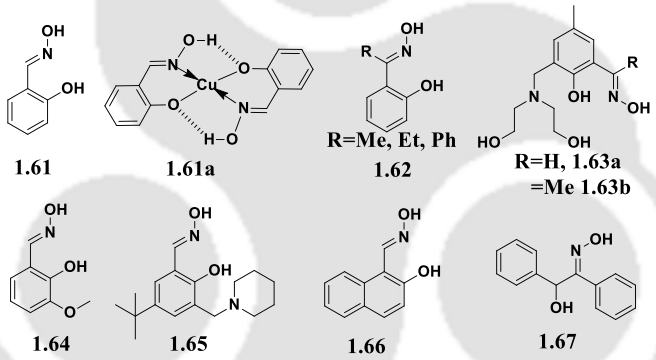

Figure 1.28: Some oxime ligands (**1.61-1.67**) and **1.61a** is a copper(II) complex with **1.61**.

Phenolic oximes **1.61** or **1.62** on double deprotonation behave as tridentate bi-nucleating ligands, which may be coordinated to the metal ions by nitrogen or oxygen atoms participating in the formation of the metallacrown ring. There are plenty of examples on polynuclear trivalent metal complexes with oxime **1.61 or 1.62** as ligands with Fe(III)[113] or Mn(III).[114] Majority of the polynuclear oxime complex reports include dinuclear,[113a] trinuclear,[114] tetranuclear,[115] hexanuclear[116] having azide,[117] halide,[116] perchlorate,[114b] and carboxylate[115] counterions or co-ligands.

Both compounds **1.61** and **1.62** form metal complexes with transitions metal ion like nickel.[118] Hexanuclear complexes of manganese and iron metal ions with **1.61** and **1.62** oxime ligands have shown **(Fig. 1.29)** single-molecule magnet property. Salicylaldoxime-based [Mn^{III}_6] complexes with general formula [$Mn^{III}_6O_2(O_2CR)_2$(**1.61**)$_6$$(EtOH)_4$] are prepared from reaction of manganese acetate dihydrate

and salicylaldoxime (**1.61**) in ethanol.[119] The metallic core of manganese complex consists of two off-set, stacked $[Mn^{III}_3(\mu_3\text{-}O)(\mathbf{1.61}^{2-})_3]^+$ triangles where each edge of the triangle is bridged by one oximate -N-O- group; thus, creating an oxo-centred $\{Mn\text{-}N\text{-}O\text{-}\}_3$ ring. Magnetic studies revealed S=4 ground states with axial anisotropies of the order D = -1.2 cm^{-1} and ''moderate'' energy barriers to magnetization reversal of U_{eff} = 28 K. Hexanuclear iron complex of oxime **1.62** with the general formula $[Fe_6O_2(OH)_2(Et\text{-}sao)_2(Et\text{-}saoH)_2(O_2CPh)_6]$ shown in **Fig. 1.29b** also showed single-molecule magnets property like the hexanuclear manganese complex (**Fig. 1.29a)**.[120]

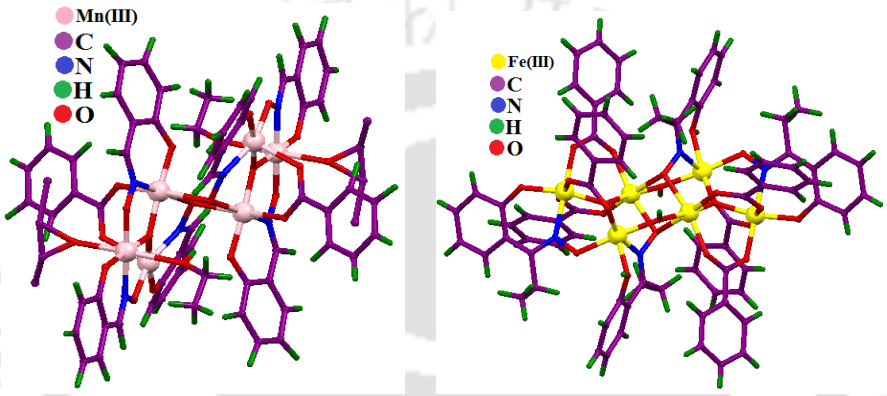

(a) (b)

Figure 1.29: Hexnuclear (a) manganese(III) and (b) iron(III) complexes of **1.61** and **1.62** oximes respectively.

Compound **1.63a** formed octametallic Cu(II) wheels on simple reaction with copper(II) salts, and also it formed single-stranded hexametallic mixed-metal Na_2Cu_4 wheel.[121] Octametallic Cu(II) wheels and hexametallic mixed-metal Na_2Cu_4 wheel of compound **1.63a** is the first examples of metalo-wheels of this compound. Similarly compound **1.63b** formed **d**odecametallic Mn(III) wheel,[122] and heterometallic complexes with Zn(II) and Ln(III) metal ions.[123] Phenolic oxime based ligand 3-methyloxysalicylaldoxime **1.64** is useful to construct 3d/4f heterometallic clusters. From this ligand a family of novel heptanuclear $[Mn_3Ln_4]$ metal complexes was obtained and structurally characterized which are represented examples of 3d/4f clusters.[124]

Powell and her co-workers have reported heteromettallic complexes of **1.64** with transition and lanthanide metal ions with interesting magnetic properties.[125] 3-Dialkylaminomethyl substituted salicylaldoxime (**1.65)** are used as an efficient metal salt extractant. Compound **1.65** forms a zwitterionic complex with copper(II) and zinc(II) metal salts, where some anions like nitrate, tetrafluoroborate and trifluoroacetate are found in outer sphere of the complex.[126] But with halides such as chloride or bromide it formed inner coordinated metal

complex, leading to high chloride selectivity and very good mass transport efficiencies of copper(II) chloride.

2-Hydroxy-1-naphthaldehyde oxime (**1.66**) forms binuclear metal complex with manganese(III) having general formula $[Mn^{III}_2(\mathbf{1.66}^{2-})_2(\mathbf{1.66}^{-})_2(MeOH)_2].4MeOH$.[127] And also it forms hexanuclear manganese complex in presence of naphthalene-1,8-dicarboxylic acid as a co-ligand.[128] Benzoin oxime **1.67** is used to prepare family of decanuclear copper(II),[129] nickel(II)[130] and manganese (III)[131] complexes, each showing anti-ferromagnetic property. Phenolic oxime ligands form different transitions metal complexes having various nuclearity are well described by Tasker and co-workers,[132] where ‘‘metal oximate’’ building blocks are used as ligands to synthesize various homo and heterometallic paramagnetic complexes. However in coordination chemistry, pyridyl oximes has significant role to synthesized transition metal oxime or metal-oximate complexes with various nuclearity. Pyridyl oximes (**1.68-1.70**; R= H, Me, Ph) have significance in synthesise of polynuclear transition metal oxime or metal-oximate complexes (**Fig. 1.30**). The first structurally characterized metal complex of pyridine-2-carbaldehyde oxime was $\{Cu_3(OH)(SO_4)^{-}(\mathbf{1.68})_3\}$.[133] The dianionic species generated from **1.68-1.70** are important as chelating and bridging (μ_2-μ_4) agents.[134] Compounds **1.68-1.70** form dodecanuclear and hexadecanuclear Ni-cluster on simple reaction with $NiCl_2.6H_2O$ in presence of base.[135]

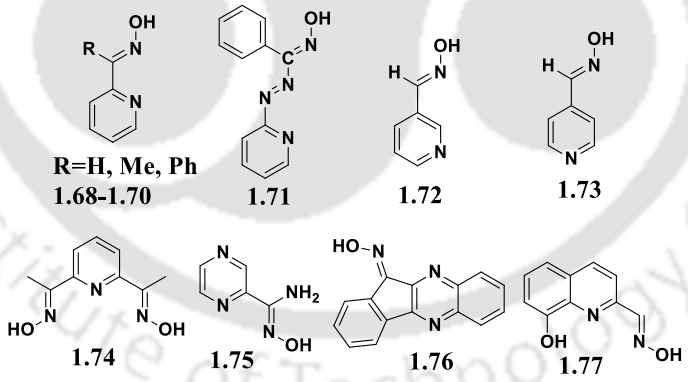

Figure 1.30: Some heterocyclic oxime derivatives are used as ligands for synthesis of metal complexes.

Methyl 2-pyridyl ketone oxime (**1.69**) forms heterometallic complexes with zinc(II) and lanthanide(III) ions such as $[ZnLn(\mathbf{1.69}^{-})_3(\mathbf{1.69})_3]^{-}(ClO_4)_2$ or $[ZnLn(NO_3)_2(\mathbf{1.69}^{-})_3(\mathbf{1.69})]$. These blue-green complexes show ligand-based photo-luminescence.[136] The compound **1.71** is a potential flexidentate pyridyl-azo-oxime, it provides a series of homoleptic complexes $[Co^{III}(L^{1-})_3]$ or $[Co^{III}(L^{1-})_2]ClO_4$. These complexes have N_6 and N_4O_2 coordination environments respectively.[137] Ligand **1.72,** has similar structural feature as that of 2-pyridyl oxime, but coordination chemistry of this ligand **1.72** is very limited. It provides example of

supramolecular assembly when complexes to ions like silver (I) or copper(I). The crystal structure of $[Ag(\mathbf{1.72})_2](PF_6)$ contains cations that is comprised of two ligands coordinated through the 3-pyridyl nitrogen atoms to one silver(I) ion.[138] In this complex the oxime moieties are *cis* with respect to each other, and cations are linked by complementary O-H···N hydrogen bonds that are formed between oxime moieties present on neighboring ligands. These interactions generate an infinite 1D chain like assembly. In crystal lattice, the adjacent chains are linked by C-H···O hydrogen bonds. But in the crystal structure of $[CuI(\mathbf{1.72})]_n$ each tetrahedral copper(I) ion is coordinated to three μ_3-I^- ligands to generate an infinite one-dimensional assembly. Porous molecular materials are formed as a consequence of oxime **1.73** coordinating to nickel(II) metal ion.[139]

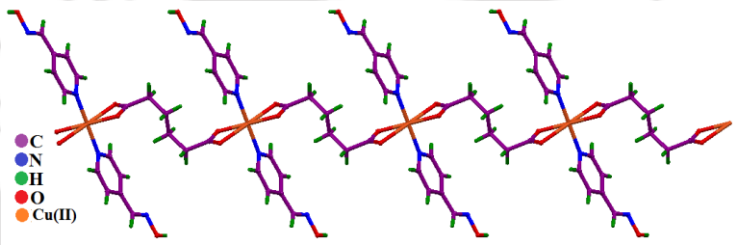

Figure 1.31: one-dimensional tape-like structure of copper(II) adipate complex with **1.73**.

Metal complexes of oxime ligand **1.73** with zinc(II) and cadmium(II) show nonlinear optical (NLO) properties.[140] Polymeric luminescent zinc(II) and cadmium(II) metal aliphatic dicarboxylate complexes of **1.72** or **1.73** with are useful for gas adsorption.[141] The soft nature of 1D coordination polymer crystals of copper(II) adipate complex of **1.73** (**Fig. 1.31**) was investigated by nano-indentation study for mechanical stress in conditions of different indentation loading.[142] Some of the polynuclear metal complexes of ligand **1.74** show single-molecular magnet proerties.[143] Ligand **1.74** forms nano-dimensional octadecanuclear heterometallic $\{Cu_6Ln_{12}\}$ clusters with assistance of bridging N_3^- Ligands. Depending on the 4f-metal ion present in these octadecanuclear complexes some of them shows single-molecule magnetic behavior with large magnetic entropy changes.[144]

Dimeric uranium complex of **1.74** $[UO_2(\mathbf{1.74})Cl]_2$ is stable in solution as shown by ESI-MS spectrometry and NMR spectroscopy.[145] Ligand **1.74** forms palladium(II) and platinum(II) chelate complexes, which shows biological activity.[146] Pyrazine-2-amidoxime (**1.75**) is another ligand having similarity to oxime **1.68.** This ligand has an extra metal binding site to form metal complexes with 3d-4f metal ions. It forms decanuclear $\{Dy_4Ni_6\}$ cluster with a central butterfly-shaped $\{Dy_4(\mu_3\text{-}OH)_2\}$ core and six peripheral diamagnetic nickel(II) ions.[147] Different nuclearities metal complexes of nickel(II) or cobalt(II/III) metal ions are formed by indeno-quinoxaline ligand **1.76** (**Fig.1.30**), in such complexes nuclearities ranges

from 3 up to 8. These complexes have shown interesting magnetic properties.[148] The reaction of 8-quinolinol-2-carboaldoxime (**1.77**) with nickel(II) and lanthanum(III) metal salts afforded different heterometallic decanuclear metal complexes and magnetic studies on these complexes reveal an overall anti-ferromagnetic behavior.[149]

The foregoing discussions have suggested that the oxime functional group or oxime together with other functional group is used as ligands for making of metal complexes with different nuclearity. The special interests on oxime complexes because of single molecular magnetic properties and unusual optical properties associated with many clusters. Porous materials can be also successfully generated from complexation of oxime with metal ions and such complexes are useful for gas adsorption study. However, many of metal complexes are sensitive to cations or anions; hence leave huge scopes to use oxime based molecules to explore interesting properties.

1.14: Scope of the present work

From the above literature survey it is clear that oxime derivatives not only have wide variations of synthons in self-assemblies but also draw special interests from wide modes of binding to metal ions. The oxime functional group containing compounds show interesting optical properties in solid state.[150] Oxime derivatives also have great potential in medicinal chemistry; it shows high antibacterial and antifungal properties,[151] high index of antitumor activity.[152] Oxime derivatives can cause several biological effects such as endothelium independent relaxation in blood vessels,[153] increased targeting of specific nucleobases of DNA,[154] and oxidative DNA cleavage.[155] Metal complexes of oxime based ligands display biological activities.[156] Some metal complexes of oxime derivatives show biological activity as well as catalytic activity for organic transformations.[157] Metal complexes of pyridine-4-carbaldoxime shows interesting supramolecular assemblies in solid state through weak interactions.[158] It form oxime-oxime dimeric synthons and O-H···O interactions to form a dimeric assembled structure (**Fig. 1.32**).

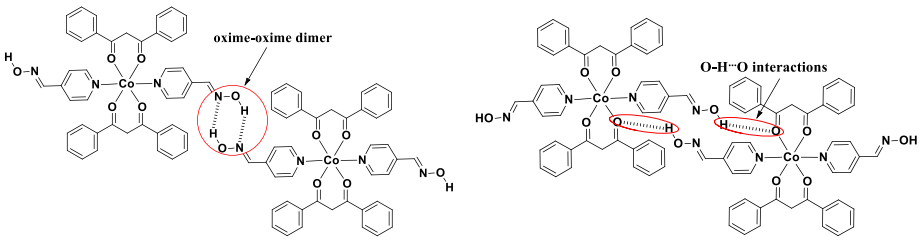

(a) (b)

Figure 1.32: (a) and (b) two different oxime synthons in metal complex of oxime derivatives.

In metal complex anion are present as counter ions in free or by occupying coordination sites of the metal ion. There are several studies on the oxime containing ligands in which the better coordinating site of the ligand coordinates with metal ion, while the oxime part remains free. In these complexes free oxime group form hydrogen bonds with anions.[159] The ability of an anion to coordinate to a metal ion or remain in uncoordinated depend on the nature of anions or hydrogen bonds provided by the ligand. One such example is $CF_3SO_3^{2-}$ anion, which a counter anion of silver(I) metal, remains in the outer sphere of the silver(I) complex but involves in O-H···anion interactions (**Fig. 1.33).**[160] Hence, by deprotonation of free oxime sites of the oxime based metal complexes, one can synthesized higher nuclearity heteromettalic metal complex as illustrated in **Fig. 1.33b**. And also we can use these metal complexes as a template for selective or sensitive detection of basic anions.

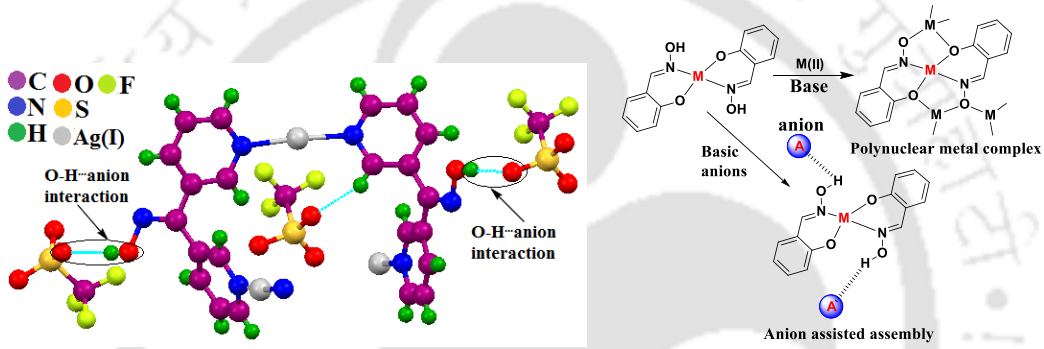

(a) (b)

Figure 1.33: (a) Anion-oxime interaction in silver(I) complex of 3,3'-bipyridyl ketone oxime and (b) Synthesis scheme of polynuclear metal complexes and anionic assemblies from bis-chelate metal(II) salicylaldoxime complex.

As mentioned earlier that the oxime functional group has applications in drugs industry, to detect chemical war-weapon as well as controlling certain biological processes, hence understanding of oxime derivatives in different supramolecular environments would be challenging topic in the field of supramolecular chemistry. Self-assemblies of oximes has also prospect to develop new materials with interesting optical properties. Another interesting aspect of oxime derivatives is they have ability to detect cation and anion. In such cases issues related to hydrolytic stability, sensitivity, selectivity, biocompatibility, solubility and cost optimization continues to generate new impetus. Thus, our approach would be to

1. Study supramolecular assemblies based on oxime containing molecules.
2. Study the self-assemblies of oximes having additional weak interacting sites within the molecule or with other molecules that have hydrogen bond ability with oximes.

3. To synthesise multi-component cocrystals of oximes having additional functions groups to study the thermal stability and molecular recognition properties.
4. To utilize non-directional properties of anions and cations for construction of different non-covalent self-assemblies of oxime derivatives.
5. Synthesized self-assemblies of metal complexes as well as metal organic frameworks[161] of oxime derivatives which selectively interact with anions or cations.

So, we chose oxime functionalized phenolic or heterocyclic compounds to establish series of supramolecular assemblies formed in various conditions and explore some interesting structural, optical and thermal properties.

1.15: References

1. J. -M. Lehn, 'Supramolecular chemistry and self-assembly special feature: Toward complex matter: Supramolecular chemistry and self-organization', *Proc. Nat. Acad. Sci*., USA, 2002, **99**, 4763.
2. (a) J. P. Sauvage, *Acc. Chem. Res*., 1998**,** **31**, 611; (b) M. Fujita, *Acc. Chem. Res*., 1999, **32**, 53-61; (c) D. L. Caulder, K. N. Raymond, *Acc. Chem. Res*., 1999, **32**, 975-982; (d) P. J. Stang, *Chem. Rev*., 2000, **100**, 853-908.
3. (a) J. M. Lehn, *Pure Appl. Chem.*, 1978, **50**, 871-892; (b) J. M. Lehn, *Acc. Chem. Res*.,1978, **11**, 49-57.
4. S. K. Burley, G. A. Petsko, *Science*, 1985, **229**, 23-28.
5. (a) J. C. Ma, D. A. Dougherty, *Chem. Rev*., 1997, **97**, 1303-1324; (b) P. B. Crowley, A. Golovin, *Proteins Struct. Funct. Bioinf*., 2005, **59**, 231-239.
6. (a) D. Quinonero, C. Garau, C. Rotger, A. Frontera, P. Ballester, A. Costa, P. M. Deya, *Angew. Chem. Int. Ed. Eng*., 2002, **41**, 3389-3392; (b) C. Garau, A. Frontera, D. Quinonero, P. Ballester, A. Costa, P. M. Deya, *ChemPhysChem*., 2003, **4**, 1344-1348; (c) D. Quinonero, A. Frontera, C. Garau, P. Ballester, A. Costa, P. M. Deya, *ChemPhysChem*., 2006, **7**, 2487-2491.
7. A. Gil, V. Branchadell, M. J. Calhorda, *RSC Adv*., 2016, **6**, 85891-85902.
8. S. Roche, C. Haslam, H. Adams, S. L. Heath, J. A. Thomas, *Chem. Commun*., 1998, 1681-1682.
9. (a) M. Chiper, M. A. R. Meier, D. Wouters, S. Hoeppener, C. A. Fustin, J. F. Gohy, U. S. Schubert, *Macromolecules*, 2008, **41**, 2771-2777; (b) S. J. Rowan, J. B. Beck, *Faraday Discuss*., 2005, **128**, 43-53.

10. A. Harada, K. Kobyashi, Y. Takashima, A. Hashidzume, H. Yamaguchi, *Nature Chem.*, 2011, **3**, 34-37.
11. F. Diederich, Symposium on Molecular Architecture Volume 67 Number 10 October 1990. 813.
12. B. H. Northrop, F. Africo, N. Tangchiavang, J. D. Badjic, J. F. Stoddart, *Org. Lett.*, 2006, **8**, 3899-3902.
13. S. Sivakova, S. J. Rowan, *Chem. Soc. Rev*., 2005, **34**, 9-21.
14. Q. Yan, K. Cai, D. Zhao, *Phys. Chem. Chem. Phys*., 2016, **18**, 1905-1910.
15. G. Beobide, O. Castillo, A. Luque, U. G-. Couceiro, J. P. Garcıa-Teran, P. Roman, *Inorg. Chem*., 2006, **45**, 5367-5382.
16. Z. Feng, T. Zhang, H. Wang, B. Xu, *Chem. Soc. Rev.*, 2017, **46**, 6470-6479.
17. J. W. Steed, J. L. Atwood, *Supramolecular chemistry, Second Edition*, 2009, 1-941.
18. D. J. Cram, *Angew. Chem. Int. Ed*., 1988, **27**, 1009-1020.
19. G. R. Desiraju, *Acc. Chem. Res*., 1991, **24**, 290-296.
20. (a) G. R. Desiraju, *Acc. Chem. Res*., 2002, **35**, 565-573; (b) G. R. Desiraju, *Angew. Chem. Int. Ed. Eng*., 2011, **50**, 52-59.
21. (a) P. Vishweshwar, A. Nangia, V. M. Lynch, *J. Org. Chem*. 2002, **67**, 556-565; (b) P. K. Goswami, R. Thaimattam, A. Ramanan, *Cryst. Growth Des*. 2016, **16**, 1268-1281; (c) D. Singh, J. B. Baruah, *Cryst.Growth Des*. 2012, **12**, 3169-3180; (d) R. J. Sarma, J. B. Baruah, *Cryst. Growth Des*. 2007, **7**, 989-1000. (e) Katarzyna N. Jarzembska, Anna A. Hoser, Sunil Varughese, Radosław Kamiński, Maura Malinska, Marcin Stachowicz, Venkatesvara R. Pedireddi, and Krzysztof Woźniak, *Cryst. Growth Des*. 2017, **17**, 4918-4931; (f) C. B. Aakeröy, S. V. Panikkattu, B. DeHaven, J. Desper, *Cryst. Growth Des*. 2012, **12**, 2579-2587.
22. (a) V. R. Thalladi, H. C. Weiss, D. Blaser, R. Boese, A. Nangia, G. R. Desiraju, *J. Am. Chem. Soc*., 1998, **120**, 8702-8710; (b) H. C. Weiss, R. Boese, H. L. Smith, M. M. Haley, *Chem. Commun*., 1997, 2403-2404.
23. (a) G. R. Desiraju, *Angew. Chem. Int. Ed. Engl*., 1995, **34**, 2311-2327; (b) G. R. Desiraju, *Chem. Commun*., 1997, 1475-1482.
24. J. D. Watson and F. H. Crick, *Nature*, 1953, **171**, 737-738.
25. G. R. Desiraju, T. Steiner, The weak hydrogen bond in structural chemistry and biology. 1999, Oxford: Oxford University Press.
26. I. Rozas, I. Alkorta, J. Elguero, *J. Phys. Chem. A*, 1998, **102**, 9925-9932.

27. M. C. Etter, *Acc. Chem. Res*., 1990, **23**, 120-126.
28. (a) M. C. Etter, J. C. MacDonald, J. Bernstein, *Acta. Cryst.*, 1990, **B46**, 256-262; (b) J. Bernstein, R. E. Davis, L. Shimoni, N. -L. Chang, *Angew. Chem. Int. Ed. Engl*., 1995, **34**, 1555-1573.
29. J. Teyssandier, S. De Feyter, K. S. Mali, *Chem. Commun.*, 2016, **52**, 11465-11487.
30. J. R. Williamson, M. K. Raghuraman, T. R. Cech, *Cell*, 1989, **59**, 871-880.
31. S. C. Zimmerman, W. Wu, *J. Am. Chem. Soc.*, 1989, **111**, 8054-8055.
32. D. E. Lynch, N. Mistry, G. Smith, K. A. Byriel, C. H. L. Kennard, *Aust. J. Chem*., 1998, **51**, 813-818.
33. E. Chekmeneva, C. A. Hunter, M. J. Packer, S. M. Turega, *J. Am. Chem. Soc*., 2008, **130**, 17718-17725.
34. E. A. Meyer, R. K. Castellano, F. Diederich, *Angew. Chem. Int. Ed. Eng*., 2003, **42**, 1210-1250.
35. (a) S. Shinkai, M. Ikeda, S. Atsushi, M. Takeuchi, *Acc. Chem. Res*., 2001, **34**, 494-503; (b) M. Ma, Y. Gong, D. Bong, *J. Am. Chem. Soc*., 2009, **131**, 16919-16926; (c) M. -K. Chung, P. S. White, S. J. Lee, M. R. Gagne, *Angew. Chem. Int. Ed. Eng*., 2009, **48**, 8683-8686.
36. R. Katoono, H. Kawai, K. Fujiwara, T. Suzuki, *J. Am. Chem. Soc*., 2009, **131**, 16896-16904.
37. (a) C. J. Pedersen, *J. Am. Chem. Soc*., 1967, **89**, 2495-2496; (b) C. J. Pedersen, *J. Am. Chem. Soc*., 1967, **89**, 7017-7036.
38. K. Zhu, M. Zhang, F. Wang, N. Li, S. Li, F. Huang, *New J. Chem*., 2008, **32**, 1827-1830.
39. J. L. Sessler, P. A. Gale, W. S. Cho, *Anion Receptor Chemistry*, The Royal Society of Chemistry, Cambridge, UK, 2006.
40. G. Lamoureux, B. Roux, *J. Phys. Chem. B*, 2006, **110**, 3308-3322.
41. A. G. Sharpe, *J. Chem. Educ*., 1990, **67**, 309-315.
42. (a) D. Esteban-Gomez, L. Fabbrizzi, M. Licchelli, E. Monzani, *Org. Biomol. Chem*. 2005, **3**, 1495-1500; (b) D. W. Kim, J. Kim, J. Hwang, J. K. Park, J. S. Kim, *Bull. Korean Chem. Soc.*, 2012, **33**, 1159-1164; (c) N. T. Dang, J. J. Park, S. Jang, J. A. Kang, *Bull. Korean Chem. Soc.*, 2010, **31**, 1204-1208; (d) E. Martínez-Gonzalez, F. J. Gonzalez, J. R. Ascenso, P. M. Marcos, C. Frontana, *J. Org. Chem*., 2016, **81**, 6329-6335.

43. P. Khakhlary, J. B. Baruah, *J. Mol. Struct.*, 2014, **1078**, 188-196.
44. (a) T. J. Mooibroek, P. Gamez, *CrystEngComm*, 2012, **14**, 1027-1030; (b) H. I. Althagbi, A. J. Edwards, B. K. Nicholson, D. A. Reason, G. C. Saunders, S. A. Sim, D. A. van der Heijden, *Cryst. Growth Des*., 2016, **16**, 174-188.
45. (a) N. Phukan, J. B. Baruah, *CrystEngComm*, 2016, **18**, 7753-7763; (b) N. Phukan, J. B. Baruah, *Cryst. Growth Des*., 2014, **14**, 2640-2653; (c) V. S. Bryantsev, B. P. Hay, *J. Phys. Chem. A*, 2006, **110**, 4678-4688; (d) A. Karmakar, J. B. Baruah, *Inorg. Chem. Commun*., 2009, **12**, 140-144.
46. (a) N. Yutronic, V. Manriquez, , P. Jara, O. Wittke, G. Gonzalez, *Supramol. Chem*., 2001, **12**, 397-403; (b) T. L. Nguyen, F. W. Fowler, J. W. Lauher, *J. Am. Chem. Soc*., 2001, **123**, 11057-11064.
47. (a) V. Amendola, L. Fabbrizzi, L. Mosca, *Chem. Soc. Rev.*, 2010, **39**, 3889-3915; (b) N. Phukan, J. B. Baruah, *CrystEngComm*, 2016, **18**, 3877-3890; (c) N. Busschaert, C. Caltagirone, W. V. Rossom, P. A. Gale, *Chem. Rev*., 2015, **115**, 8038-8155.
48. M. Boiocchi, L. D. Boca, D. E. Gómez, L. Fabbrizzi, M. Licchelli, E. Monzani, *J. Am. Chem. Soc*., 2004, **126**, 16507-16514.
49. S. J. Brooks, P. R. Edwards, P. A. Gale, M. E. Light, *New J. Chem*., 2006, **30**, 65-70.
50. D. A. Jose, D. K. Kumar, B. Ganguly, A. Das, *Org. Lett*., 2004, **6**, 3445-3448.
51. S. Kondo, Y. Hiraoka, N. Kurumatani, Y. Yano, *Chem. Commun*., 2005, 1720-1722.
52. Z. Yin, Z. Li, A.Yu, J. He, J. -P. Cheng, *Tetrahedron Lett*., 2003, **44**, 6679-6681.
53. G. W. Bates, P. A. Gale, M. E. Light, *Chem. Commun*., 2007, 2121-2123.
54. V. K. Bhardwaj, M. S. Hundal, G. Hundal, *Tetrahedron*, 2009, **65**, 8556-8562.
55. P. Zhang, B.B. Shi, X.M. You, Y.M. Zhang, Q. Lin, H. Yao, T.B. Wei, *Tetrahedron*, 2014, **70**, 1889-1894.
56. S. Sen, M. Mukherjee, K. Chakrabarty, I. Hauli, S. K. Mukhopadhyay, P. Chattopadhyay, *Org. Biomol. Chem*., 2013, **11**, 1537-1544.
57. Y. Chang, S. Wu, C. H. Hu, C. Cho, M. X. Kao, A. T. Wu, *Inorg. Chim. Acta*, 2015, **432**, 25-31.
58. S. Liu, L. Zhang, P. Zhou, W. Zan, X. Yao, J. Yang, Y. Yang, *RSC Adv*., 2015, **5**, 19983-19988.
59. H. Khanmohammadi, K. Rezaeian, *RSC Adv*., 2014, **4**, 1032-1038.
60. M. Ajmal, S. Demirci, M. Siddiq, N. Aktasd, N. Sahiner, *New J. Chem*., 2016, **40**, 1485-1496.
61. J. Donohue, *J. Am. Chem. Soc*., 1956, **78**, 4172-4172.

62. (a) C. B. Aakeröy, A. S. Sinha, *RSC Adv.*, 2013, **3**, 8168-8171; (b) C. B. Aakeröy, A. S. Sinha, K. N. Epa, C. L. Spartz, J. Desper, *Chem. Commun*., 2012, **48**, 11289-11291.
63. (a) D. P. Jindal, R. Chattopadhaya, S. Guleira, R. Gupta, *Eur. J. Med. Chem*., 2003, **38**, 1025-1034; (b) D. B. Garcia, R. G. Brown, J. N. Delgado, *J. Pharmaceut. Sci*., 1980, **69**, 995-999; (c) I. H. Lone, K. Z. Khan, B. I. Fozdar, F. Hussain, *Steroids*, 2013, **78**, 945-950.
64. I. B. Wilson, S. Ginsburg, *Biochim. Biophys. Acta*, 1955, **18**, 168-170.
65. E. J Poziomek, B. E. J. Hackley, G. M Steinberg, *J. Org. Chem*., 1958, **23**, 714-717.
66. A. Luttringhaus, I. Hagedorn, *Arzneimittelforschung*, 1964, **14**, 1-5.
67. I. Hagedorn, W. H Gundel, K. Schoene, *Arzneimittelforschung*, 1969, **19**, 603-606.
68. A. Emmerson, *J. Antimicrob. Chemother*., 1988, **22**, 101-104.
69. (a) R. Graves, S. P. Weaver, *J. Am. Board Fam. Med*., 2008, **21**, 246-248; (b) L. -W. Zheng, Y. Li, D. Ge, B. -X. Zhao, Y. -R. Liu, H. -S. Lv, J. Ding, J. -Y. Miao, *Bioorg. Med. Chem. Lett*., 2010, **20**, 4766-4770.
70. V. Bertalosi, G. Gilli, A. Veronese, *Acta. Crystallogr. Sect. B*., 1982, **B38**, 502-511.
71. J. N. Lowa, L. M. N. B. F. Santos, C. F. R. A. C. Lima, P. Brandão, L. R. Gomes, *Eur. J. Chem.*, 2010, **1**, 61-66.
72. E. A. Burton, L. Brammer, F. C. Pigge, C. B. Aakeröy, D. S. Leinen, *New J. Chem*., 2003, **27**, 1084-1094.
73. A. S. Sinha, K. N. Epa, P. D. Chopade, M. M. Smith, J. Desper, C. B. Aakeröy, *Cryst. Growth Des*., 2013, **13**, 2687-2695.
74. C. B. Aakeroy, D. J. Salmon, M. M. Smith, J. Desper, *Cryst. Growth Des*., 2006, **6**, 1033-1042.
75. C. B. Aakeröy, S. Panikkattu, P. D. Chopade, J. Desper, *CrystEngComm*, 2013, **15**, 3125-3136.
76. C. B. Aakeroy, M. Fasulo, N. Schultheiss, J. Desper, C. Moore, *J. Am. Chem. Soc*., 2007, **129**, 13772-13773.
77. C. B. Aakeroy, K. N. Epa, S. Forbes, J. Desper, *CrystEngComm*, 2013, **15**, 5946-5949.
78. C. B. Aakeroy, J. Desper, M. M. Smith, *Chem. Commun*., 2007, 3936-3938.
79. C. B. Aakeroy, D. J. Salmon, M. M. Smith, J. Desper, *CrystEngComm*, 2009, **11**, 439-443.
80. C. B. Aakeroy, M. M. Smith, J. Desper, *CrystEngComm*, 2012, **14**, 71-74.

81. Z. Radić, T. Dale, Z. Kovarik, S. Berend, E. Garcia, L. Zhang, G. Amitai, C. Green, B. Radić, B. M. Duggan, D. Ajami, Jr. J. Rebek, P. Taylor, *Biochem. J.*, 2013, **450**, 231-242.
82. K. J. Wallace, J. Morey, V. M. Lynch, E. V. Anslyn, *New J. Chem.*, 2005, **29**, 1469-1474.
83. K. J. Wallace, R. I. Fagbemi, F. J. F. Andersen, J. Morey, V. M. Lynth, E. V. Anslyn, *Chem. Commun.*, 2006, 3886-3888.
84. (a) T. J. Dale, Jr. J. Rebek, *Angew. Chem., Int. Ed.*, 2009, **48**, 7850-7852; (b) I. S. K. Kerkines, I. D. Petsalakis, G. Theodorakopoulos, Jr. J. Rebek, *J. Phys. Chem. A*, 2011, **115**, 834-840.
85. I. Walton, M. Davis, L. Munro, V. J. Catalano, P. J. Cragg, M. T. Huggins, K. J. Wallace, *Org. Lett.*, 2012, **14**, 2686-2689.
86. H. Lee, H.-J. Kim, *Tetrahedron*, 2014, **70**, 2966-2970.
87. Y. J. Jang, O. G. Tsay, D. P. Murale, J. A. Jeong, A. Segev, D. G. Churchill, *Chem. Commun.*, 2014, **50**, 7531-7534.
88. Y.-C. Cai, C. Li, Q. -H. Song, *J. Mater. Chem. C*, 2017, **5**, 7337-7343.
89. O. G-. Beltrán, B. K. Cassels, N. Mena, M. T. Nuñez, O. Yañez, J. Caballero, *Tetrahedron Lett.*, 2014, **55**, 873-876.
90. B. K. Deshmukh, M. G. Awari, *Chem. Anal.*, 1987, **32**, 369-372.
91. A. E. Mahgoub, N. A. Darwish, M. M. Shoukry, *Analyst*, 1978, **103**, 879-883.
92. M. Wang, Y. Yuan, H. Wang, Z. Qin, *Analyst*, 2016, **141**, 832-835.
93. V. Bravo, S. Gil, A. M. Costero, M. N. Kneeteman, U. Llaosa, P. M. E. Mancini, L. E. Ochando, M. Parra, *Tetrahedron*, 2012, **68**, 4882-4887.
94. K.Chen, J. W. Bats, M. Schmittel, *Inorg. Chem.*, 2013, **52**, 12863-12865.
95. A. Balamurugan, H.-il Lee, *Sens. Actuators B*, 2015, **216**, 80-85.
96. J. Sivamani, V. Sadhasivam, A. Siva, *Sens. Actuators B*, 2017, **246**, 108-117.
97. W. Y. Lin, L. L. Long, B. B. Chen, W. Tan, *Chem. - Eur. J.*, 2009, **15**, 2305-2309.
98. X. H. Cheng, H. Z. Jia, T. Long, J. Feng, J. G. Qin and Z. Li, *Chem. Commun.*, 2011, **47**, 11978-11980.
99. G. F. Wu, F. Zeng, S. Z. Wu, *Anal. Methods*, 2013, **5**, 5589-5596.
100. S. -Y. Yu, C. -Y. Hsu, W. -C. Chen, L. -F. Wei, S. -P. Wu, *Sens. Actuators B*, 2014, **196**, 203-207.
101. J. Shi, Q. Li, X. Zhang, M. Peng, J. Qin, Z. Li, *Sens. Actuators B*, 2010, **145**, 583-587.

102. N. Zhao, Y. H. Wu, R. M. Wang, L. X. Shi, Z. N. Chen, *Analyst*, 2011, **136**, 2277-2282.

103. C. B. Rosen, D. J. Hansen, K. V. Gothelf, *Org. Biomol. Chem*., 2013, **11**, 7916-7922.

104. P. Khakhlary, J. B. Baruah, *RSC Adv.*, 2014, **4**, 64643-64648.

105. S. Borah, B. P. Das, G. Konwar, S. P. Mahanta, N. Gogoi, *RSC Adv.*, 2015, **5**, 75187-75194.

106. H. -S. Yu, W. -T. Liao, C. -Y. Chai, *J. Biomed. Sci*., 2006, **13**, 657-666.

107. A. S. M. Islam, R. Alam, A. Katarkar, K. Chaudhuri, M. Ali, *Analyst*, 2015, **140**, 2979-2983.

108. M. Dolai, R. Alam, A. Katarkar, K. Chaudhuri, M. Ali, *Analytical Sciences*, 2016, **32**, 1295-1300.

109. S. -Y. Na, J. -Y. Kim, H. -J. Kim, *Sens. Actuators B*, 2013, **188**, 1043-1047.

110. (a) P. Chaudhuri, *Coord. Chem. Rev*., 2003, **243**, 143-190; (b) V. Yu. Kukushkin, D. Tudela, A. J. L. Pombeiro, *Coord. Chem. Rev*., 1996, **156**, 333-362; (c) V. Yu. Kukushkin, A. J. L. Pombeiro, *Coord. Chem. Rev*., 1999, **181**, 147-175.

111. (a) L. Tschugaeff, *Chem. Ber*., 1905, **38**, 2520-2522.

112. P. A. Tasker, P. G. Plieger, L. C. West, *Compr. Coord. Chem. II*, 2004, **9**, 679-759.

113. (a) C. N. Verani, E. Bothe, D. Burdinski, T. Weyhermüller, U. Flörke, P, Chaudhuri, *Eur. J. Inorg. Chem*., 2001, **2001**, 2161-2169; (b) P. Chaudhuri, E. Rentschler, F. Birkelbach, C. Krebs, E. Bill, T. Weyhermüller, U. Flörke, *Eur. J. Inorg. Chem*., 2003, **2003**, 541-555.

114. (a) R. Inglis, C. J. Milios, L. F. Jones, S. Piligkos, E. K. Brechin, *Chem. Commun*., 2012, **48**, 181-190; (b) C. Yang, K. Cheng, S. Hung, M. Nakano, H. Tsai, *Polyhedron*, 2011, **30**, 3272-3278.

115. C. P. Raptopoulou, A. K. Boudalis, K. N. Lazarou, V. Psycharis, N. Panopoulos, M. Fardis, G. Diamantopoulos, J. -P. Tuchagues, A. Mari, G. Papavassiliou, *Polyhedron*, 2008, **27**, 3575-3586.

116. C. Yang, P. Feng, Y. Chen, Y. Tsai, G. Lee, H. Tsai, *Polyhedron*, 2011, **30**, 3265-3271.

117. C. Yang, S. Hung, G. Lee, M. Nakano, H. Tsai, *Inorg. Chem*., 2010, **49**, 7617-7619.

118. Q. -L. Wang, L. -H. Yu, D. -Z. Liao, S. -P. Yan, Z. -H. Jiang, P. Cheng, *Helve. Chim. Acta*, 2003, **86**, 2441-2451.

119. C. J. Milios, C. P. Raptopoulou, A. Terzis, F. Lloret, R. Vicente, S. P. Perlepes, A. Escuer, *Angew. Chem. Int. Ed*., 2004, **43**, 210-212.

120. K. Mason, I. A. Gass, F. J. White, G. S. Papaefstathiou, E. K. Brechin, P. A. Tasker, *Dalton Trans*., 2011, **40**, 2875-2881.

121. J. M. Frost, R. J. Stirling, S. Sanz, N. Vyas, G. S. Nichol, G. Rajaraman, E. K. Brechin, *Dalton Trans*., 2015, **44**, 10177-10187.

122. S. Sanz, J. M. Frost, M. B. Pitak, S. J. Coles, S. Piligkos, P. J. Lusby, E. K. Brechin, *Chem. Commun*., 2014, **50**, 3310-3312.

123. W. Sethi, S. Sanz, K. S. Pedersen, M. A. Sørensen, G. S. Nichol, G. Lorusso, M. Evangelisti, E. K. Brechin, S. Piligkos, *Dalton Trans*., 2015, **44**, 10315-10320.

124. H. Chen, C. -B. Ma, M. -Q. Hu, H. -M. Wen, C. -N. Chen, *Dalton Trans*., 2014, **43**, 16737-16744.

125. (a) I. A. Kühne, N. Magnani, V. Mereacre, W. Wernsdorfer, C. E. Anson, A. K. Powel, *Chem. Commun*., 2014, **50**, 1882-1885; (b) Y. Peng, V. Mereacre, C. E. Anson, A. K. Powell, *Dalton Trans*., 2017, **46**, 5337-5343.

126. (a) R. S. Forgan, J. E. Davidson, F. P. A. Fabbiani, S. G. Galbraith, D. K. Henderson, S. A. Moggach, S. Parsons, P. A. Tasker, F. J. White, *Dalton Trans*., 2010, **39**, 1763-1770; (b) R. S. Forgan, J. E. Davidson, S. G. Galbraith, D. K. Henderson, S. Parsons, P. A. Tasker, F. J. White, *Chem. Commun*., 2008, 4049-4051.

127. E. Houton, S. M. Taylor, C. C. Beedle, J. Cano, S. Piligkos, S. Hill, A. G. Ryder, E. K. Brechin, L. F. Jones, *Dalton Trans*., 2012, **41**, 8340-8347.

128. A. Perivolaris, A. M. Fidelli, R. Inglis, V. G. Kessler, A. M. Z. Slawin, E. K. Brechin, G. S. Papaefstathiou, *J. Coord. Chem*., 2014, **67**, 3972-3986.

129. (a) G. C. Vlahopoulou, T. C. Stamatatos, V. Psycharis, S. P. Perlepes, G. Christou, *Dalton Trans*., 2009, 3646-3649; (b) T. C. Stamatatos, G. Vlahopoulou, C. P. Raptopoulou, V. Psycharis, A. Escuer, G. Christou, S. P. Perlepes, *Eur. J. Inorg. Chem*., 2012, **2012**, 3121-3131.

130. G. Karotsis, C. Stoumpos, A. Collins, F. White, S. Parsons, A. M. Z. Slawin, G. S. Papaefstathiou, E. K. Brechin, *Dalton Trans*., 2009, 3388-3390.

131. E. S. Koumousi, M. J. Manos, C. Lampropoulos, A. J. Tasiopoulos, W. Wernsdorfer, G. Christou, T. C. Stamatatos, *Inorg.. Chem*., 2010, **49**, 3077-3079.

132. A. G. Smith, P. A. Tasker, D. J. White, *Coord. Chem. Rev*., 2003, **241**, 61-85.

133. R. Beckett, B. F. Hoskins, *J. Chem. Soc. Dalton Trans*. 1972, 291-295.

134. K. F. Konidaris, C. D. Polyzou, G. E. Kostakis, A. J. Tasiopoulos, O. Roubeau, S. J. Teat, E. Manessi-Zoupa, A. K. Powell, S. P. Perlepes, *Dalton Trans*., 2012, **41**, 2862-2865.

135. C. G. Efthymiou, L. Cunha-Silva, S. P. Perlepes, E. K. Brechin, R. Inglis, M. Evangelisti, C. Papatriantafyllopoulou, *Dalton Trans*., 2016, **45** ,17409-17419.

136. N. C. Anastasiadis, C. D. Polyzou, G. E. Kostakis, V. Bekiari, Y. Lan, S. P. Perlepes, K. F. Konidaris, A. K. Powell, *Dalton Trans*., 2015, **44**, 19791-19795.

137. S. Pramanik, S. Roy, T. Ghorui, S. Ganguly, K. Pramanik, *Dalton Trans*., 2014, **43**, 5317-5334.

138. (a) C. B. Aakeröy, A. M. Beatty, D. S. Leinen, *J. Am. Chem. Soc*., 1998, **120**, 7383-7384; (b) C. B. Aakeröy, A. M. Beatty, D. S. Leinen, K. P. Lorimer, *Chem. Commun*. 2000, 935-936.

139. C. B. Aakeröy, A. M. Beatty, D. S. Leinen, *Angew. Chem., Int. Ed*., 1999, **38**, 1815-1819.

140. L. Croitor, E. B. Coropceanu, A. E. Masunov, H. J. Rivera-Jacquez, A. V. Siminel, M. S. Fonari, *J. Phys. Chem. C*, 2014, **118**, 9217-9227.

141. L. Croitor, E. B. Coropceanu, A. E. Masunov, H. J. Rivera-Jacquez, A. V. Siminel, V. I. Zelentsov, T. Ya. Datsko, M. S. Fonari, *Cryst. Growth Des*., 2014, **14**, 3935-3948.

142. L. Croitor, D. Z. Grabco, E. B. Coropceanu, C. Pyrtsac, M. S. Fonari, *CrystEngComm*, 2015, **17**, 2450-2458.

143. (a) A. Escuer, B.Cordero, M. Font-Bardia, T. Calvet, O. Roubeau, S. J. Teat, S. Fedi, F. F. de Biani, *Dalton Trans*., 2010, **39**, 4817-4825; (b) A. Escuer, J. Esteban, O. Roubeau, *Inorg. Chem*., 2011, **50**, 8893-8901; (c) C. Lampropoulos, T. C. Stamatatos, K. A. Abboud, G. Christou, *Inorg. Chem*., 2009, **48**, 429-431.

144. D. I. Alexandropoulos, K. M. Poole, L. Cunha-Silva, J. A. Sheikh, W. Wernsdorfer, G. Christou, T. C. Stamatatos, *Chem. Commun.***,** 2017, **53**, 4266-4269.

145. D. I. Alexandropoulos, E. C. Mazarakioti, S. A. Corrales, J. T. Bryant, L. V. Gasparov, C. Lampropoulos, T. C. Stamatatos, *Inorg. Chem. Comm*., 2017, **78**, 13-16.

146. E. S. Koumousi, M. Zampakou, C. P. Raptopoulou, V. Psycharis, C. M. Beavers, S.J. Teat, G. Psomas, T. C. Stamatatos, *Inorg. Chem*., 2012, **51**, 7699-7710.

147. H. -M. Dong, Y. Li, Z. -Y. Liu, E. -C. Yang, X. -J. Zhao, *Dalton Trans*., 2016, **45**, 11876-11882.

148. (a) A. B. Canaj, L. E. Nodaraki, A. Philippidis, D. I. Tzimopoulos, E. Fotopoulou, M. Siczek, T. Lis and C. J. Milios, *RSC Adv*., 2013, **3**, 13214-13224; (b) A. B. Canaj, L. E. Nodaraki, K. Slepokura, M. Siczek, D. I. Tzimopoulos, T. Lis, C. J. Milios, *RSC Adv*., 2014, **4**, 23068-23077.

149. S. Hossain, S. Das, A. Chakraborty, F. Lloret, J. Cano, E. Pardob, V. Chandrasekhar, *Dalton Trans*., 2014, **43**, 10164-10174.

150. H. Durmus, H. Safak, H. Z. Akbas, G. Ahmetli, *J. Appl. Poly. Sc*., 2011, **120**, 1490-1495.

151. R. Sun, Y. Li, M. Lu, L. Xiong and Q. Wang, *Bioorg. Med. Chem. Lett*., 2010, **20**, 4693-4699.

152. S. Grigalevicius, S. Chierici, O. Renaudet, R. Lo-Man, E. Deriaud, C. Leclerc, P. Dumy, *Bioconjugate Chem*., 2005, **16**, 1149-1159.

153. J. Reedijk, *Inorg. Chim. Acta*, 1992, **200**, 873-881.

154. T. W. Hambley, E. C. H. Ling, S. O'Mara, M. J. Mckeage and P. Russell, *J. Biol. Inorg. Chem*., 2000, **5**, 675-681.

155. N. Saglam, A. Colak, K. Serbest, S. Duelger, S. Guener, S. Karaboecek, A. O. Belduez, *Biometals*, 2002, **15**, 357-365.

156. K. Karami, Z. M. Lighvan, A. M. Alizadeh, M. P-. Shirani, T. Khayamian, J. Lipkowsk, *RSCAdv*., 2016, **6**, 78424-78435.

157. J. -Y. Song, Y. Liu, H. -Y. Zhao, H. -T. Han, Z. -F. Li, W. -H. Guo, W. -Y. Chu, Z. -Z. Sun, *New J.Chem*., 2017, **41**, 12288-12292.

158. B. -M. Kukovec, M. Malik, I. Kodrin, C. B. Aakeroy, M. Dakovic, *Cryst. Growth Des*., 2016, **16**, 7308-7317.

159. (a) J. W. Lee, E. A. Kim, Y. J. Kim, Y. -A. Lee, Y. Pak, O. -S. Jung, *Inorg. Chem*., 2005, **44**, 3151-3155; (b) O. -S. Jung, Y. J. Kim, Y. -A. Lee, K. -M. Park, S. S. Lee, *Inorg. Chem*., 2003, **42**, 844-850.

160. V. J. Argyle, L. M. Woods, M. Roxburgh, L. R. Hanton, *CrystEngComm*, 2013, **15**, 120-134.

161. (a) D. Masih, V. Chernikova, O. Shekhah, M. Eddaoudi, O. F. Mohammed, *ACS Appl. Mater. Interfaces*, 2018, **10**, 11399-11405; (b) A. Karmakar, P. Samanta, A. V. Desai, S. K. Ghosh, *Acc. Chem. Res.*, 2017, **50**, 2457-2469; (c) J. -P. Ma, Y. Yu, Y. -B. Dong, *Chem. Commun.*, 2012, **48**, 2946-2948; (d) B. Manna, A. V. Desai, S. K. Ghosh, *Dalton Trans*., 2016, **45**, 4060-4072.

Chapter 2

Part A: Anion Assisted Supramolecular Assemblies of Oxime Derivatives and Recognition of Fluoride ion

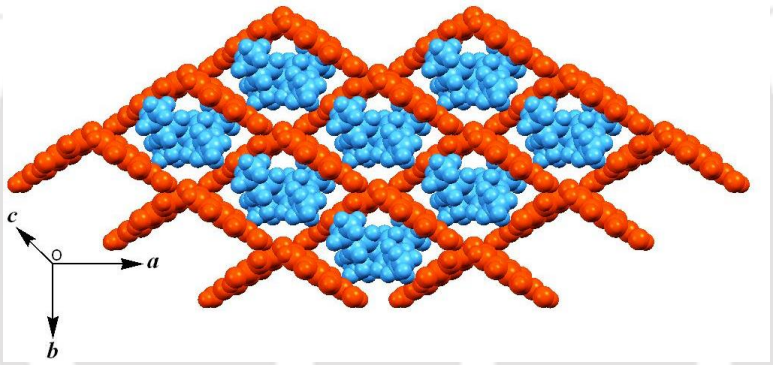

CrystEngComm, 2015, **17**, 2301-2309.

2.1.1: Introduction

Anions regulate various processes in biological systems, bioinorganic or bioorganic chemistry and mineralogy.[1] Anions are highly polarizable hence soft in nature and have higher ionic radii in comparison to cations with identical electrons count. Anions are also involved in supramolecular assemblies in a variety of ways. They are part of a neutral molecule contributing to various hydrogen bonded schemes. In addition to conventional hydrogen bonds, anions provide avenues for anion-π interactions, C-H···anion interactions, anion-anion interactions. Each of these interactions contributes to overall stability of a non-covalent self-assembly. Anions also provide avenues for electrostatically assisted hydrogen bonds which have higher bond strength. The electrostatically guided hydrogen bonded self-assemblies have extra stability and they are subject to extensive research. On the other hand, supramolecular assemblies formed due to complementary hydrogen bonds provide selectivity in binding of a receptor molecule. The directional behaviours of weak interactions play a major role in deciding such assemblies. As the anions are associated with different charge or size or shape and it depends on the number or location of binding sites available in a receptor to form anion-receptor assembly. Anion-receptor binding is very selective in nature. As an illustration, few anions and their complementing receptors[2] are shown in **Fig. 2.1.1**.

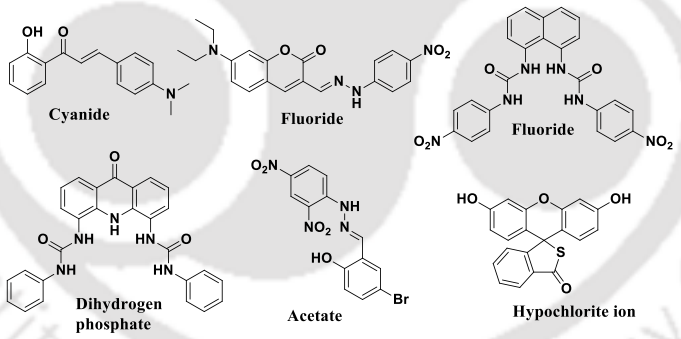

Figure 2.1.1: Some neutral receptors with their complementing anions.

There are also alternative ways to look at the supramolecular aspects of anions. A specific anion is basically a counter ion of the corresponding acid or metal ions. Anions participate in weak interaction scheme of neutral or partially protonated receptors. Alternatively anions may also have different extent of protonation while participating as a component to form supramolecular assembly. Accordingly, a mono-protonated anion differs from di or tri-protonated anions or the neutral acid. For example, phosphoric acid remains as either mono, di or tri protonated species while interacting with receptors in supramolecular chemistry. The anions can transform to form cationic or anionic species such as H_2F^+ or HF_2^-, which have distinct ways to form hydrogen bonds with a receptor that differ from HF or F^-.

The anions form hydrated or solvated species to participate in formation of hydrogen bonds to form different supramolecular assemblies.[3] Anions may act as base to form self-assemblies; for example fluoride ion deprotonates or forms strong hydrogen bond with receptors to provide fluoride assisted assemblies.[4] Anions may also be in the form of metal complex; in which central metal ion has definite role to guide directional properties of the participating self-assemblies.[5] Based on these processes, specific interactions with the anion takes place to show recognition and these recognition processes are reflected in signal transductions. Fluoride ion is capable of deprotonating hydroxyl groups and such deprotonation of a hydroxyl group directly attached to a chromophore changes colour.[6] It is also well known fact that the hydrogen bond of a receptor with tetrabutylammonium fluoride (TBAF) also causes change in colour and such changes are caused specifically by TBAF among a series of tetrabutylammonium salts.[7] It may be noted that there are large numbers of receptor molecules show characteristic changes in absorption and emission properties upon interactions with fluoride ions and some of which are fluoride specific. But some of them do not differentiate fluoride ion from basic anions such as hydroxide and acetate. This is primarily due to the mechanism of interactions of fluoride ions with a receptor. A hydrogen bonded receptor without getting protonated and participating only in hydrogen bonding is suitable for specific detection of fluoride ion. Thus, understanding of self-assemblies formed by interactions of a receptor with fluoride ion is important. Since, tetrabutylammonium cation bearing fluoride ion is easily dissolve in organic solvents and are well known to form stable adducts, they are of general interest.

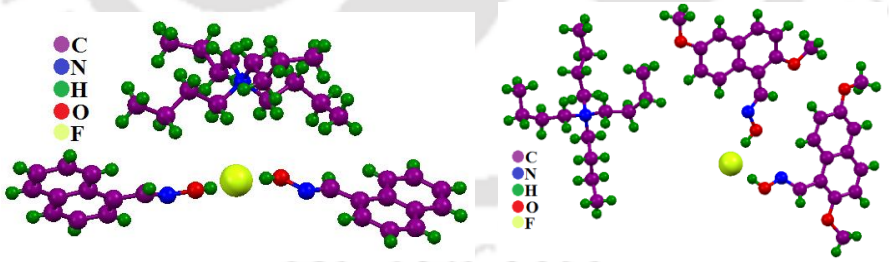

(a) (b)

Figure 2.1.2: 2:1 Cocrystals of (a) 1-naphthaldoximes and (b) 2,6-dimethoxy-1 naphthaldehyde with tetrabutylammonium fluoride (TBAF).

Gothelf and his co-workers reported some simple oxime based sensor for selective detection of fluoride ion in protic and aprotic solvent.[7] They determined fluoride assisted assemblies of oxime derivatives and typical examples are shown in **Fig. 2.1.2**. The 2:1 cocrystals formed between 1-naphthaldoximes or 2,6-dimethoxy-1-naphthaldehyde oxime derivatives with tetrabutylammonium fluoride (TBAF) have O-H···F interactions as the principal hydrogen

bond interactions. Furthermore, the fluoride ions interacting with phenolic or oxime compounds are well known, but there was no study relating to fluoride assisted assemblies of hydroxyaromatic aldoximes. We felt that the understanding of self-assemblies of hydroxyaroamtic aldoximes would enable us to understand oxime-oxime and oxime-phenol interactions as these two functional groups are weak acids and would compete in forming hydrogen bonds among them. Such molecules also would provide chromophoric and fluorophoric sites for signal modulation by interacting with anions or neutral molecules. With such anticipations, structures and optical properties associated with different supramolecular assemblies generated by oximes **2.1.1-2.1.3** (**Fig. 2.1.3a**) and respective assemblies generated by reacting with tetrabutylammonium fluoride (TBAF) are studied.

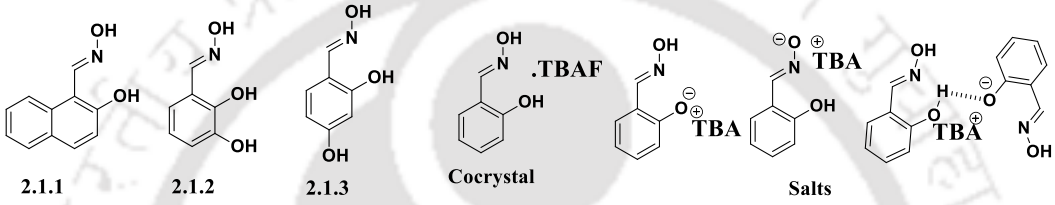

Figure 2.1.3: (a) Structures of oxime derivatives **2.1.1-2.1.3** and (b) Different form of cocrystals or salts of 2-hydroxyphenylaldoxime with TBAF that may be expected from interactions of **2.1.1-2.1.3** with TBAF.

There are different ways to form salts or cocrystals of 2-hydroxybenzaldoxime by interacting with a tetrabutylammonium fluoride (TBAF) as shown in **Fig. 2.1.3b**. Number of such possibilities increase when more hydroxyl-groups are introduced to the aromatic ring. There is also additional possibility to form fluoride assisted assemblies involving HF_2^-.[8] This chapter deals with self-assemblies of hydroxyaromatic aldoximes **2.1.1-2.1.3** to ascertain the role of hydroxyl-groups on aromatic oxime derivatives and understand the ability of these oxime derivatives for recognition of fluoride ion or to form self-assemblies assisted by fluoride ions.

2.1.2: Crystal structure of oxime derivatives 2.1.1-2.1.3

The crystal structure of oxime **2.1.1** was reported earlier.[9] The self-assembly of oxime **2.1.1** is comprised of $R^2_2(8)$ type homosynthons formed through aldoxime C-H···O interactions as illustrated in **Fig. 2.1.4a**. But the structure of oxime **2.1.2** or **2.1.3** has shown that it has $R^4_4(10)$ O-$H_{aldoxime}$....O-$H_{hydroxy}$ heterosynthons similar to the heterosynthons found in the structure of the 2-hydroxyphenylaldoxime.[10] In the self-assembly of the oximes shows

intramolecular hydrogen bond of O-H of the 2-hydroxy group with the nitrogen atom of the oxime as illustrated in **Fig. 2.1.4b**.

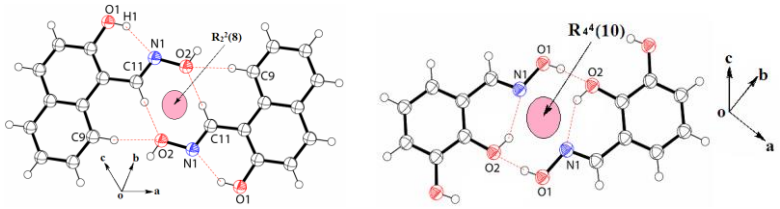

(a) (b)

Figure 2.1.4: The dimeric assemblies of the oximes (a) **2.1.1** and (b) **2.1.2**.

Thus assemblies of these compounds differ in the type of interactions present within their respective self-assemblies. The dimeric self-assembly of the **2.1.2** has two O-H···O interactions to stabilise a ten-membered ring. From the stability point of view, the former has lower stability for obvious reason of the hierarchy of the bond strength between the O-H···O interaction over a C-H···O interaction.

2.1.3: Adducts of oximes 2.1.1-2.1.3 with tetrabutylammonium fluoride

Tetrabutylammonium fluoride (TBAF) forms cocrystals **2.1.1**.TBAF (**2.1.4**) with 2-hydroxynaphthaldoxime **(2.1.1**) in 1:1 molar ratio between host and coformer, on the other hand, 2,3-dihydroxyphenylaldoxime (**2.1.2**) forms cocrystal $(\mathbf{2.1.2})_2$.TBAF (**2.1.5**) with TBAF which is in 2:1 ratio. Similar reaction between 2,4-dihydroxyphenylaldoxime (**2.1.3**) and TBAF causes deprotonation of one phenolic hydroxy group of **2.1.3** to form salt **2.1.6** (**Fig. 2.1.5**). Structures of cocrystals **2.1.4-2.1.5** and salt **2.1.6** are determined by single crystal X-ray diffraction and they are also characterized by other spectroscopic techniques. The difference in their molecular compositions are reflected as cocrystal **2.1.4** has 1:1 and the other has 2:1 oxime and TBAF molar ratio, which is evident in their elemental analysis and integration of protons in ^{1}H-NMR spectra.

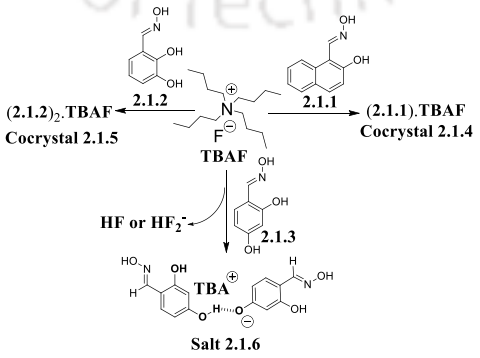

Figure 2.1.5: Cocrystals of oximes **2.1.1-2.1.2** with TBAF and tetrabutylammonium salt of oxime **2.1.3.**

Whereas, the salt **2.1.6** has 2:1 molar ratio between oxime molecules and TBAF. Each cocrystal or salt and oxime derivative is characterized by X-ray diffraction as well as FT-IR spectroscopic technique. The FT-IR spectra of oxime derivatives have characteristic peak at 1620-1632 cm^{-1} for C=N stretching, but on crystallization with TBAF these peaks are shifted to 1614-1624 cm^{-1}. Similar -OH stretching of oxime functional group show characteristic peak at 3313-3454 cm^{-1} which were not found in the crystalline products with TBAF. This peak is shifted or disappearance because formation of strong hydrogen bond between oxime -OH and fluoride anion.

2.1.4: Anion assisted supramolecular assemblies of oximes 2.1.1-2.1.3

Solid state self-assembly of cocrystal **2.1.4** has oxime molecules arranged in chain-like structures. The chain-like structures are formed along *c*-crystallographic axis by hydrogen bonds bridging oxime molecules by fluoride ions. Each fluoride ion is connected to two oxime molecules from two opposite directions. One side of fluoride ion is connected through O-H···F interaction involving OH group of oxime functionality. Other side has an O-H···F interaction with phenolic hydroxy group and a C-H···F interaction of a hydrogen atom at *ortho*-position to the hydroxy group to form a chelate-like motif. Such interactions inhibit the *ortho*-hydroxy group to form conventional intramolecular hydrogen bond. Carbon-fluorine covalent bonds have role in oximes to form cocrystals.[11] In the present case, we observed a weak C-H···F interaction and a O-H···F interactions that contribute to form hydrogen bonded cyclic motif. In this particular case, such cyclic motif is more favorable than formation of an intramolecular cyclic hydrogen bonded motif which was found in ortho-hydroxyaromatic oxime derivatives.[9,10] Due to the interaction of the phenolic hydroxyl O-H with fluoride, the hydrogen atom of this group projects outwards from the oxime group unfavorable for intramolecular hydrogen bond.

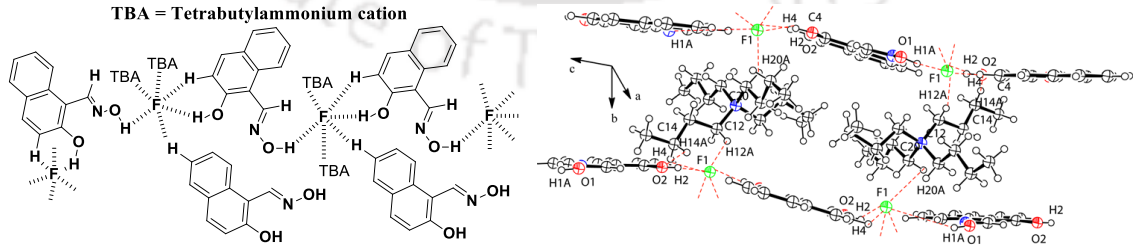

(a) (b)

Figure 2.1.6: (a) Representation of chain formed through fluoride ions interacting with O-H and C-H bond at one end and through OH of oxime at other end and (b) Chain-like arrangement of oximes in structure of cocrystal **2.1.4** holding tetrabutylammonium cations in between layers (30% thermal ellipsoids in ORTEP diagram).

Different weak interactions contributing to form the chain-like structures are shown in **Fig. 2.1.6a**. Although oximes can self-assemble to form various catemers, strong participation of fluoride ions in hydrogen bond do not allow formation of any of the conventional catemers.[12] Hence, it is clear that the fluoride ions does not allow formation of oxime-oxime or oxime-phenol interactions. In the crystal lattice of cocrystal **2.1.4**, tetrabutylammonium ions are held between two such chains, which are stabilized by C-H···O and C-H···F interactions. Some of the important hydrogen bond parameters are listed in **Table 2.1.1**. Fluoride ion of cocrystal **2.1.4** (**Fig. 2.1.6b**) also interacts with two tetrabutylammonium cations through C-H···F interactions. Thus, fluoride ions make a conjugated system for proton transfer by bridging two different types of hydroxy groups at two ends of oxime molecules. Structure has crystallographically disordered tetrabutylammonium cation, which could not be resolved.

Table 2.1.1: Prominent hydrogen bond parameters of cocrystals **2.1.4**, **2.15** and salt **2.1.6.**

Cocrystals/salt	D-H···A	d_{D-H}(Å)	$d_{H\cdots A}$ (Å)	$d_{D\cdots A}$(Å)	∠D−H···A (°)
2.1.4	O(1)-H(1A)···F(1) [-x, 1/2+y, 1/2-z]	0.82	1.74	2.555	173
	C(8)-H(8)···F(1) [1-x, 1/2 +y,1/2 -z]	0.93	2.59	3.468	158
	C(20)-H(20A)···F(1) [x, 1/2 -y,1/2 +z]	0.97	2.45	3.276	142
	C(14)-H(14A)···O(2) [x, y, z]	0.97	2.70	3.529	143
2.1.5	O(3)-H(3A)···F(1) [x, -1+y, -1+z]	0.82	1.79	2.579	161
	O(1)-H(1)···F(1) [x, y, -1+z]	0.82	1.74	2.556	171
	O(6)-H(6)···F(1) [1+x, y, z]	0.82	1.77	2.576	165
	C(30)-H(30A)···O(1) [x, y, z]	0.97	2.63	3.599	174
2.1.6	O(3)-H(3A)···O(1) [1/2+x, 1/2+ y, z]	0.82	1.90	2.679	169

Cocrystal **2.1.5** is formed between oxime **2.1.2** and TBAF is in 2:1 molar ratio. Composition of this cocrystal is also established from integration of proton signals in ^{1}H-NMR spectra. The ^{1}H-NMR spectra of cocrystal **2.1.5**, shows clearly discernible signals from tetrabutylammonium cations in aliphatic region due to two sets of methylene proton and methyl groups with chemical shifts at 3.5-0.5 ppm; integration of this set of signals correspond to one TBAF molecule with respect to two molecules of oxime **2.1.2**. The ^{1}H-NMR spectra of the cocrystal is suggestive of a stable self-assembly in solution. Assembling process in the solid state in this case is also guided by strong O-H···F interactions, which results 4+4 cyclic units between four molecules of oximes with four fluoride ions (**Fig. 2.1.7a**). Fluoride ions act as central point to grow such cyclic structures to make 2D rectangle like grid arrangements. Lengths of the grid-like structure are shown in inset of **Fig. 2.1.7b**. Each cyclic unit holds tetrabutylammonium cations within them. Two hydroxyl groups and two oxime groups from four independent oxime **2.1.2** molecules are involved in O-H···F interactions to contribute to coordination environment of fluoride ions in cocrystal **2.1.5** (**Fig. 2.1.7b**). Fluoride ions adopt tetrahedral hydrogen bond environment around them.

Fluoride ions act as central point to grow such cyclic structures to make grid-like arrangements, they assist in encapsulation of tetrabutylammonium cations within the grids through weak C-H···O interactions. Thus, this structure provides an example of a fluoride assisted assembly to encapsulate tetrabutylammonium cations. Each oxime **2.1.2** molecule possesses intramolecular hydrogen bond between nitrogen atom of oxime and hydroxy-group present at *ortho*-position. Thus, presence and absence of intramolecular hydrogen bond between hydroxy group and oxime nitrogen is a prime difference in structures of cocrystals **2.1.4** and **2.1.5**. It may be noted that hydroxy group of oxime interacts with fluoride ions[7] but we have dealt with hydroxy-aromatic oximes, of which phenolic hydroxy groups play important roles to guide their packing patterns. Hence such a factor makes much different packing from a packing present in simple oximes. In both cocrystals **2.1.4** and **2.1.5** participation of hydroxy group of phenolic part in construction hydrogen bond bridges with fluoride ions are observed.

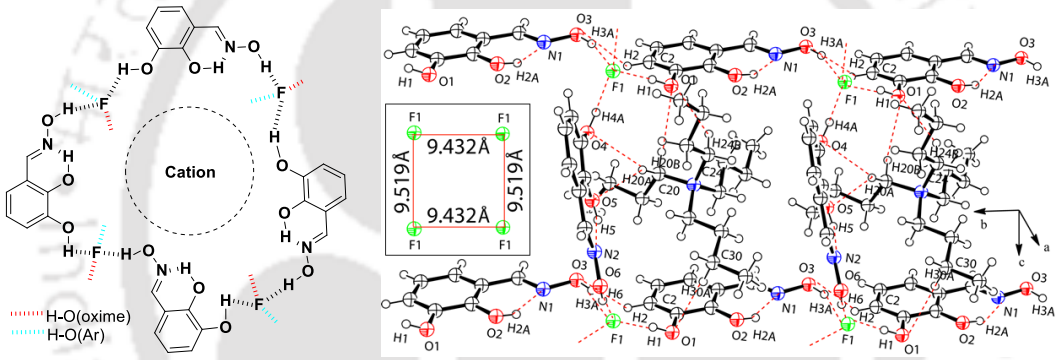

(a) (b)

Figure 2.1.7: (a) Representation of fluoride assisted cyclic motif in cocrystal **2.1.5** and (b) Encapsulation of tetrabutylammonium cations in fluoride assisted assembly of cocrystal **2.1.5** (30% thermal ellipsoids in ORTEP diagram). In the inset lengths of grid-like structure.

The comparison between the structural aspects of these two cocrystals **2.1.4** and **2.1.5** shows that one has layered structure encapsulating cations whereas the other has grid-like structure encapsulating cations. In the former case, intermolecular hydrogen bonds are absent but it is present in the latter case. Due to additional hydroxyl group with the oxime, oxime-fluoride and oxime-phenol interactions are observed in the latter case.

Reaction of oxime **2.1.3** with TBAF resulted in abstraction of a proton from a hydroxy group at *para*-position of the ring with respect to oxime group to form a salt **2.1.6**, which crystallized as a cocrystal of oxime **2.1.3.** Structure of the salt **2.1.6** determined by single crystal X-ray diffraction is comprised of self-assemblies of V-shaped dimeric anionic motifs comprised of a mono-deprotonated oxime molecules and a neutral oxime molecule.

Such dimeric motifs form chain-like structures and chains interact among themselves to make voids to encapsulate tetrabutylammonium cations as illustrated in **Fig. 2.1.8a**. In the case of salt **2.1.6**, hydroxyl group present at *para*-position of phenyl ring with respect to the oxime group is deprotonated. It is involved in intramolecular hydrogen bonds to form assemblies. This allows formation of intramolecular hydrogen bonds between hydroxyl groups present at *ortho*-position with nitrogen atom of oxime. 2D-rectangular grid-like structure having TBA cations within grids is shown in **Fig. 2.1.8b**. Deprotonated oxime **2.1.3** has strong hydrogen bonds between phenolic units through O-H···O hydrogen bonds having electrostatic property (**Fig. 2.1.8b**). Due to this a short donor-acceptor bond distance between O1-H···O1 of 2.47Å is observed. Once such assemblies are connected to each other through hydrogen bonds (O3-H···O1) of oxime group of another molecule, rectangular grid-like structures are formed. Alternatively, structures of such grids can be explained as combination of linear chains in two different directions to form self-assemblies of anions and neutral oxime molecules.

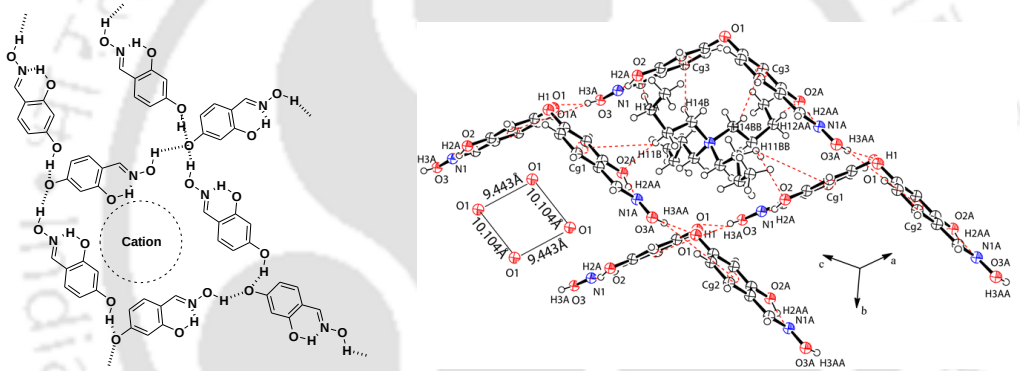

(a) (b)

Figure 2.1.8: (a) Diagram to show assemblies of dimeric motif of monoanion and neutral oxime **2.1.3** and (b) Encapsulation of tetrabutylammonium cation in anionic assembly of oximes in salt **2.1.6** (30% thermal ellipsoids). In the inset lengths of grid-like structure.

Each chain are perpendicular to each other is linked by hydrogen bond, forming grid-like structure. There is difference between grid-like structure in cocrystal **2.1.5** and in salt **2.1.6**; in the former case electrostatic interactions of fluoride ions are involved which is absent in the latter case. The two dihydroxyaromatic aldoximes retain intramolecular hydrogen bonds between oxime and phenol. The fluoride assisted assembly of the self-assembly of cocrystal **2.1.5** is based on oxime-fluoride and phenol-fluoride interactions whereas the salt **2.1.6** is guided by phenolate-phenol interactions, which is exceptional. Fluoride ions are special due to their small size and ability to act as a base.[13] Deprotonation of phenolic compounds by fluoride ions are well established[14] but so far self-assemblies of anionic species generated by fluoride ion without being a part is not reported.

Self-assembly of cocrystal of a salt formed by assembly of mono-deprotonated oxime **2.1.3** with a neutral molecule of **2.1.3** generated by fluoride ion without being a part of the assembly is exceptional. For hydrogen bonds and short contacts parameters of cocrystals **2.1.4**, **2.1.5** and salt **2.1.6** please see **Table 2.1.1** and page 227 of appendix.

2.1.5: UV-vis spectroscopic studies of oximes 2.1.1-2.1.3 with fluoride ion

Fluoride ions are very useful to deprotonate hydrogen atom from various groups to cause signal transduction. Since in solid state studies different types of self-assemblies of oximes are observed, one can anticipate hydrogen bonded assembly in solution to distinguish fluoride ions from other anions. Thus a solution study is taken up and it is found that oximes **2.1.1-2.1.3** interact with tetrabutylammonium fluoride (TBAF), which selectively changes colour of the solutions of these oximes. The oximes **2.1.1-2.1.3** has absorption at 351 nm, 269 nm and 274 nm respectively. Upon addition of different tetrabutylammonium salts other than tetrabuylammonium fluoride to these solutions there is no change in these absorptions. Thus, tetrabutylammoinum salts such as chloride, bromide, iodide, acetate, nitrate, bisulphate, biphosphate do not change the absorption spectra of oxime derivatives **2.1.1-2.1.3**.

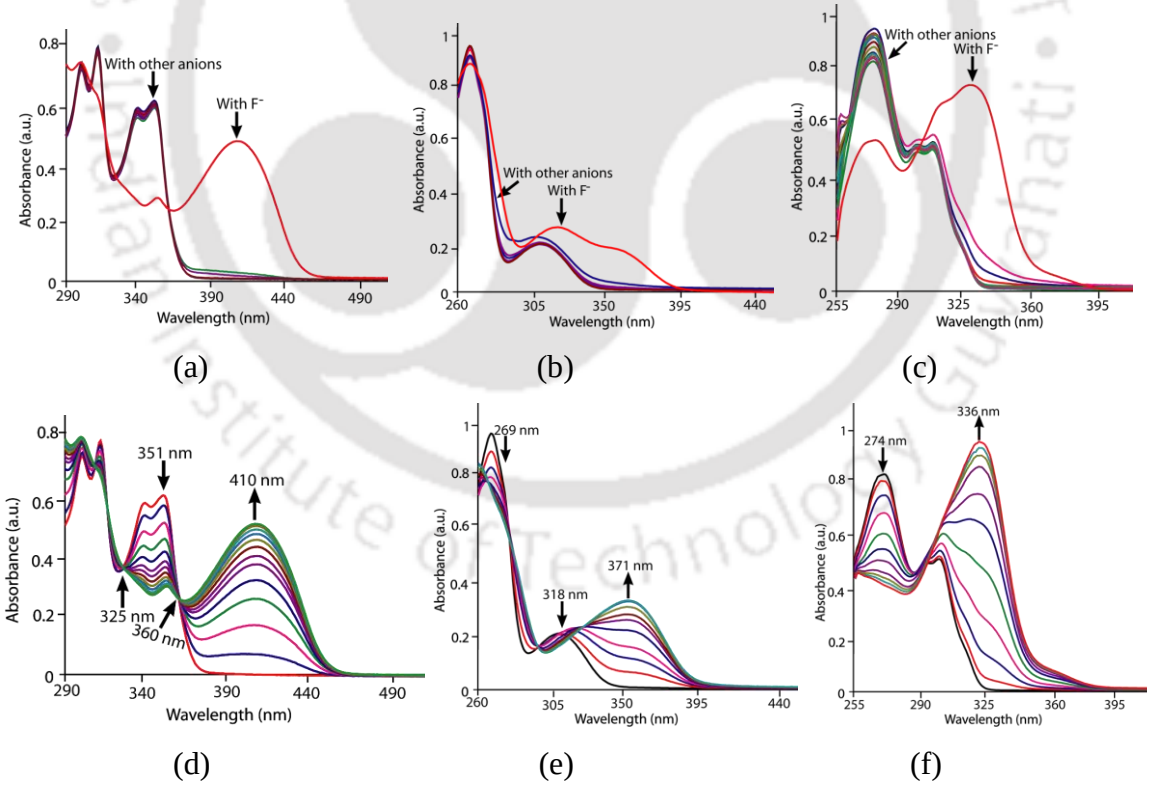

Figure 2.1.9: UV-vis spectra of oxime (a) **2.1.1,** (b) **2.1.2,** (c) **2.1.3** (10^{-5}M) with different tetrabutylammonium salts (100 µl of 10^{-5} M) showing fluoride salt only can cause changes in absorptions. UV-vis spectroscopic titration of oxime (d) **2.1.1,** (e) **2.1.2,** (f) **2.1.3** (10^{-5} M) with TBAF (0µl-100µl of 10^{-5} M) in dimethyl suphoxide (DMSO).

But independent experiments carried out by adding TBAF to compounds **2.1.1**-**2.1.3** show new absorption peak at 410 nm for oxime **2.1.1**, shoulder around 371 nm for oxime **2.1.2** and 336 nm for oxime **2.1.3** respectively (**Fig. 2.1.9a-c**). Changes in UV-vis absorption of oxime derivatives **2.1.1**-**2.1.3** are observed in corresponding titration carried out with each compound by adding solution of TBAF. Increase in concentration of TBAF reduces intensity of absorption peak at shorter wavelength while intensity of new absorption at longer wavelength increases which are shown in **Fig. 2.1.9d-f**. Shifts in absorbance to longer wavelength are due to formation of stable complex with TBAF through weak interactions, while it shows change in colour visibly. Thus, oxime derivatives **2.1.1**-**2.1.3** is suitable for detection of fluoride. Fluoride ions cause deprotonation of phenols[14] and related compounds which helps to detect fluoride ions. On the other hand, there are also examples of hydroxy-naphthalenes[15] and hydroxy-anthraquinones[16] which show colour change on interaction with fluoride ions without getting deprotonated. Specific deprotonation by fluoride ions of intramolecular hydrogen bonded naphthol derivative was demonstrated earlier.[17] Metal complex of receptors containing several hydroxyl groups show O-H···F interactions[18] and selective colour changes takes place while cocrystals of naphthylaldoxime with fluoride salt are formed.[7] It was earlier suggested[19] that adduct formation of a fluoride ion versus deprotonation of acidic compound by fluoride ions are to be carefully distinguished. In fact this is true in the present cases and differences in shift of wavelengths in these cases stems from different types of assemblies. An assembly containing no fluoride ion and the neutral assembly containing fluoride ions make a wide difference. Accordingly, absorption peak of **2.1.3** on interaction of fluoride ions appear at 336 nm which is much lower than absorptions shown by oximes **2.1.1** and **2.1.2** at 410 nm and 371 nm respectively. Furthermore, the peak observed at 336 nm is identical to absorption maximum shown by a solution of the salt **2.1.6**, hence it can be easily suggested that the peak arises from phenoxide ion. This example suggests that fluoride ion can act as substrate to generate new coloured assemblies without its participation in the assembly which is generally not observed in sensors for fluoride ions.[20] Selective colour change caused by fluoride ions allows easy detection of fluoride by dipping a filter paper that is pre-soaked with any of the oxime among **2.1.1**-**2.1.3** in a solution of fluoride ions in DMSO. A series of experiments by independently dipping filter paper in different solutions are depicted in **Fig. 2.1.10a**. It is clear that aqueous solution containing fluoride ions only develops yellow colour on these papers. Thus, these oxime derivatives **2.1.1**-**2.1.3** have practical utility to test for presence of fluoride ion in water. When a solution of TBAF is added to a solution of oxime **2.1.1** in DMSO, it shows fluorescence emission at

468 nm on excitation at 320 nm, similar peaks are not observed from solution of **2.1.1** containing other tetrabutylammonium salts.

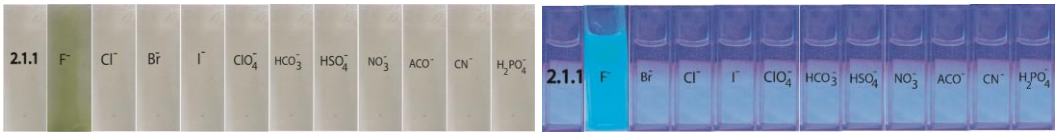

(a) (b)

Figure 2.1.10: (a) Colour of filter papers pre-soaked with oxime **2.1.1** followed by soaking in solutions of different tetrabutylammonium salts and (a) Fluorescence of oxime 2.**1.1** in DMSO in presence of different tetrabutylammonium salts on exposure to UV-light at 254 nm (For each tetrabutylammonium salt, respective anions are shown in figures).

On the basis of this observation, we have developed a technique to visually detect fluoride ions by exposing solutions containing different anions with **2.1.1** by exposing them to UV-light. Solution containing fluoride ions with oxime **2.1.1**, exclusively shows a blue fluorescence as illustrated in **Fig. 2.1.10b**. Thus, oxime **2.1.1** could be used as a fluorescence sensor for fluoride ions. Even though oximes **2.1.2** or **2.1.3** are useful in detection of fluoride ions by UV-vis spectroscopy, these two oximes are weakly fluorescent, hence are not suitable to detect fluoride ions by fluorescence technique. However, tetrabutylammonium hydroxide and acetate shows similar changes (**Fig. 2.1.17** and **2.1.8**, experimental section) to that of fluoride ions in the case of **2.1.1** and **2.1.2** but with a lower intensity at 410 nm and 371 nm at comparable concentrations. However, no noticeable change was found in UV-vis spectra of oxime **2.1.3** with tetrabutylammonium hydroxide and acetate.

2.1.6: Conclusions

This study clearly shows that the ability of fluoride ion to deprotonate as well as form hydrogen bond can be independently explored to construct self-assemblies of hydroxyaromatic aldoximes with fluoride ion. The retention and cleavage of intramolecular hydrogen bonded motifs in self-assemblies are guided by the additional hydroxyl group other than the one located at the *ortho* position of these three hydroxyaromatic aldoximes. The fluoride-hydroxyl as well as fluoride-oxime hydrogen bonds found in one of the dihydroxyaromatic aldoxime suggests that competition between intramolecular hydrogen bonds and oxime-phenol interactions exists. These assemblies carry specific optical properties and enable to provide information to detect fluoride ions visually and distinguish it from other anions. Assembly with or without fluoride ion provided layer or grid like structures which encapsulate cations in electrostatically guided hydrogen bonded self-assemblies.

2.1.7: Experimental section

Synthesis and characterization of oxime derivatives 2.1.1-2.1.3 and their cocrystals or salt:

Oxime derivatives **2.1.1-2.1.3** were prepared from the respective hydroxy-aromatic aldehyde by reacting them with hydroxylamine hydrochloride in presence of pyridine. Typical procedure for synthesis of 2-hydroxynapthaldoxime (**2.1.1**) is as follows: Pyridine (1 mL) was added drop wise to a solution of hydroxylamine hydrochloride (0.138 g, 2 mmol) dissolved in ethanol (20 mL). Resulting solution was stirred at room temperature for 15 mins followed by which 2-hydroxy-1-naphthaldehyde (0.344 g, 2 mmol) was added and continued stirring at room temperature for 1 hr. Yellow precipitate of oxime **2.1.1** was obtained from the reaction mixture, which was extracted by ethylacetate and water solvent mixture. Removal of ethylacetate in a rotavapor yielded oxime **2.1.1**. Yield: 82 %. ^{1}H-NMR (400 MHz, DMSO-d_6): 11.53 (s, 1H), 9.04 (s, 1H), 8.48 (d, J = 8 Hz, 1H), 7.86 (d, J = 4 Hz, 1H), 7.84 (d, J = 4 Hz , 1H), 7.52 (t, J = 8 Hz, 1H), 7.37 (t, J = 4 Hz, 1H), 7.21 (d, J = 8 Hz, 1H). IR (KBr, cm^{-1}): 3331 (br, m), 3013 (w), 2924 (w), 2766 (w), 1947 (w), 1758 (w), 1632 (s), 1591 (s), 1526 (w), 1464 (w), 1463(m), 1414 (m), 1369 (w), 1310 (m), 1268 (s), 1239 (s), 1182 (s), 1163 (w), 1143 (w), 1079 (w), 1034 (w), 1014 (s) 938 (s), 878 (w), 854 (w), 814 (s), 776 (s), 744 (m), 718 (w), 649 (w), 541(w). Mass (ESI) m/z: 188.0698 (m+1); (Calculated exact mass 187.0633 for $C_{11}H_9NO_2$).

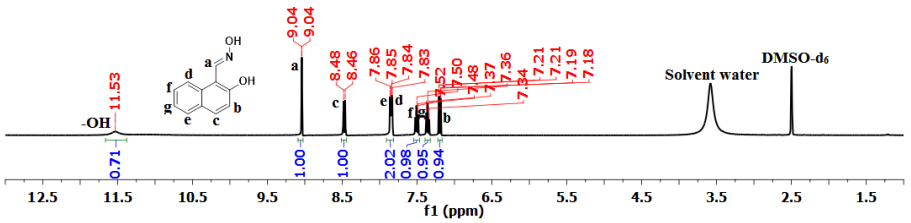

Figure 2.1.11: ^{1}H-NMR (400 MHz, DMSO-d_6) of oxime **2.1.1**.

Oxime **2.1.2**: Isolated yield: 83%. ^{1}H-NMR (400MHz, DMSO-d_6): 11.31 (s, 1H), 9.58 (s, 1H), 9.28 (s, 1H), 8.31 (s, 1H), 6.91 (d, J = 8 Hz, 1H), 6.78 (d, J = 8 Hz, 1H), 6.68 (t, J = 8 Hz, 1H). IR (KBr, cm^{-1}): 3454 (br, m), 1620 (s), 1592 (w), 1478 (s), 1444 (m), 1412 (w), 1347 (m), 1308 (m), 1285 (m), 1251 (m), 1165 (s), 1075 (m), 1030 (s), 967(s), 850 (s), 782(s), 744 (m), 727 (m), 626 (s), 566 (w). Mass (ESI) m/z: 154.1049. (Calculated exact mass 153.0426 for $C_7H_7NO_3$).

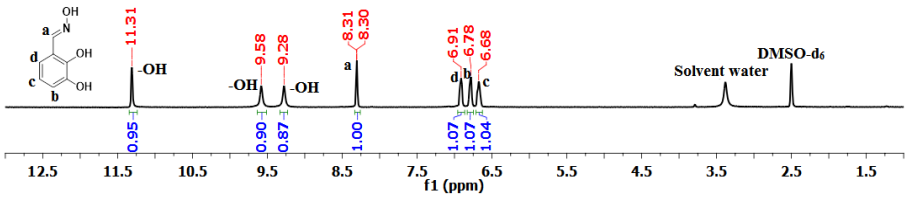

Figure 2.1.12: ^{1}H-NMR (400 MHz, DMSO-d_6) of oxime **2.1.2**.

Oxime **2.1.3**: Isolated yield: 84%. ^{1}H-NMR (400MHz, DMSO-d_6): 10.95 (s, 1H), 10.09 (s, 1H), 9.73 (s, 1H), 8.19 (s, 1H), 7.25 (d, J = 12 Hz, 1H), 6.28 (m, 2H). IR (KBr, cm^{-1}): 3363 (br, m), 1643 (m), 1623 (m), 1598 (w), 1524 (s), 1488 (m), 1446 (w), 1365 (w), 1344 (w), 1304 (s), 1255 (s), 1208 (s), 1170 (m), 1117 (m), 1003 (s), 973 (s), 957 (m), 933 (w), 857 (w), 830 (s), 801 (m), 733 (w), 712 (w), 631 (w), 594 (m), 573 (w). Mass (ESI) m/z: 154.1049; (Calculated exact mass 153.0426 for $C_7H_7NO_3$).

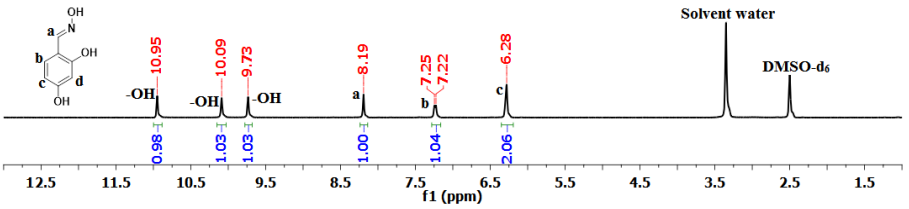

Figure 2.1.13: ^{1}H-NMR (400 MHz, DMSO-d_6) of oxime **2.1.3**.

Crystals of cocrystals **2.1.4**-**2.1.5** and salt **2.1.6** were obtained by slow evaporation of solution of respective aldoxime (0.1 mmol) and tetrabutylammonium fluoride (0.1 mmol) in methanol. Cocrystal **2.1.4**: ^{1}H-NMR (400 MHz, $CDCl_3$): 9.10 (s, 1H, H-C=), 8.03 (d, J = 8 Hz, 1H, H_{ar}), 7.74 (d, J = 8 Hz, 1H, H_{ar}), 7.67 (d, J = 12 Hz, 1H, H_{ar}), 7.47 (t, J = 8 Hz, 1H, H_{ar}), 7.31 (t, J = 8 Hz, 1H, H_{ar}), 7.17 (d, J = 8 Hz, 1H, H_{ar}), 3.26 (m, 8H, N-CH_2), 1.61 (m, 8H, -CH_2-), 1.39 (m, 8H, -CH_2-), 0.97 (m, 12H, -CH_2-). There are deuterium exchangeable signals at 2.62 (s, OH) and 1.5 (s, OH). IR (KBr, cm^{-1}): 2959 (s), 2872 (s), 2851 (w), 1783 (w), 1621 (s), 1594 (m), 1571 (s), 1569 (s), 1431 (s), 1373 (m), 1344 (s), 1306 (m), 1274 (w), 1246 (w), 1211(w), 1167 (m), 1108 (w) 1074 (w), 1035 (w), 1002 (w), 937 (s), 880 (m), 828 (s), 783 (w), 760 (m), 668 (w), 582 (w).

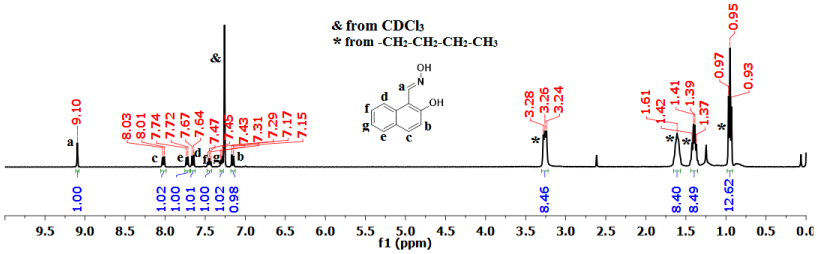

Figure 2.1.14: ^{1}H-NMR (400 MHz, $CDCl_3$) of cocrystal **2.1.4**.

Cocrystal **2.1.5**: ^{1}H-NMR (400MHz, DMSO-d_6): 8.30 (s, 1H, H-C=), 6.92 (d, J = 8 Hz, 1H, H_{ar}), 6.66 (d, J = 8 Hz, 1H, H_{ar}), 6.56 (t, J = 8 Hz, 1H, H_{ar}), 3.17 (t, J = 8 Hz , 4H, N-CH_2-), 1.56 (m, 4H, -CH_2-), 1.33-1.28 (m, 4H, -CH_2-), 0.95-0.91 (m, 6H, -CH_3). IR (KBr, cm^{-1}): 2961 (w), 2874 (w), 2723 (w), 1624 (m), 1577 (m), 1515 (w), 1473 (m), 1379 (s), 1321 (s), 1269 (s), 1243 (w), 1209 (w), 1166 (w), 1108 (w), 1077 (w), 1011 (s), 941 (w), 882 (w), 846 (s), 780(s), 735(s), 622 (s), 587 (m).

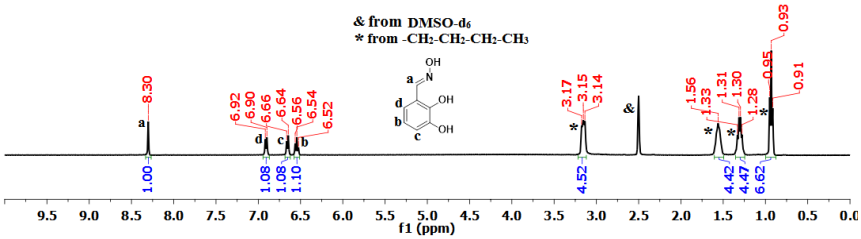

Figure 2.1.15: ^{1}H-NMR (400 MHz, $CDCl_3$) of cocrystal **2.1.5**.

Salt **2.1.6**: ^{1}H-NMR (400MHz, DMSO-d_6): 8.16 (s, 2H, H-C=), 7.16 (d, J= 8 Hz, 2H, H_{ar}), 6.28 (s, 4H, H_{ar}), 3.14 (m, 8H, N-CH_2-), 1.55 (m, 8H, -CH_2-), 1.30 (m, 8H, -CH_2-), 0.93 (m, 12H, -CH_3). IR (KBr, cm^{-1}): 2965 (m), 2876 (w), 1614 (s), 1515 (m), 1477 (w), 1381 (w), 1328 (w), 1311 (m), 1267 (w), 1208 (s), 1117 (m), 994 (m), 969 (m), 887 (w), 757 (w), 733 (w), 651 (w), 576 (m), 506 (m).

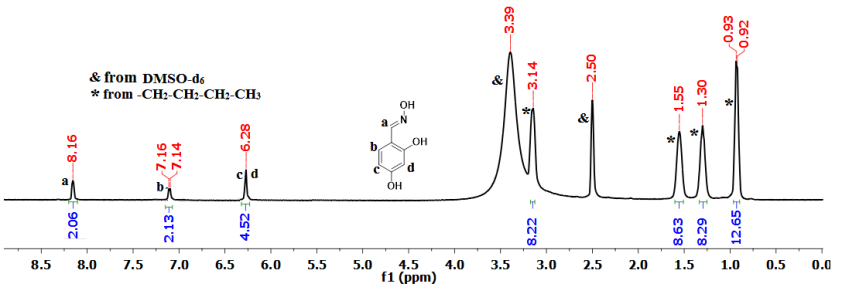

Figure 2.1.16: ^{1}H-NMR (400 MHz, DMSO-d_6) of salt **2.1.6**.

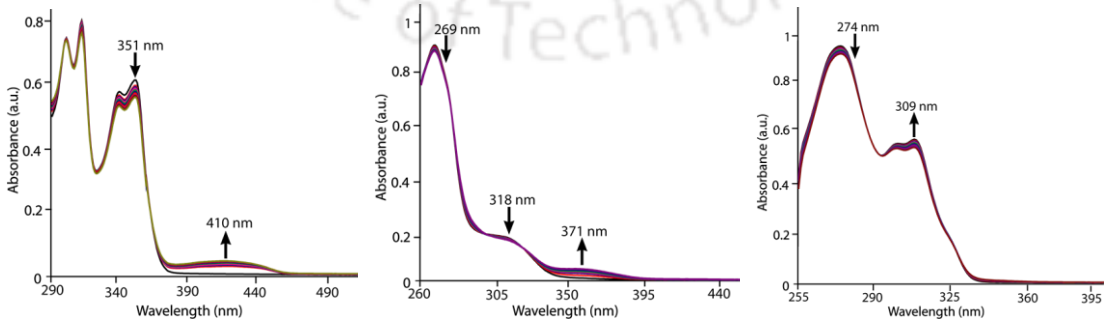

(a) (b) (c)

Figure 2.1.17: UV-vis spectroscopic titration of oxime (a) **2.1.1,** (b) **2.1.2,** (c) **2.1.3** (10^{-5}M) with TBAOAc (0µl-100µl of 10^{-5} M) in dimethylsuphoxide (DMSO).

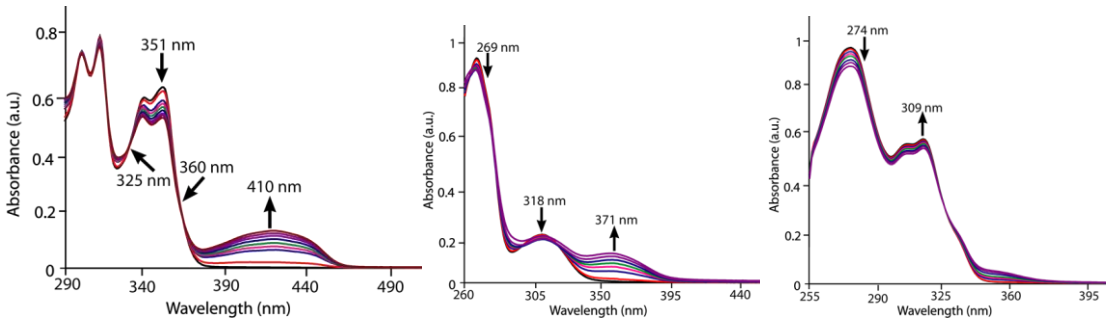

(a) (b) (c)

Figure 2.1.18: UV-vis spectroscopic titration of oxime (a) **2.1.1,** (b) **2.1.2,** (c) **2.1.3** (10^{-5} M) with TBAOH (0µl-100µl of 10^{-5} M) in dimethylsuphoxide (DMSO).

2.1.8: References

1. (a) T. Gunnlaugsson, M. Glynn, G. M. Tocci (née Hussey), P. E. Kruger and F. M. Pfeffer, *Coord. Chem. Rev*., 2006, **250**, 3094-3117; (b) R. Martinez-Máñez and F. Sancenón, *Chem. Rev*., 2003, **103**, 4419-4476.
2. (a) S. Park, H. J. Kim, *Chem. Commun*., 2010, **46**, 9197-9199; (b) X. Zhuang, W. Liu, J. Wu, H. Zhang, P, Wang, *Spectrochim. Acta, Part A: Mol. Biomol. Spectrosc*., 2011, **79**, 1352-1355; (c) E. J. Cho, B. J. Ryu, Y. J. Lee, K. C. Nam, *Org. Lett*., 2005, **7**, 2607-2609; (d) S. E. Garcıa-Garrido, C. Caltagirone, M. E. Light, P. A. Gale, *Chem. Commun.*, 2007, 1450-1452; (e) J. Shao, H. Lin, M. Yu, Z. Cai, H. Lin, *Talanta*, 2008, **75**, 551-555; (f) Q. Xu, K. -A. Lee, S. Lee, K. M. Lee, W. -J. Lee, J. Yoon, *J. Am. Chem. Soc.*, 2013, **135**, 9944-9949.
3. (a) M. Arunachalam, P. Ghosh, *Inorg. Chem.*, 2010, **49**, 943-951; (b) M. Arunachalam, S. Chakraborty, S. Marivel, P. Ghosh, *Cryst. Growth Des*., 2012, **12**, 2097-2108; (c) P. Sokkalingam, S. -Y. Kee, Y. Kim, S. -J. Kim, P. H. Lee, C. -H. Lee, *Org. Lett.*, 2012, **14**, 6234-6237.
4. (a) R. Dutta, P. Ghosh, *Eur. J. Inorg. Chem*., 2012, **2012**, 3456-3462; (b) R. Dutta, P. Ghosh, *Chem. Commun.*, 2014, **50**, 10538-10554.
5. (a) R. Zhang, Y. Zhao, J. Wang, L. Ji, X. -J. Yang, B. Wu, *Cryst. Growth Des*., 2014, **14**, 544-551; (b) J. M. Stauber, G. E. Alliger, D. G. Nocera, C. C. Cummins, *Inorg. Chem*., 2017, **56**, 7615-7619.
6. (a) J. Ma, Z. Li, Y. Zong, Y. Men, G. Xing, *Tetrahedron Lett*., 2013, **54**, 1348-1351; (b) J. Wang, Y. Hou, C. Li, B. Zhang, X. Wang, *Sens. Actuators B*, 2011, **157**, 586-593; (c) H. Khanmohammadi, K. Rezaeian *RSC Adv.*, 2014, **4**, 1032-1038.
7. C. B. Rosen, D. J. Hansen, K. V. Gothelf, *Org. Biomol. Chem*., 2013, **11**, 7916-7922.

8. R. J. Sarma, J. B. Baruah, *Chem. Eur. J.*, 2006, **12**, 4994-5000.
9. Z. Guo, L. Li, G. Liu, J. Dong, *Acta Cryst.*, 2008, **E64**, o568-o569.
10. P. A. Wood, P. A. Forgan, D. Henderson, S. Parsons, E. Pidcock, P. A. Tasker, J. E. Warren, *Acta Cryst.*, 2006, **62B**, 1099-1111.
11. C. B. Aakeröy, S. Panikkattu, P. D. Chopade, J. Desper, *CrystEngComm*, 2013, **15**, 3125-3136.
12. C. B. Aakeröy, A. M. Baety, D. S. Leinen, *CrystEngComm*, 2000, **27**, 1-6.
13. (a) F. G. Bordwell, *Acc. Chem Res.*, 1988, **21,** 456-463; (b) L. S. Evans, P. A. Gale, M. E. Light, R. Quesada, *Chem. Commun*., 2006, 965-967; (c) P. Ashokkumar, V. T. Ramakrishnan, P. Ramamurthy, *Chem. Eur. J.*, 2010, **16,** 13271-13277.
14. (a) J. Ma, Z. Li, Y. Zong, Y. Men, G. Xing, *Tetrahedron Lett*., 2013, **54**, 1348-1351; (b) J. Wang' Y. Hou, C. Li, B. Zhang, X. Wang, *Sens. Actuators B*, 2011, **157**, 586-593; (c) H. Khanmohammadi, K. Rezaeian *RSC Adv.*, 2014, **4**, 1032-1038.
15. S. Devaraj, D. Sarvannakumar, M. Kundaswamy, *Tetrahedron Lett.*, 2007, **48,** 3077-3081.
16. V. Luxami, S. Kumar, *Tetrahedron Lett.*, 2007, **48**, 3083-3087.
17. (a) C. R. Rice, *Coord. Chem. Rev.*, 2006, **250**, 3190-3199. (b) E. R. Libra, M. J. Scott, *Chem Commun.*, 2006, 1485-1487.
18. J. -S. Wu, J. -H. Zhou, P. -F. Wang, X. -H. Zhang, S. -K. Wu, *Org. Lett.*, 2005, **7**, 2133-2136.
19. P. D. Beer, P. A. Gale, *Angew. Chem. Int. Ed. Engl.*, 2001, **40**, 486-516.
20. (a) A. Roy, D. Kand, T. Saha, P. Talukdar, *Chem. Commun.*, 2014, **50,** 5510-5513; (b) M. Boiocchi, L. D. Boca, D. E. Gomez, L. Fabbrizzi, M. Licchelli, E. Monzani , *J. Am. Chem. Soc.*, 2004, **126**, 16507-16514; (c) D. Buckland, S. V. Bhosale, S. J. Langford, *Tetrahedron Lett.*, 2011, **52**, 1990-1992; (d) X. Cao, W. Lin, Q. Yu, J. Wang, *Org. Lett.*, 2011, **13,** 6098-6101; (e) L. Fu, F. -L. Jiang, D. Fortin, P. D. Harvey, Y. Liu, *Chem Commun.*, 2011, **47,** 5503-5505; (f) M. Jo, J. Lim, M. S. Ognjen, *Org. Lett.*, 2013, **15,** 3518-3521; (g) H. Lu, Q. Wang, Z. Li, G. Lai, J. Jiang, Z. Shen, *Org. Biomol. Chem.*, 2011, **19,** 4558-4562; (h) M. Mascal, I. Yakovlev, E. B. Nikitin, J. C. Fettinger, *Angew. Chem. Int. Ed. Engl.*, 2007, **46,** 8782-8784; (i) M. R. Rao, S. M. Mobin, M. Ravikanth, *Tetrahedron*, 2010, **66,** 1728-1734; (j) Z. Xu, N. J. Singh, S. K. Kim, D. R. Spring, K. S. Kim, J. Yoon, *Chem. Eur. J.*, 2011, **17,** 1163-1170; (k) S. Yamaguchi, T. Shirasaka, K. Tamao, *Org. Lett.*, 2000, **2,** 4129-4132; (l) J. F. Zhang, C.S. Lim, S. Bhuniya, B. R. Cho, J. S. Kim, *Org. Lett.*, 2011,

13, 1190-1193; (m) V. Amendola, G. Bergamaschi, M. Boiocchi, L. Fabbrizzi, L. Mosca, *J. Am. Chem. Soc.*, 2013, **135,** 6345-6355; (n) E. J. Cho, W. Moon, S. W. Ko, J. Y. Lee, S. K. Kim, J. Yoon, K. C. Nam, *J. Am. Chem. Soc.*, 2003, **125,** 12376-12377; (o) L. S. Evans, P. A. Gale, M. E. Light, R. Quesada, *Chem. Commun*., 2006, 965-967; (p) T. Guchhait, G. Mani, *J. Org. Chem.*, 2011, **76,** 10114-10121; (q) T. H. Kim, T. M. Swager, *Angew. Chem. Int. Ed. Engl.*, 2003, **42,** 4803-4806; (r) J. Y. Lee, E. J. Cho, A. Mukamel, K. C. Nam, *J. Org. Chem.*, 2004, **69,** 943-950.

Chapter 2

Part B: Anion Assisted Conformationally Guided Dendrimer-like Self-assemblies of Multi-component Cocrystals of Dioxime

CrystEngComm, 2016, **18**, 5482-5491.

2.2.1: Introduction

Physico-chemical properties associated with self-assemblies have contributed significantly to material sciences.[1] Conformers in self-assembled structures are important to guide self-assemblies formed through non-covalent interactions.[2] Among different self-assemblies dendritic assemblies have interest in nano-sciences,[3] thus and there is definite need to generate new dendrimer-like non-covalent assemblies. Dendritic molecules[4] and dendritic guest interacting[4a] with host to form dendrimer-like aggregates are known and there is definite possibilty to study such assemblies through crystal enginnering approach. Directional properties of the weak interactions and conformation adjustments[5] have a constructive role or be a barrier for construction of a desired assembly. Local effects such as interactions of solvent and ions with a substrate are common factors to guide selective orientations of a molecule while crystallisation.[5] Crystal engineering approach helps in studying self-assembly of multi-functional compounds such as tetracarboxylic acids;[6] but dendrimer-like non-covalent assemblies of polyfunctional compounds requires more efforts to make a headway. Anions may be used as connects[7] and the coordination effect of anions plays role in non-covalent synthesis. Two types of receptors are generally found in anion assisted assemblies; they are protonated and neutral receptors.[7] Neutral oximes form hydrogen bonds with anions and they behave as donor or acceptor for hydrogen bonds.[8] As mentioned that the conformation plays role in self-assemblies *syn* or *anti* conformers of aldoximes are well known for control of reactivity of oximes.[9] Specific conformer of certain oximes[10] are efficient as neurotoxic agent. Oximes form assemblies suitable for molecular recognition.[11] Hence, there is need to explore the assemblies of oximes.[12] Such studies will also enhance understanding on the role of anions to generate well defined packing patterns.[13] Cocrystals with multiple numbers of oxime functional groups provide avenues to study O-H···anion interactions suitable to synthesise multi-component assemblies. Due to such factors and directional coordination behaviour of anions, specific conformers of host molecules in such assemblies may be possible.

1,3-Benzenedialdoxime[12a] (**2.2.1**) has three hydrogen bonding sites whose orientations decide geometry of a conformer. Several conformers may arise from the orientations of the active hydrogen atoms of this molecule (**Fig. 2.2.1a**). The dispositions of the functional groups across C=N bonds (**Fig. 2.2.1b**) also causes different geometries of this molecule. The orientations of the C-$H_{(oxime)}$ across the phenylene ring causes different structural changes depicted in **Fig. 2.2.1c**.

Thus beyond *syn-anti* forms **I-III** there are other sub-sets of conformers like **IV-V** (**Fig. 2.2.1c**). Conformers like *anti-anti* and *H-out-out* are apparently identical but may have differences from the projection of the O-H bonds.

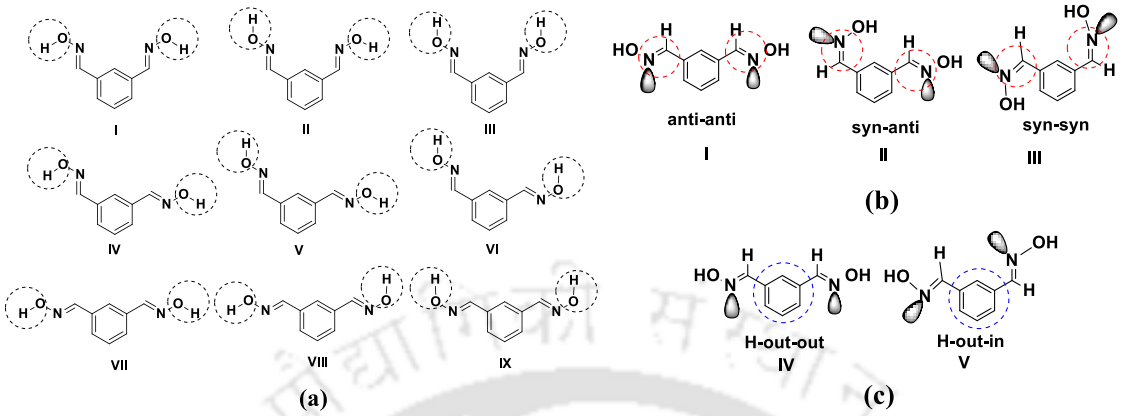

Figure 2.2.1: Some conformers of oxime **2.2.1** due to orientations of (a) O-H bonds, (b) functional groups across C=N bonds and (c) across phenylene unit. (Dotted circles represent the sites under consideration).

The conformers due to inward or outward orientations of the C-H_{oxime} across the phenylene unit would control the directional properties of non-covalent interactions associated with the oxime. The conformations of the host molecules in various non-covalently linked self-assemblies contribute to their better understanding.[14] We explored the conformers from different orientations across oxime groups and their role in formation of dendrimer-like non-covalently linked self-assemblies of oxime **2.2.1** by utilizing coordination effect of anions.

2.2.2: Adducts of oxime 2.2.1 with different tetrabutylammonium salts

In solid state oxime **2.2.1**, it adopts *anti-anti* conformer[11a] (**I**, of **Fig. 2.2.1b**); alternatively, it may be described to possess *H-out-out* conformer (**IV** of **Fig. 2.2.1c**). It reacts with tetrabutylammonium hydroxide to form cocrystal **2.2.2.** This cocrystal is comprised of a tetrabutylammonium cation, mono-deprotonated oxime anion along with a molecule of neutral oxime **2.2.1**.

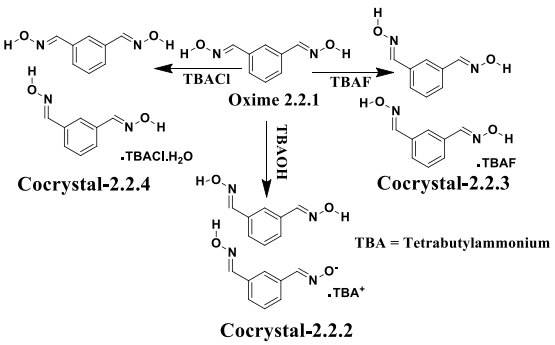

Scheme 2.2.1: Different cocrystals of oxime **2.2.1** with different tetrabutylammonium salts.

While with terabutylammonium chloride (TBACl) it forms a hydrated 2:1 cocrystal **2.2.3**, but with tetrabutylammonium fluoride (TBAF) it forms an anhydrous 2:1 cocrystal **2.2.4** (**Scheme 2.2.1**). Cocrystal **2.2.2** has both anionic and neutral oximes in *H-out-in* conformations; but cocrystal **2.2.3** has two oximes in *H-out-in* conformations; whereas cocrystal **2.2.4** has one oxime with *H-out-out* and other *H-out-in* conformation.

2.2.3: Supramolecular assemblies of oxime 2.2.1 and cocrystals 2.2.2-2.2.4

The solid state self-assembly of oxime **2.2.1** has $R_2^2(6)$ hydrogen bonded cyclic motifs possessing O-H···N hydrogen bonds.[12a] Due to such motifs one-dimensional chain-like structures (**Fig. 2.2.2a**) are observed. Asymmetric unit of the cocrystal **2.2.2** contains a tetrabutylammonium cation, a mono-deprotonated oximate anion and one neutral oxime molecule. The oxime molecules and the oximate molecules are connected by O-H···O bonds which contribute to the self-assembly of the cocrystal **2.2.2**. Considering the anionic side of the mono-anionic oximate as head and the oxime end as tail, two mono-anionic oximates form dimeric sub-assemblies which are held to each other in a head to tail fashion. These hydrogen bonded dimeric sub-assemblies have $R_2^2(7)$ graph set notation.[15] They are formed by C-H···N and O-H···O interactions. For hydrogen bonds and short contacts parameters of cocrystals **2.2.2**-**2.2.4** please see page 227 of appendix.

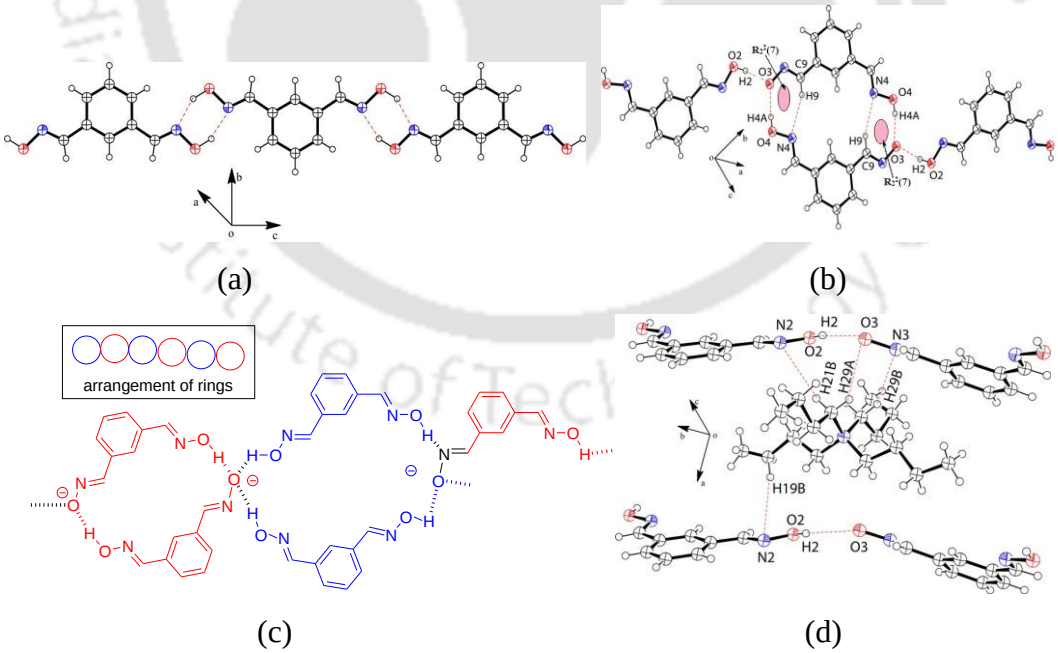

Figure 2.2.2: (a) Chain-like structure of oxime **2.2.1**; (b) Self-assembling between oxime and oximate anion in cocrystal **2.2.2**; (c) Representation of anionic part of self-assembly of cocrystal **2.2.2** inset is chains of ring-like assemblies (cations are not shown for clarity); (d) Layered structure found in cocrystal **2.2.2** (30% thermal ellipsoids in ORTEP diagram).

Such hydrogen bonded dimers of anions interact with two neutral oxime molecules at two ends via O-H ··O interactions (**Fig. 2.2.2b**). The two ends of these dimeric sub-assemblies are bridged by neutral oxime molecules to form cyclic dimeric sub-assemblies across two sides (**Fig. 2.2.2c**). Dimeric sub-assemblies are in alternative positions to form chain-like arrangement of two different cyclic motifs. The anionic part of self-assembly has layered structure where tetrabutylammonium cations are (**Fig. 2.2.2d**) held. We observe that the alternate cyclic units are held by N-O$^-$ through bifurcated or trifurcated hydrogen bonds. This may be attributed to the ability of oxyanion to hold two hydrogen bonds. The bifurcated hydrogen bonds in N-oxides have found utility in construction of predesigned non-covalent synthesis.[16] Hence, cyclic motifs guided by electrostatic contribution of N-O$^-$ bonds to generate patterns like alternate macrocycles type arrangements. The packing pattern of these motifs may be considered to be analogous to cyclic unit present in metallacycles of covalently linked systems.[17a-b] Conformation of a molecule guides architecture of a self-assembly;[18] whereas, resurge on multi-component systems necessitates a systematic understanding of such factors.[19] Generally, energy required for a conformation change can be of the order of 1-8 kcal/mole and this is comparable to the energy of a weak hydrogen bond.[20] Flexiblity due to multiple numbers of methylene groups in the chain of tetrabutylammnonium cation may also influence conformational change during crystallisation.

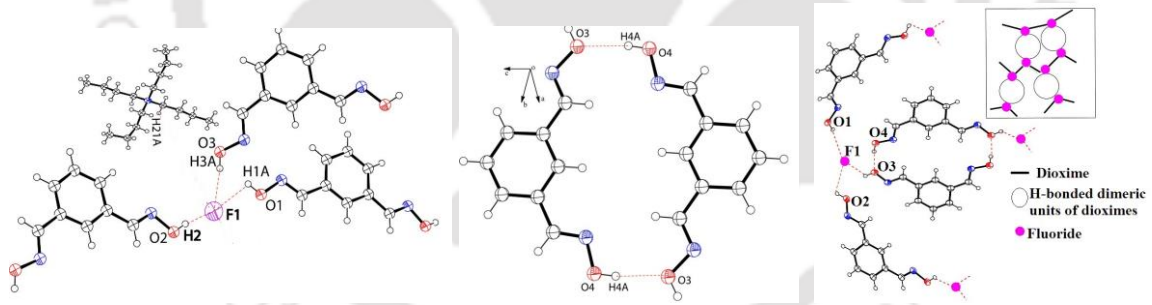

(a) (b) (c)

Figure 2.2.3: (a) Anion coordination environment in cocrystal **2.2.3** (a proximal cation is also shown); (b) Sub-assembly of oxime **2.2.1** within self-assembly of cocrystal **2.2.3**; (c) First generation dendrimer-like self-assemblies of cocrystal **2.2.3** (cations are not shown for clarity); inset is the representation of combination of dimeric sub-assemblies of ring and monomeric dioximes connected to fluoride ions (30% thermal ellipsoids in ORTEP diagram).

But, cocrystals in the present study are cation specific, for example we did not obtained similar cocrystals with tetramethylammonium or ammonium cation. Thus, two conformationally dissimilar units with very close energy differences crystallised as cocrystal **2.2.2** to meet those synergic effects. Tetrabutylammonium fluoride formed a three component

cocrystal **2.2.3** with oxime **2.2.1** having a composition **$(2.2.1)_2$.(TBAF)**. The asymmetric unit of this cocrystal contains two neutral oxime **2.2.1** molecules and a tetrabutylammonium fluoride. In this cocrystal oxime **2.2.1** molecules are in *H-out-in* orientations. In this cocrystal one fluoride ion form three strong hydrogen bonds with three hydroxy group of oxime unit via O-H···F interactions (**Fig. 2.2.3a**). The H···F bonds are strong as evident from the hydrogen bond distances, which are in the range of 1.64-1.71 Å. These distances are shorter than the conventional H···F distance which is 1.96 Å. The self-assembly of two oxime molecules has $R_2^2(20)$ hydrogen bonded cyclic motifs formed via O-H···O interactions (**Fig. 2.2.3b**). Among the three coordination sites in trigonal planar geometry[21] adopted by each fluoride ion; two sites are connected to two independent oxime molecules and rest is connected to a hydrogen bonded sub-assembly formed between two oxime molecules. Anionic part is a dendrimer-like self-assembly possessing cyclic hydrogen bonded sub-assemblies and discrete oxime molecules connected in regular manner. Tetrabutylammonium cations are accommodated in the interstitial concave spaces. The representation of the structure of the anionic part of the assembly without the cations is shown in the **Fig. 2.2.3c**; inset of the figure is the model arrangement of the assembly. The biggest challenge in dendrimer synthesis is to continue uniformity in the repeat units.[19] In conventional synthetic chemistry, bringing together cyclic and open chain compounds to connect to a common point involves multiple steps and is often difficult. The fluoride assisted dendrimer-like assembly reported here represents connectivity of cyclic and linear motif tethered by fluoride ions providing robust uniform arms. Semi-rigid protonated derivatives such as nicotinamides show conformational adjustments[22] but in the present case changes are brought about by anion on neutral oximes keeping the compositional integrity of the host. To check phase purity of each cocrystal, powder XRD patterns of the bulk sample of cocrystal **2.2.2-2.2.4** were recorded and they were compared with the powder XRD pattern generated from the CIF file of the single crystal data. They show matching of the all the prominent peaks showing the integrity on the presence of one type crystals in bulk sample.

The multi-component cocrystal **2.2.4** has a composition **$(2.2.1)_2$.(TBACl).H_2O**. The cocrystal **2.2.4** is a hydrate whereas cocrystal **2.2.3** is anhydrous. Two oxime molecules of the cocrystal **2.2.4** comprise of different conformers; one of them is *H-out-out* and other is *H-out-in*. Self-assembly of two conformationally similar oxime molecules form $R_2^2(6)$ type hydrogen bond cyclic motifs. The sub-assemblies of dimer of *H-out-out* oximes interact by C-H···O interactions with other sub-assemblies of dimers constitued by *H-out-in* conformers (**Fig. 2.2.4a**). Each chloride ion form three hydrogen bonds with hydroxy groups of oximes.

Accordingly, one chloride ion interact with three oxime molecules through O-H···Cl interactions to construct the distorted trigonal bipyramidal (**tbp**) geometry. Such distorted **tbp** geometry is generally choice of chloride ions in hydrogen bond environments.[21] The assembly can be explained by Ettter's rule[15], as strongly O-H···Cl hydrogen bonds are formed to satisfy the three coordinated distorted **tbp** geometry around each chloride ion as higher priority. Each water molecule interacts with three oxime molecules through O-H···N and O-H···O interactions. Self-assembly (**Fig. 2.2.4b**) is thus assisted by chloride ions and water molecules. Due to the difference in the size and electronegativity between chloride and fluoride ion, packing patterns in respective assemblies are affected. The self-assembly assisted by chloride ions required help of water molecules to make up the packing difference caused by size. This caused wide differences between the self-assembly between cocrystal **2.2.3** and **2.2.4**. Water molecules act as bridge to connect the nitrogen atoms of two oxime groups of independent molecules at the connecting points of the oximes to chloride ions. Such bridges are formed by two O-H···N bonds in each junction. Overall, the self-assembly is formed by chloride ions as pivots to generate dendrimer-like arrangement (**Fig. 2.2.4c**). Dendrimer-like arrangement is grown by interactions of three OH of three independent oxime molecules with one chloride ion, which completes the first generation dendrimer-like assembly.

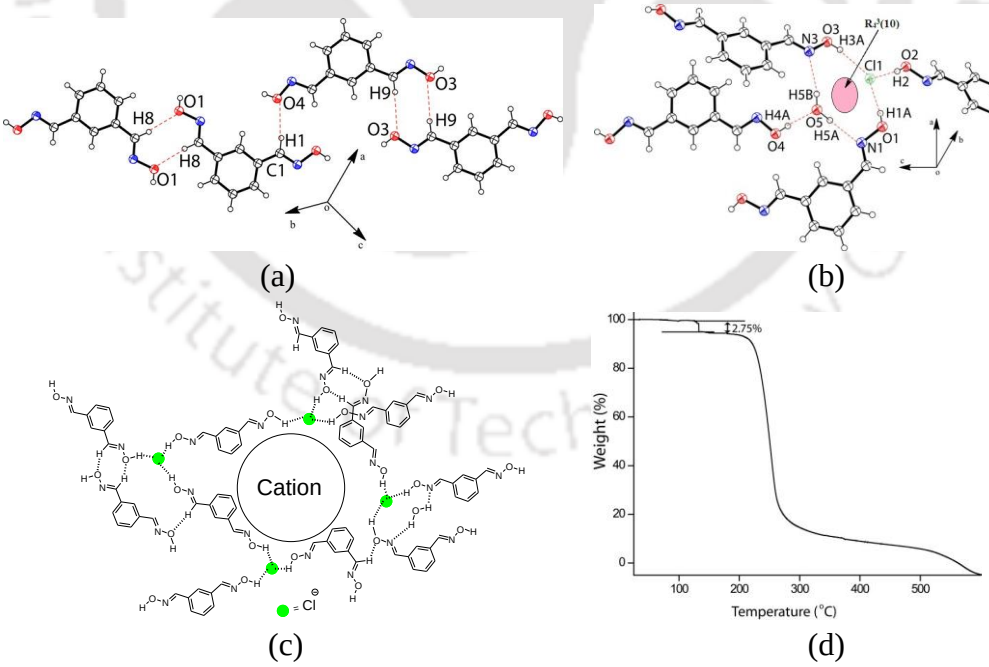

Figure 2.2.4: (a) Self-assembly of **2.2.1** in cocrystal **2.24**; (b) Anion and water assisted assembly of oxime **2.2.1** in cocrystal **2.2.4**; (c) A part of dendrimer-like assembly of cocrystal **2.2.4** providing space for TBA cations in cocrystal **2.2.4**; (d) TGA of the cocrystal **2.2.4** (heating rate 10°C/min) (30% thermal ellipsoids in ORTEP diagram).

Similar building around all the chloride ions on other ends of the first generation unit leads to the second generation. The interactions with water molecules allow formation of cyclic hydrogen bonded sub-assemblies as illustrated in **Fig. 2.2.4c**. The overall self-assembly form well defined cavities to hold the tetrabutylammonium cations. Thus, in this case water molecules also assist in encapsulation of cations. Inclusion of water in the cocrystal **2.2.4** apparently modifies the uniform dendrimer-like assembly present in the cocrystal **2.2.3**. The thermal stability of cocrystal **2.2.2** and cocrystal **2.2.3** were determined by thermogravimetry which showed them to be unstable above 200 °C. Whereas, support for the presence of water molecules in the cocrystal **2.2.4** was apparent in thermogram showing a weight loss in the region of 100-110°C (**Fig. 2.24d**) due to loss of water molecule. Examinations of the assemblies showed that *H-out-out* and *H-out-in* conformers were present in the hydrogen bonded motifs of these cocrystals. In the self-assemblies of the cocrystal **2.2.3** and cocrystal **2.2.4** the coordination environment of anions are similar (**Fig. 2.2.3a** and **Fig. 2.2.4b**) each has distorted trigonal geometry. The packing differences in the two cocrystals originate from the size of anions and hydration. Defining $\Delta_{X...O}$ as the difference between $d_{Cl...O}$ of the cocrystals **2.2.3** and similar $d_{F...O}$ distance in cocrystal **2.2.4**; $\Delta_{X...O1}$ = 0.481Å, $\Delta_{X...O2}$ = 0.511Å, $\Delta_{X...O3}$ = 0.503Å. This difference helps to generate more spaces among the directly hydrogen bonded oxime molecules connecting the chloride in the case of cocrystal **2.2.4**. As a result of this convulsion in arrangement of molecules, a water molecule is accommodated between two oximes connected to a chloride, and helps in the conformational adjustments to show two different conformers in the case of chloride assisted assembly. Alternative explanation is also possible by invoking the H···F and H···Cl bond strengths. Generally H···F bonds are stronger than H···Cl, thus former will provide better opportunity to the conformer namely oxime molecules while forming the cocrystals. Thus in the case of fluoride cocrystal stretch geometry is preferred whereas in chloride case two conformers are found in the lattice.

2.2.4: Gas phase DFT calculation and ^{1}H-NMR studies

A DFT calculation using as B3LYP functional with 6-31+G (d,p) basis set have revealed that the difference between the *H-out-out* and *H-out-in* are comparable and energetically latter is more stable by 0.168 kcal/mole. On the other hand, the HOMO-LUMO gap of the two conformers is very close to make a distinction in UV-spectra. The energy difference being smaller as compared to hydrogen bond energies which lie between 5 to 20 kcal/mole (**Fig. 2.2.12)**; Thus, it should not be possible to distinguish in solution at ordinary conditions. This is reflected in the ^{1}H-NMR spectra of oxime **2.2.1** independently recorded in CD_3OD,

CD_3CN, DMSO-d_6 and acetone-d_6 (**Fig. 2.2.13**). The signals observed in ^{1}H-NMR spectra in all these solvents were identical except in the positions of chemical shift of the O-H protons.

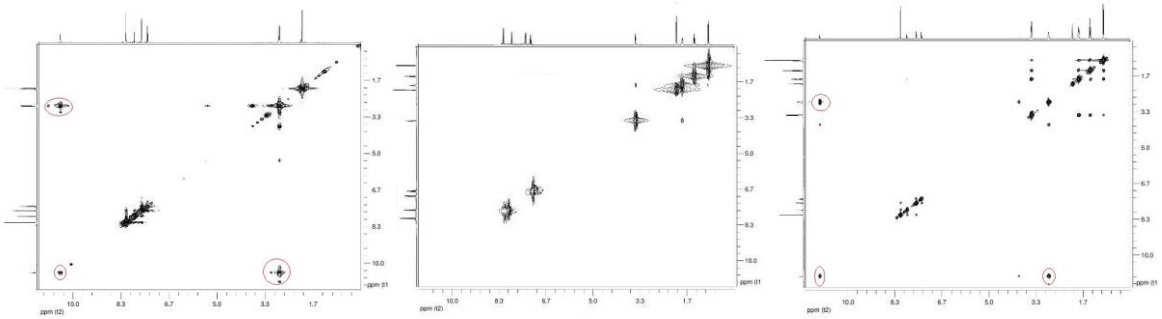

(a) (b) (c)

Figure 2.2.5: ^{1}H-NOESY spectra (600MHz, Acetone-d_6) of (a) oxime **2.2.1** and cocrystal (b) **2.2.3** and (c) **2.2.4**.

The OH signal appeared at 9.09, 10.44 and 11.30 ppm in CD_3CN, DMSO-d_6 and acetone-d_6 respectively. However, in CD_3OD the signal of O-H merged with the residual OH peak of solvent. This suggested that the interactions of the labile OH protons on oxime groups with different solvents are different. We have compared ^{1}H-NOESY spectra of the cocrystal **2.2.3** and cocrystal **2.2.4** with respective ^{1}H-NOESY spectra of oxime **2.2.1** (**Fig. 2.2.5**). Other than the exchange of the labile protons of the oxime groups with water molecules present with the deuterated solvent, no other NOE effect was observed. Titrations of oxime **2.2.1** with TBACl showed no change in peak positions other than the OH peak. However, peak positions of aromatic protons of oxime **2.2.1** were shifted at high concentration of TBAF (**Fig. 2.2.14,** experimental section). Careful observation has revealed that at 0.5 mole equivalent of TBAF did not affect the spectra of oxime **2.2.1**. Since cocrystal **2.2.3** is 2:1 ratio of oxime **2.2.1** and TBAF, this experiment also could not distinguish conformational change in solution.

2.2.5: FT-IR and Raman spectroscopic studies

IR spectra and Raman spectra of oxime **2.2.1** and cocrystals (**Fig. 2.2.6a-b**) were recorded to see distinctions among them. Raman spectroscopy is identified to be an important tool to study solid state conformation in polymorphs.[23] Oxime **2.2.1** has O-H bond stretching vibration in IR-spectra at 3258 cm^{-1} and it also has C-H vibrations at 3000-2950 cm^{-1}. In the cocrystals **2.2.2** and **2.2.3**, the O-H stretches are broad, but due to the water molecule in the cocrystal **2.2.4** there is a sharp O-H stretch at 3190 cm^{-1}. IR spectra of cocrystals **2.2.2-2.2.4** have sharp signals for C=N stretching in the range of 1480-1491 cm^{-1} (**Fig. 2.2.6a**). Raman spectra (**Fig. 2.2.6b**) showed distinct features in each case in the region 1530-1685 cm^{-1}. Due to *H-out-out* orientation of oxime **2.2.1**, it showed two absorptions at 1626 cm^{-1} and 1599 cm^{-}

[1]. These peaks are attributed to C=N stretch based on the Raman absorptions reported for aromaticaldoximes.[24] Cocrystals showed more numbers of Raman peaks in this particular region than **2.2.1**. More precisely, cocrystal **2.2.2** has showed a peak at 1537 cm^{-1}; this peak is additional to the peaks at 1648 cm^{-1} 1608 cm^{-1} and 1582 cm^{-1}.

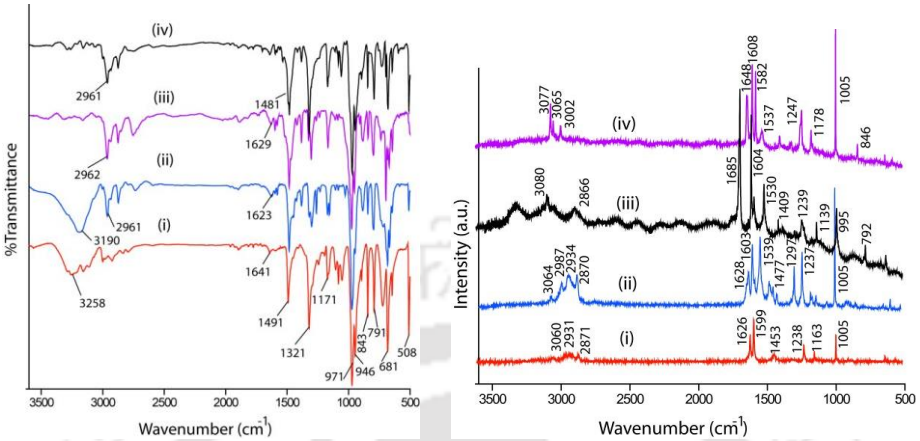

(a) (b)

Figure 2.2.6: (a) FT-IR and (b) Raman spectra of (i) oxime **2.2.1**; (ii) Cocrystal **2.2.4**; (iii) Cocrystal **2.2.3** and (iv) Cocrystal **2.2.2**.

Similarly, cocrystal **2.2.3** has Raman absorptions at 1685 cm^{-1}, 1604 cm^{-1} and 1530 cm^{-1}. Whereas, similar sets of peaks for cocrystal **2.2.4** at 1628 cm^{-1} and 1603 cm^{-1} which are similar to **2.2.1** and an addition peak at 1539 cm^{-1} was observed. The common point among the conformers of the cocrystals is the *H-out-in* orientation of one oxime molecule in each case. Thus, the signal at 1537cm^{-1} of cocrystal **2.2.2**, 1530 cm^{-1} of cocrystal **2.2.3** and 1539 cm^{-1} of cocrystal **2.2.4** are attributed to the contribution from *H-out-in* conformer. Another common peak observed in Raman for all these cases occurs at 1005 cm^{-1} due to N-O stretching.

2.2.6: Conclusions

Several hydrogen bonded cyclic synthons in dioxime cocrystals are identified (**Fig. 2.2.7**) suggesting that conventional hydrogen bonded $R_2^2(6)$ type motif of oxime **2.2.1** got modified to $R_2^2(7)$ type in cocrystal **2.2.2**. In fluoride assisted self-assembly of cocrystal **2.2.3** robust dimeric sub-assemblies formed by O-H···O interactions between two oxime molecules, whereas in chloride assisted assembly of cocrystal **2.2.4** $R_2^2(8)$ synthons were observed. The multi-component cocystals **2.2.2-2.2.4** has dissimilar motifs; suggests role of anions to guide packing patterns. Hydrogen bond motifs in the cocrystals are formed as per hierarchy of the bond strengths availing good donors and acceptors to follow Etter's rules.[15] Bifurcated

hydrogen bond of N-O$^-$ provides the connectivity between cyclic motifs in cocrystal **2.2.2** to make chain-like hydrogen bonded arrangements.

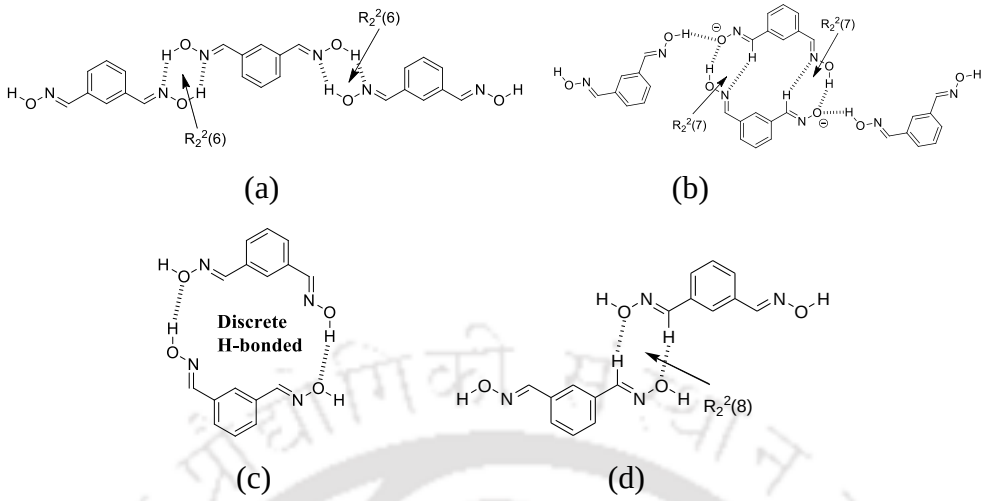

Figure 2.2.7: Hydrogen bonded cyclic motifs found in the self-assemblies of (a) oxime **2.21**; (b-d) cocrystals **2.2.2-2.2.4**.

Robust cyclic sub-assemblies within the self-assembly guided by strong O-H···F bonds in cocrystal **2.2.3**, adds value to utility to stabilize cyclic hydrogen bonded motifs of robust molecules. Combination of *H-out-out* and *H-out-in* conformers are found in cocrystals **2.2.4**, where the self-assembly has water molecules acting as fillers of dendrimer-like structure. Observation of *H-out-in* conformers in the cocrystals which is not present in **2.2.1** is attributed to built-up of large ensembles to stabilize TBA cations. This study on generating dendrimer-like packing patterns from anion guided assemblies of neutral host molecules opens up new avenues for multi-component cocrystals from another perspective.

2.2.7: Experimental section

Synthesis and characterization of oxime 2.2.1 and cocrystals 2.2.2-2.2.4:

Oxime **2.2.1** was prepared by reported procedure.[12a] Slow evaporation of solution of oxime **2.2.1** (16.5 mg, 0.1 mmol) and corresponding tetrabutylammonium salts (namely hydroxide, fluoride or chloride) (0.1 mmol) in mixture of solvents comprising of methanol and acetone (20 ml, 1:1, v/v) yielded crystals of corresponding cocrystals.

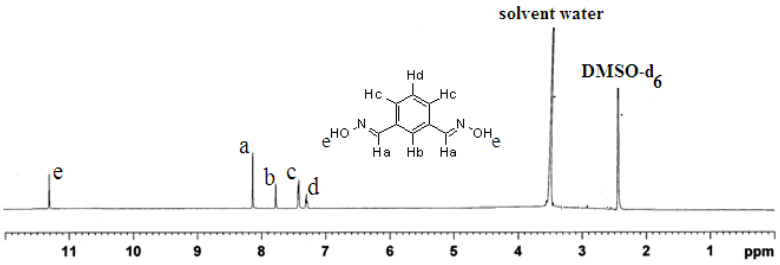

Figure 2.2.8: ^{1}H-NMR (600 MHz, DMSO-d_6) of oxime **2.2.1**.

Cocrystal **2.2.2:** Isolated yield: 70 %. ^{1}H-NMR (600 MHz, DMSO-d_6): 8.14 (s, 4H), 7.78 (s, 2H), 7.43 (d, J = 7.2 Hz, 4H), 7.31 (t, J = 7.8 Hz, 2H), 3.15 (m, 8H, N-CH_2), 1.56 (m, 8H, -CH_2-), 1.30 (m, 8H, -CH_2-), 0.93 (m, 12H, -CH_2-). IR (KBr, cm^{-1}): 2961 (s), 1481 (s), 1420 (w), 1383 (s), 1170 (s), 1082 (w), 1059 (s), 970 (s), 947 (s), 893 (w), 844 (s), 792 (s), 729 (w), 696 (s), 679 (s), 644 (s), 508 (s).

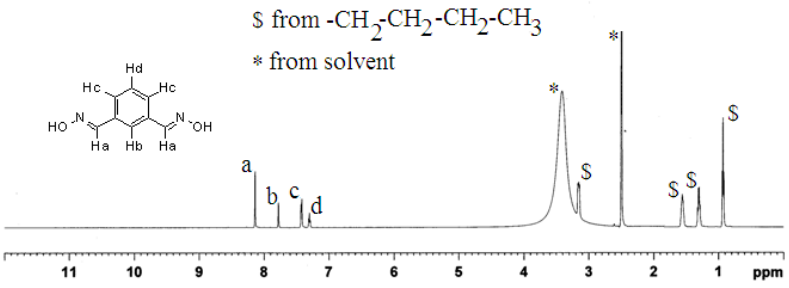

Figure 2.2.9: ^{1}H-NMR (600 MHz, DMSO-d_6) of cocrystal **2.2.2**.

Cocrystal **2.2.3:** Isolated yield: 71 %. ^{1}H-NMR (600 MHz, DMSO-d_6): 11.32 (s, 2H), 8.15 (s, 4H), 7.80 (s, 2H), 7.59 (d, J = 7.8 Hz, 4H), 7.43 (t, J = 7.8 Hz, 2H), 3.17 (m, 8H, N-CH_2), 1.56 (m, 8H, -CH_2-), 1.32 (m, 8H, -CH_2-), 0.94 (m, 12H, -CH_2-). IR (KBr, cm^{-1}): 3190 (br, m), 2961 (s), 1483 (s), 1382 (m), 1300 (s), 1261 (s), 1171 (s), 1155 (w), 1084 (w), 971 (s), 884 (s), 843 (s), 795 (s), 722 (s), 682 (s), 666 (s), 509 (s).

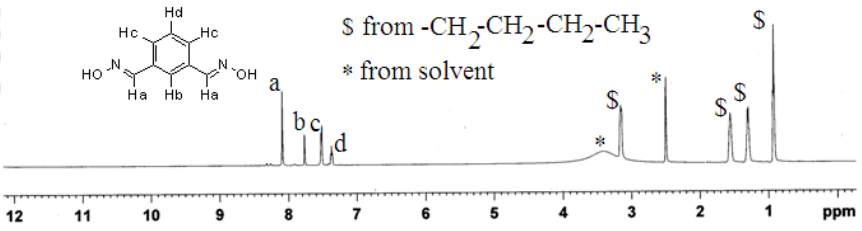

Figure 2.2.10: ^{1}HNMR (600 MHz, DMSO-d_6) of cocrystal **2.2.3**.

Cocrystal **2.2.4:** Isolated yield: 74 %. ^{1}H-NMR (600 MHz, DMSO-d_6): 8.09 (s, 4H), 7.76 (s, 2H), 7.52 (d, J = 7.8 Hz, 4H), 7.38 (t, J = 7.2 Hz, 2H), 3.15 (m, 8H, N-CH_2), 1.56 (m, 8H, -CH_2-), 1.30 (m, 8H, -CH_2-), 0.93 (m, 12H, -CH_2-). IR (KBr, cm^{-1}): 2962 (s), 1482 (s), 1420 (s), 1382 (s), 1324 (m), 1303 (s), 1167 (s), 973 (s), 952 (m), 908 (w), 882 (s), 841 (s), 798 (s), 737 (w), 696 (s), 683 (w), 670 (m), 644 (s), 500 (s).

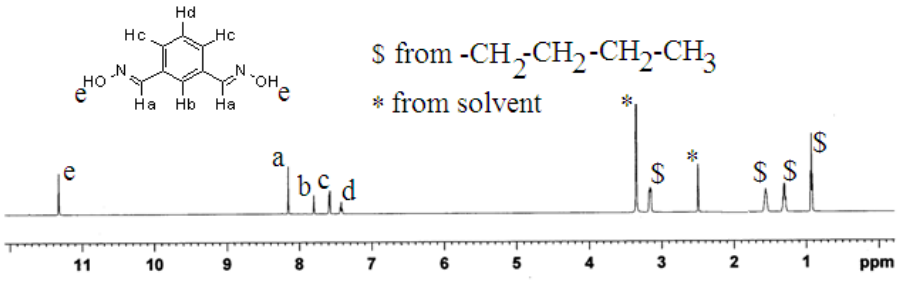

Figure 2.2.11: ^{1}H-NMR (600 MHz, DMSO-d_6) of cocrystal **2.2.4**.

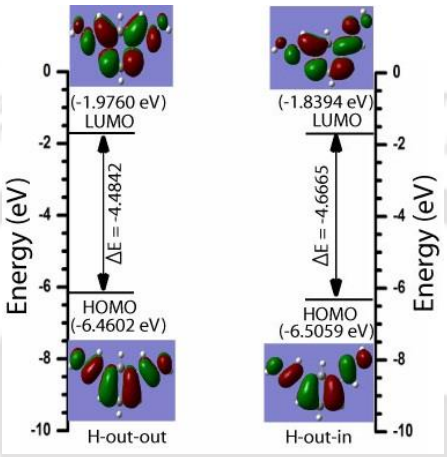

Figure 2.2.12: HOMO and LUMO gap in two conformers of oxime **2.2.1,** calculated by DFT using B3LYP/6-31+G (d,p) as basis set.

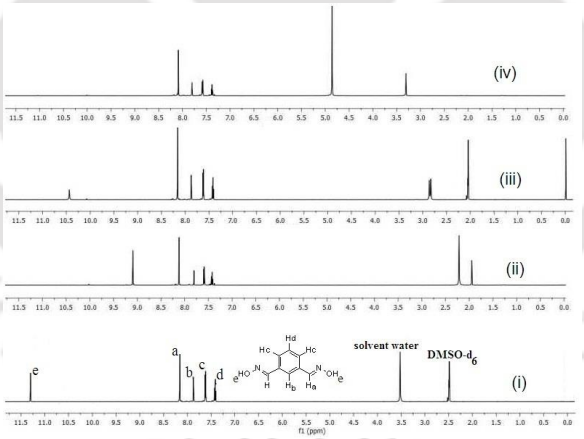

Figure 2.2.13: Solvent dependent ^{1}H-NMR spectra of oxime **2.2.1** in (i) DMSO-d_6, (ii) Acetonitrile-d_3, (iii) Acetone-d_6 and (iv) Methanol-d_4.

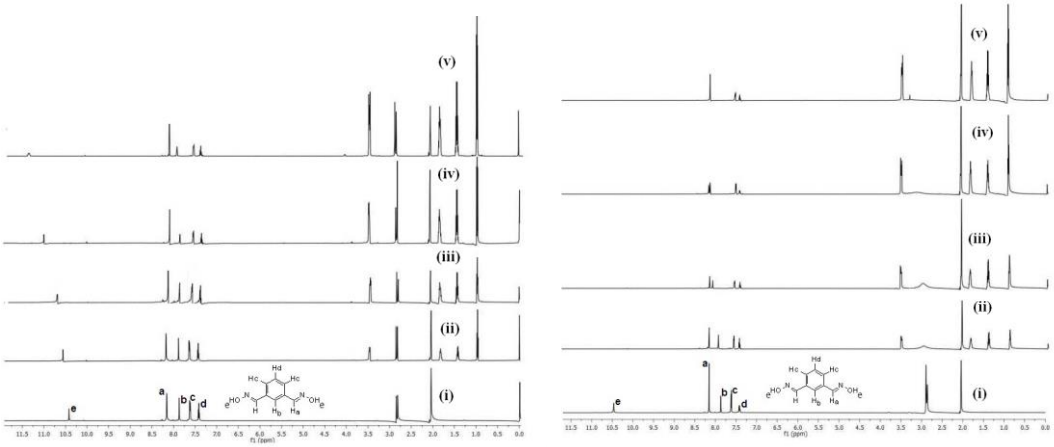

(a) (b)

Figure 2.2.14: ^{1}H-NMR (Acetone-d_6) spectra during titration of oxime **2.2.1** with tetrabutyl ammonium (a) chloride and (b) fluoride using (i) 0.0, (ii) 0.5, (iii) 1 (iv) 1.5, (v) 2 equivalents.

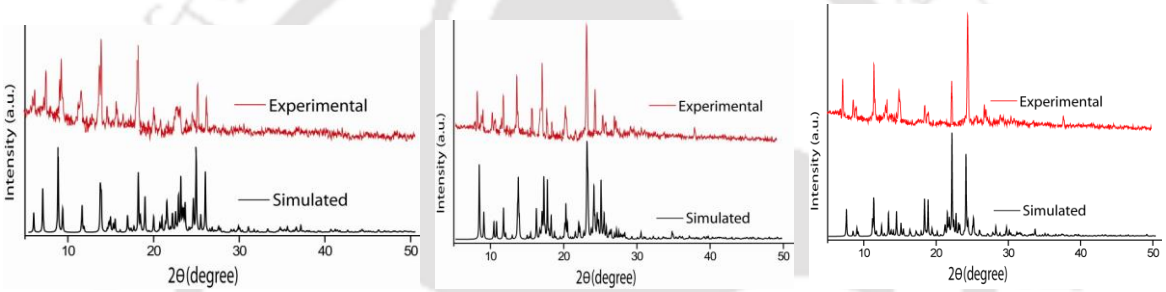

(a) (b) (c)

Figure 2.2.15: PXRD of cocrystal **(a) 2.2.2**, (b) **2.2.3** and (c) **2.2.4** (Red = Experimental, Black = Simulated), Simulated pattern generated from CIF file.

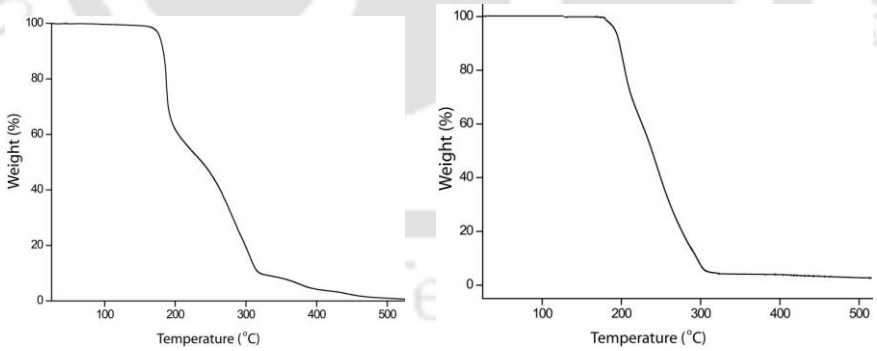

(a) (b)

Figure 2.2.16: TGA of Cocrystal (a) **2.2.2** and (b) **2.2.3**.

2.2.8: References

1. (a) V. Balzani, P. Ceroni, M. Maestri, V. Vicinelli, *Curr. Opin. Chem. Biol.*, 2003, **7,** 657-665; (b) A. E. Hargrove, S. Nieto, T. Zhang, J. L. Sessler, E. V. Anslyn, *Chem. Rev.*, 2011, **111,** 6603-6782; (c) K. S. Wimbush, W. F. Reus, W. G. van-der Wiel, D.

N. Reinhoudt, G. M. Whitesides, C. A. Nijhuis, A. H. Velders, *Angew. Chem. Int. Ed*., 2010, **49,** 10176-10180; (d) M. D. Pluth, R. G. Bergman, K. N. Raymond, *Acc. Chem. Res*., 2009, **42**, 1650-1659; (e) B. Escuder, J. F. Miravet, J. A. Saez, *Org. Biomol. Chem.*, 2008, **6**, 4378-4383.

2. (a) G. M. Whitesides, J. P. Mathias, C. T. Seto, *Science*, 1991, **254,** 1312-1319; (b) A. Langner, S. L. Tait, N. Lin, R. Chandrasekar, M. Ruben, K. Kern, *Angew. Chem., Int. Ed.*, 2008, **47,** 8835-8838; (c) S. Stepanow, R. Ohmann, F. Leroy, N. Lin, T. Strunskus, C. Wo, K. Kern, *ACS Nano,* 2010, **4**, 1813-1820; (d) A. Theobald, N. S. Oxtoby, M. A. Phillips, N. R. Champness, H. P. Beton, *Nature*, 2003, **424,** 1029-1031; (e) Y. Xie, X. Wang, R. Huang, W. Qi, Y. Wang, R. Su, Z. He, *Langmuir*, 2015, **31,** 2885-2894.
3. (a) J. Sebestík, M. Reinis, J. Jezek, Biomedical Applications of Peptide-, Glyco- and Glycopeptide Dendrimers, and Analogous Dendrimeric Structures. *Springer Vienna*, 2012, 115-129; (b) D. A. Tomalia, H. M. Brothers II, L. T. Piehler, H. D. Durst, D. R. Swanson, *Proc. Natl. Acad. Sci. USA*, 2002, **99**, 5081-5087; (c) A. Theodore, T. A. Betley, J. A. Hessler, A. Mecke, M. M. B. Holl, B. G. Orr, S. Uppuluri, D. A. Tomalia, Jr. J. R. Baker, *Langmuir*, 2002, **18**, 3127-3133; (d) T. Faal, P. T. Wong, S. Tang, A. Coulter, Y. Chen, C. H. Tu, Jr., J. R. Baker, Sk. Choi, M. A. Inlay, *MolBiosys*, 2015, 783-790; (e) M. H. Li, Sk. Choi, P. Leroueil, Jr., J. R Baker, *ACS Nano*, 2014, **8**, 5600-5609; (f) A. Witte, A. Leistra, P. T. Wong, S. Bharathi, K. Refior, P. Smith, O. Kaso, K. Sinniah, Sk. Choi, *J. Phys. Chem. B*, 2014, **118**, 2872-2882; (g) K. Manthiram, Y. Surendranath, A. P. Alivisatos, *J. Am. Chem. Soc.*, 2014, **136**, 7237-7240; (h) D. Bracha, R. H. Bar-Ziv, *J. Am. Chem. Soc.*, 2014, **136**, 4945-4953; (i) S. Chen, M. Schulz, B. -D. Lechner, C. Appiah, W. H. Binder, *Polym. Chem.*, 2015, **6**, 7988-7994.
4. (a) M. A. C. Broeren, B. F. M. Waal, M.H. P. Van Genderen, H. M. H. F. Sanders, G. Fytas, E.W. Meijer, *J. Am. Chem. Soc.*, 2005, **127**, 10334-10343; (b) M. W. P. L. Baars, A. J. Karlsson, V. Sorokin, B. F. W. De Waal, E. W. Meijer, *Angew. Chem. Int. Ed*., 2000, **39,** 4262-4265; (c) U. Boas, S. H. M. Sontjens, K. J. Jensen, J. B. Christensen, E. W. Meijer, *ChemBioChem*, 2002, **3**, 433-439; (d) M. A. C. Broeren, J. L. J. V. Dongen, M. Pittelkow, J. B. Christensen, M. H. P. V. Genderen, E. W. Meijer, *Angew. Chem. Int. Ed*., 2004, **43,** 3557-3562; (e) D. Banerjee, M. A. C. Broeren, M. H. P. van Genderen, E. W. Meijer, P. L. Rinaldi, *Macromolecules*, 2004, **37,** 8313-8318; (f) D. de Groot, B. F. M. de Waal, J. N. H. Reek, A. P. H. J. Schenning, P. C. J.

Kamer, E. W. Meijer, P. W. N. M. van Leeuwen, *J. Am. Chem. Soc.*, 2001, **123,** 8453-8458.

5. (a) A. J. Cruz-Cabeza, J. Bernstein, *Chem. Rev.*, 2014, **114**, 2170-2191; (b) J. V. Barth, *Surf. Sci.*, 2009, **603**, 1533-1541.
6. (a) A. Dey, S. Bera, K. Biradha, *Cryst. Growth and Des.*, 2015, **5,** 318-325; (b) S. Roy, K. Biradha, *Cryst. Growth Des*., 2013, **13,** 3232-3241.
7. R. Castelcean, *Chem. Soc. Rev.*, 2010, **39**, 3675-3685.
8. (a) A. Tarai, J. B. Baruah, *CrystEngComm*, 2015, **17,** 2301-2309; (b) A. Tarai, J. B. Baruah, *CrystEngComm*, 2016, **18**, 298-308.
9. (a) P. M. Collins, *Chem. Commun.*, 1966, 164-165; (b) A. V. Afonin, I. A. Ushakov, D. V. Pavlov, A. V. Ivanov, A. I. Mikhalov, *Magn. Reson. Chem.*, 2010, **48**, 685-692; (c) H. Rosemeyer, G. Toth, B. Golankiewicz, Z. Kazimierczuk, W. Bourgeois, U. Kretschmer, H. P. Muth, F. Seela, *J. Org. Chem.*, 1990, **55,** 5784-5790.
10. (a) F. J. Ekstrom, C. Astot, Y. P. Pang, *Clin. Pharmacol. Ther.*, 2007, **82**, 282-293; (b) A. P. Guimaraes, T. C. C. Franca, T. C. Ramalho, M. N. Renno, E. F. F. da Cunha, K. S. Matos, D. T. Mancini, K. Kuca, *J. Appl. Biomed.*, 2011, **9**, 163-171.
11. A. Tarai, J. B. Baruah, *Cryst. Growth Des.*, 2016, **16,** 126-135.
12. (a) E. A. Bruton, L. Brammer, F. C. Pigge, C. B. Aakeroy, D. S. Leinen, *New J. Chem.*, 2003, **27**, 1084-1094; (b) C. B. Aakeroy, A. M. Beatty, D. S. Leinen, *Cryst. Growth Des.*, 2001, **1**, 47-52; (c) C. B. Aakeroy, A. S. Sinha, K. N. Epa, P. D. Chopade, M. M. Smith, J. Desper, *Cryst. Growth Des.*, 2013, **13**, 2687-2695.
13. (a) P. D. Beer, A. D. Keefe, *J. Organomet. Chem.*, 1989, **375**, C40-C42; (b) M. C. T. Fyfe, P. T. Glink, S. Menzer, J. F. Stoddart, A. J. P. White, D. J. Williams, *Angew. Chem. Int. Ed.*, 1997, **36**, 2068-2070; (c) C. -Y. Zheng, D. -J. Wang, L. Fan, J. Zheng, *Struct. Chem.*, 2013, **24**, 705-711.
14. (a) A. Mukherjee, S. Tothadi, G. R. Desiraju, *Acc. Chem. Res.*, 2014, **47,** 2514-2524; (b) C. B. Aakeroy, J. Desper, J. Urbina, *Chem. Commun.* 2005, 2820-2822; (c) C. B. Aakeroy, D. Salmon, *CrystEngComm* 2005, **7,** 439-448; (d) C. L. Seaton, T. Munshi, S. E. William, I. J. Scown, *CrystEngComm* 2013, **15,** 5250-5260; (e) S. Aitipamula, A. B. H. Wong, P. S. Chow, B. H. Tan, *CrystEngComm*, 2013, **15,** 5877-5887; (f) R. Dubey, G. R. Desiraju, *IUCrJ* 2015, **2,** 402-417; (g) S. Tothadi, P. Sanphui, G. R. Desiraju, *Cryst. Growth Des.* 2014, **14,** 5293-5302; (h) N. A. Mir, Dubey, R.; Desiraju, G. R. *IUCrJ*, 2016, **3**, 96-101.

15. (a) M. C. Etter, *Acc. Chem. Res.*,1990, **23,** 120-126; (b) M. C. Etter, J. C. McDonald, J. Bernstein, *Acta Crystallogr.*, 1990, **B46**, 256-262.
16. C. B. Aakeroy, T. K. Wijethunga, J. Desper, *CrystEngComm*, 2014, **16,** 28-31.
17. (a) E. Zangrando, M. Cassanova, E., Alessio, *Chem. Rev.*, 2008, **108**, 4979-5013; (b) V. Haridas, A. R. Sapala, J. P. Jasinski, *Chem. Commun.*, 2015, **51**, 6905-6908.
18. Y. Yang, F. Huang, C. F. Chen, M. Xia, Q. Cai, F. J. Qian, J. Xiang, *Sci. Rep.*, 2013, **3**, 10590.
19. (a) C. B. Aakeroy, J. Desper, J. Urbina, *Chem. Commun.*, 2005, 2820-2822; (b) G. Bolla, A. Nangia, *Chem. Commun.*, 2015, **51**, 15578-15581; (c) N. A. Mir, R. Dubey, G. R. Desiraju, *IUCrJ* 2016, **3,** 96-101; (d) C. L. Seaton, T. Munshi, S. E. William, I. J. Scown, *CrystEngComm*, 2013, **15,** 5250-5260.
20. (a) D. Buttar, M. H. Charlton, R. Docherty, J. Starbuck, *J. Chem. Soc. Perkin Trans. 2*, 1998, 763-772; (b) A. Nangia, *Cryst Growth and Des.*, 2008, **8**, 1079-1081.
21. J. W. Steed, J. L. Atwood, Spramolecular Chemistry, Wiley 2nd. ed. 2009, Chichester.
22. Z. Ma, S. Han, V. Ch. Kravtsov, B. Moulton, *Inorg. Chim. Acta*, 2010, **363**, 387-394.
23. M. Drancinsky, E. Prochazkova, J. Sebestik, P. Matejka, P. Bour, *J. Phys.Chem. B*, 2013, **117**, 7297-7307.
24. S. Jeyavijayan, M. Arivazhagan, *Indian J. Pure Appl. Phys.*, 2012, **50,** 623-632; (b) T. Stepanenko, L. Lapinski, M. J. Nowak, L. Adamowicz, *Vibrational Spectrosc.*, 2001, **26**, 65-82.

Chapter 3

Recognition of Aggregation Induced Emission Active Oxime Derivatives by Nitrogen Containing Compounds in Solid and Solution

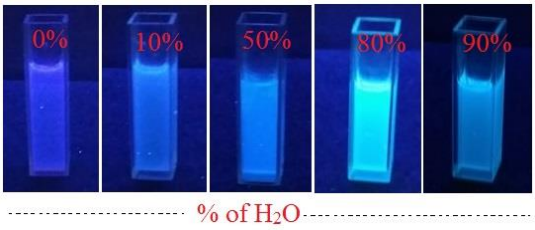

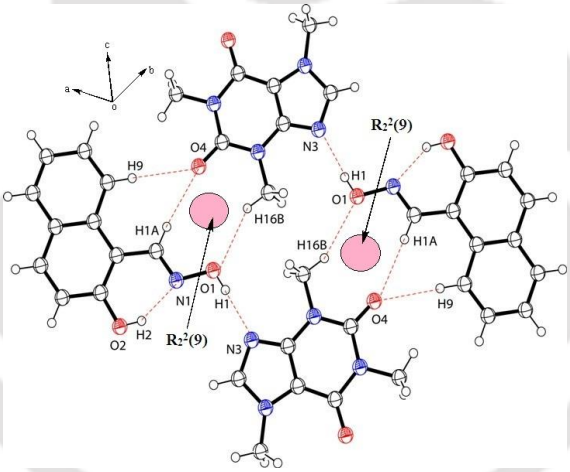

Some results have been reported in *Cryst. Growth Des*., 2016, **16**, 126-135.

3.1: Introduction

In supramolecular chemistry recognition of a molecule means specific and selective interactions between two or more molecules through non-covalent interactions to form a stable host-guest complex.[1] There are different approaches useful to study molecular recognition; spectroscopic titrations, determination of binding constants, thermodynamic parameters, morphology study and crystal engineering are some conventional means. Generally, properties of host-guest complexes are different from the original properties associated with individual host or guest molecules.[2] On the other hand, while a host molecule interact with a specific guest molecule significant and distinguishable signal transductions may take place. Among various spectroscopic tools fluorescence spectroscopy is a very sensitive process.[3] The advantage of the fluorescence emission is reflected on large intensity or wavelength shifts due to change in weak interactions among hosts, guests, host-guest, and solute-solvent interactions.[4] The changes in emission on host-guest binding passes through different mechanisms as photo-induced electron transfer (PET),[5] excited state intramolecular proton transfer (ESIPT),[6] forster resonance energy transfer (FRET),[2] internal charge transfer (ICT),[7] chelation enhanced fluorescence (CHEF)[8] etc. Among them photo-electron transfer mechanism is one of the very conventional mechanism which results in enhancement or quenching of emission.[5] On the other hand, exciplex and excimer formation are also common to cause changes in the emission of aromatic molecules.[9] The conventional fluorescence processes contributing to emission changes are shown in **scheme 3.1**. There are also other mechanisms such as aggregation induced emission that contribute to fluorescence changes.[10] Aggregation induced emission (AIE) enhancement as well as quenching are common phenomenon of fluorophoric compounds that can easily form aggregates.[10]

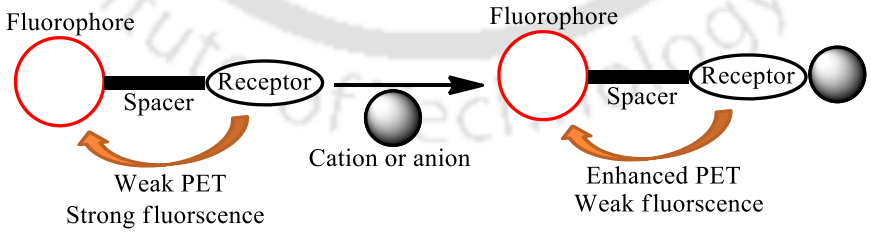

Scheme 3.1: Emission changes through photo-induced electron transfer (PET) mechanism.

Generally, π-stacked compounds cause fluorescence quenching but in AIE active fluorophores the fluorescence enhances under appropriate conditions with or without interactions with a substrate participating in aggregation. Molecules that show AIE emission are useful in various fields such as optoelectronics, sensors, probes.[11]

Interplay of weak interactions and conformations of a fluorophore play important roles in aggregation induced emission.[12] The mechanistic aspect of AIE are related to weak interactions and factors like conformational changes, geometrical changes, self-assembling, weak interactions, orbital symmetry.[13] Fluorescence properties of naphthalene derivatives are utilized to recognize *cis*- or *trans*-isomers[14] and biologically important metal ions.[15] Fluorescence emissions of certain hydroxy-aromatic imines are influenced by supramolecular environments due to keto-imine inter-conversion.[16] Quaternary ammonium salts influence fluorescence properties of hydroxy-aromatic compounds.[17] These literatures suggest possibilities to suitably arrange molecules through hydrogen bonds to achieve aggregation induced emission from compounds having naphthalene unit tethered or directly connected to a unit for weak interactions such as hydrogen bonds.[18] In this regard, hydroxy-aromatic oximes are suitable to form inter or intra molecular hydrogen bonds involving hydroxy-groups as well as to act as templates for π-interactions. Interplay of the weak interactions involving hydroxy-groups on hydroxy-aromatic aldoximes as seen in chapter 2 alters the hydrogen bonding patters of oxime counterparts. These occur upon change of position on a ring or increase in the number of hydroxy-groups attached to an aromatic ring. It is also an established fact that 2-hydroxynaphthalene derivatives[19] are fluorescent due to excited state intra-molecular proton transfer process. In the case of 2-hydroxynaphthalene oxime this is due to the possibility of oxime-quinoid form shown in **Fig. 3.1a**.

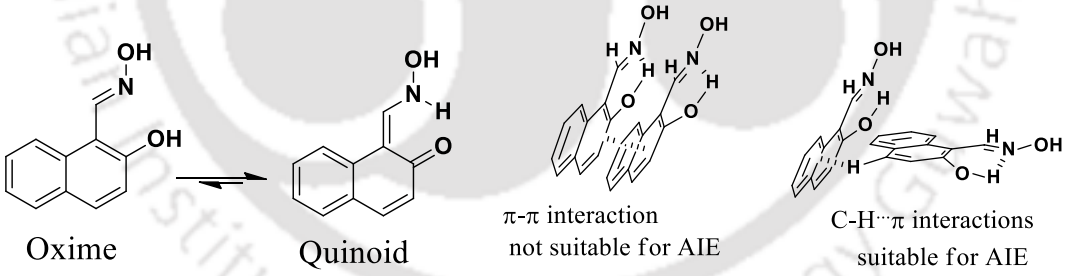

Figure 3.1: (a) Oxime-quinoid forms and (b) Two different arrangements of aromatic rings of 2-hydroxynaphthalene oxime (**2.1.1**), one is suitable for quenching of fluorescence and other is for AIE.

Due to these points, there are scopes to study the fluorescence of 2-hydroxynaphthalene derivatives through modulation of such non-covalent weak interactions. Reason to choose such molecules for structural and fluorescence emission study is explained with the two possible stacking arrangements among 2-hydroxynaphthalene oxime derivative (**2.1.1**) shown in **Fig. 3.1b**.

The molecule 2-hydroxynaphthaldoxime shown in **Fig. 3.1b** has set of disc-like naphthalene molecules that may aggregate in parallel arrangements which are favourable arrangement to cause quenching of fluorescence as observed in aromatic fluorophores with π-stacking. This kind of quenching is known as Foster quenching process.[20] But an arrangement involving C-H···π interactions as shown in **Fig. 3.1b** may be suitable for aggregation induced emission.[21] It is also well known fact that non-covalently linked self-assemblies of fluorescent oxime molecules show interesting optical properties.[22]

In this chapter we have studied structural and emission properties of different hydroxy-aromatic oximes to understand their self-assemblies, molecular recognition and signal transduction properties.

3.2: Aggregation induced emission (AIE) of 2-hydroxynaphthaldoxime (2.1.1)

Oxime **2.1.1** shows solvatochromism behaviour in different solvent such as DMSO, DMF, DMA, THF, MeOH, acetonitrile and EtOH. But the fluorescence emission intensity of oxime **2.1.1** is different in each solvent. A strong emission was observed at 392 nm (**Fig. 3.2a**) upon excitation at 315 nm in DMSO solvent whereas in presence of other solvent it showed very weak emission at 392 nm. The emission at 392 nm in different solvents is due to excited state proton transfer. The exceptional high intensity of fluorescence emission observed from a solution in DMSO was due to higher basicity of DMSO helping proton transfer in excited state.[23]

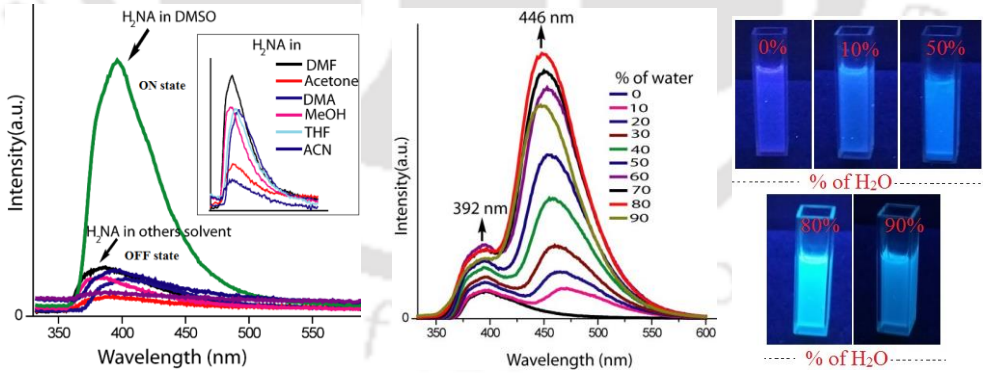

(a) (b) (c)

Figure 3.2: (a) Emission spectra of oxime **2.1.1** (10^{-4} M) in solvents (inset is expanded spectra other than the one recorded in DMSO), (b) Emission spectra of oxime **2.1.1** (10^{-4} M) in solvents comprising of different proportions of DMSO and water (λ_{ex} = 315 nm) and (c) fluorescence emission (under UV light) observed by naked eyes.

Oxime **2.1.1** in DMSO solvent shows a drastic change in fluorescence emission upon addition of water was due to its higher basicity induce proton transfer. A new emission peak

at 446 nm was observed on addition of water to a solution of the oxime **2.1.1** in DMSO (**Fig. 3.2b**). The intensity of the new emission peak at 446 nm was increased with amounts of added water to the solution and it continuously increased till the volume of water was 80% with respect to DMSO. The new emission peak appearing at higher wavelength is attributed to aggregation induced emission based on the literature on similar effect on emission spectra to show emission at higher wavelength on addition of water in related compounds.[24] It may be noted that certain 2-naphthol tethered Schiff bases show fluorescence emissions due to excited state intramolecular proton transfer (ESIPT).[25] In present case while growing the new AIE peak at 446 nm, it is also observed at intensity of emission peak at 392 nm due to ESIPT was enhanced upon adding water. Thus, the present example provided scope to study effect of water on ESIPT as well as on the generation of aggregation induced emission by adding water to a solution of it. Furthermore the crystal structure of the compound is known[26] hence there is a scope to correlate packing pattern of the compound with fluorescence in solid state. To a solution of oxime **2.1.1** in DMSO upon addition of water the AIE peak at 446 nm and ESIPT at 392 nm increase simultaneously. Upon excitation by UV-light the changes in emission intensities are noticeable naked eyes as shown in **Fig. 3.2c**. The oxime **2.1.1** is insoluble in pure water; hence it was not possible to record spectra of this compound in pure water. Similar trend in fluorescence spectral changes were observed in solutions of 2-hydroxynaphthaldoxime in other solvents such as methanol and tetrahydrofuran (THF), methanol upon addition of water. The fluorescence emissions in these two solvents at 392 nm were significant. There was also drastic increase in intensity of the new peak at 446 nm on addition of water in each case. Clear differences in enhancement of peak at 392 nm by water in different solvents were observed. This is attributed to the fact that, added water to other solvents enhanced ESIPT. Due to inherent basicity of DMSO, ESIPT occurred without water. Upon addition of water ESIPT (ON state) is not significantly affected relative to the solutions of oxime **2.1.1** in other solvents. But in each case, aggregation induced emission occurred at 446 nm irrespective of the solvents under consideration.

Dynamic light scattering study of a solution of oxime **2.1.1** in DMSO and mixture of solvents DMSO-H_2O (1:9, v/v) showed average particle size in each case to be different. In pure DMSO the average particle size was 561.2 nm with polydispersity 0.643; whereas average particle size was 623.5 nm with polydispersity 0.265 in 90 % water with 10 % DMSO solvent (**Fig. 3.3a**).

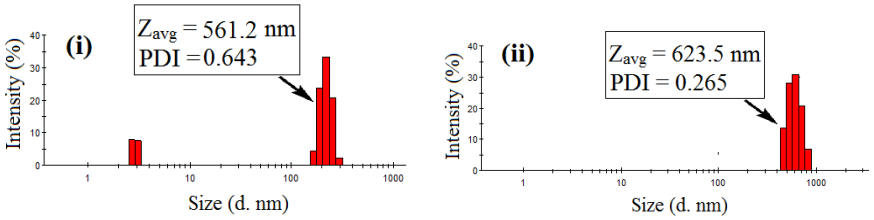

(a)

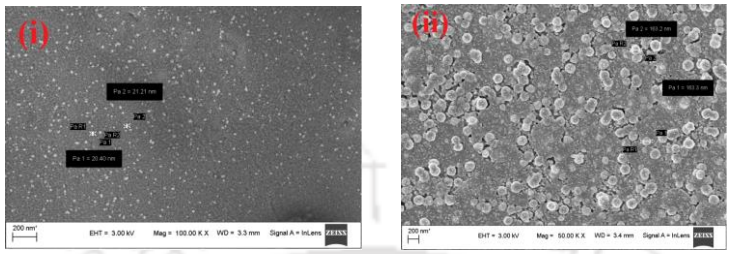

(b)

Figure 3.3: (a) Dynamic light scattering (DLS) based particle size and (b) FESEM images (by drop caste method) of oxime **2.1.1** from (i) DMSO and (ii) DMSO-H_2O (1:9, v/v) mixed solvent. Average particles size in **Fig. b** is (i) 26.2 nm and (ii) 163.2 nm.

These result showed that aggregate formed by oxime **2.1.1** in pure DMSO was different from mixed solvents of DMSO and water. In DMSO oxime **2.1.1** aggregated as relatively smaller average size particles than that in DMSO-H_2O (1:9, v/v) mixed solvent. Similar result was found from Field Emission Scanning Electron Microscope (FESEM) studies, which are shown in **Fig. 3.3b**. The images were indicative of the changes in the sizes of the particles in DMSO and in mixed solvent of water and DMSO. ^{1}H-NMR titration was performed by adding different amounts of D_2O to a solution of oxime **2.1.1** in DMSO-d_6 (**Fig. 3.4**). As the D_2O concentration was increased in solution of the compound in DMSO-d_6, the exchangeable OH proton appearing at chemical shift 11.53 ppm disappeared. There was no significant shift of the chemical shifts of the aromatic protons other than the proton labelled as b in **Fig. 3.4**.

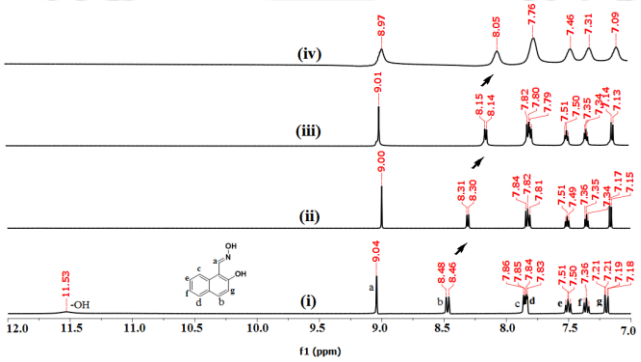

Figure 3.4: ^{1}H-NMR (600 MHz) spectra of oxime **2.1.1** in (i) DMSO-d_6, (ii) 20 % D_2O, (iii) 40% D_2O and (iv) 50% D_2O (aromatic regions are given for clarity).

^{1}H-NMR signal for hydrogen of N=CH of **2.1.1** appeared at 9.04 ppm, it was slightly shifted but the shift was not significant. Only drastic change in chemical shift position of the proton b was observed. The proton b originally appeared as a doublet of doublet 8.48 ppm which was shifted to 8.08 ppm (marked by arrows in **Fig. 3.4**).This shift is correlated to weak interactions involving concerned C-H bond between the oxime molecules caused by the changes in concentrations of D_2O in the medium. The contribution of hydrogen bond with water to the weak interactions helped the molecules to organise such that self-assembly had C-H$\cdots\pi$ interactions (**Fig. 3.1b**). The ^{1}H NMR spectra recorded in different solvents pointed out that the solvents not only influenced the chemical shifts of exchangeable OH protons, but also effected the CH=N proton. The trend in chemical shift ($\delta_{CH=N}$) of this proton was acetonitrile-d_3 > methanol-d_4 > dimethylsulphoxide-d_6. This has been attributed to the interactions of the solvents with labile OH changing the C=N character slightly. This could be a reason that the ESIPT is dependent on solvent as propensity to stabilise imine structure was guided by proton exchange process at the excited state. On the other hand, the aromatic C-H proton *b* appeared at 8.48, 8.26, 8.10 ppm in dimethylsulphoxide-d_6, acetonitrile-d_3, methanol-d_4 respectively. The rest of the peaks were not affected to show significant differences.

We have extended the study to examine the solid state self-assemblies of the compounds to correlate fluorescence properties of oximes **2.1.1** and **2.1.2** with anticipation that solid and solution property are cause difference in recognising of various guest molecules. We attempted crystallisation of these oxime derivatives in presence of different nitrogen containing molecules or nitrogen containing API molecules (Active Pharmaceutical Ingredient) such as 4,4'-bipyridine (44'-bipy), hexamethylenetetramine (HMTA), caffeine and theophylline.

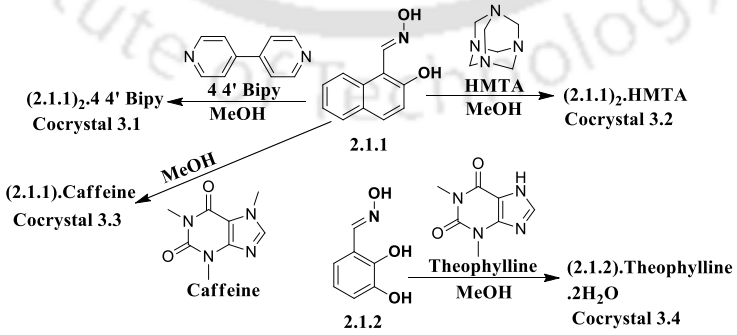

Scheme 3.2: Synthesis of different cocrystals of oxime derivatives **2.1.1** and **2.1.2**.

The oxime **2.1.1** formed cocrystals with 44'-bipy, HMTA and caffeine namely cocrystals **3.1**, **3.2** and **3.3** having composition (**2.1.1**)$_2$.44'-bipy, (**2.1.1**)$_2$.HMTA and (**2.1.1**).caffeine

respectively. But no cocrystal of **2.1.1** with theophylline was obtained whereas oxime **2.1.2** yielded cocrystal with theophylline having composition (**2.1.2**).theophylline.$2H_2O$ (**Scheme 3.2**).

3.3: Structural descriptions of cocrystals 3.1-3.4

Aakeröy's group had established various synthons of oximes and their cocrystals.[27] Moreover, available green synthetic methods for preparation of oximes make these class of molecules more easily amenable for constructions of new assemblies with future prospects in material sciences.[28] Due to the directional nature of hydrogen bonds there are large scopes for different conformations of hydroxyaromaticaldoximes or in their host-guest complexes in solid state to construct new synthons.[27] Concept of synthons[29] for designed synthesis in crystal engineering[30] put forward by Desiraju has left large scope to analyze different synthons of aromaticaldoximes in varieties of hydrogen bonded assemblies.[31] Generally aldoximes form assemblies having $R^2_2(8)$ homosynthon[27] as shown in **Fig. 3.5a** but introduction of an hydroxy-group to the aromaticaldoximes such as in 2-hydroxyphenylaldoxime[26] changes self-assemblies. In hydroxyphenylaldoxime $R^4_4(10)$ heterosynthons as illustrated in **Fig. 3.5b** were observed due to competition of phenolic O-H group contributing to self-assembly. Thus it is of interest to know about synthons in poly aromaticaldoximes and polyhydroxyaromaticaldoximes.

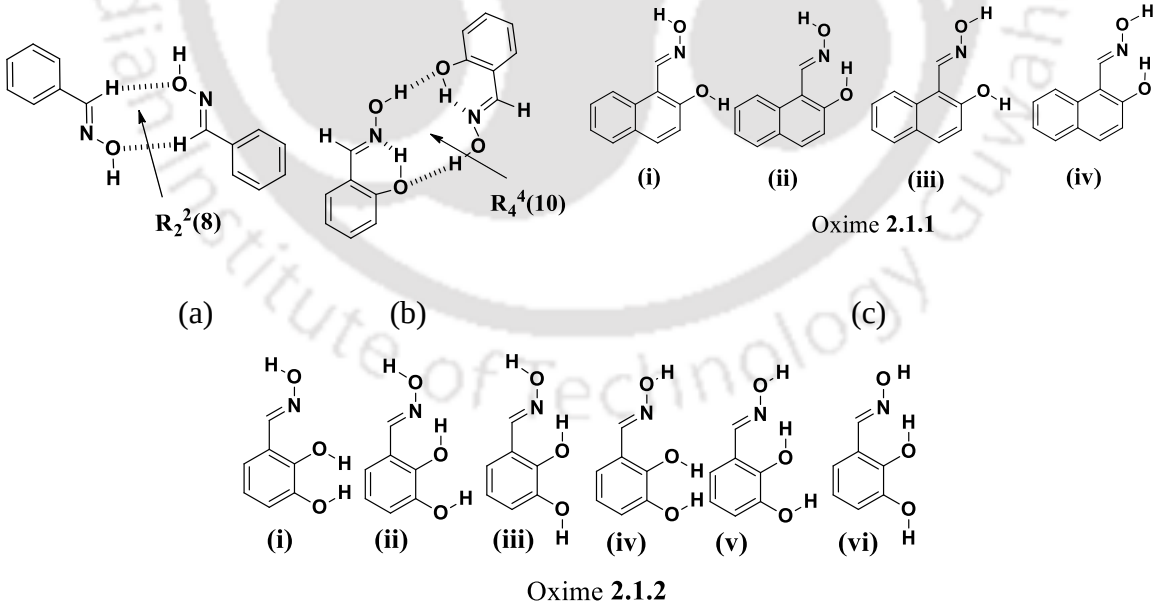

Figure 3.5: (a) Homosynthon observed in aldoximes and (b) Heterosynthon observed in 2-hydroxyphenylaldoxime. Orientations of active hydrogen atoms in (c) **2.1.1** and (d) **2.1.2**.

These compounds would differ in their respective packing pattern due to presence of the polyaromatic rings or the additional hydroxy groups to participate in weak non-covalent interaction schemes. Two such examples are 2-hydroxynapthaldoxime (**2.1.1**) and 2,3-dihydroxyphenylaldoxime (**2.1.2**) for which different possibilities of arranging hydroxyl groups as shown in **Fig. 3.5c** and **3.5d**. Upon crystallisation of the various solutions of oxime **2.1.1** with 4,4'-bipyridine or HMTA or caffeine or theophylline cocrystals from three out of four such independent combinations were formed. Accordingly cocrystals **3.1-3.3** namely; (**2.1.1**)$_2$.44'-bipy, (**2.1.1**)$_2$.HMTA and (**2.1.1**).caffeine respectively (**scheme 3.2**) were isolated but failed to get crystals from the solutions of oxime **2.1.1** with theophylline. The interesting feature is that the cocrystals **3.1-3.3** of oxime **2.1.1** with the 4,4'-bipyridine and the HMTA were in 2:1 molar ratio whereas with caffeine it was a 1:1 cocrystal. It may be mentioned that polymorphic forms and solvates of caffeine with anthranilic acid was reported in literature,[32] moreover same host molecule can form cocrystals with caffeine and theophylline differing in molar ratios.[33] Water bridged assemblies in the cocrystals of caffeine or theophylline was also reported.[34] Hence in anticipation of hydrated cocrystals in the present study the powder XRD patterns of the bulk samples of the cocrystals were examined to ascertain their phase purity. All the cocrystals **3.1-3.3** of oxime **2.1.1** reported in this study are anhydrous and no solvated cocrystals were observed from any of the solvent used for crystallisation. But the cocrystal of oxime **2.1.2** with theophylline was a dihydrate. The structures of the cocrystal **3.1** of oxime **2.1.1** with 4,4'-bipyridine or HMTA possesses similar O-H···N interactions as shown in **Fig. 3.6a-6b**; but the packing patterns of both cocrystals widely differ. Packing patterns are guided by O-H···N, C-H···O and C-H···π interactions in the cocrystals **3.1**, but in case of cocrystals **3.2**, the packing pattern is guided by O-H···N, C-H···O, C-H···π and π···π interactions. Here π···π interaction play a crucial role which differ the packing patterns of both cocrystals. Parent oxime **2.1.1** has a conformer II shown in **Fig. 3.5c**, whereas in the cocrystals oxime part has structure of conformer I of **Fig. 3.5c**.

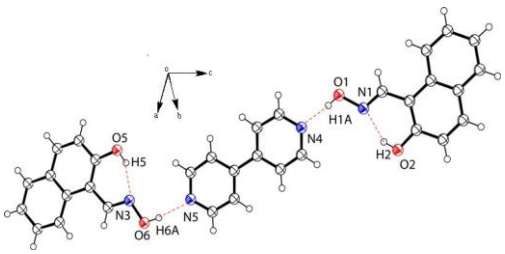

(a)

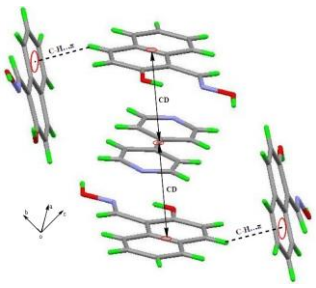

(d)

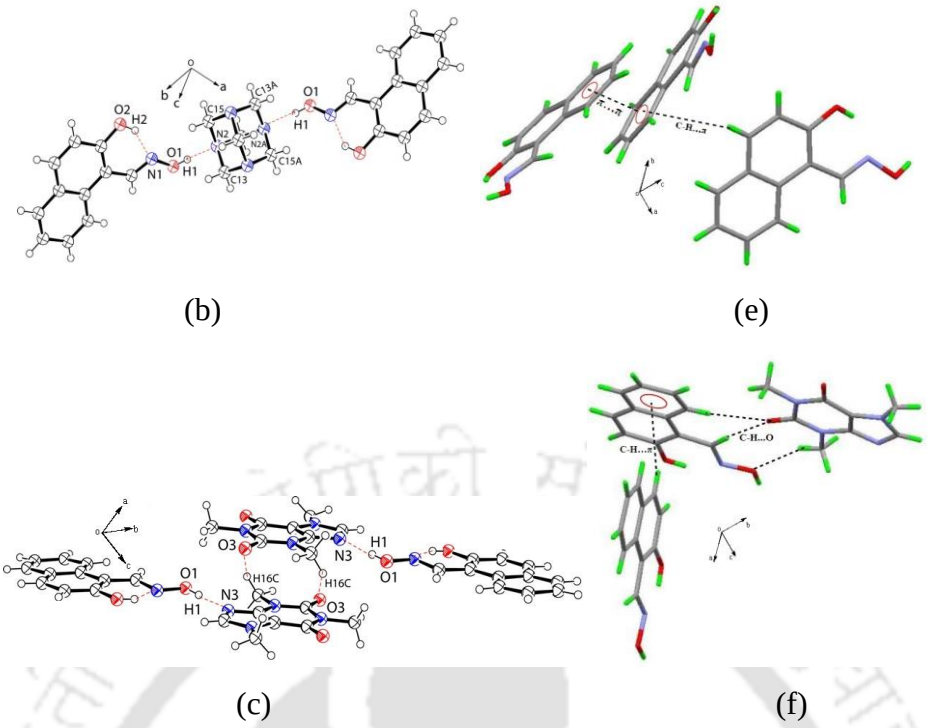

Figure 3.6: Cocrystals of oxime **2.1.1** with (a) 4,4'-bipyridine, (b) hexamethylenetetramine and (c) caffeine. (d-f) Different weak interactions present in the packing patterns of the three cocrystals **3.1-3.3** (30% thermal ellipsoids in ORTEP diagram).

In general the structures of the three cocrystals **3.1-3.3** of oxime **2.1.1** may be suggested to be composed of oxime **2.1.1** molecules held by weak interactions with respective coformers in two different ways. In the first two cocrystals **3.1** or **3.2** are based on either a planar or a non-planar bridging unit anchoring two guest molecules through O-H···N hydrogen bonds. Whereas, the third cocrystal **3.3** has two guest molecules stacked holding two oxime **2.1.1** molecules (**Fig. 3.6c**). The prominent weak interactions of these cocrystals **3.1-3.3** are shown in **Fig. 3.6d-3.6f** and the hydrogen bond parameters of the oxime **2.1.1**, **2.1.2** and cocrystals **3.1-3.4** are given as **Table 3.1**. For other hydrogen bonds and short contacts parameters of oxime **2.1.1**, **2.1.2** and cocrystals **3.1-3.4** please see page 228 of appendix.

Table 3.1: Prominent hydrogen bond parameters of oxime **2.1.1**, **2.1.2** and cocrystals **3.1-3.4**.

Oximes/cocrystals	D-H···A	d_{D-H}(Å)	$d_{H\cdots A}$ (Å)	$d_{D\cdots A}$(Å)	∠D−H···A (°)
2.1.1	O(2)-H(2)···O(1) [-x,-1/2+y,1/2-z]	0.82	1.99	2.7808(19)	163
2.1.2	O(1)-H(1)···O(2) [-x,-y,-z]	0.82	2.13	2.866(5)	149
	O(3)-H(3)···O(1) [x,1/2-y,1/2+z]	0.82	2.16	2.833(5)	139
3.1	O(1)-H(1A)···N(4) [1-x,1/2+y, 1/2-z]	0.82	1.93	2.738(3)	169
	O(3)-H(3)···N(6) [-1+x, y, z]	0.82	1.93	2.739(3)	171
	O(6)-H(6A)···N(5) [1+x, 1/2-y, -1/2+z]	0.82	1.88	2.694(3)	173
3.2	O(1)-H(1)···N(2) [3/2-x,y,-1/2+z]	0.82	1.97	2.767(2)	163
	C(12)-H(12A)···O(2) [1-x,-y,1+z]	0.97	2.50	3.315(3)	141
	C(12)-H(12B)···O(2) [x,y,1+z]	0.97	2.50	3.315(3)	141

3.3	O(1)-H(1)···N(3) [-1+x,y,-1+z]	0.82	1.96	2.777(4)	176
	C(1)-H(1A)···O(4) [1-x,-y,-z]	0.93	2.46	3.386(3)	175
	C(9)-H(9)···O(4) [1-x,-y,-z]	0.93	2.53	3.460(3)	175
3.4	N(3)-H(3A)···O(1) [-1/2+x,1/2-y,1/2+z]	0.86	2.47	3.107(18)	131
	O(7)-H(7A)···N(2) [-1/2+x,1/2-y,-1/2+z]	0.88	1.99	2.879(19)	177
	N(3)-H(3A)···O(2) [-1/2+x,1/2-y,1/2+z]	0.86	2.05	2.838(18)	152

Slow evaporation of the respective solution (in methanol, dimethylsulphoxide, acetonitrile, ethanol etc.) of oxime **2.1.2** with 4,4'-bipyridine or hexamethylenetetramine or caffeine or theophylline yielded crystals from only one of these combinations namely from the solution of oxime **2.1.2** with theophylline (**Scheme 3.1**). The cocrystal **3.4** was a dihydrate of 1:1 cocrystal between oxime **2.1.2** and theophylline. Crystal structure of the cocrystal **3.4** has showed that it formed self-assemblies through hydrogen bonds with the water molecules to hold the oxime and the coformer molecules. Self-assembly of the cocrystal **3.4** has shown in the **Fig. 3.7**, the dimeric sub-assemblies that were present in the packing pattern of the parent structure of oxime **2.1.2** were disrupted. In the cocrystal **3.4** each aldoxime molecule forms water assisted assemblies with theophylline. One O-H bond of water molecule hydrogen bonds with the carbonyl oxygen atom of theophylline and the oxygen atom of the same water molecule connects to the oxime O-H bond of oxime **2.1.2**. The carbonyl group of theophylline is involved in a bifurcated hydrogen bond by connecting the phenolic O-H group located at 2-position of the aromatic ring and these interactions yield a $R^3_3(7)$ motif which holds the key to the formation of this three component cocrystal.

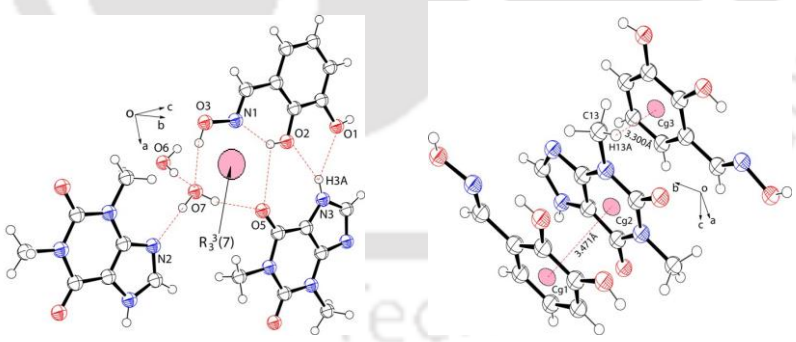

(a) (b)

Figure 3.7: (a) Self-assemblies of hydrated cocrystal **3.4** of oxime **2.1.2** with theophylline. (b) π-π interactions between oxime **2.1.2** and theophylline (30% thermal ellipsoids).

The conformation of oxime **2.1.2** due to the orientations of the active hydrogen atoms of oxime in the cocrystal **3.4** is different with respect to the conformation observed in the parent compound. Parent oxime has the conformation IX of the **Fig. 3.5d**, but the cocrystal possesses the conformation X presented in the **Fig. 3.5d**. Interesting feature of this cocrystal

3.4 is the stacking interactions between theophylline and oxime **2.1.2** molecules. The molecules show π-stacking (**Fig. 3.7b**) between the rings with a separation distance 3.471 Å, which is conducive to have strong π-π interactions.[35] This interaction originates from the dipolar nature of the theophylline molecule which has an electron-deficient ring to interact with electron-rich ring of oxime **2.1.2**. On the other hand, the analysis of the structure of oxime **2.1.1** shows that it is comprised of $R^2_2(8)$ type homo-synthons formed by aldoxime involving C-H···O interactions. But oxime **2.1.2** formed a $R^4_4(10)$ $O\text{-}H_{aldoxime}....O\text{-}H_{hydroxy}$ hetero-synthons similar to the hetero-synthons found in the structure of the 2-hydroxyphenylaldoxime (please refer to chapter 2).[26] Comparing these synthons with the structures of different cocrystals of these compounds it may be concluded that the nitrogen containing heterocycles disrupts the original oxime synthons altogether to generate new hetero-synthons.

The FT-IR spectrum of oxime **2.1.1** has O-H stretching frequency at 3331 cm^{-1}. This peak shifts to higher wave number in the case of each cocrystal and appear in the region 3445-3460 cm^{-1}. Such shifts are attributed to the formation of hydrogen bonds in the cocrystals through the oxime OH and nitrogen atom of the respective coformer. O-H frequency of oxime **2.1.1** is shifted in cocrystals **3.1-3.3** at 3445 cm^{-1}, 3446 cm^{-1} and 3460 cm^{-1} respectively. This trend is reflected in the O-H···N bond parameters, as the caffeine has the higher donor-acceptor distance with the largest O-H···N angle among the three.

The oxime **2.1.1** has C=N stretching at 1632 cm^{-1}, and the cocrystals **3.1-3.3** of oxime **2.1.1** shows characteristic C=N bond stretching in the region of 1628-1658 cm^{-1}. This shows that the C=N bond is intact in the cocrystals and the nitrogen atom of this unit do not directly participate in formation of hydrogen bond. Cocrystal **3.3** has a strong C=O stretching at 1704 cm^{-1} from the carbonyl group of the caffeine part. A similar carbonyl stretching absorption in the IR spectra of the cocrystal **3.4** (**2.1.2.theophylline.2H_2O**) appears at 1706 cm^{-1}.

3.4: Recognition of oxime 2.1.1 or 2.1.2 in solid and solution state by nitrogen containing compounds

To ascertain the suitable wavelengths for fluorescence excitation studies, UV-vis spectra of solid samples of each cocrystal **3.1-3.4** were recorded. They show broad absorption in the region of 350-400 nm originating from the host oxime molecules. The broadening arises due to a proximity broadening effect from self-interacting molecules in the vicinity in solid-state. The absorbance peaks of individual oxime molecules and the corresponding cocrystals are given in the **Fig. 3.17**. On the basis of the observation on the UV-vis absorption shown by the oximes and cocrystals, the emission spectrums in each case was investigated by exciting at

368 nm (**Fig. 3.8**). The oxime **2.1.1** exhibited a broad emission band around 475-530 nm. The cocrystal **3.3** of oxime **2.1.1** with caffeine showed a relatively higher fluorescence emission intensity with a shift toward a shorter wavelength, whereas the cocrystals **3.1-3.2** of oxime **2.1.1** with 4,4′-bipyridine or hexamethylenetetramine (HMTA) are weakly fluorescent.

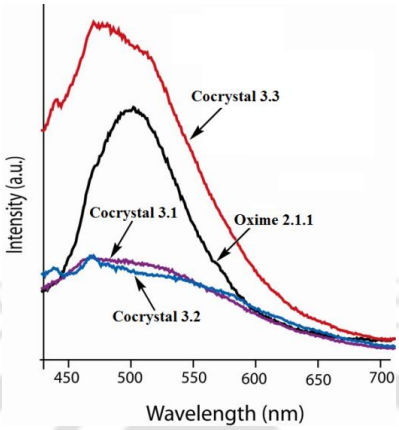

Figure 3.8: Fluorescence emission spectra of oxime **2.1.1** and cocrystals **3.1-3.3** of solid samples. (Excitation in each case at 368 nm).

This suggests that upon cocrystal formation with 4,4′-bipyridine or HMTA the fluorescence of oxime **2.1.1** gets quenched by the respective coformer. In these experiments uniformity in preparation of samples were ensured by carrying out experiments with similar amounts, and the fluorescence was measured under identical conditions. It is a well-known fact that fluorescence of organic compounds in the solid state depends on the architecture of crystal packing,[36] and π···π stacking interactions cause fluorescence quenching.[37] On the other hand it was also suggested that C-H···π interactions can contribute to fluorescence changes.[38]

Table 3.2: Different cocrystal of oximes and fluorescence properties

Coformers	Oxime **2.1.1**	Fluorescence behavior* In solid-state	Oxime **2.1.2**	Fluorescence behavior[#] In solution
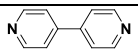	2:1 cocrystal **3.1**	Non-fluorescent	No cocrystal was obtained	Quenching
	2:1 Cocrystal **3.2**	Non-fluorescent	No cocrystal was obtained	Quenching
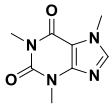	1:1 Cocrystal **3.3**	Fluorescent	No cocrystal was obtained	Quenching
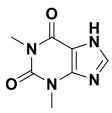	No cocrystal was obtained	……..	1:1:2 Cocrystal **3.4**[$]	Quenching

* In solution no change. # No cocrystal was obtained, hence solid state fluorescence not measured. $ Nonfluorescent in solid

Jones and co-workers[39] showed that in stacking arrangements guided by weak interactions with leading to face-to-face aromatic interactions of chromophoric compounds with other coformers can tune the fluorescence properties. Aggregation such as H-aggregate formed by assembling of the same type of molecules on top of each other results in shifting of fluorescence to shorter wavelength, whereas a J-aggregate does it in an opposite manner.[40] The difference of fluorescence in the present cocrystals illustrated in **Table (3.2** and **3.3)** can be attributed to the respective packing patterns. Close analyses of the structures of oxime **2.1.1** and cocrystals have shown that self-assemblies of the oxime molecules are guided by several weak interactions. The weak interactions like O-H···N, C-H···O, and O-H···O in oxime **2.1.1** and cocrystals are shown in **Fig. 3.9a-d**. The packing pattern of each cocrystal is different from the packing pattern observed in the parent oxime. From the crystal densities among these cocrystals, the cocrystal **3.1** has a lower crystal density than the cocrystal **3.2**, and both have several weak interactions, but the latter has additional π···π interactions. Since the cocrystals **3.1** and **3.2** are in 1:2 molar ratio, this factor contributes to cause a large difference between the packing patterns of these two crystals with respect to the packing pattern of the cocrystal **3.3** of oxime **2.1.1** with caffeine which has a 1:1 molar ratio of host and coformer.

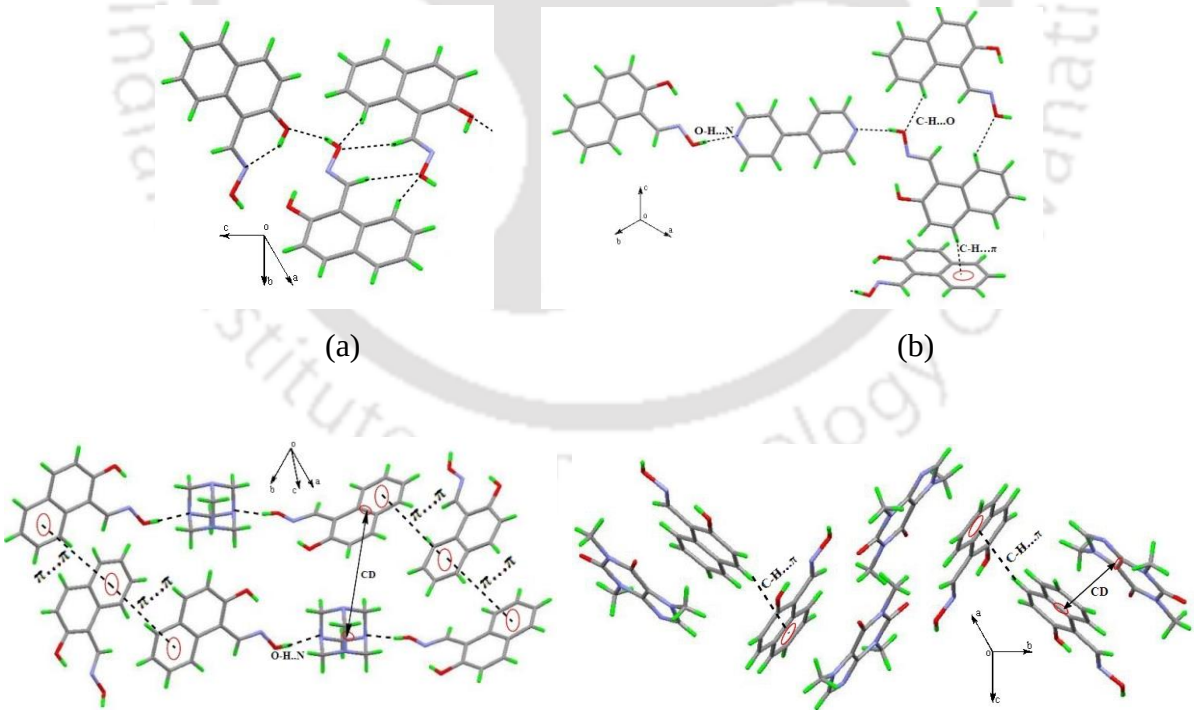

(a) (b)

(c) (d)

Figure 3.9: Packing diagram of (a) oxime **2.1.1**, (b) Cocrystal **3.1**, (c) Cocrystal **3.2** and (d) Cocrystal **3.3**

The caffeine molecules in the cocrystal **3.3** are positioned on top of the oxime **2.1.1** molecule, and the center core distance is 3.718 Å. The carbonyl group of caffeine molecule forms a hydrogen bond with oxime. The naphthalene unit of oxime **2.1.1** in cocrystal **3.3** is involved in C-H···π interaction with the neighboring naphthalene unit present in the lattice. To have effective π···π stacking interactions between two planar fluorophoric π-units, they should have a parallel arrangement, and each of the interacting ring must be positioned on top of each other, whereas to have a center-dot C-H···π interaction the interacting C-H of one ring should appear at a position which is perpendicular to the central point of the other ring.

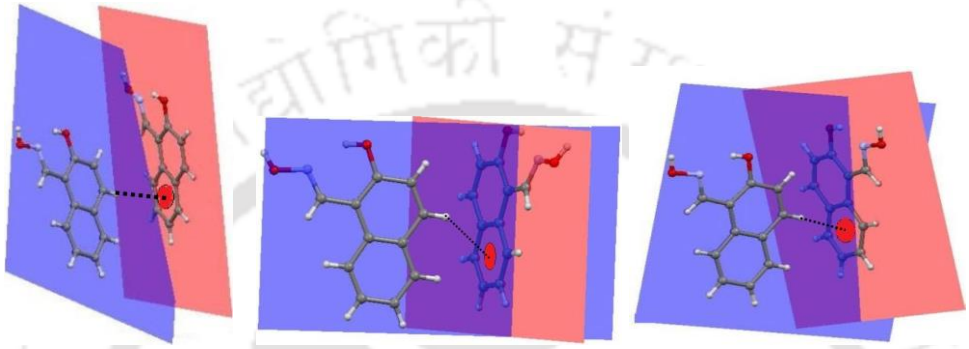

(a) (b) (c)

Figure 3.10: The stacking of the fluorphoric **2.1.1** in the cocrystals (a) **3.1** [∠67.17°], (b) **3.2** [∠76.06°], and (c) **3.3** [∠86.12°]. In each case the angle between the planes of oxime **2.1.1** is shown in the third bracket.

Thus, we examined the arrangements of the fluorophoric π-units, namely, **2.1.1** in the cocrystals, and compared with the packing pattern of the oxime **2.1.1**. The angles between such planes are shown in **Fig. 3.10a-c**. In the case of cocrystal **3.3** it is ∠86.12°, which is very close to a perpendicular arrangement and hence has the least π···π stacking interactions but it has better C-H···π interactions among the others. On the other hand, the parent compound does not have similar C-H···π interactions, but the packing has rings at a slightly translated parallel position to each other, so that a highly effective π···π stacking interaction is not feasible. Further analysis of other two cocrystals show a less than 90° angle between the planes suggesting the positions of the rings to be nonparallel. However, the deviations from perpendicular positions are not enough to cut off the effective C-H···π interactions. Such qualitative analysis is not good enough to form an overall picture to explain the fluorescence changes. It can easily explain fluorescence changes in three cases leaving aside the 4,4′-bipyridine cocrystals **3.1** as an exception. Complete segregation of oxime **2.1.1** molecules in the cocrystal **3.3** with caffeine leads to monomer type arrangements to show emission with

higher intensity with a slight blue shift. This may be compared to J-aggregate (oxime **2.1.1**) transformed to an arrangement of discrete monomers (**2.1.1** in caffeine cocrystal **3.3**).[40]

Table 3.3: Characteristic fluorescence properties of oxime **2.1.1** and cocrystals in solid state

Oxime/cocrystals	λ_{ab} (nm)	λ_{ex} (nm)	λ_{em} (nm)	(Quantum yields) Φ_F
2.1.1	390 nm	368 nm	510 nm	0.095
3.3	395 nm	368 nm	468 nm	0.052
3.1	397 nm	368 nm	470 nm	0.15
3.2	395 nm	368 nm	470 nm	0.14

The parent compound can be considered as a partially quenched state, and the π-stacking induced by the HMTA cocrystal **3.2** causes quenching of the fluorescence in the case of the cocrystal with HMTA. To provide even a qualitative explanation of the solid state fluorescence property of the cocrystal **3.1** with 4,4′-bipyridine, an explanation has to account for three symmetry independent host molecules, which is difficult. Nonetheless we can suggest with the data available from the experiments that parallel stacking of the pyridine ring of bipyridine units could be the major factor contributing to the quenching of fluorescence in this particular case.

To ascertain interactions between the oxime **2.1.1** with the coformers in solution, the fluorescence emission spectra at 392 nm of solution of oxime **2.1.1** by adding coformers were recorded. No changes in fluorescence emissions were observed by these coformers in solution (**Fig. 3.11a**). Hence these results suggest that dilute solution interactions between the respective coformer and oxime **2.1.1** are too weak to detect. Similar results are reflected in the ^{1}H-NMR titrations between selected coformers with oxime **2.1.1** where no change in peak positions was observed (**Fig. 3.18-3.19**). These results clearly demonstrate that the optical properties of the oxime **2.1.1** is not affected by coformers in solution but in solid coformers play a major role to either enhance or reduce the intensities and positions. The oxime **2.1.2** is non-fluorescent, and its cocrystal with theophylline is also non-fluorescent in the solid state. But oxime **2.1.2** shows fluorescence in solution, whereas the respective solution of oximes **2.1.1** or **2.1.2** in DMSO-H_2O mixture has an emission peak at 392 and 387 nm upon excitation at 315 and 270 nm, respectively. The fluorescence emission of oxime **2.1.2** at 387 nm was gradually decreased upon addition of theophylline as shown in the **Fig. 3.11b**. Similar changes were also observed at pH = 3 and pH = 10 (**Fig. 3.20**). A relatively higher quenching effect was observed at pH = 3 as compared to pH = 10; hence it may be suggested that it is the exchange of hydrogen between the hydrogen bond donor and acceptor that holds

the key to the quenching of fluorescence. The differences observed in fluorescence by theophylline have generated interest to screen aldoximes by theophylline. For this purpose fluorescence spectra of oximes **2.1.1** (at 392 nm), **2.1.2** (at 387 nm), **2.1.3** (at 356 nm) and 2-hydroxyphenylaldoxime (at 354 nm) (the latter two compounds were taken as screening compounds) were monitored by adding a solution of theophylline to the respective oxime solution (**Fig. 3.11a-d**). Addition of theophylline to a respective solution of **2.1.1** or **2.1.3** or 2-hydroxyphenylaldoxime did not cause fluorescence spectral changes.

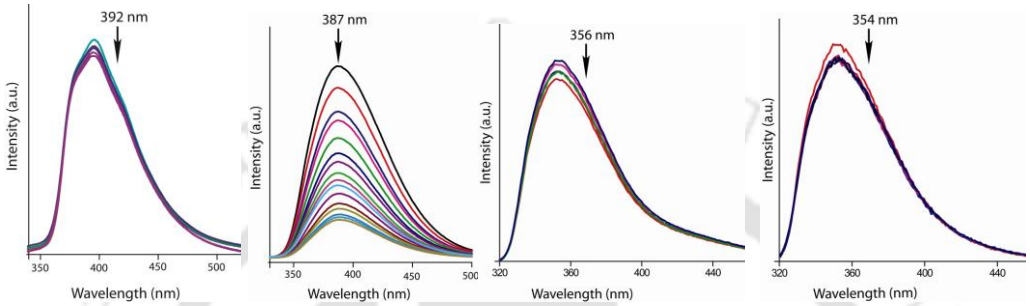

(a) (b) (c) (d)

Figure 3.11: Changes in the fluorescence emission spectra of oximes (a) **2.1.1**, (b) **2.1.2**, (c) **2.1.3** and (d) 2-hydroxyphenylaldoxime (10^{-5} M solution in DMSO-H_2O) on addition of theophylline (10^{-5} M in DMSO-H_2O, 10µl aliquot).

These oximes were not recognized by theophylline to cause changes in their respective emission spectra. We have also examined the effect on fluorescence emission of oxime **2.1.2** by adding a solution of caffeine or 4,4′-bipyridine or HMTA; in each case fluorescence quenching was observed, but these compounds could not change the fluorescence emissions of oxime **2.1.1** or **2.1.3** or 2-hydroxyphenylaldoxime. Even though all four coformers resulted in fluorescence quenching of oxime **2.1.2** in the solution state, only one of them (theophylline) formed a cocrystal. Hence the solution study clearly tells that careful choice of nitrogen aromatic compounds can screen a series of oximes to identify a particular oxime **2.1.2**. Theophylline is the most important metabolite of caffeine, and it is found in tea, coffee, cocoa beans, and chocolate.[41] Theophylline forms cocrystal with phenols,[42] carboxylic acids,[43] and various other organic molecules.[44] On the other hand, caffeine has the ability to form cocrystals with carboxylic acids[45] and nicotinamides.[46] Since the quenching process is very selective to oxime **2.1.2** by coformers; it is attributed to the effect of the 3-hydroxy group which is participating in proton transfer in this particular example. Three other examples of oximes lack a hydroxy group at the 3-position with respect to the oxime functional group of the aromatic ring.

It may be noted that among the oximes **2.1.1**, **2.1.2**, **2.1.3** and 2-hydroxyphenylaldoxime, only oxime **2.1.2** has the distinction of having a hydroxy group at the 3-position of the ring with respect to the oxime functional group. This hydroxy-group is not in conjugation with the oxime functional group through the intervening π-electrons of the ring. This makes the fluorescence behavior of this oxime different from the other three oximes in the presence of coformers in solution.

3.5: Conclusions

The intensities of fluorescence emission of oxime **2.1.1** due to ESIPT in dimethylsulphoxide as well as aggregation induced emission occurring at 446 nm increased with amount of water. Depending on solvent the water induced AIE reaches maximum intensity at different ratio of water added to solution. The C-H···π interactions involving the C-H located at the *para* position with respect to oxime group of the naphthalene ring is suggested to be facilitate formation of aggregate suitable to show AIE. The compound remains in aggregated form in non-aqueous solution but the particle size of aggregates increase on addition of water. And also two different hydrogen bonded cyclic motifs of oxime **2.1.1** and **2.1.2** are modified by coformers. In solution 4,4′-bipyridine, HMTA and caffeine cause quenching of fluorescence of oxime **2.1.2**, suggesting that interactions of these compounds with **2.1.2** involve the hydroxyl group at the 3-position, whereas in the theophylline cocrystal **3.4** all the hydrogen bonding sites are used, causing complete quenching of fluorescence. On the other hand, the cocrystals of oxime **2.1.1** with 4,4′-bipyridine or HMTA or caffeine were formed easily. π-Stacking plays the decisive role to increase or decrease fluorescence intensity of **2.1.1** and cocrystals of **2.1.1** in the solid state. In solution no interactions of **2.1.1** with coformers were observed. By virtue of such properties different oximes can be distinguished by the fluorescence technique either in the solid state or in solution. The differences in fluorescent behavior among aldoximes could be exploited for their identification and separation.

3.6: Experimental section

Synthesis and characterization of cocrystals 3.1-3.4:

Oximes **2.1.1-2.1.3** and 2-hydroxyphenylaldoxime were prepared from their respective hydroxyaromatic aldehyde reacting them with hydroxylamine hydrochloride in the presence of base by followed reported procedure[47] as mention in Chapter-2. Cocrystals were obtained by slow evaporation of a solution of the respective aldoxime and the guest molecules with respective molar ratio in methanol.

Cocrystal 3.1: Isolated yield: 76 %. ^{1}H-NMR (600 MHz, DMSO-d_6): 11.52 (s, 1H), 11.14 (s, 1H), 9.03 (s, 1H), 8.72 (d, J = 5.4 Hz, 3H), 8.47 (d, J = 8.4 Hz, 1H), 7.85 (m, 4H), 7.50 (t, J = 7.2 Hz, 1H), 7.35 (t, J = 6.8 Hz, 1H), 7.20 (d, J = 9 Hz, 1H). IR (KBr, cm^{-1}): 3445 (bs), 1631 (s), 1596 (s), 1537 (w), 1467 (m), 1405 (m), 1369 (w), 1344 (w), 1307 (m), 1276 (s), 1239 (s), 1215 (s), 1183 (m), 1161 (w), 1145 (w), 1080 (w), 1062 (w), 1038 (s), 1023 (m), 999 (m), 940 (s), 880 (w), 825 (s), 799 (s), 776 (w), 744 (m), 671 (w), 645 (w), 620(s).

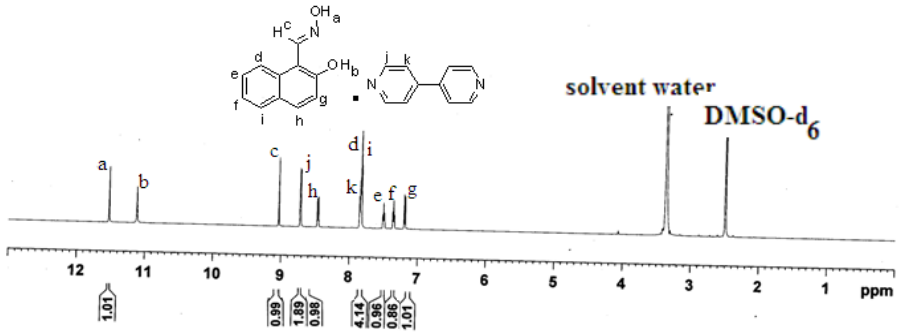

Figure 3.12: ^{1}H-NMR (600 MHz, DMSO-d_6) of cocrystal **3.1**.

Cocrystal 3.2: Isolated yield: 78 %. ^{1}H-NMR (600 MHz, DMSO-d_6): 11.50 (s, 1H), 11.10 (s, 1H), 9.03 (s, 1H), 8.47 (d, J = 8.4 Hz, 1H), 8.00 (s, 1H), 7.85 (t, J = 8 Hz, 2H), 7.51 (t, J = 7.2 Hz, 1H), 7.37 (t, J = 6.8 Hz, 1H), 7.20 (d, J = 9 Hz, 1H), 4.55 (s, 12H). IR (KBr, cm^{-1}): 3446 (bs), 2959 (w), 2924 (w), 2875 (w), 1628 (m), 1591 (s), 1525 (w), 1464 (s), 1424 (w), 1370 (m), 1348 (w), 1312 (s), 1276 (s), 1238 (s), 1227 (s), 1180 (m), 1163 (w), 1144 (w), 1083 (w), 1007 (s), 947 (w), 933 (s), 870 (m), 825 (w), 813 (s), 800 (s), 738 (s), 723 (m), 693 (s), 673 (m), 665 (m), 644 (m).

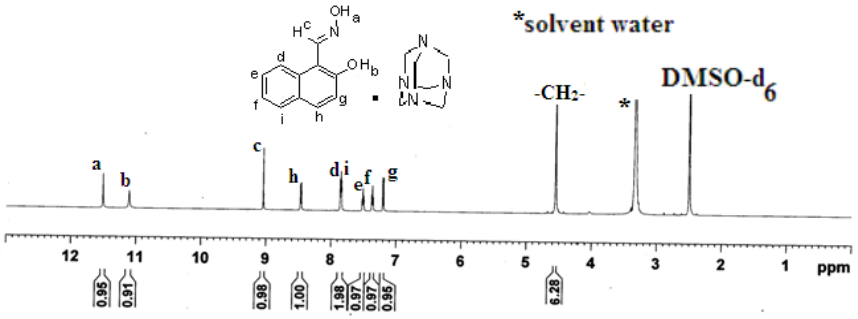

Figure 3.13: ^{1}H-NMR (600 MHz, DMSO-d_6) of cocrystal **3.2**.

Cocrystal 3.3: Isolated yield: 82%. ^{1}H-NMR (600 MHz, DMSO-d_6): 11.50 (s, 1H), 11.10 (s, 1H), 9.03 (s, 1H), 8.47 (d, J = 8.4 Hz, 1H), 8.00 (s, 1H), 7.85 (t, J = 8.4 Hz, 2H), 7.51 (t, J = 7.2 Hz, 1H), 7.37 (t, J = 6.8 Hz, 1H), 7.20 (d, J = 9 Hz, 1H), 3.87 (s, 3H), 3.41 (s, 3H), 3.21 (s, 3H). IR (KBr, cm^{-1}): 3460 (bs), 3003 (w), 2922 (w), 1704 (s), 1658 (s), 1593 (w), 1553 (s), 1496 (s), 1468 (m), 1407 (w), 1362 (w), 1326 (m), 1282 (s), 1240 (s), 1211 (w), 1181 (s),

1140 (w), 1037 (m), 1022 (m), 978 (w), 938 (s), 878 (w), 829 (s), 780 (m), 757 (w), 744 (s), 669 (m), 645 (m), 607 (m).

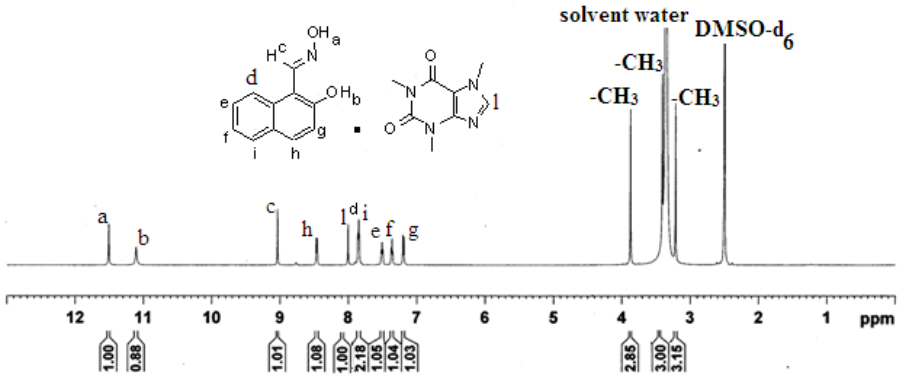

Figure 3.14: ^{1}H-NMR (600 MHz, DMSO-d$_6$) of cocrystal **3.3**.

Cocrystal 3.4: Isolated yield: 86%. ^{1}H-NMR (600 MHz, DMSO-d$_6$): 11.29 (s, 1H), 9.56 (s, 1H), 9.25 (s, 1H), 8.30 (s, 1H), 8.02 (s, 1H), 6.91 (d, J = 7.2 Hz, 1H), 6.79 (d, J = 8.4 Hz, 1H), 6.68 (t, J = 7.8 Hz, 1H), 3.44 (s, 3H), 3.23 (s, 3H). IR (KBr, cm^{-1}): 3479 (s), 3218 (bs), 1706 (s), 1650 (s), 1558 (s), 1505 (s), 1465 (w), 1440 (w), 1421 (w), 1385 (m), 1315 (m), 1259 (s), 1232 (s), 1190 (s), 1099 (w), 1058 (m), 994 (s), 959 (w), 933 (m), 849 (m), 780 (m), 764 (m), 741 (s), 711 (w), 654 (w), 620 (w), 505 (s).

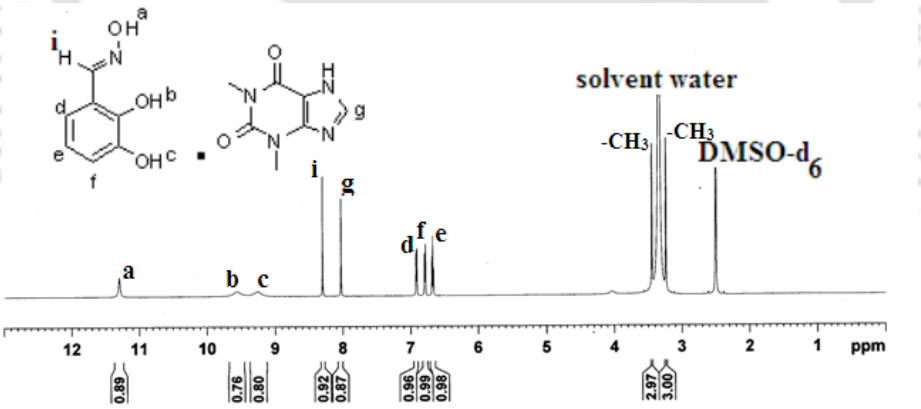

Figure 3.15: ^{1}H-NMR (600 MHz, DMSO-d$_6$) of cocrystal **3.4**.

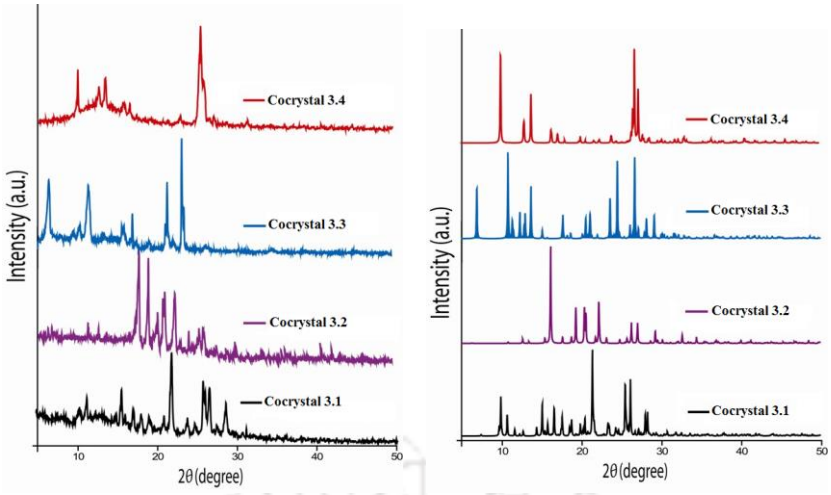

(a) (b)

Figure 3.16: PXRD of cocrystals **3.1-3.4**: (a) Experimental and (b) Simulated. Simulated PXRD pattern generated from cif file.

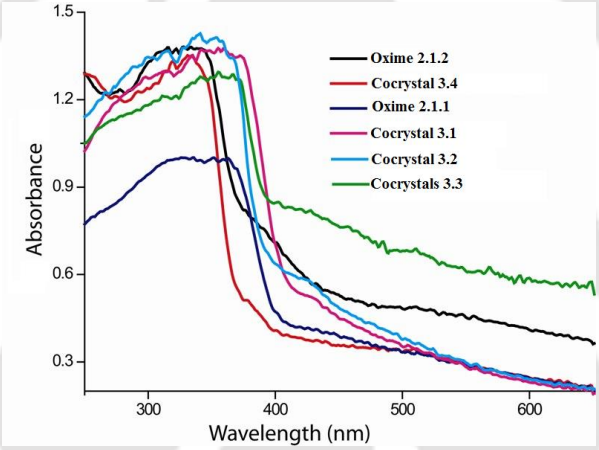

Figure 3.17: Solid state UV-visible spectra of the oximes **2.1.1-2.1.2** and cocrystals **3.1-3.4**.

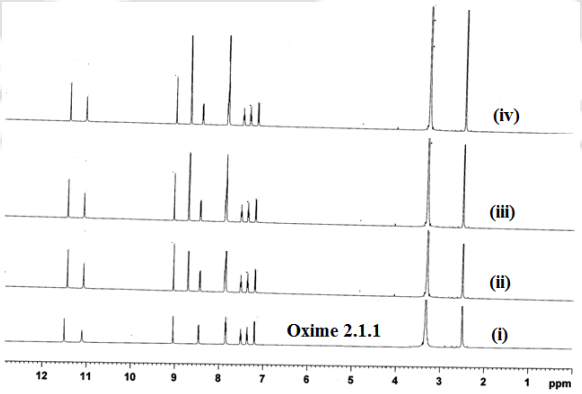

Figure 3.18: ^{1}H-NMR (DMSO-d_6) titration of oxime **2.1.1** upon addition (i) 0.0, (ii) 1.0 (iii) 2.0 and (iv) excess equivalents of 4,4'-bipyridine.

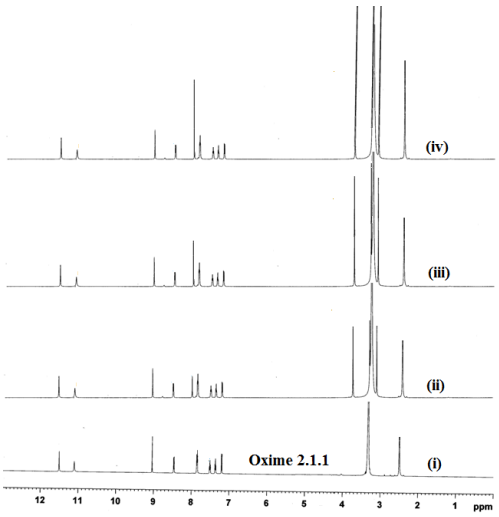

Figure 3.19: ^{1}H-NMR (DMSO-d_6) titration of oxime **2.1.1** upon addition (i) 0.0, (ii) 1.0, (iii) 2.0 and (iv) excess equivalents of caffeine.

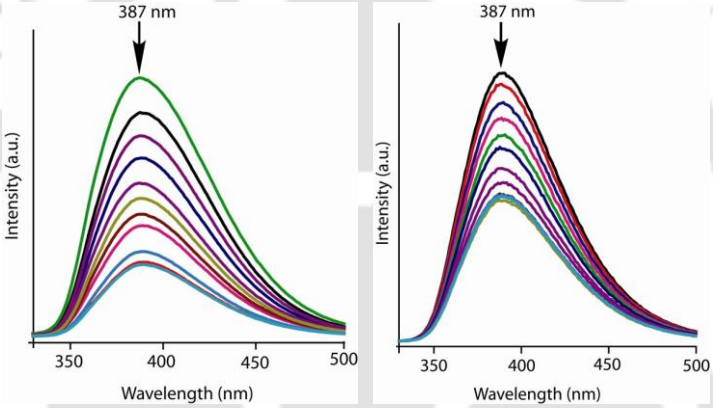

(a) (b)

Figure 3.20: Changes in fluorescence emission spectra of oxime **2.1.2** (10^{-5} M solution in DMSO-H2O) on addition of theophylline (10^{-5} M) at (a) pH 3 and (b) pH 10 respectively.

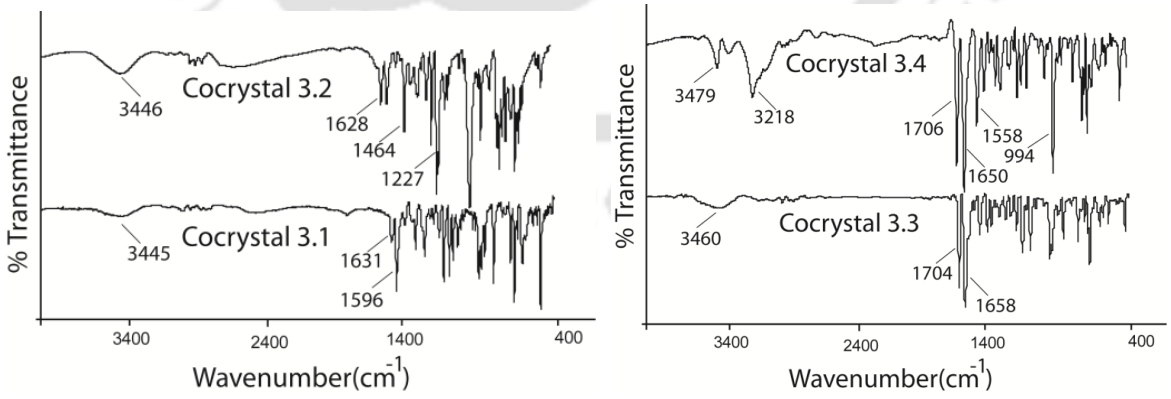

(a) (b)

Figure 3.21: FT-IR spectra of (a) cocrystals **3.1-3.2** and (b) cocrystals **3.3-3.4**.

3.7: References

1. H. Jiang, B. D. Smith, *Chem. Commun*., 2006, 1407-1409.
2. A. Tarai, J. B. Baruah, *Chemistry Select*, 2017, **2**, 10101-10106.
3. K. R. Murphy, C. A. Stedmon, D. Graeber, R. Bro, *Anal.Methods*, 2013, **5**, 6557-6566.
4. K. Santhosh, G. K. Grandhi, S. Ghosh, A. Samanta, *Pure Appl.Chem.*, 2013, **85**, 1451-1463.
5. (a) T. Kowalczyk, Z. Lin, T. V. Voorhis, *J. Phys. Chem. A*, 2010, **114**, 10427-10434; (b) P. Ashokkumar, V. T. Ramakrishnan, P. Ramamurthy, *J. Phys. Chem. A*, 2011, **115**, 14292-14299.
6. X. Bi, B. Liu, L. McDonald, Y. Pang *J. Phys. Chem. B*, 2017, **121**, 4981-4986.
7. L. He, B. Dong, Y, Liu, W. Lin, *Chem. Soc. Rev*., 2016, **45**, 6449-6461.
8. H. Lee, H. -S. Lee, J. H. Reibenspies, R. D. Hancock, *Inorg. Chem*., 2012, **51**, 10904-10915.
9. D. W. Cho, M. Fujitsuka, K. H. Choi, M. J. Park, U. C. Yoon, T. Majima, *J. Phys. Chem. B*, 2006, **110**, 4576-4582.
10. J. Mei, N. L. C. Leung, R. T. K. Kwok, J. W. Y. Lam, B. Z. Tang, *Chem. Rev*., 2015, **115**, 11718-11940.
11. (a) C. W. T. Leung, Y. Hong, S. Chen, E. Zhao, J. W. P Lam, B. Z. Tang, *J. Am. Chem. Soc*., 2013, **135**, 62-65; (b) D. Ding, K. Li, B. Liu, B. Z. Tang, *Acc. Chem. Res*., 2013, **46**, 2441-2453; (c) S. Li, S. M. Langenegger, R. Haner, *Chem. Commun*., 2013, **49**, 5835-5837; (d) J. Wang, J. Mei, R. Hu, J. Z. Sun, A. Qin, B. Z. Tang, *J. Am. Chem. Soc*., 2012, **134**, 9956-9966.
12. Y. Hong, J. W. Y. Lam, B. Z Tang, *Chem. Soc. Rev*.**,** 2011, **40**, 5361-5388.
13. J. Mei, Y. Hong, J. W. Y. Lam, A. Qin, Y. Tang, B. Z. Tang, *Adv. Mater*., 2014, **26**, 5429-5479.
14. S. Samanta, B. Nath, J. B. Baruah, *Inorg. Chem. Commun*., 2012, **22**, 98-100.
15. (a) N. Phukan, J. B. Baruah, *Inorg. Chem. Commun*., 2013, **37**, 89-92; (b) Y. K. Jang, U. C. Nam, H. L. Kwon, I. H. Hwang, C. Kim, *Dyes Pigments*, 2013, **99**, 6-13.
16. A. K. Das, S. Goswami, *Sens. Actuators B*, 2017, **245**, 1062-125.
17. A. Tarai, J. B. Baruah, *CrystEngComm*, 2015, **17**, 2301-2309.
18. H. Xiao, K. Chen, D. Cui, N. Jiang, G. Yin, J. W. R. Wang, *New J. Chem*., 2014, **38**, 2386-2393.

19. (a) R. B. Singh, S. Mahanta, S. Kar, N. Guchhait, *Chem. Phys*., 2007, **331**, 373-384; (b) I. S. K. Kerkines, I. D. Petsalakis, G. Theodorakopoulos, Jr. J Rebek, *J. Phys. Chem. A*, 2011, **115**, 834-840.
20. B. Wang, X. Wang, W. Wang, F. Liu, *J. Phys. Chem. C*, 2016, **120**, 21850-21857.
21. Y. Hong, J. W. Y. Lamand, B. Z. Tang, *Chem.Commun*., 2009, 4332-4353.
22. T. J. Dale, Jr. J. Rebek, *Angew. Chem., Int. Ed*., 2009, **48**, 7850-7852.
23. D. B. Smithrud, E. M. Sanford, I. Chao, S. B. Ferguson, D. R. Carcanague, J. D. Evanseck, K. N. Houk, F. Diederich, *Pure. Appl. Chem*., 1990, **62**, 2227-2236.
24. M. Pannipara, A. G. Al-Sehemi, A. Kalam, A. M. Asiri, *Optical Materials*, 2017, **72**, 442-446.
25. L. McDonald, J. Wang, N. Alexander, H. Li, T. Liu, Y. Pang, *J. Phys. Chem. B*, 2016, **120**, 766-772.
26. Z. Guo, L. Li, G. Liu, J. Dong, *Acta Cryst.* 2008, **64**, 568-569.
27. (a) A. M. Beatty, D. S. Leinen, C. B. Aakeroy, *Cryst. Growth Des*., 2002, **1**, 47-51; (b) C. B. Aakeroy, K. N. Epa, S. Forbes, J. Desper, *CrystEngComm.*, 2013, **15**, 5946-5949; (c) A. S. Sinha, K. N. Epa, P. D. Chopade, M. M. Smith, J. Desper, C.B. Aakeroy, *Cryst. Growth Des*., 2013, **13**, 2687-2695; (d) E. A. Bruton, L. Brammer, F. C. Pigge, C. B. Aakeroy, D. S. Leinen, *New J. Chem*., 2003, **27**, 1084-1094.
28. (a) C. B. Aakeroy, A. S. Sinha, K. N. Epa, C. L. Spartz, J. Desper, *Chem. Commun*., 2012, **48**, 11289-11291; (b) C. B. Aakeroy, A. S. Sinha, *RSC Adv*., 2013**,** **3**, 8168-8171.
29. G. R. Desiraju, *Angew. Chem. Int. Ed.*, 1995, **34**, 2311-2327.
30. (a) A. Dey, M. T. Kirchner, V. R. Vangala, G. R. Desiraju, R. Mondal, J. A. K. Howard, *J. Am. Chem. Soc*., 2005, **127**, 10545-10559; (b) J. A. R. P. Sarma, G. R. Desiraju, *Cryst. Growth Des*., 2002, **2**, 93-100; (c) T. S. Thakur, G. R. Desiraju, *Cryst. Growth Des*., 2008, **8**, 4031-4044.
31. D. J. Salmon, M. M. Smith, J. Desper, C. B. Aakeroy, *Cryst. Growth Des*., 2006, **4**, 1033-1042.
32. N. Madusanka, M. D. Eddleston, M. Arhagelskis, W. Jones, *Acta Crystallogr*., 2014, **B70**, 72-80.
33. A. Jacobs, F. M. A. Noa, *CrystEngComm*, 2015, **17**, 98-106.
34. B. Das, J. B. Baruah, *Cryst.Growth Des.*, 2011, **11**, 278-286.
35. C. A. Hunter, J. K. M. Sanders, *J. Am. Chem. Soc*., 1990, **112**, 5525-5534.
36. B. Kupcewicz, M. Malecka, *Cryst. Growth Des*., 2015, **15**, 3893-3904.

37. Q. Feng, M. Wang, B. Dong, C. Xu, J. Zhao, H. Zhang, *CrystEngComm*, 2013, **15**, 3623-3629.
38. Z. Zhang, Y. Zhang, D. Yao, H. Bi, I. Javed, Y. Fan, H. Zhang, Y. Wang, *Cryst Growth Des.*, 2009, **9**, 5069-5076.
39. D. Yan, A. Delori, G. O. Lloyd, T. Friscic, G. M. Day, W. Jones, J. Lu, M. Wei, D. G. Evans, X. Duan, *Angew. Chem. Int. Ed*., 2011, **50**, 12483-12486.
40. F.C. Spano, *Acc. Chem Res*., 2010, **43**, 429-439.
41. M. T. Jafari, B. Rezaei, M. Javaheri, *Food Chem*., 2011, **126**, 1964-1970.
42. (a) N. Schultheiss, M. Roe, S. X. M. Boerrigter, *CrystEngComm*, 2011, **13**, 611-619; (b) Z. -L. Wang, L. -H. Wei, *Acta Crystallogr*. *Sect. E*, 2007, **63**, o1681-o1682; (c) S. Chattoraj, L. Shi, C. C. Sun, *CrystEngComm*, 2010, **12**, 2466-2472; (d) B. Sarma, B. Saikia, *CrystEngComm*, 2014, **16**, 4753-4765.
43. H. Abourahma, J. M. Urban, N. Morozowich, B. Chan, *CrystEngComm*, 2012, **14**, 6163-6169.
44. (a) S. Aitipamula, A. B. H. Wong, P. S. Chow, R. B. H. Tan, *CrystEngComm*, 2014, **16**, 5793-5801; (b) A. Delori, P. T. A. Galek, E. Pidcock, M. Patni, W. Jones, *CrystEngComm*, 2013, **15**, 2916-2928.
45. S. Karki, T. Friscic, W. Jones, W. D. S. Motherwell, *Mol. Pharmaceutics*, 2007, **4**, 347-354.
46. J. Lu, S., Rohani, *Org. Process Res. Dev.*, 2009, **13**, 1269-1275.
47. A. Tarai, J. B. Baruah, *CrystEngComm*, 2015, **17**, 2301-2309.

Chapter 4

Part A: Transition Metal Complexes of Hydroxyaromatic Aldoximes and Their Interactions with Fluoride ions

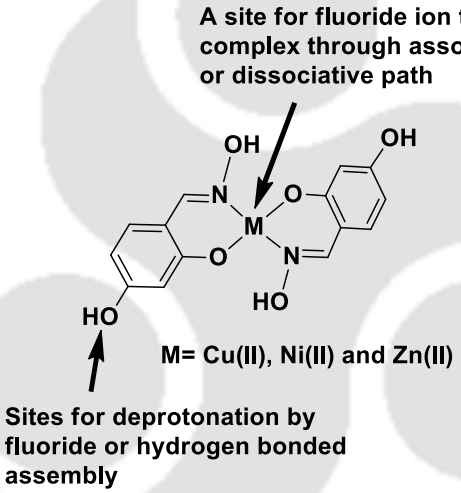

RSC Adv., 2015, **5**, 82144-82152.

4.1.1: Introduction

Chelation of metal ions by oximes and related ligands are of great interest for many years in the area of coordination chemistry.[1] Dimethylglyoxime (H_2DMG) is one such metal chelator, it used as reagent for the gravimetric analysis of nickel(II). Typically a bivalent nickel metal ion reacts with two equivalents of H_2DMG form a neutral $Ni(HDMG)_2$ complex (**Fig. 4.1.1a**).[2] Salicylaldoxime is another such ligand which was first used by Ephraim as a ligand for synthesis of square planar metal complexes with Ni(II), Pd(II) and Pt(II) metal ions.[3] Salicylaldoxime contains oxime or phenolic groups, can be single deprotonated at phenolic group or can be double deprotonated by loss of both the active hydrogen atoms from phenolic and oxime groups by base.

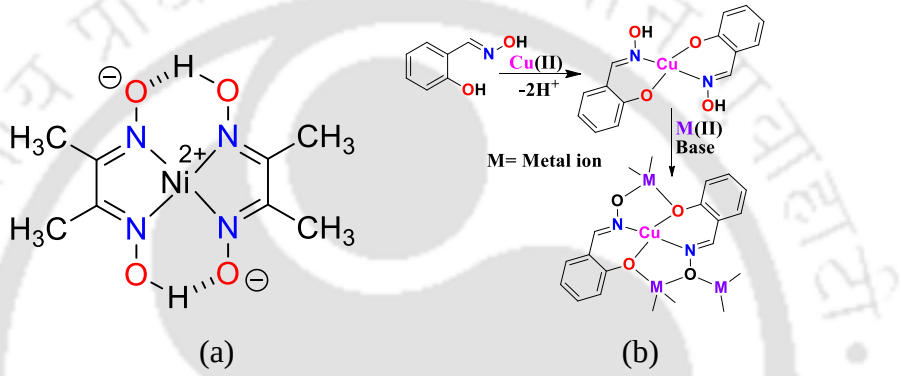

(a) (b)

Figure 4.1.1: (a) Nickel(II) dimethylglyoximate complex and (b) Formation of mono and mixed metal polynuclear copper(II) salicyloximate complexes.

Mono-deprotonation at the phenolic O-H group of salicylaldoxime forms pseudo-mononuclear metal complex (**Fig. 4.1.1b**). Such deprotonation of salicylaldoxime is very selectively caused by Cu(II) and Ni(II) metal ions over other metal ions such as Fe(III) or Mn(II). Therefore, the single deprotonated phenolic oximes are extensively used in extraction of Cu(II) or Ni(II) metal ions. Similar pseudo-mononuclear metal complexes of Zn(II), Pd(II) and Co(II) were reported. In these complexes hydrogen bonds between oximic and phenolic group exist.[4] Double deprotonation at oximic and phenolic groups provides opportunities to form polynuclear metal complexes with same metal or with different metal ions. Carboxylic acid or azide acts as bridge in certain metal such as Fe(III), Mn(III) and Co(II)-oxime complexes to form polynuclear metal complexes. Some polynuclear metal oximate complexes show interesting magnetic properties.[5] Metal chelate complexes of oximes provide avenues to prepare new supramolecular self-assemblies. To form such complexes free hydroxy-group or other functional groups that are attached to such ligands are utilised. Polyhydroxyaromatic oximes belong to such a category of ligands.

In those complexes may have free hydroxy groups for weak interactions or for further deprotonation to make new self-assemblies. Thus, such metal complexes of polyhydroxyaromatic aldoximes[6] (**Fig. 4.1.2**) have scopes to form different self-assemblies and utilisation of such complexes for signal transductions has general interest.

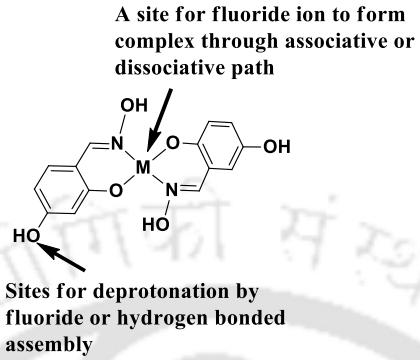

Figure 4.1.2: Sites for interaction with a basic ion such as fluoride with a *bis*-chelated metal complex of 2,4-dihydroxybenzaldoxime (Oxime **2.1.3**).

Bis-chelated metal-oxime complexes having fluorophoric or chromophoric groups have applications as sensor for detection of ions.[7] In this chapter we have chosen to study the metal complexes of polyhydroxy aromatic aldoximes with first-row transition metal ions to understand the self-assemblies and interactions of fluoride. Use of the metal complexes of the polyhydroxyaromatic aldoxime such as one shown in **Fig. 4.1.2** would have several possibilities to interact with fluoride ions as that of the free oximes as discussed in chapter 2. The possible site of interaction with fluoride ions on hydroxyaromaticoxime metal complex is shown in **Fig. 4.1.2**. With this background, we prepared a series of model complexes of 2,4-dihydroxybenzaldoxime (Oxime **2.1.3**) with divalent copper, nickel and zinc ions to explore their interactions with fluoride ions.

4.1.2: Synthesis of bivalent copper, nickel and zinc metal complexes of oxime 2.1.3

A series of divalent copper, nickel and zinc complexes of oxime **2.1.3** (Refer to chapter-2) were prepared by reacting oxime **2.1.3** with respective metal salts in different solvents as illustrated in **Scheme 4.1.1**. The copper complexes **4.1.1**-**4.1.4** have a general composition [Cu(**2.1.3**)$_2$].solvent [when solvent = DMF (**4.1.1**), DMA (**4.1.2**), DMSO (**4.1.3**) and 4,4'-bipyiridine (**4.1.4**)]. The two nickel complexes **4.1.5** and **4.1.6** has composition [Ni(**2.1.3**)$_2$].DMF and [Ni(**2.1.3**)$_2$] respectively. But the zinc complex **4.1.7** has one extra coordinating ligand 1, 3-bis(4 pyridyl)propane and it forms an octahedral zinc(II) complex.

These complexes **4.1.1-4.1.7** have been characterized by conventional spectroscopic tools and X-ray single crystal and powder diffraction techniques.

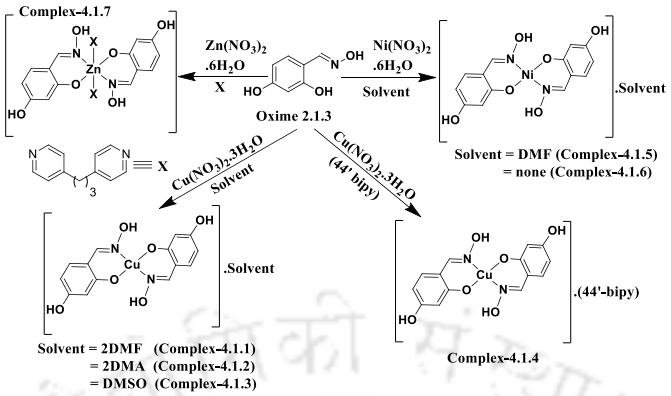

Scheme 4.1.1: Synthesis of transition metal complexes of oxime **2.1.3**.

Three different solvates of the copper complexes **4.1.1-4.1.3** have enabled us to understand the hydrogen bond directed assemblies involving the free hydroxy-group of the complex to guide the respective self-assemblies of these complexes formed as different solvates. And a guest 4,4'-bipyridine encapsulated copper complex **4.1.4** was synthesised to see the difference in self-assemblies of solvated copper complexes **4.1.1-4.1.3** and guest encapsulated copper complex **4.1.4**.

4.1.3: Structural descriptions of metal(II) complexes 4.1.1-4.1.7

The complexes **4.1.1-4.1.7** are *bis*-chelated complexes, their structures are similar to the common metal chelated salicyaldoxime complexes.[4] The copper complexes **4.1.1-4.1.4** have same core which varies with the solvent of crystallisation. Hydrogen bonded self-assemblies of the solvated copper complexes are shown in **Fig. 4.1.3.** The differences in each assembly arise due to the dissimilar complementary hydrogen bond forming abilities with the solvent molecule present in outer sphere of these complexes. The complex **4.1.1** has a dimethylformamide (DMF) molecule that forms a cyclic type hydrogen bonded assembly. Such cyclic hydrogen bonded structures involve two DMF molecules are held through O-H···O hydrogen bonds (**Fig. 4.1.3a**). The non-covalent self-assemblies of the complexes **4.1.2** and **4.1.3** have similarities but they have large difference from the self-assemblies of **4.1.1**. One is guided by oxime-oxime synthons and other is guided by π···π interactions along with O-H···O hydrogen bonds (**Fig. 4.1.3b-c**). On the other hand, guest 4,4'-bipyiridine encapsulate copper complex **4.1.4** was self-assembled through O-H···N hydrogen bonds. For hydrogen bonds and short contacts parameters of complexes **4.1.1-4.1.7** please see page 228-229 of appendix.

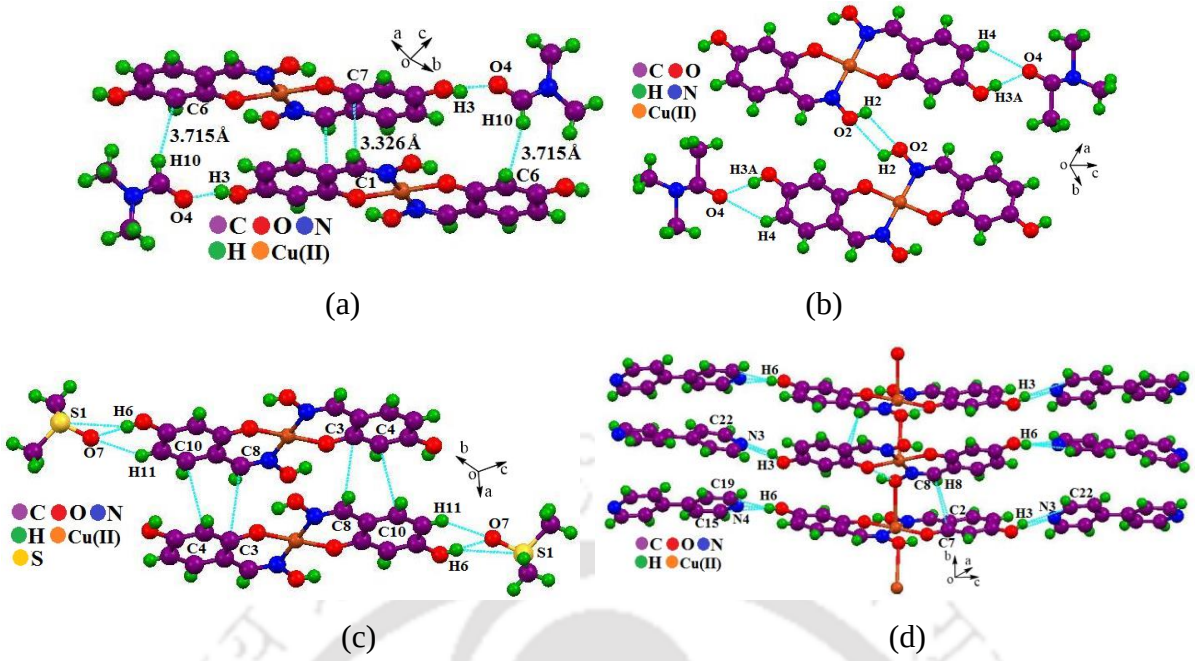

Figure 4.1.3: Hydrogen bonded Self-assembies of copper complexes (a) **4.1.1**, (b) **4.1.2**, (c) **4.1.3** and (d) **4.1.4**.

Complexes **4.1.1-4.1.3** have similar coordination environment around copper but they have distinct differences in bond parameters. The metal-ligand bond lengths are dependent on the nature of solvent of crystallization molecules present in their lattices. Such differences in turn affect respective packing pattern. As a representative example, the structure of complex **4.1.1** is shown in **Fig. 3a** and the rest are shown as supporting figures. Bond parameters of complexes **1-3** are compared in **Table 4.1.1**.

Table 4.1.1: Some of the selective metal-ligand bond parameters in complexes **4.1.1-4.1.4**

Complex No.	**M-L**	Length (Å)	∠L-M-L	Angle (°)	∠L-M-L	Angle (°)
4.1.1	Cu1-O1	1.895(3)	O1-Cu1-O1'	180.0	O1'-Cu1-N1	92.40(13)
	Cu1-N1	1.945(3)	O1-Cu1-N1	87.60(13)	N1-Cu1-N1'	180.0
4.1.2	Cu1-O1	1.892(2)	O1-Cu1-O1'	179.99(1)	O1'-Cu1-N1'	87.64(11)
	Cu1-N1	1.937(3)	O1-Cu1-N1	92.36(11)	N1-Cu1-N1'	180.00
4.1.3	Cu-O2	1.895(2)	O2-Cu-O1	179.48(12)	O1-Cu-N1	92.32(11)
	Cu-O1	1.907(2)	O2-Cu-N2	92.01(11)	N2-Cu-N1	179.37(13)
	Cu-N2	1.934(3)	O1-Cu-N2	88.05(11)		
	Cu-N1	1.940(3)				
4.1.4	Cu1-O2	1.898(2)	O2-Cu1-O1	178.52(14)	O2-Cu1-N2	92.00(11)
	Cu1-O1	1.915(2)	O2-Cu1-N1	86.79(11)	O1-Cu1-N2	88.48(11)
	Cu1-N1	1.930(3)	O1-Cu1-N1	92.63(11)	N1-Cu1-N2	175.58(15)
	Cu1-N2	1.941(3)				

In all the four coordinated complexes the nitrogen atoms of the two oxime ligands are at trans dispositions in the coordination sphere. The bond distances of two copper-oxygen as well as the two copper-nitrogen bond distances in the complex **4.1.1** and **4.1.2** are identical. Thus these pairs of bonds are related by C2-axes. Whereas, the complexes **4.1.3** and **4.1.4** have

four different copper-nitrogen and copper-oxygen bond distances. Such differences are attributed to the packing requirement of different guest molecules in respective lattice to accommodate solvent molecules of different shapes, sizes and each having independent direction hydrogen bonds in the lattice to form tight packed structures. As a result of packing requirement, two other oxygen atoms of neighbouring molecules of complex **4.1.4** in crystal lattice are at close vicinities. Thus, in solid state the complex **4.1.4** appears to be a hexa-coordinated complex to form a coordination polymer. However, the axial copper-oxygen distance of these Cu···O interactions is 2.654 Å, which is a relatively long enough to describe such interactions as adequate distance to be a dative bond. On the other hand, the other Cu-O bonds of the complex lie between 1.8-1.9 Å. There are many examples of 4,4'-bipyridine bridged copper complexes bridging through axial positions of the copper ions of paddle-wheel geometry.[8] 4,4'-bipyridine is a good coordinating ligand to form copper complexes,[8] but in the present case it does not coordinate to the copper ion in the complex **4.1.4**; it remain as guest molecule.

The nickel complexes **4.1.5** and **4.1.6** are similar in structures in which coordination environments are similar as that of the copper complexes **4.1.1-4.1.3**. But these complexes have differences in the obvious metal-ligand bond parameters; due to the nickel ion in lieu of the copper. The complex **4.1.5** is a DMF solvate, whereas the complex **4.1.6** is devoid of solvent of crystallization. Among the divalent copper and nickel complexes there is difference in their packing patterns. Packing patterns of the nickel complexes have nickel ions positioned on the top of aromatic rings of a neighbouring molecule showing weak stacking interactions (**Fig. 4.1.4a**). Whereas copper complexes also have layered packing patterns in which copper ions are found to be present on the top of each other with or without an intervening atom.

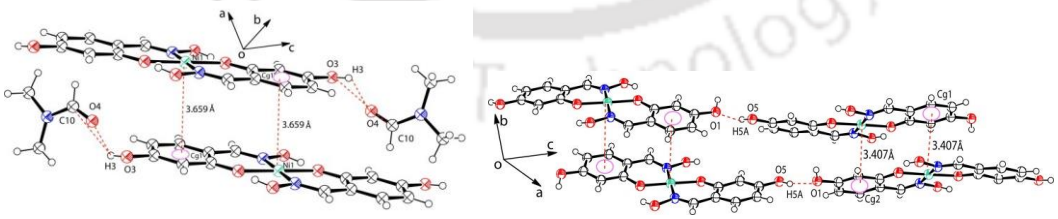

(a) (b)

Figure 4.1.4: Hydrogen bonded self-assemblies of nickel complexes (a) **4.1.5** and (b) **4.1.6** (30% thermal ellipsoids).

The DMF solvated nickel complex **4.15** and the anhydrous nickel complex **4.1.6** has large packing differences. Shortest distance between a nickel ion and the centriod of an aromatic ring above it is 3.407 Å for the complex **4.1.6 (Fig. 4.1.4b)** and 3.695 Å for the complex

4.1.5. DMF molecules are responsible to hold the layered packing structure of the complex **4.1.5**, whereas the layered packing of the complex **4.1.6** is held by intermolecular hydrogen bonds between free hydroxy-groups of ligands.

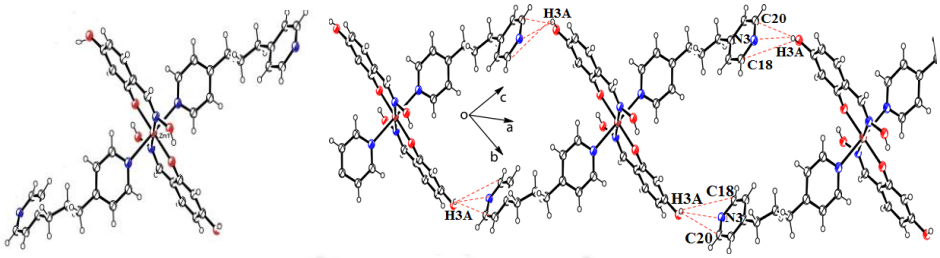

(a) (b)

Figure 4.1.5: (a) Crystal structure of zinc complex **4.1.7** and (b) Hydrogen bonded self-assembly of zinc complex **4.1.7** (30% thermal ellipsoids).

The zinc complex **4.1.7** is a hexa-coordinated mononuclear complex; it has 1,3-bis(4-pyridyl)propane ligand coordinating through nitrogen atom at one end and the other end remains free (**Fig. 4.1.5a**). Nitrogen atom of the free end of pep is hydrogen bonded to a hydroxy-group of a neighbouring complex to form 1D hydrogen bonded chain-liked structure (**Fig. 4.1.5b**). Phase purity of the bulk samples of the metal complexes **4.1.1-4.1.7** were checked by powder X-ray diffraction technique. It is clear from the experimental patterns of the solvates resembles the corresponding simulated pattern, showing that the bulk of the complexes are in one phase, that is only one form of solvate is formed in each case.

FT-IR spectra of the complex **4.1.1** has stretching frequency at 2925 cm^{-1} due to C-H stretching, and C=O stretching of the DMF appear at 1663 cm^{-1}, beside this there are C=N and C=C stretching's at 1643 cm^{-1} and 1621 cm^{-1} respectively (**Fig. 4.1.6a**). On the other hand, the complex **4.1.2** has dimethylacetamide (DMA) molecules which shows the C=O stretching at 1637 cm^{-1}; similarly the complex **4.1.3** shows a sharp S=O stretching at 1129 cm^{-1} due to the dimethyl sulfoxide (DMSO).

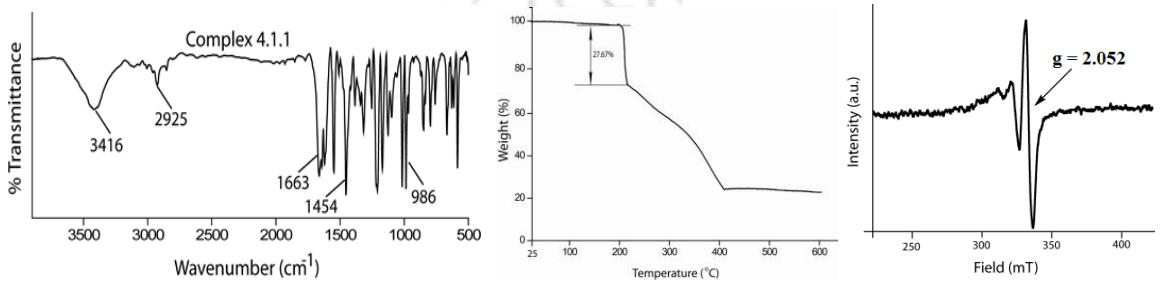

(a) (b) (c)

Figure 4.1.6: (a) FT-IR spectrum, (b) TGA diagram and (c) EPR spectrum of complex **4.1.1**.

Thermogravimetric analysis have revealed that these solvated complexes are thermally stable to about 200 °C and they loss respective solvent of crystallization molecules around 200-250 °C (**Fig. 4.1.6b**). All these complexes decompose around 450 °C to form the respective metal oxide (please refer to thermograms in experimental section). Copper complexes **4.1.1-4.1.4** shows characteristic $g_{\perp}$ value 2.052, 2.056, 2.054 and 2.065 in EPR spectrum respectively in solid state is due to presence of unpaired electron in copper(II) metal ion.

4.1.4: UV-vis and fluorescence spectroscopic studies of metal complexes of oxime with fluoride ion

Due to small size and high charge density on fluoride ion act as base to interact with fluorophore or chromophore containing phenols,[9] ureas,[10] thioureas,[11] oximes,[12] sulphonamides[13] and amides.[14] Such complexations of the oxime derivatives to cause specific signal transductions. Fluorescent sensors based on high chemical affinity of the fluoride ions towards silicon[15] or boron[16] atoms are reported in literature. The silicon based receptors in aqueous solution, requires several minutes to complete the detection process,[15] which is a disadvantage to use such compounds as receptors. In an another approach, the fluoride ions are detected on the basis of their specific tendency to coordinate to a hard metal ion for example, divalent calcium,[17] trivalent iron[18] or tetravalent zirconium ions.[19] Such metal complexes require pre-treatment to avoid interference of other metal ions such trivalent aluminium or iron ions while detecting fluoride ions.[18] Platinum(II) complexes possessing triarylboron group containing ligands show distinct phosphorescent response on interaction with fluoride ions.[20]Among the other metal complexes, ruthenium-2,2'-bipyridine,[21] Fe(III)-thiourea complexes[22] have been used to detect fluorides ions. Fluorescence receptor having a rhodamine unit senses fluoride ions and was used in imaging of fluoride ions in living cell.[23] Conventionally, the ligand exchange reactions of fluoride ions from a complex help to detect of fluoride ions by spectroscopic tools. In such reactions, one or more ligands are released to generate spectroscopic or electrochemical signals. Despite of known utility of hydroxyaromaticaldoximes in the detection of fluoride ions,[24] there are also many organic compounds[25] which selectively interact with fluoride ion. Hydroxyaromatic oxime metal complexes have not been explored for such a purpose. UV-Vis spectra of these complexes were recorded in water, DMSO-water and aprotic polar solvents such as DMSO, DMF, DMA and THF with or without adding of different solution of tetrabutylammonium salts (chloride, bromide, acetate, fluoride, phosphate). The changes on addition of anions do not affect the spectra of the complexes in water or DMSO-water mixture (**Fig. 4.1.15-4.1.16**), but a definite change was found in each case in aprotic polar solvents with fluoride and hydroxide ions.

Independent UV-vis spectra of copper, nickel and zinc complexes with different tetabutylammonium salts such as fluoride, chloride, bromide, phosphate and carbonate are shown in **Fig. 4.1.7a-c**.

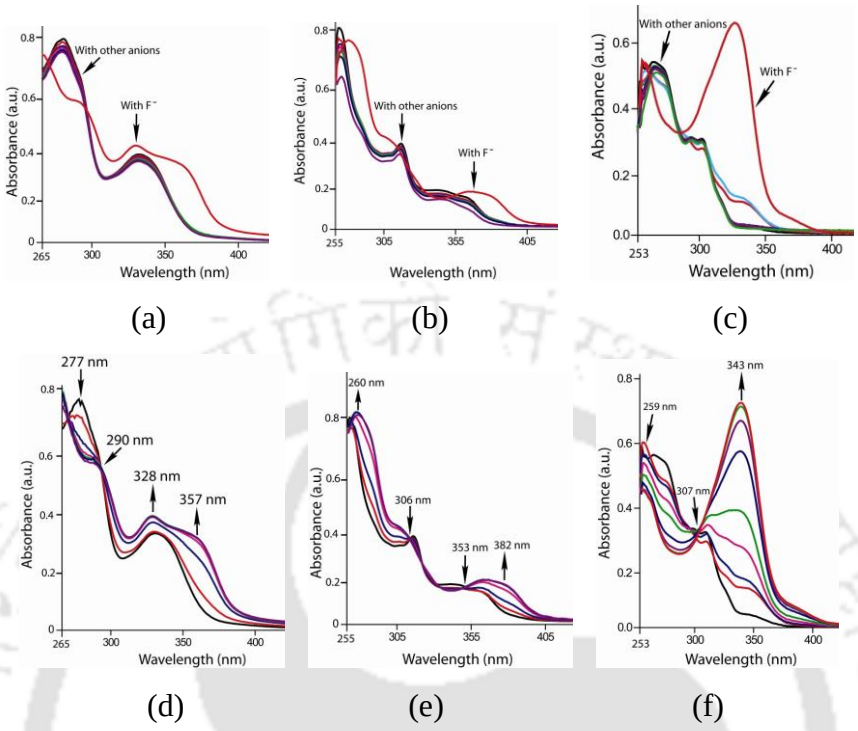

Figure 4.1.7: UV-vis spectra of (a) copper, (b) nickel and (c) zinc complex (10^{-5} M) with different tetrabutylammonium salts (50 µl of 10^{-3} M) and UV-vis spectroscopic titration of (d) copper, (e) nickel and (f) zinc complex (10^{-5} M) with TBAF (10 µl aliquot of 10^{-3} M) in dimethylsuphoxide (DMSO).

It shows that only the terabutylammonium fluoride or hydroxide causes change in the UV-vis spectra of these complexes and effect on the rest of the salts are negligible (**Fig. 4.1.7a-c**). The parent ligand as well as the zinc complex **4.1.7** has a strong absorption at 259 nm, whereas copper and nickel complex has absorption at 277 nm and 256 nm respectively. The changes caused by the fluoride ions are shown separately in **Fig. 4.1.7d-f**, which shows that the gradual increase of the fluoride ions yields a new absorption peak at 357 nm (for copper complex) or 382 nm (for nickel complex) or 343 nm (for zinc complex) and such a change passes through an isobestic point at 290 nm, 306 nm and 307 nm. Positions of the new absorptions peak in the case of the complexes **4.1.1-4.1.3** on interacting with tetrabutylammonium fluoride are independent of solvents of crystallization. However, the position of the new peak generated upon interactions with fluoride ions is dependent on the central metal ions. From the shifts in absorption of nickel, copper and zinc complexes has a definite trend, the zinc complex shows shift shorter than the copper and the nickel shows the highest shift. This is attributed to the electronic factors of these metal ions.

The electron occupancies in *d*-orbitals follow the sequence Ni(II), Cu(II) and Zn(II). The metal complexes having polyhydroxy-groups have been shown to form hydrogen bonds with fluoride ions to cause a colour change.[26] We have also shown earlier that the oxime **2.1.3** acts as fluoride sensor showing spectral changes in UV region.[27] The UV-vis spectra of the copper complex **4.1.1** and the nickel complex **4.1.5** in acidic (pH = 6), neutral and basic (pH = 9) medium in dimethylsulphoxide. In basic medium complexes show a peak longer wavelength which is similar to the peak that was observed in presence of fluoride ions (**Fig. 4.1.17**). Whereas, the UV-vis spectra of the complexes in acidic medium tally with the peak of the ligand, suggesting that the complexes decompose in acid medium. These experiments also show that the fluoride detection by these complexes is possible only at a neutral condition in aprotic medium.

The zinc complex **4.1.7** has a fluorescence emission at 346 nm on excitation at 270 nm. However, a new fluorescence emission at 415 nm (**Fig. 4.1.8**) on addition of fluoride ions to the complex **4.1.7** was observed. This emission peak was very selective to the fluoride ions among different ions tested (**Fig. 4.1.8**). Further to these we have examined the fluorescence emission of the zinc complex **4.1.7** in different pH (**Fig. 4.1.17e-f**). The zinc complex is very weakly fluorescent in neutral and in acidic medium. To the solution of this complex at pH = 6 when tetrabutylammonium fluoride was added, no change in fluorescence emission took place.

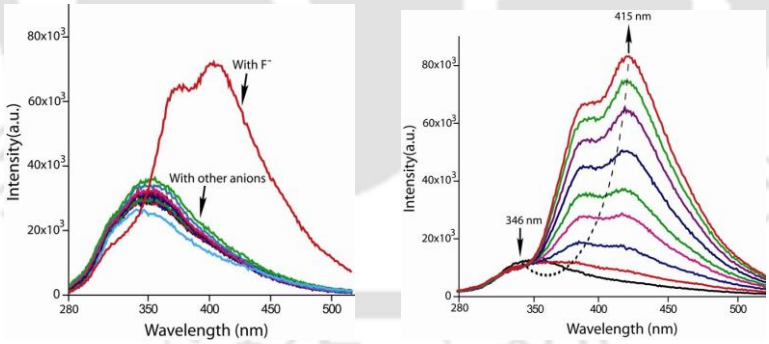

(a) (b)

Figure 4.1.8: The changes in the fluorescence emission spectra of zinc complex **4.1.7** (10^{-5} M solution in DMSO) on addition of (a) tetrabutylammonium salts (fluoride, chloride, bromide, phosphate, carbonate) (50 µl of 10^{-3}M) and (b) tetrabutylammonium fluoride (10 µl aliquot of 10^{-3} M in DMSO).

This suggests that the complex is stable at such pH and does not respond to fluoride ions. But this complex at pH = 9 showed a strong emission at 415 nm. This showed that a substrate have ability to abstract the acidic hydrogen of the ligand cause a similar effect with the

complexes. The emission peak at 415 nm was associated with a shoulder at 375 nm (**Fig. 4.1.8b**). At lower concentration of fluoride ions the shoulder of this peak is not observed but peak at 415 nm was observed. Hence the peak at 375 nm is attributed to hydrogen bond formation. As the concentration of fluoride ions were increased proton transfer took place showing the prominent peak at 415 nm arising from the anionic form of the complex. At lower concentration of fluoride ions, there is equilibrium between hydrogen bonded assembly of metal complex and deprotonated metal complex caused by fluoride ions. Once more amounts of fluoride ions are added the equilibrium shifts toward deprotonated metal complex which emits at 415 nm.

A series of anions were tested for changes in fluorescence emission with the solution of complex **4.1.7** and also the relative sensitivity of the complexes were tested. The emission profiles are shown (**Fig. 4.1.18a,** experimental section, page-122**)** by a bar graph diagram. Beside this, the effect of the sensitivity of the emission caused by various anions were checked and found that the fluoride ions can be easily detected in the presence of other ions such as acetate, biphosphate, bromide, carbonate, chloride, perchlorate etc (**Fig. 4.1.18b**). Hence, complex **4.1.7** is a highly sensitive fluorophore for the detection of fluoride ions. Comparing the fluorescence emission spectra of the complex **4.1.7** in basic medium with the medium in presence fluoride ions showed that deprotonation of hydroxy group of the ligand was responsible for such an increase in intensity of emission with a shift of fluorescence towards longer wavelength. Hence, a highly sensitive zinc-oxime complex for the detection of fluoride ions is identified. The complexation of divalent metal ions having a d^{10} configuration through deprotonation of ligands generally causes fluorescence enhancement of fluorophoric units.[8] The detection limit of the complex **4.1.7** was found to be 4.86×10^{-6} M which was calculated by using $3\alpha/k$ as the detection limit, whereas, α is the standard deviation of the complex and k is the slope of intensity vs. concentration plot (**Fig. 4.1.19a,** experimental section, page-123). Thus, the basic behavior of the fluoride ion deprotonate all these complexes to form resonance stabilized anions shown in **Scheme 4.1.2**. Divalent zinc possess a d^{10} configuration, generates less resonance stabilized anion; whereas, the d^9 and d^8 configuration of the central metal ions have comparatively higher delocalization, hence the absorption occurs at a longer wavelength than the corresponding zinc complex. Phenols shows absorption changes on deprotonation by fluoride ions,[10] but such a change may occur without a proton transfer.[11] Specific changes in absorption by the fluoride ions in the present case but not caused by the respective acetate or hydroxide tetrabutylammonium salt showed that proton-transfer is not necessarily required for such a process. In basic medium these

complexes are deprotonated, hence fail to detect fluoride ions. Based on these observations, **Scheme 4.1.2** is proposed to explain the absorption changes.[28]

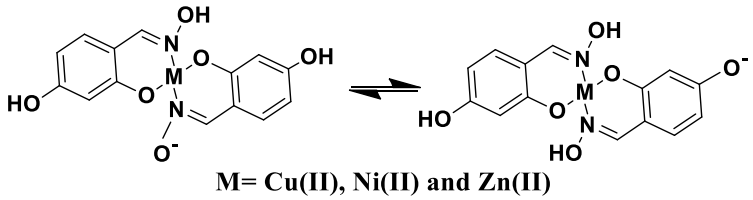

Scheme 4.1.2: Tautomeric structures generated from the complexes by the interactions of fluoride ion.

Further support to the mechanism is drawn from EPR spectra for copper complexes and ^{1}H NMR spectroscopy of zinc and nickel complexes. EPR spectral features of the copper complexes in DMSO (**Fig. 4.1.19b**) do not show change in after addition of tetrabutylammonium fluoride. This suggests that the copper sites are not affected by the presence of fluoride ions and the effect of fluoride ion is on the external periphery of the complex. In the ^{1}H NMR titration of the nickel and zinc complexes (**Fig. 4.1.20**-**4.1.21**) with different amounts of tetrabutylammonium fluoride did not shift the chemical shift positions of other signals then the hydroxy signals of the complexes, showing that complex is not decomposed in solution upon interaction with fluoride and a fast exchange of proton by fluoride ion takes place. However, the exchange process could not be ascertained as we could not clearly get the exchangeable protons of the hydroxy groups of the complexes in solution (merges with water from solvent peak). The role of fluoride is further clarified by recording the UV-vis spectra of the complexes in presence of tetrabutylammonium hydroxide (**Fig. 4.1.22**). These complexes behave similarly as the tetrabutylammonium fluoride establishing the proposed mechanism. The deprotonation and hydrogen bond formation allows such interactions, but in the present case it is complete deprotonation as the fluoride ions and hydroxy ions behave in similar manner. Disadvantage of using these complexes is that the detection of fluoride ions is not possible by these complexes in pure water.

4.1.5: Conclusions

The hydrogen bond involving the oxime as well as phenolic O-H groups play crucial role in the self-assemblies of the polyhydroxyaromatic oxime complexes. Though the DMF and DMA belong to similar class of compounds there complementing effect in formation of hydrogen-bonded assemblies differs. In the case of DMA, the carbonyl group is connected to the phenolic O-H in complex **4.1.2** and the C-H group is involved in C-H$\cdots\pi$ interactions. In analogous DMF solvate the phenol-carbonyl interactions are prominent and in this case the

O-H of oximes of two molecules form oxime-oxime interactions; due to such complementary hydrogen bonds, differences in solid state self-assemblies are widely different from each other. The 4,4´-bipyridine hydrogen bonds with phenolic O-H and makes arrangement of molecules in which the oxime groups are close to axial position of the copper showing weak interactions to make an apparently a six coordinated metal complex which is not observed in other solvates. The nickel complexes and zinc complex has wide difference in the directional arrangement of molecules, whereas the zinc complex **4.1.7** has shown extension of grid-like structures through coordination of one nitrogen atom of 1, 3-bis(4 pyridyl)propane to zinc and phenol-pyridine hydrogen bonds. These examples have shown that besides the changes caused in the packing by presence and absence of a guest or solvent molecules, the directional hydrogen bonds are crucial in generating the overall architecture of the respective non-covalent assembly in each case. Interactions of fluoride ions with metal complexes in solution clearly tell that divalent metal ions other than the conventional hard ions can also be used for the fluoride detection by putting them as a part of a receptor. Population of d-electron in the central metal ions in a delocalized chelate system plays a key role in shifting the emission or absorption spectra with respect to the parent ligand during the detection of fluoride ions. Depending on the metal ions such as in the zinc complex **4.1.7** fluorescence emission can be a tool for the detection of fluoride ions despite the parent ligand does not have such a capability. Interesting aspect of the zinc complex **4.1.7** is that it has a very weakly fluorescent counterpart, but the zinc complex **4.1.7** on the interactions with the fluoride ions becomes strongly fluorescent to show an emission at longer wavelength. Incorporation of the basic aromatic heterocyclic compounds as ligands or solvent of crystallization do not interfere in the fluoride detection.

4.1.6: Experimental section

UV-vis and fluorescence experiments:

For study of interactions with fluoride ions separate solutions of the complexes **4.1.4**, **4.1.5** and **4.1.7** (10^{-5} M solution) as well as the solutions of different tetrabutyl ammonium ions (10^{-3} M solution) were prepared in dimethylsuphoxide or water or DMSO-water mixture (1:1 v/v). To record the UV-vis spectra or fluorescence spectra 3 ml solution of the complex was placed in quartz cell of a 10 mm path length at room temperature. Absorption or emission spectra were recorded after each addition, by adding definite amounts of solutions of anions in aliquot to such a solution using micropipette

Synthesis and characterization of metal complexes 4.1.1-4.1.7:

2,4-dihydroxyphenylaldoxime (oxime **2.1.3)** was prepared followed by reported procedure[27] as mention in Chapter-2.

Complex 4.1.1: To a well-stirred solution of oxime **2.1.3** (0.153 g, 1 mmol) in methanol (10 ml), copper(II) nitrate trihydrate (0.120 g, 0.5 mmol) was added. A dark green precipitate obtained was dissolved by adding minimum amount of dimethylformamide (DMF). Reaction mixture was filtered and transparent liquid was kept for crystallization. After 5 days crystals were obtained. Isolated yield: 60 %. IR (KBr, cm^{-1}): 3416 (bs), 2925 (m), 1663 (s), 1643 (s), 1621 (s), 1548 (s), 1510 (w), 1454 (s), 1384 (w), 1341 (w), 1317 (m), 1253 (m), 1209 (s), 1170 (s), 1126 (s), 1098 (m), 1016 (s), 986 (s), 968 (w), 849 (m), 836 (w), 796 (s), 759 (s), 667 (s), 630 (w), 614 (w). TGA: 200-250°C (-2DMF; exptl. wt. loss 27.67 %, calcd. 28.40 %). Elemental anal. calcd for $C_{20}H_{26}CuN_4O_8$; C: 46.69 %, H: 5.05 %, N: 10.89 %; found, C: 46.56 %, H: 5.01 %, N: 10.78 %.

Complex 4.1.2: Complex **4.1.2** was prepared by similar procedure of complex **4.1.1** using dimethylacetamide (DMA) as solvent for crystallization. After 7 days needle type crystals were obtained. Isolated yield: 62 %. IR (KBr, cm^{-1}): 3400 (bw), 3106 (bs), 1637 (s), 1613 (bs), 1546 (s), 1457 (s), 1414 (w), 1397 (m), 1344 (w), 1312 (m), 1257 (s), 1215 (s), 1174 (s), 1137 (s), 1012 (s), 985 (s), 970 (w), 858 (m), 842 (s), 814 (m), 761 (s), 796 (s), 661 (w), 620 (m), 630 (m). TGA: 200-250°C (-2DMA; exptl. wt. loss 29.56 %, calcd. 32.14 %). Elemental anal. calcd for $C_{22}H_{30}CuN_4O_8$; C: 48.70%, H: 5.53 %, N: 10.33%; found, C: 48.66 %, H: 5.50 %, N: 10.28 %.

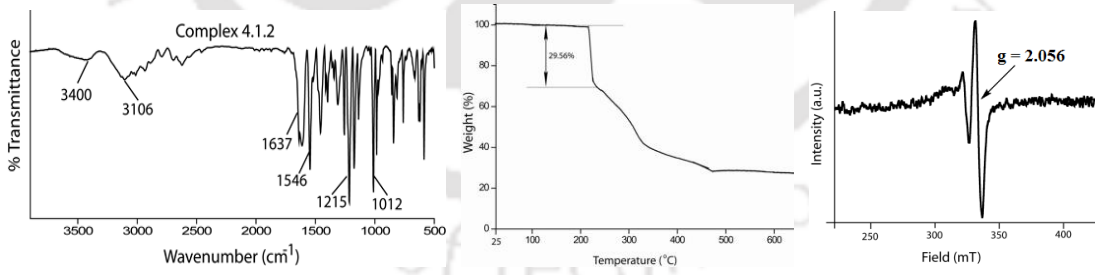

(a) (b) (c)

Figure 4.1.9: (a) FT-IR spectrum, (b) TGA diagram and (c) EPR spectrum of complex **4.1.2**.

Complex 4.1.3: Complex **4.1.3** was prepared by a similar procedure of complex **4.1.1** using dimethyl sulfoxide (DMSO) instead of DMF. After 8 days black plate type crystals were obtained. Isolated yield: 60 %. IR (KBr, cm^{-1}): 3332 (bs), 2922 (w), 1648 (s), 1606 (s), 1481 (s), 1453 (s), 1376 (m), 1347 (w), 1328 (w), 1314 (w), 1284 (m), 1247 (m), 1212 (s), 1190 (w), 1129 (s), 1014 (s), 987 (s), 953 (w), 850 (m), 834 (s), 795 (w), 786 (m), 761 (m), 698 (m), 651 (m), 630 (s), 610 (m). TGA: 200-250°C (-DMSO; exptl. wt. loss 17.16 %, calcd.

17.52%). Elemental anal. calcd for $C_{16}H_{18}CuN_2O_7S$; C: 43.05 %, H: 4.03 %, N: 6.27 %, S: 7.17 %.; found, C: 43.01 %, H: 4.01 %, N: 6.21 %, S: 7.10 %.

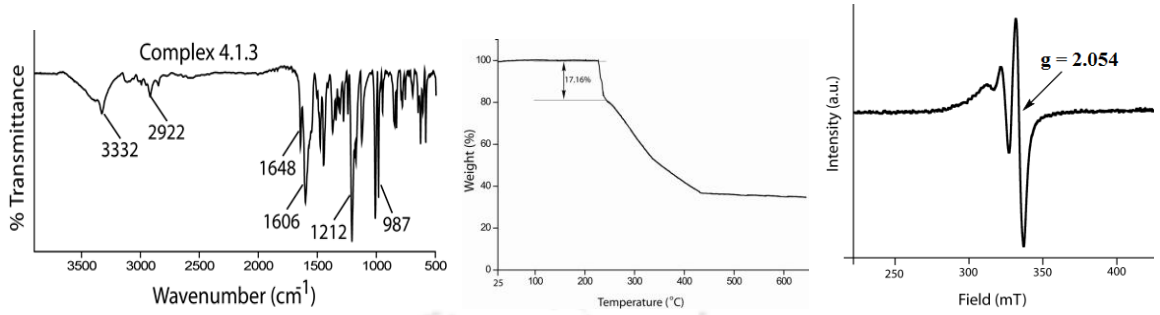

(a) (b) (c)

Figure 4.1.10: (a) FT-IR spectrum, (b) TGA and (c) EPR spectrum of complex **4.1.3**.

Complex 4.1.4: Complex **4.1.4** was prepared by a procedure similar to synthesis of complex **4.1.1**, but adding 4,4'-bipyiridine (4,4'-bipy). After 15 days black needle shaped crystals were obtained. Isolated yield: 58%. IR (KBr, cm^{-1}): 3452 (bs), 1620 (s), 1606 (s), 1597 (w), 1549 (s), 1516 (w), 1491 (w), 1455 (s), 1408 (s), 1377 (w), 1321 (s), 1256 (s), 1222 (w), 1212 (s), 1173 (s), 1134 (m), 1058 (s), 1015 (s), 1001 (w), 982 (s), 964 (w), 846 (m), 832 (s), 799 (s), 760 (s), 668 (w), 633 (s), 621 (s), 609 (w). Elemental anal. calcd for $C_{24}H_{20}CuN_4O_6$; C: 54.96 %, H: 3.81 %, N: 10.68 %; found, C: 54.91 %, H: 3.76 %, N: 10.61 %.

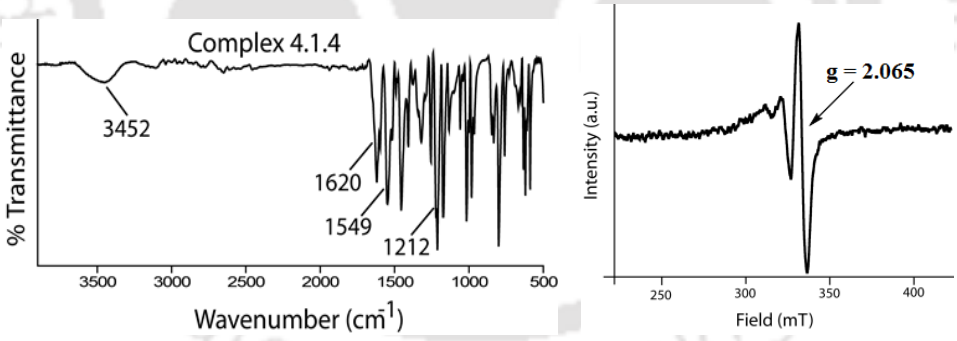

(a) (b)

Figure 4.1.11: (a) FT-IR and (c) EPR spectrum of complex **4.1.4**.

Complex 4.1.5: To a well-stirred solution of oxime **2.1.3** (0.153 g, 1 mmol) in methanol (10 ml), nickel(II) nitrate hexahydrate (0.145 g, 0.5 mmol) was added. A green precipitate was obtained, which was dissolved in a minimum amount of DMF and filtered, transparent filtrate after 7 days gave green block type crystals. Isolated yield: 65 %. IR (KBr, cm^{-1}): 3380 (bs), 2925 (w), 1659 (s), 1643 (s), 1615 (s), 1569 (w), 1555 (s), 1514 (w), 1494 (w), 1451 (s), 1386 (w), 1346 (w), 1310(s), 1261 (w), 1228 (w), 1216 (s), 1170 (s), 1124 (s), 1102 (w), 1020 (s), 987 (s), 955 (w), 861 (m), 845 (m), 831 (s), 794 (s), 769 (m), 668 (s), 647 (s). TGA: 250-

300°C (-2DMF; exptl. wt. loss 27.85 %, calcd. 28.71 %). Elemental anal. calcd for $C_{20}H_{26}N_4NiO_8$; C: 47.13 %, H: 5.10 %, N: 10.99 %; found, C: 47.08 %, H: 5.06 %, N: 10.92 %.

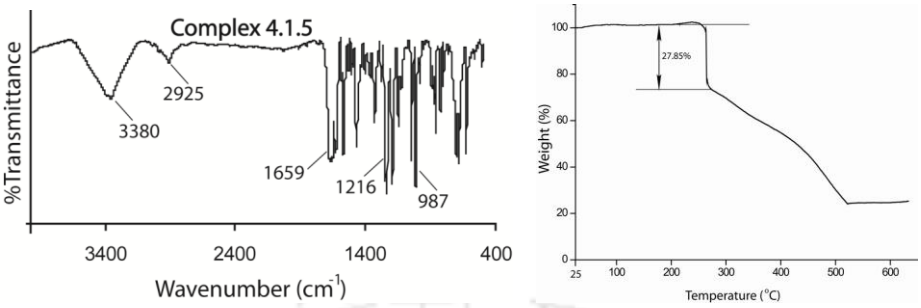

(a) (b)

Figure 4.1.12: (a) FT-IR spectra and (b) TGA diagram of complex **4.1.5**.

Complex 4.1.6: Complex **4.1.6** was obtained from an identical reaction that was used in preparation of **4.1.5** but in this case it was carried out in DMSO. After 6 days green crystals were obtained. Isolated yield: 67 %. IR (KBr, cm^{-1}): 3372 (bs), 2923 (w), 1635 (w), 1607 (s), 1574 (w), 1553 (s), 1514 (w), 1483 (w), 1449 (s), 1381 (m), 1308 (s), 1261 (m), 1214 (s), 1167 (s), 1122 (s), 1019 (s), 986 (s), 955 (w), 862 (m), 832 (s), 794 (m), 768 (m), 673 (w), 647 (s). Elemental anal. calcd for $C_{14}H_{12}N_2NiO_6$; C: 46.28 %, H: 3.30 %, N: 7.71 %; found, C: 46.22 %, H: 3.25 %, N: 7.66 %.

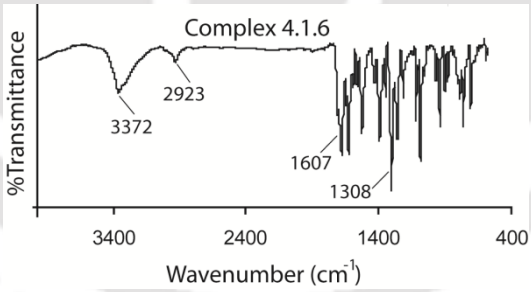

Figure 4.1.13: FT-IR spectra of complex **4.1.6**.

Complex 4.1.7: To a solution of oxime **2.1.3** (0.153 g, 1mmol) and 4-(2-(pyridine-4-yl)propyl)pyridine (pep) (0.198g, 1mmol) in methanol (10 ml), zinc(II) nitrate hexahydrate (0.148g, 0.5mmol) was added and stirred. A white precipitate was obtained. Precipitate was dissolved in a minimum amount of DMF and filtered. Filtrate on standing, resulted in formation of crystals after 15 days. Isolated yield: 70 %. IR (KBr, cm^{-1}): 3039 (w), 2923 (w), 1646 (m), 1605 (s), 1557 (m), 1500 (s), 1477 (s), 1452 (s), 1419 (s), 1383 (s), 1332 (w), 1274 (s), 1245 (s), 1207 (s), 1177 (s), 1119 (s), 1070 (m), 1008 (s), 998 (s), 983 (s), 957 (w), 840 (s), 794 (s), 761 (m), 613 (s). Elemental anal. calcd for $C_{40}H_{40}N_6O_6Zn$; C: 62.64 %, H: 5.22 %, N: 10.96 %; found, C: 62.60 %, H: 5.16 %, N: 10.88 %.

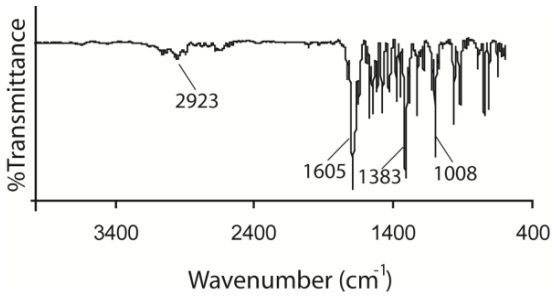

Figure 4.1.14: FT-IR spectra of complex **4.1.7**.

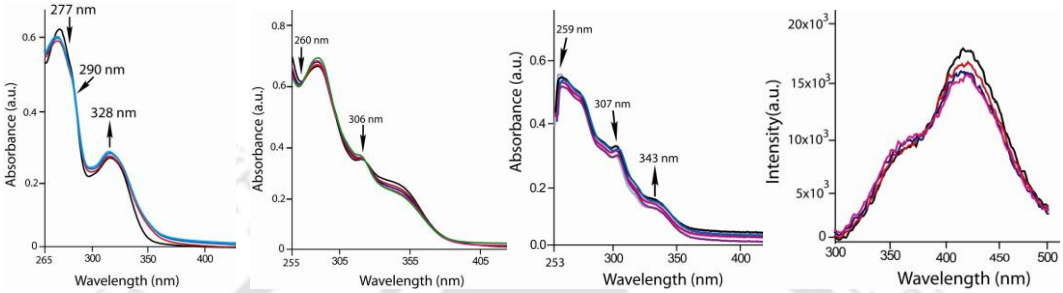

(a) (b) (c) (d)

Figure 4.1.15: UV-vis spectra of complex (a) **4.1.1**, (b) **4.1.5** and (c) **4.1.7** in water on addition of different amounts of the tetrabutylammonium fluoride (100µl aliquot of 10^{-5} M in water). (d) Fluorescence spectra of complex **4.1.7** in water on addition of different amount of the tetrabutylammonium fluoride (100µl aliquot of 10^{-3} M in water).

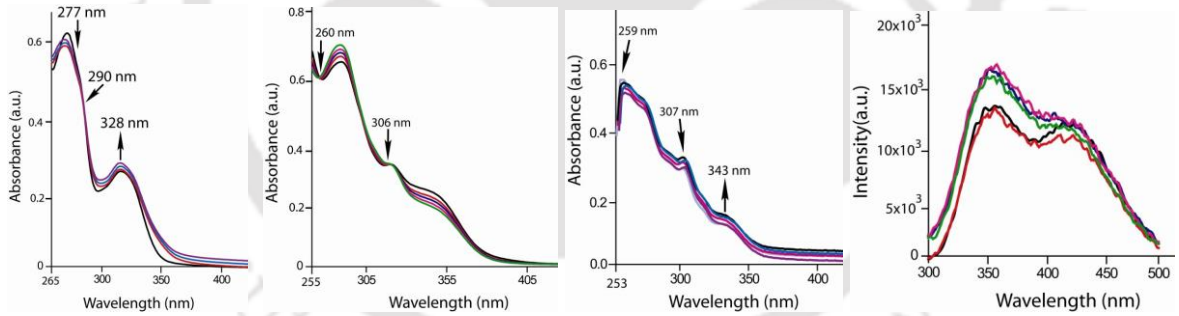

(a) (b) (c) (d)

Figure 4.1.16: UV-vis spectra of complex (a) **4.1.1**, (b) **4.1.5** and (c) **4.1.7** in DMSO-water mixture on addition of different amounts of the tetrabutylammonium fluoride (100µl aliquot of 10^{-3} M in water). (d) Fluorescence spectra of complex **4.1.7** in DMSO-water mixture on addition of different amount of the tetrabutylammonium fluoride (100µl aliquot of 10^{-3} M).

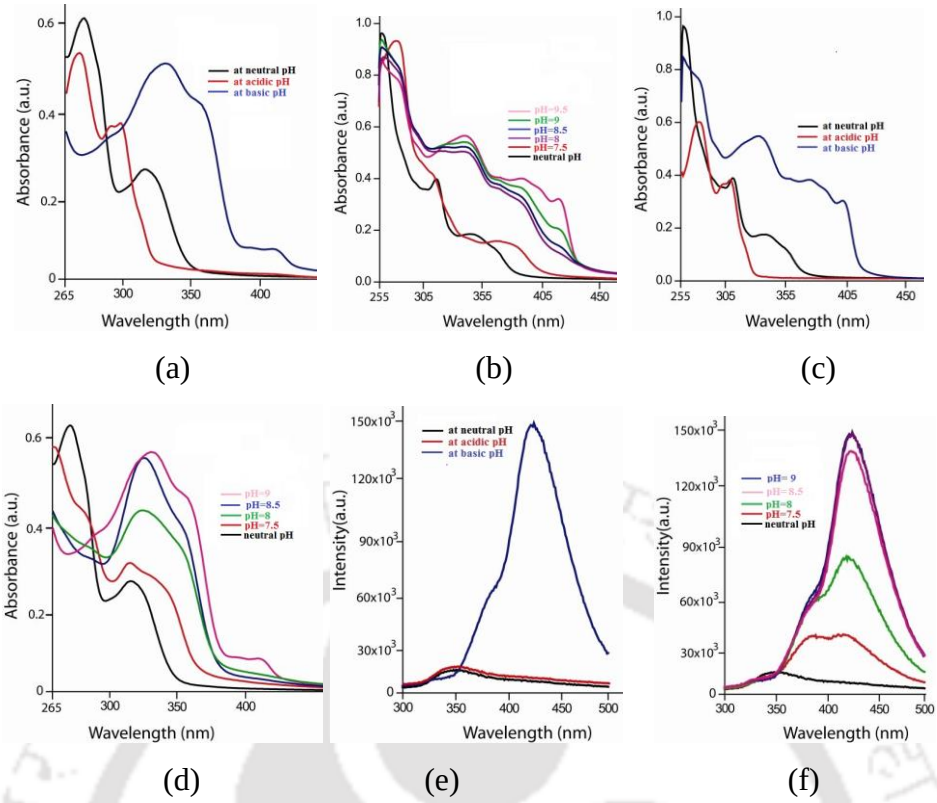

Figure 4.1.17: UV-vis spectra of complex (a) **4.1.1**, (b) **4.1.5** at different pH and (c) and (d) are basic pH titration spectra of complex **4.1.1** and **4.1.5**. Fluorescence spectra of complex **4.1.7** (e) at different pH and (f) basic pH titration spectra.

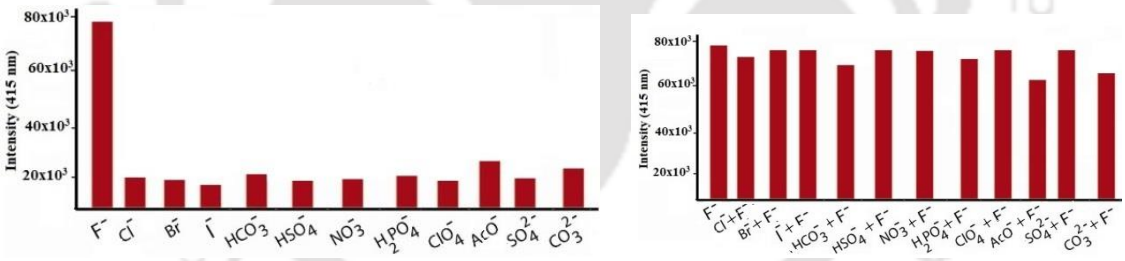

Figure 4.1.18: Fluorescence intensities at 415 nm for the complex **4.1.7** (10^{-5} M) in the presence of (a) different anions (10^{-3} M) and (b) Fluoride (10^{-3} M) with the addition of 10^{-3}M of different anions respectively.

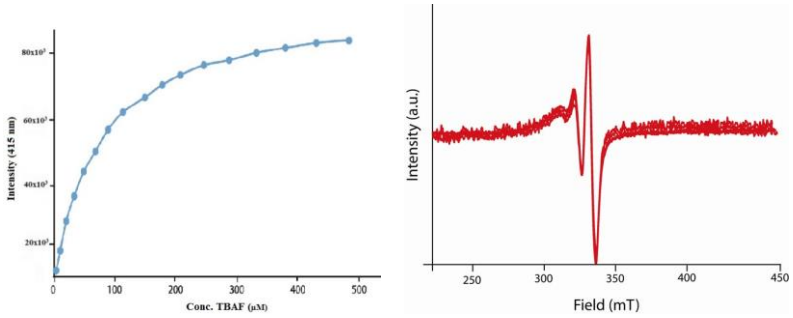

(a) (b)

Figure 4.1.19: (a) Fluorescence intensity versus [TBAF] plot of zinc complex **4.1.7** at 415 nm and (b) EPR spectrum of copper complex **4.1.7** with addition of different amounts of tetrabutyl ammonium fluoride.

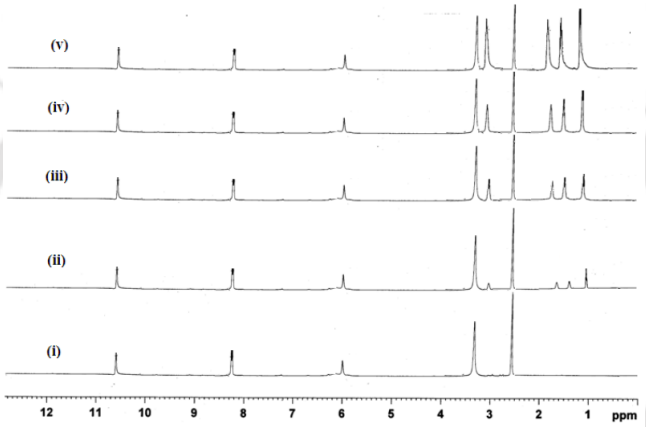

Figure 4.1.20: ^{1}H-NMR (DMSO-d_6) spectra during titration of complex **4.1.5** with tetrabutyl ammonium fluoride (i) 0.0, (ii) 0.5, (iii) 1.0, (iv) 1.5 and (v) 2 equivalents.

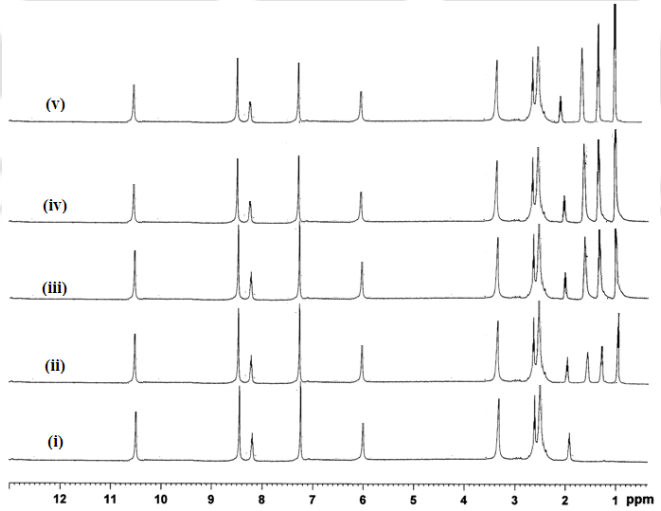

Figure 4.1.21: ^{1}H-NMR (DMSO-d_6) spectra during titration of complex **4.1.7** with tetrabutyl ammonium fluoride (i) 0.0, (ii) 0.5, (iii) 1.0, (iv) 1.5 and (v) 2 equivalents.

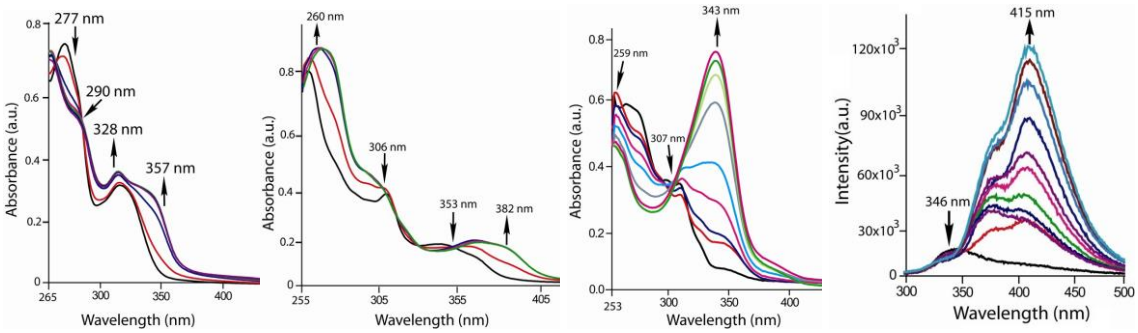

(a) (b) (c) (d)

Figure 4.1.22: UV-vis spectra of complex (a) **4.1.1**, (b) **4.1.5** and (c) **4.1.7** on addition of different amount of tetrabutylammonium hydroxide. (d) Fluorescence spectra of complex **4.1.7** on addition of different amount of tetrabutylammonium hydroxide.

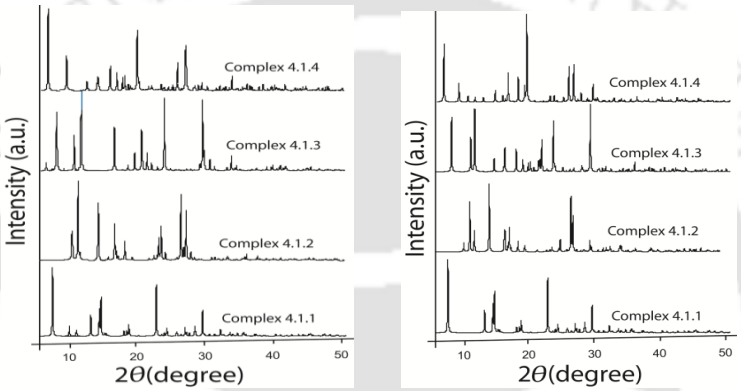

(a) (b)

Figure 4.1.23: (a) Experimental and (b) Simulated powder X-ray diffraction patterns of the complexes **4.1.1-4.1.4**.

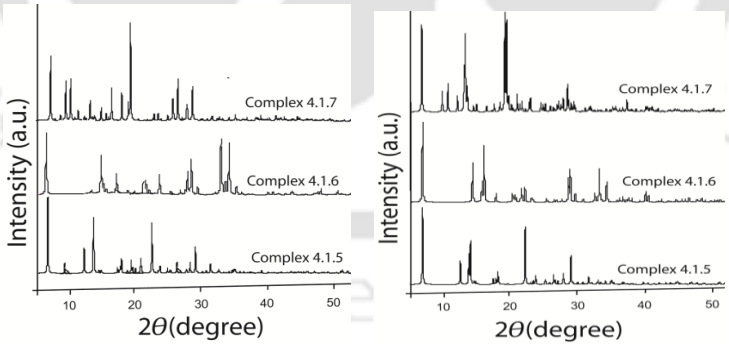

(a) (b)

Figure 4.1.24: (a) Experimental and (b) Simulated powder X-ray diffraction patterns of the complexes **4.1.5-4.1.7**.

4.1.7: References

1. A. Chakravorty, *Coord. Chem. Rev*., 1974, **13**, 1-46.
2. L. E. Godycki, R. E. Rundle, *Acta. Cryst*., 1953, **6**, 487.
3. (a) F. Ephraim, *Berichte*, 1930, **63**, 1928; (b) E. G. Cox, F. W. Pinkard, W. Wardlaw, K. C. Webster, *J. Chem. Soc*., 1935, 459-462.
4. A. G. Smith, P. A. Tasker, D. J. White, *Coord. Chem. Rev*., 2003, **241**, 61-85.
5. (a) R. Inglis, C. Milios, L. F. Jones, S. Piligkos, E. K. Brechin, *Chem. Commun*., 2011, **48**, 181-190; (b) I. A. Gass, C. J. Milios, A. Collins, F. J. White, L. Budd, S. Parsons, M. Murrie, S. P. Perlepes, E. K. Brechin, *Dalton Trans*., 2008, 2043-2053; (c) K. Mason, I. A. Gass, F. J. White, G. S. Papaefstathiou, E. K. Brechin, P. A. Tasker, *Dalton Trans*., 2011, **40**, 2875-2881.
6. (a) P. S. Reddy K. H. Reddy, *Polyhedron*, 2000, **19,** 168-174; (b) D. Mandal, B. D. Gupta, *Organometallics* 2005, **24,** 1501-1510; (c) V. Y. Kukushikin, A. J. L. Pomberio, *Coord. Chem. Rev.*, 1999, **181,** 147-181.
7. W. Lu, H. Jiang, F. Hu, L. Jiang, Z. Shen, *Tetrahedron*, 2011, **67**, 7909-7912.
8. D. L. Reger, A. Debreczeni, B. Reinecke, V. Rassolov, M. D. Smith, R. F. Semeniuc, *Inorg. Chem.*, 2009, **48,** 8911-8924.
9. V. Bhalla, R. Tejpal, M. Kumar, *Tetrahedron*, 2011, **67,** 1266-1271.
10. C. -H. Chen, M. -K., Leung, *Tetrahedron*, 2011, **67,** 3924-3935.
11. D. A. Jose, D. K. Kumar, B. Ganguly, A. Das, *Org. Lett.*, 2004, **6,** 3445-3448.
12. C. B. Rosen, D. J. Hansen, K. V. Gothelf, *Org. Biomol. Chem.*, 2013, **11,** 7916-7922.
13. (a) C. Chen, D. Zhu, *Org. Lett.*, 2005, **7,** 4629-4632; (b) S. V. Bhosale, M. B. Kalyankar, S. J. Langford, *Org. Lett.*, 2009, **11,** 5418-5421.
14. C. Caltagirone, A. Mulas, F. Isaia, V. Lippolis, P. A. Gale, M. E. Light, *Chem. Commun.* 2009, 6279-6281.
15. (a) T. H. Kim, T. M. Swager, *Angew. Chem., Int. Ed.*, 2003, **42,** 4803-4806; (b) S. Y. Kim, J. I. Hong, *Org. Lett.*, 2007, **9**, 3109-3112; (c) X. F. Yang, *Spectrochim. Acta, Part A*, 2007, **67,** 321-330; (d) R. Hu, J. Feng, D. H. Hu, S. Q. Wang, S. Y. Li, Y. Li, G. Q. Yang, *Angew. Chem., Int. Ed.*, 2010, **49,** 4915-4918; (e) X. F. Yang, H. Qi, L. Wang, Z. Su, G. Wang, *Talanta*, 2009, **80,** 92-97; (f) S. Y. Kim, J. Park, M. Koh, S. B. Park, J. I. Hong, *Chem. Commun.*, 2009, 4735-4737.
16. (a) L. Weber, D. Eickhoff, J. Kahlert, L. Bohling, A. Brockhinke, H. Stammler, B. Neumanna, M. A. Fox, *Dalton Trans.*, 2012, **41,** 10328-10346; (b) S. Arimori, M. G.

Davidson, T. M. Fyles, T. G. Hibbert, T. D. James, G. I. Kociok-Kohn, *Chem. Commun.,* 2004, 1640-1641.

17. S. Rochat, K. Severin, *Chem. Commun.,* 2011, 4391-4393.
18. H. Parham, N. Rahbar, *Talanta,* 2009, **80**, 664-669.
19. (a) O. A. Zaporozhets, L. Y. Tsyukalo, *Anal. Chim. Acta,* 2007, **597,** 171-177; (b) K. Okazaki, M. Mifune, J. Odo, Y. Tanaka, Y. Saito, *Anal. Sci.,* 1992, **8,** 567-569; (c) P. Sahu, J. D. Panda, B. C. Sinha, *Talanta,* 1992, **39,** 541-545; (d) L. Kanwar, K. K. Rao, *Sens. Actuators, B,* 2010, **149**, 245-251; (e) R. F. Devine, G. L. Partington, *Environ. Sci. Technol.,* 1975**, 9,** 678-679.
20. S. B. Zhao, T. McCormick, S. Wang, *Inorg. Chem.,* 2007, **46,** 10965-10967.
21. Z. Lin, Y. Zhao, C. Duan, B. Zhang, Z. Bai, *Dalton Trans.,* 2006, 3678-3684.
22. W. Lu, H. Jiang, F. Hu, L. Jiang, Z. Shen, *Tetrahedron,* 2011, **67,** 7909-7912.
23. G. Sivaraman, D. Chellappa, *J. Mater. Chem. B,* 2013, **1**, 5768-5772.
24. (a) S. Li, C. Zhang, S. Huang, F. Hu, J. Yin, S. H. Liu, *RSC Adv.,* 2012, **2,** 4215-4219; (b) W. Guan, S. Yamabe, S. Sakaki, *Dalton Trans.,* 2013, **42,** 8717-8728; (c) D. A. Jose, P. Kar, D. Koley, B. Ganguly, W. Thiel, H. N. Ghosh, A. Das, *Inorg. Chem.,* 2007, **46**, 5557-5564.
25. (a) F. Zheng, C. Yu, X. Hou, S. Wu, *Chem. Eur. J.,* 2013, **19**, 936-942; (b) X. Yong, M. Su, W. Wan, W. You, X. Lu, J. Qu, R. Liu, *New J. Chem.,* 2013, **37**, 1591-1594
26. J. -S. Wu, J. -H. Zhou, P. -F. Wang, X. -H. Zhang, S. -K. Wu, *Org. Lett.,* 2005, **7,** 2133-2136.
27. A. Tarai, J. B. Baruah, *CrystEngComm,* 2015, **17,** 2301- 2309.
28. (a) M. Cometti, K. Rissanen, *Chem. Commun.,* 2009, 2809-1829; (b) X. Yong, M. Su, W. Wang, Y. Yan, J. Qu, R. Liu, *Org. Biomol. Chem.,* 2013, **11,** 2254-2257; (c) J. Wang, Y. Hou, C. Li, B. Zhang, X. Wang, *Sensors and Actuators B,* 2011, **157,** 586-593; (d) P. D. Beer, P. A. Gale, *Angew. Chem. Int. Ed.* 2001, **40,** 486-516.

Chapter 4

Part B: Inclusion of Aldehyde or Oxime in Cadmium Coordination Polymer and Conversion of Aldehyde to Oxime

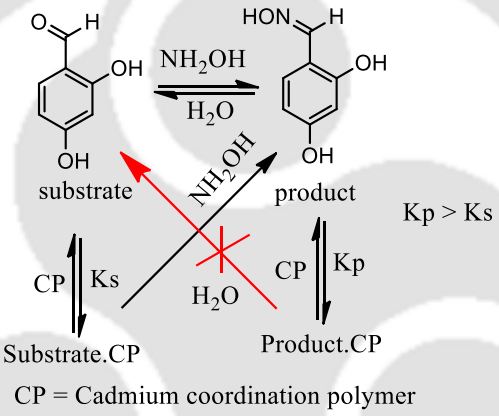

ChemistrySelect, 2017, **2**, 11482-11486.

4.2.1: Introduction

Coordination polymers (CPs) or metal-organic frameworks (MOF, a porous coordination polymer) are new generation molecular materials.[1a-b] Both class of compounds are constructed by reacting metal ions with organic ligands via coordination bonds. From past few decades CPs or MOF have received significant interest from researchers because of their real life applications[1c] in varies areas, such as gas storage or separation,[2] magnetism,[3] drug delivery,[4] and luminescence.[5] Certain coordination polymers (CPs) catalyze photochemical reactions.[6] Coordination polymers also undergo crystal to crystal transformations[7] and reactions by solvents.[8] CPs or MOF are widely used as catalyst for organic transformations[9] and certain porous frameworks serve as container to perform catalytic or stoichiometric reactions.[10] One of the way to activate a substrate for a chemical transformation may be achieved by placing the reactants into voids of a MOF. For such a process, sizes of the voids should be conducive to accommodate the reactant molecule and there should be a mechanism through which the product/s is/are released from the MOF.[11] A flexible MOF would have high storage or release due to their high selectivity and low energy in the recovery of adsorbed molecules as compared to a rigid porous adsorbents.[12] Flexible organic ligands may provide more possibilities for the construction of unique MOFs because of their freedom of conformation. Such flexible MOFs are very limited and leave scope for preparation of new flexible functional materials for catalytic studies.

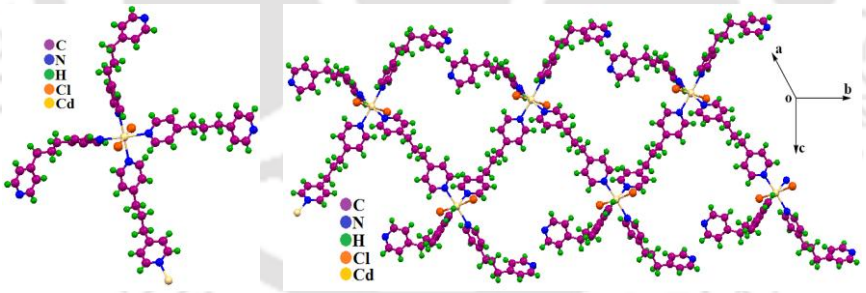

(a) (b)

Figure 4.2.1: (a) Crystal structure of cadmium(II)-1,3-bis(4-pyridyl)propane complex and (b) its corresponding hydrogen bonded self-assembies.

One of such flexible organic ligands is 1,3-bis(4-pyridyl)propane is frequently used for constructing various MOFs.[13] It forms hydrogen bonded one dimensional cadmium coordination polymer (**Fig. 4.2.1**).[14] Cadmium(II) containing coordination polymers also have attracted considerable attention because the large radius, various coordination modes, and special physical properties of Cadmium(II) ion.[15] Reversible assembling and disassembling of building blocks of coordination polymer are also possible,[16] hence an

originally nonporous material may be used to encapsulate a guest and again release through assembling and disassembling properties. Furthermore, assembling of a coordination polymer with a reactant or a product of a reaction[17] may selectively hold either of them. The coordination polymers also change dimensions upon reaction conditions[18] and solvents.[19] One-dimensional (1-D) coordination polymers are advantageous as catalyst to provide multiple sites for reactant or product in varieties of ways. Hence, it is an open ended research area to search for coordination polymers that would weakly bind to a reactant or a product of a reversible reaction. Such processes on formation of self-assembled 1-D coordination polymers with or without a substrate and product is described schematically in **Fig. 4.2.2a**.

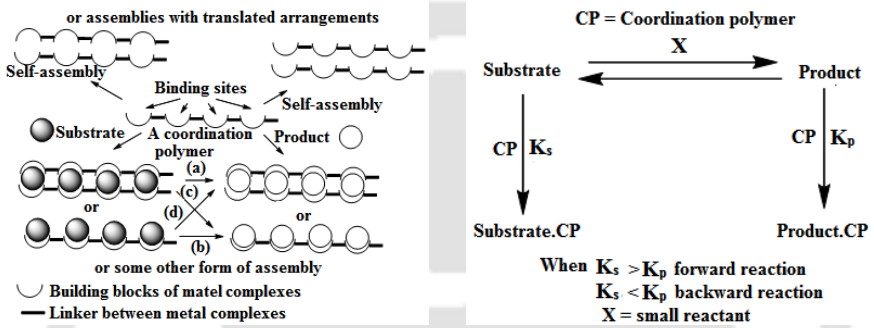

(a) (b)

Figure 4.2.2: (a) Various self-assemblies, interactions of substrate or product with 1-D coordination polymer and (b) Different equilibrium of coordination polymer with substrate.

The ability of a substrate or product to reversibly bind or associate with a coordination polymer will be a deciding factor to shift the equilibrium between reactant and product (**Fig. 4.2.2b**). In this part of this chapter the association ability of an aldehyde and corresponding aldoxime with cadmium coordination polymer having identical linker is described.

4.2.2: Synthesis of different cadmium coordination polymers of 1,3-bis(4-pyridyl)propane ligand

Cadmium coordination polymer with 1,3-bis(4-pyridyl)propane as linkers (abbreviated as **CP-4.2.1)** is formed by reaction of 1,3-bis(4-pyridyl)propane and cadmium nitrate in methanol-dimethylformamide solvent mixture. The cadmium coordination polymers of 1,3-bis(4-pyridyl)propane having guests namely 2,4-dihydroxybenzaldehyde and 2,4-dihydroxybenzaldoxime, abbreviated as **CP-4.2.2** and **CP-4.2.3** (**Scheme 4.2.1**) respectively are prepared by three component reactions of cadmium nitrate, 1,3-bis(4-pyridyl)propane together with 2,4-dihydroxybenzaldehyde or 2,4-dihydroxybenzaldoxime (oxime **2.1.3**).

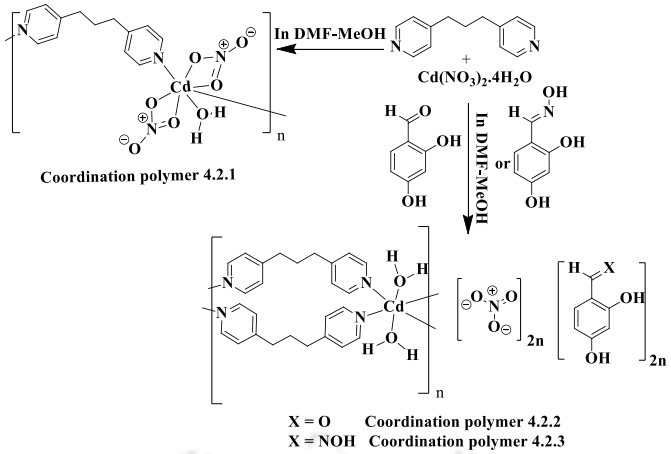

Scheme 4.2.1: Synthesis of cadmium coordination polymer and guest encapsulation.

The coordination polymers are characterized by conventional spectroscopy, X-ray structure determination and by comparing the experimentally observed powder X-ray diffraction data with the generated diffraction pattern from the crystallographic information files.

4.2.3: Structural descriptions of cadmium coordination polymers 4.2.1-4.2.3

The coordination polymer **4.2.1** that was prepared from the reaction of 1,3-bis(4-pyridyl)propane with cadmium nitrate tetrahydrate was a 1:1 coordination polymer having monohydrated cadmium nitrate bridged by 1,3-bis(4-pyridyl)propane. In this coordination polymer each cadmium ion is in six coordinated environment and connected to two nitrogen atoms of pyridine rings of 1,3-bis(4-pyridyl)propane bridging ligands. There are two bis-chelating nitrates and a water molecule coordinated to each cadmium ion. Interpenetrated structures are generally observed in coordination polymers of 1,3-bis(4-pyridyl)propane with cadmium,[20] present example is a simple one-dimensional coordination polymers was prepared at mild conditions. Structure of CP-**4.2.1** complements reported one-dimensional cadmium CPs of flexible bridging ligands, 4-pyridyl-(CH_2)n-4-pyridyl (n = 1, 2).[21]

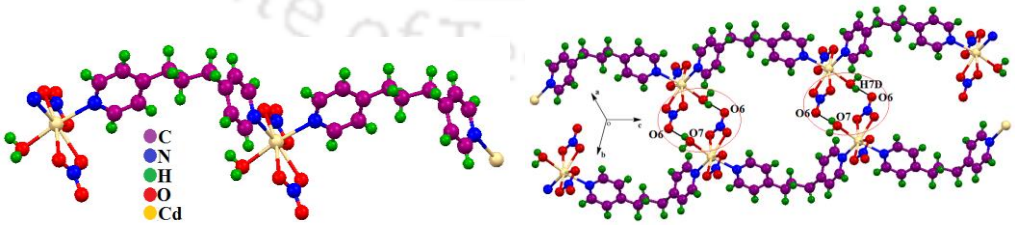

(a) (b)

Figure 4.2.3: (a) Structure of CP-**4.2.1** and (b) Hydrogen bonded self-assembly formed by interactions of coordinated nitrates in one chain with coordinated water of another chain of CP-**4.2.1**.

Hydrogen bonds of coordinated water molecules with nitrate anions make 2-dimensional sheet-like structure of CP-**4.2.1**(**Fig. 4.2.3**). For hydrogen bonds and sort contacts parameters of supramolecular assembly please see **Table 4.2.1** and page 229 of appendix. CP-**4.2.1** is relatively less soluble in common solvents, it can be modified to CP-**4.2.2** or CP-**4.2.3** by treating with 2,4-dihydroxybenzaldehyde or 2,4-dihydroxybenzaldoxime (oxime **2.1.3**) respectively. However, these reactions provide low yields of CP-**4.2.2** and CP-**4.2.3**. The low yield from such method of synthesis is attributed to the required stoichiometry of ligand for such transformation. Guest included coordination polymers require 1: 2 metal to 1,3-bis(4-pyridyl)propane stoichiometry; whereas CP-**4.2.1** has such 1:1 ratio. Alternative procedure by starting with cadmium nitrate tetrahydrate and 1,3-bis(4-pyridyl)propane in appropriate stoichiometry in the presence of respective guest molecules provided good yields of CP-**4.2.2** and CP-**4.2.3** (**Scheme 4.2.1**).

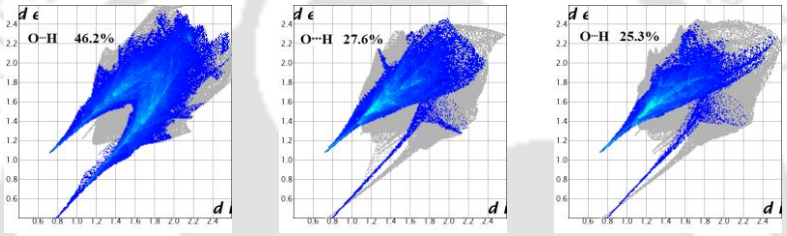

(a) (b) (c)

Figure 4.2.4: Fingerprint plots for (a) CP-**4.2.1**, (b**) CP-4.2.2** and (c) CP-**4.2.3** with O···H interactions highlighted in colour.

Hirshfeld surface[22] analysis of the three coordination polymers show that the percentage of O-H interactions (**Fig. 4.2.4)** in the case of CP-**4.2.1** there is 46.2 % interactions involving O-H hydrogen bonds, whereas in the case of the guest encapsulated coordination polymers the contribution of O-H interactions to overall weak interactions are 27.5 % in CP-**4.2.2** and 25.3 % in CP-**4.2.3**. These distributions of weak interactions suggest that the two guest included compounds have comparable hydrogen bonds involving O-H hence for any interconversion there is only slight reorganization of such weak interactions would be required.

Earlier study had shown that carboxylic acid was included as guest in sub-assemblies of 4 × 4 metallacycles of cadmium coordination polymer.[23] The present frames of the guest-included coordination polymers are comprised of 2 × 2 metallacycles as repeat units where two independent molecules of 1,3-di(pyridin-4-yl)propane hold two cadmium ions. Hence, guest as well as counter ions has important roles to stabilize their respective self-assemblies. Domain adjustments in these assemblies happen to accommodate guest molecules. Domain expansion is suggested by us as a major issue to reshuffle a non-covalent assembly for

molecular recognition.[24] Structures of the two guests included coordination polymers not only have similar metallacycle repeat units but also have similar self-assemblies. Both these guest included coordination polymers have cadmium ions with six coordination number; among which four coordination sites are occupied by ligating nitrogen atoms and other two sites in axial positions are occupied two water molecules.

Table 4.2.1: Hydrogen bond parameters of coordination polymers **4.2.1**-**4.2.3**.

CP	D-H···A	d_{D-H} (Å)	$d_{H\cdots A}$ (Å)	$d_{D\cdots A}$ (Å)	∠D-H···A (°)
CP-**4.2.1**	O(7)-H(7C)···O(2) [2-x, 2-y, -z]	0.87(4)	1.90(3)	2.773(3)	172(4)
	O(7)-H(7D)···O(6) [2-x, 1-y, -z]	0.79(5)	2.04(2)	2.809(2)	168(3)
	C(2)-H(2)···O(5) [2-x, 2-y, 1-z]	0.93(3)	2.59(4)	3.508(3)	168(4)
	C(4)-H(4)···O(3) [-1+x, y, z]	0.93(3)	2.39(3)	3.214(3)	147(3)
CP-**4.2.2**	O(3)-H(3)···O(6) [1+x, -1+y, z]	0.82(3)	2.01(5)	2.788(5)	158(6)
	O(7)-H(7A)···O(4) [1+x, -1+y, z]	0.87(6)	1.92(5)	2.790(5)	178(7)
	O(7)-H(7B)···O(6) [x, y, z]	0.82(6)	2.02(6)	2.837(5)	175(3)
	C(10)-H(10)···O(1) [1-x, 1-y, 1-z]	0.93(8)	2.55(7)	3.345(6)	143(6)
	C(13)-H(13)···O(4) [x, -1+y, z]	0.93(7)	2.54(4)	3.197(5)	128(4)
CP-**4.2.3**	O(1)-H(1A)···O(4) [-x, -y, 1-z]	0.88(5)	1.91(2)	2.788(3)	171(4)
	O(1)-H(1B)···O(2) [x, -1+y, 1+z]	0.88(6)	2.00(4)	2.847(3)	162(3)
	O(5)-H(5A)···O(3) [1-x, 1-y, 1-z]	0.82(5)	2.11(6)	2.864(3)	152(7)
	O(6)-H(6)···O(2) [x, y, z]	0.82(7)	2.25(4)	2.916(3)	138(6)
	O(6)-H(6)···O(4) [x, y, z]	0.82(3)	2.38(4)	3.181(3)	166(5)

Coordination polymer **4.2.2** having 2,4-dihydroxybenzaldehyde is shown in **Fig. 4.2.5**. In this case the layer-like supramolecular assembly (**Fig. 4.2.5b**) is formed by cationic chains in which the each cadmium ion is connected to four 1,3-bis(4-pyridyl)propane ligand. The repeat units are comprised of 2 × 2 metallacycles as illustrated in **Fig. 4.2.5a**. The two layers are connected by hydrogen bonds between nitrate anions and coordinate water molecules located in the spaces between the layers making compartments; those compartments include guest molecules (**Fig. 4.2.5c)**. The 2,4-dihydroxybenzaldehyde interacts with such partitioned self-assemblies by forming hydrogen bonds involving oxygen atom of nitrate and O-H of phenolic group located at 4-position of the ring (**Fig. 4.2.5d)**. Neighbouring guest molecules also interact between them through weak C-H···O interactions involving the phenolic hydroxy-group located at 2-position of the phenyl-ring as shown in **Fig. 4.2.5d**.

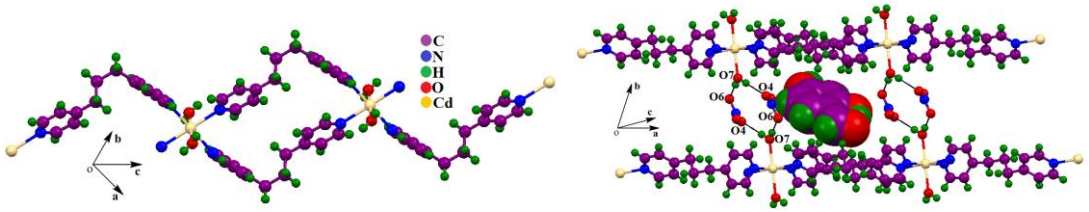

(a) (b)

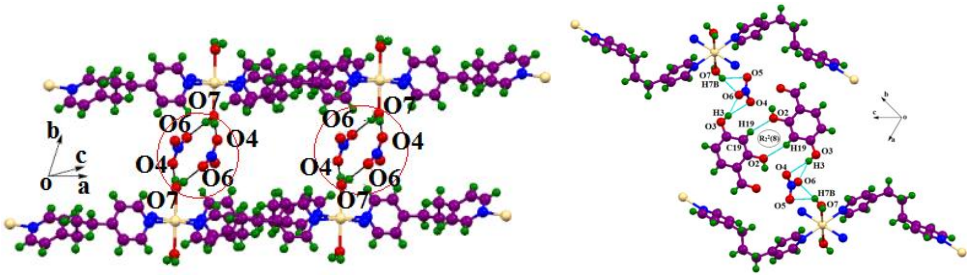

(c) (d)

Figure 4.2.5: (a) Cationic part of CP-**4.2.2**, (b) Guest encapsulated packing pattern of CP-**4.2.2**, (c) An enclosure formed by nitrate anions interacting with coordinated water molecules (without guest) and (d) Self-assembly formed by 2,4-dihydroxybenzaldehyde nitrate and coordinated water molecules in CP-**4.2.2**.

The coordination polymer **4.2.3** has 2,4-dihydroxybenzaldoxime (oxime **2.1.3**) as inclusion complex; it possesses exactly similar self-assembly as that of the CP-**4.2.2** as shown in **Fig. 4.2.6a**. The dissimilarity between the structures of the two guest included coordination polymer arises from the hydrogen bonds between the nitrate ions with the oxime molecules. The oxime **2.1.3** forms hydrogen bonds (**Fig. 4.2.6b)** involving more sites than the corresponding aldehyde in the respective coordination polymers. These hydrogen bonds are from the O-H of the oxime at one site, and the phenolic O-H located at 4-position at other site. For such hydrogen bonds two independent nitrate ions of different cationic chains are involved.

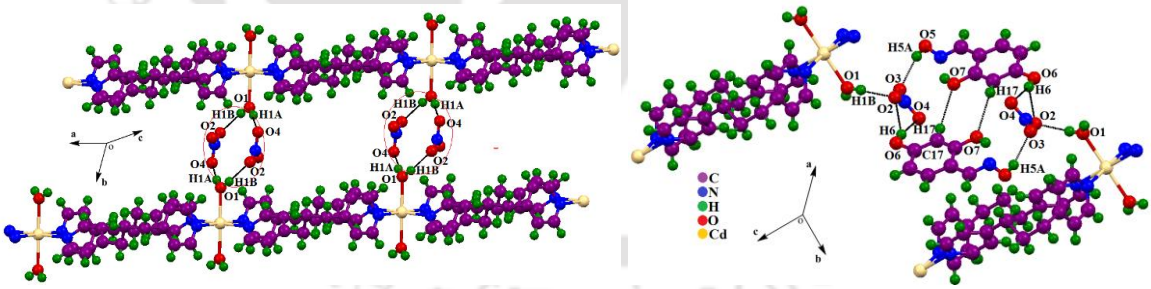

(a) (b)

Figure 4.2.6: (a) Nitrate and coordinated water molecules form hydrogen bonded layers structure in CP-**4.2.3** and (b) The assembling between oxime **2.1.3** molecules in CP-**4.2.3**.

Fundamental difference of self-assemblies of CP-**4.2.1** from other two coordination polymer in term of their respective hydrogen bonds. CP-**4.2.1** has water molecules and nitrate anions that are coordinated to cadmium ions, whereas in CP-**4.2.2** or CP-**4.2.3** has only the coordinated water molecules, but nitrate anions in the latter two cases are outside the coordination sphere.

4.2.4: Conversion of aldehyde to oxime transformation studied by the help of isothermal calorimetric titration (ICT) and FT-IR

Aldoximes are generally prepared from corresponding aldehydes. They also undergo hydrolysis to form parent aldehydes under suitable conditions.[25] Difference in binding or affinity of such substrates would shift the equilibrium of formation and decomposition between an aldehyde and corresponding oxime. Such possibilities are explored and found that the reaction of 2,4-dihydroxybenzaldehyde with hydroxylamine is catalysed by cadmium coordination polymer **4.2.1**. The reaction proceeds in approximately 30 minutes time to form 2,4-dihydroxybenzaldoxime (1mmol) from 2,4-dihydroxybenzaldehyde (1mmol) at room temperature with one mole percentage of the catalyst, whereas without the catalytic amount of the catalyst the reaction proceeds in about 3-4 hrs. After the reaction the coordination polymer **4.2.1** transforms to oxime included coordination polymer as illustrated in **scheme 4.2.2**. The coordination polymer has ability to catalyse the reaction of aldehyde to oxime. It is also found that a reaction of hydroxylamine with CP-**4.2.2** yields CP-**4.2.3**, whereas CP-**4.2.3** in water does not get hydrolyzed to form CP-**4.2.2**. Thus the reaction schemes are confirmed by comparing the IR spectra of the CP-**4.2.2**, CP-**4.2.3** and crude product of reaction between CP-**4.2.2** and hydroxylamine. The IR spectra of the CP-**4.2.2** has carbonyl stretching at 1628 cm^{-1} and 1654 cm^{-1}, which upon conversion to C=N appears at 1615 cm^{-1} (**Fig. 4.2.7**). There may be also an alternative suggestion for such an oximation reaction to suggest that the degraded product of cadmium complex in solution plays a role in catalysis. For such a happening on transformation of CP-**4.2.1** to CP-**4.2.3** a disproportionation reaction would be required. The guest included coordination polymers have 1:2 metals to linker ratio, whereas starting polymer has 1:1. Hence a disproportionation reaction of CP-**4.2.3** will require change in stoichiometry of linkers and free cadmium ions. We have negated the participation of free cadmium ion in the catalytic deoximation process, as externally added 1,3-bis(4-pyridyl)propane did not affect the catalytic oximation reaction by CP-**4.2.1** and nor the oximation reaction is facilitated by cadmium nitrate alone. A reaction carried out by adding additional cadmium ions to a reaction mixture of oxime containing catalytic amount of CP-**4.2.1**, showed the same result without improving overall yield.

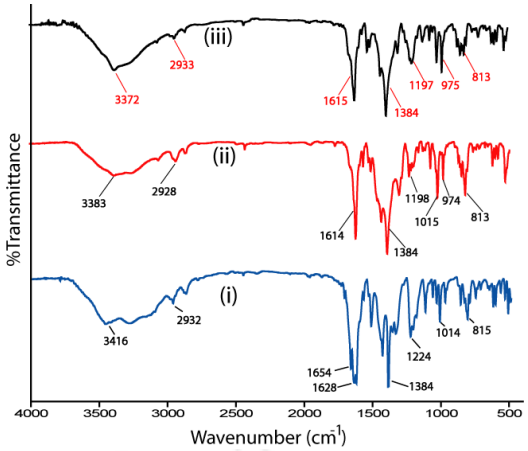

Figure 4.2.7: FTIR (KBr, cm^{-1}) of the coordination polymer (i) CP-**4.2.2**; (ii) CP-**4.2.3**; (iii) Crude product of CP-**4.2.2** upon recation with hydroxylamine.

Thermodynamic parameters for association of CP-**4.2.1** with 2,4-dihydroxybenzaldehyde or 2,4-dihydroxybenzaldoxime (oxime **2.1.3**) in solution are determined by isothermal calorimetric titrations studied. Association ability of the oxime is about three times higher than the aldehyde (**Table 4.2.2**). The interactions of host and guest shows higher enthalpy and entropy change upon association of oxime to CP-**4.2.1** than the association of aldehyde with this coordination polymer.

Table 4.2.2: Thermodynamic parameters of host-guest association

Titrant	K_a (M^{-1})	ΔH (kcal/mol)	ΔS (cal/mol/deg)
A	1×10^2	-5.197×10^4	-1.65×10^2
B	2.92×10^2	-1.107×10^4	-2.58×10^1

A = 2,4-dihydroxybenzaldehyde, B = 2,4-dihydroxybenzaldoxime (oxime **2.1.3**)

Accordingly, conversion of aldehyde to oxime is facilitated by the CP-**4.2.1**; this is evident from reaction between 2,4-dihydroxybenzaldehyde with hydroxylamine in methanol. One mole percent of CP-**4.2.1** helps instantaneous formation of 2,4-dihydroxybenzaldoxime from such a reaction, whereas in its absence incomplete conversion is observed.

Fluorescence spectroscopy is used to study the reactivity of the coordination polymers with guest molecules. A solution of CP-**4.2.1** is weakly fluorescent upon excitation at 306 nm; it shows an emission peak at 403 nm. A similar excitation of solution of CP-**4.2.2** or CP-**4.2.3** show similar emission peak of CP-**4.2.1** and but the peak is shifted from original place to 413 or 416 nm respectively (**Fig. 4.2.12**). These emissions are not affected by addition of solution of cadmium nitrate. This suggests that the backbones of coordination polymers remain intact in solution.

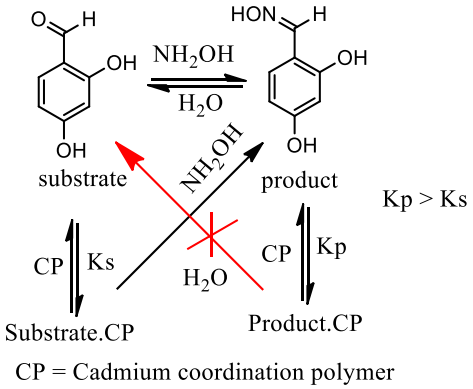

Scheme 4.2.2: Competitive equilibrium for formation hydrogen bonded assemblies.

The inclusion of oximes to the enclosures constructed through hydrogen bonds by interacting nitrate anions with water. Hence, the interaction of aldehyde with coordination polymer CP-**4.2.1** to form the coordination polymer CP-**4.2.2** facilitates the activation of the aldehyde. This activation cause easy transformation from aldehyde to oxime and finally converts the CP-**4.2.1** to polymer CP-**4.2.3**. The difference in bindings of aldehyde and oxime to coordination frame controls the inflow of aldehyde and outflow of oxime to maintain cyclic reaction path that occurred due to binding differences to form non-covalently linked self-assemblies (**scheme 4.2.2**).

4.2.5: Conclusions

In this study we have shown the ability of nitrate ion to control supramolecular features, stoichiometry and the guest inclusion of cadmium coordination polymers with 1,3-bis(4-pyridyl)propane as linker. Coordinated nitrate ions in the coordination polymer without guest prevents it to have 1:2 stoichiometry between cadmium ion and linkers, whereas the ionic nitrate form hydrogen bond with coordinated water provided partition in self-assemblies of coordination polymers to encapsulate oxime or aldehyde as guests. The aldehyde included in self-assembly is easily converted to oxime by reaction with hydroxylamine as (a) aldehyde has lower association ability and (b) oximes formed from such reactions adopt similar guest included structures with least reorganisations. This study clarifies that formation of self-assembled host-guest complexes through reorganisation of a coordination polymer by guest molecules help the guest to serve as a reactant to form product. The hydrolysis of C=N bond to carbonyl by the coordination polymer is not favoured. The oximes and aldehydes used for inclusion study are derived from oxidisable hydroxyaromatic compounds; these oxidisable compounds get stabilized in supramolecular environment and utilized for chemical transformation as per necessity namely in the conversion CP-**4.2.2** to CP-**4.2.3** in presence of hydroxylamine.

4.1.6: Experimental section

Synthesis and characterization of cadmium coordination polymers 4.2.1-4.2.3:

1,3-bis(4-pyridyl)propane (0.198gm, 1 mmol) and cadmium nitrate tetrahydrate (0.308 gm, 1 mmol) were dissolved in 20 ml methanol and stirred for overnight. A white precipitate was obtained; the reaction mixture was filtered and dried at room temperature. Dried product was CP-**4.2.1**, which was further recrystallized from dimethylformamide solution to get crystal of CP-4.2.1. The CP-**4.2.2** and CP-**4.2.3** were prepared by following procedure identical to CP-**4.2.1**, but by changing the stoichiometry as 1,3-bis(4-pyridyl)propane (0.40 gm, 2 mmol) and cadmium nitrate tetrahydrate (0.308 gm, 1 mmol) with guest (2 mmol) 2,4-dihydroxybenzaldehyde or 2,4- dihydroxybenzaldoxime (oxime **2.1.3**).

CP-**4.2.1**: Isolated yield: 72 %. ^{1}H-NMR (600 MHz, DMSO-d_6): 8.45 (d, J = 6 Hz, 4H), 7.27 (d, J = 6 Hz, 4H), 2.63 (t, J = 6 Hz, 4H), 1.94 (p, J = 6 Hz, 2H). IR (KBr, cm^{-1}): 3451 (br, s), 2929 (w), 1615 (s), 1560 (s), 1460 (w), 1431 (w), 1384 (s), 1292 (m), 1275 (m), 1225 (s), 1069 (s), 1018 (s), 842 (m), 816 (s), 734 (w), 668 (m), 613 (m).

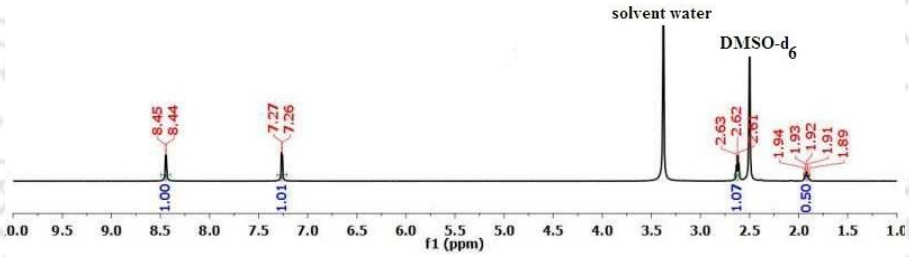

Figure 4.2.8: ^{1}H-NMR (DMSO-d_6) spectra of CP-**4.2.1**.

CP-**4.2.2**: Isolated yield: 75 %. ^{1}H-NMR (600 MHz, DMSO-d_6): 10.90 (s, 1H), 10.64 (s, 1H), 9.92 (s, 1H), 8.45 (d, J = 6 Hz, 4H), 7.53 (d, J = 6 Hz, 1H), 7.25 (d, J = 6 Hz, 4H), 6.40 (d, J = 6 Hz, 1H), 6.31 (s, 1H), 2.63 (t, J = 6 Hz, 4H), 1.94 (p, J = 6 Hz, 2H). IR (KBr, cm^{-1}): 3416 (br, w), 2932 (w), 1654 (s), 1628 (w), 1613 (w), 1560 (w), 1507 (s), 1425 (s), 1384 (s), 1330 (w), 1224 (s), 1117 (s), 1065 (w), 1014 (s), 975 (m), 863 (m), 815 (s), 798 (w), 630 (m), 613 (m).

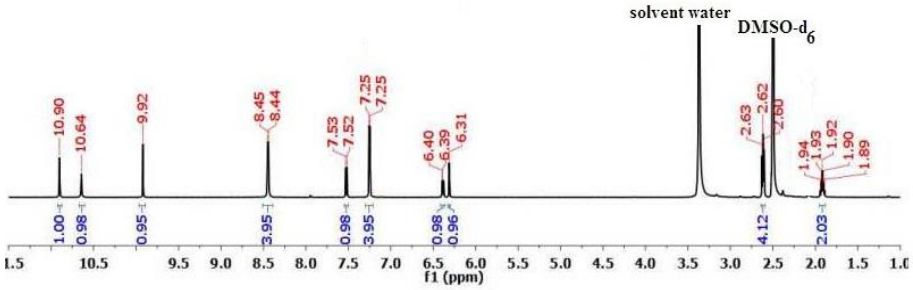

Figure 4.2.9: ^{1}H-NMR (DMSO-d_6) spectra of CP-**4.2.2**.

CP-**4.2.3**: Isolated yield: 70 %. ^{1}H-NMR (600 MHz, DMSO-d_6): 10.97 (s, 1H), 10.10 (s, 1H), 9.76 (s, 1H), 8.45 (d, J = 6 Hz, 4H), 8.19 (s, 1H), 7.26 (d, J = 6 Hz, 4H), 7.23(s, 1H), 6.29 (d, J = 6 Hz, 2H), 2.63 (t, J = 6 Hz, 4H), 1.94 (p, J = 6 Hz, 2H). IR (KBr, cm^{-1}): 3372 (br, s), 2933 (w), 1615 (s), 1522 (m), 1504 (w), 1426 (w), 1384 (s), 1298 (m), 1197 (s), 1117 (s), 1066 (m), 1013 (s), 975 (s), 864 (w), 840 (w), 798 (w), 612 (m).

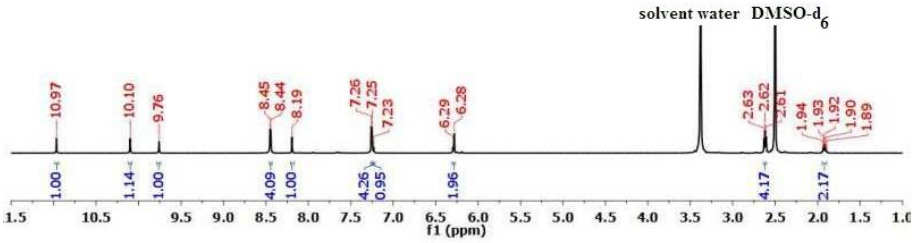

Figure 4.2.10: ^{1}H-NMR (DMSO-d_6) spectra of CP-**4.2.3**.

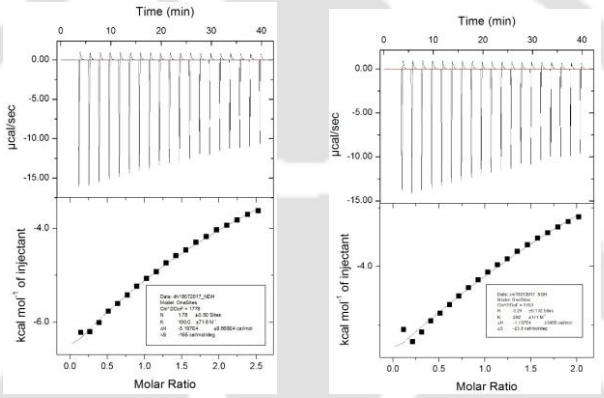

(a) (b)

Figure 4.2.11: ITC titration of CP-**4.2.1** with (a) 2,4-dihydroxybenzaldehyde and (b) 2,4-dihydroxybenzaldoxime.

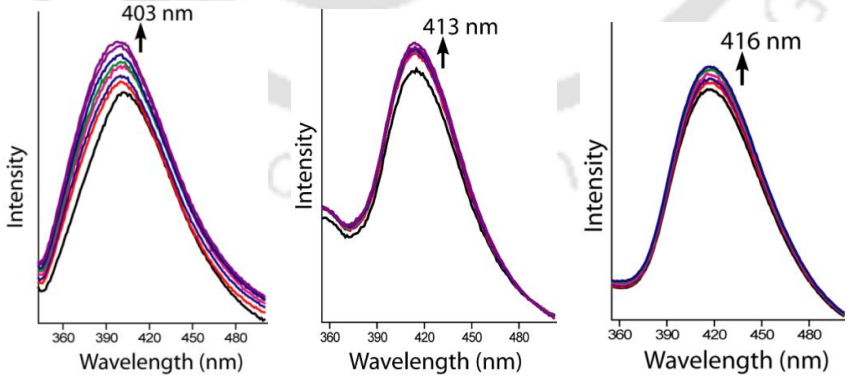

(a) (b) (c)

Figure 4.2.12: Fluorescence emission of (a) CP-**4.2.1** (10^{-4} M) with different amount of 1,3-di(pyridin-4- yl)propane (10^{-3} M), (b) CP-**4.2.2** (10^{-4} M) and (c) CP-3 (10^{-4} M) with different amount of cadmium (10^{-3} M) (each excitation at 306 nm, solutions are in dimethylformamide).

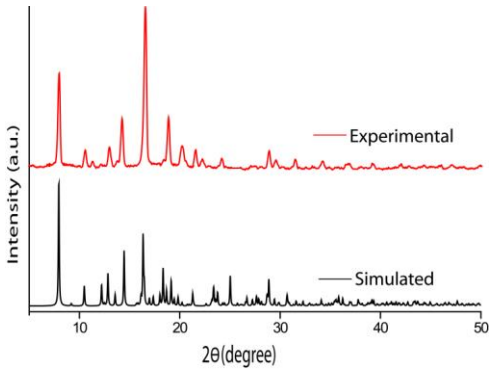

Figure 4.2.13: PXRD pattern of CP-**4.2.1** (Red= Experimental, Black= Simulated). Simulated pattern generated from cif file.

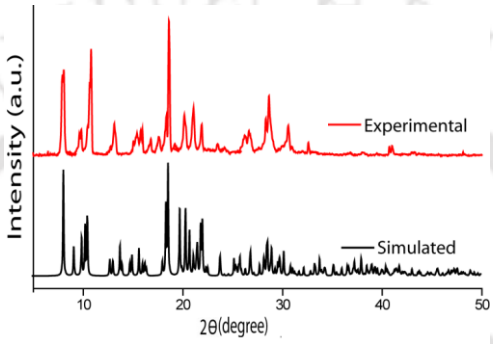

Figure 4.2.14: PXRD pattern of CP-**4.2.2** (Red= Experimental, Black= Simulated). Simulated pattern generated from cif file.

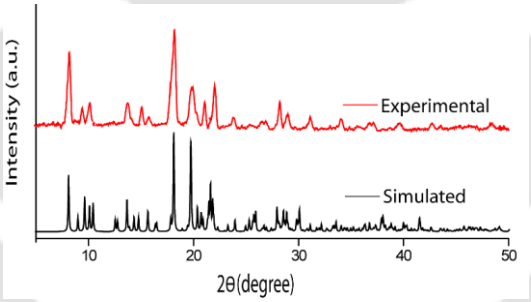

Figure 4.2.15: PXRD pattern of CP-**4.2.3** (Red= Experimental, Black= Simulated). Simulated pattern generated from cif file.

Table 4.2.3: Relative contributions of various interactions in percentage to Hirshfeld surface area in different coordination polymers **4.2.1-4.2.3**.

	CP-**4.2.1**	CP-**4.2.2**	CP-**4.2.3**
O···O	2.4	0.0	0.0
N···O	1.3	0.1	0.0
C···O	5.2	0.2	0.1
H···O	46.2	27.6	25.3
C···N	1.4	0.1	0.0
N···H	3.8	5.6	6.4

C···H	10.3	27.8	27.7
C···C	0.0	2.8	2.2
H···H	28.1	34.1	36.4

4.2.7: References

1. (a) H. C. Zhou, S. Kitagawa, *Chem. Soc. Rev*., 2014, **43**, 5415-5418; (b) J. Heine, K. Müller-Buschbaum, *Chem. Soc. Rev*., 2013, **42**, 9232-9242; (c) H. Zhang, J. Nai, L. Yu, X. W. Lou, *Joule*, 2017, **1**, 77-107.
2. (a) Q. G. Zhai, X. H. Bu, X. Zhao, D. S. Li, P. Y. Feng, *Acc. Chem. Res*., 2017, **50**, 407-417; (b) G. Ferey, C. Serre, T. Devic, G. Maurin, H. ́ Jobic, P. L. Llewellyn, G. D. Weireld, A. Vimont, M. Daturi, J. S. Chang, *Chem. Soc. Rev*., 2011, **40**, 550-562.
3. (a) K. Liu, X. J. Zhang, X. X. Meng, W. Shi, P. Cheng, A. K. Powell, *Chem. Soc. Rev*., 2016, **45**, 2423-2439; (b) X. J. Zhang, V. Vieru, X. W. Feng, J. L. Liu, Z. J. Zhang, B. Na, W. Shi, B. W. Wang, A. K. Powell, L. F. Chibotaru, S. Gao, P. Cheng, J. R. Long, *Angew. Chem., Int. Ed*., 2015, **54**, 9861-9865.
4. (a) P. Horcajada, T. Chalati, C. Serre, B. Gillet, C. Sebrie, T. Baati, J. F. Eubank, D. Heurtaux, P. Clayette, C. Kreuz, J. S. Chang, Y. K. Hwang, V. Marsaud, P. N. Bories, L. Cynober, S. Gil, G. Ferey, P. Couvreur, R. Gref, *Nat. Mater*., 2010, **9**, 172-178; (b) R. C. Huxford, K. E. deKrafft, W. S. Boyle, D. Liu, W. B. Lin, *Chem. Sci*., 2012, **3**, 198-304.
5. (a) Z. C. Hu, B. J. Deibert, J. Li, *Chem. Soc. Rev*., 2014, 43, 5815-5840; (b) W. P. Lustig, S. Mukherjee, N. D. Rudd, A. V. Desai, J. Li, S. K. Ghosh, *Chem. Soc. Rev*., 2017, **46**, 3242-3285; (c) Y. J. Cui, Y. F. Yue, G. D. Qian, B. L. Chen, *Chem. Rev*., 2012, **112**, 1126-1162; (d) M. D. Allendorf, C. A. Bauer, R. K. Bhakta, R. J. T. Houk, *Chem. Soc. Rev*., 2009, **38**, 1330-1352.
6. (a) V. Ramamurthy, K. Venkatesan, *Chem. Rev*., 1987, 87, 433-481; (b) P. Garcia-Garcia, J. M. Morenol, U. Diazl, M. Bruix, A. Corma, *Nature Commun*. 2016, **7**, 10835.
7. (a) W. M. Bloch, C. J. Sumby, *Chem. Commun*., 2012, **48**, 2534-2536; (b) J. Shi, Y. Zhang, B. Zhang, D. Zhu, *Dalton Trans*., 2016, **45**, 89-92.
8. J. Nath, A. Kirillov, J. B. Baruah, *RSC Adv*., 2014, **4**, 47876-47886.
9. (a) J. W. Liu, L. F. Chen, H. Cui, J. Y. Zhang, L. Zhang, C. Y. Su, *Chem. Soc. Rev*., 2014, **43**, 6011-6061; (b) A. Dhakshinamoorthy, H. Garcia, *Chem. Soc. Rev*., 2014, **43**, 5750-5765; (c) T. Zhang, W. B. Lin, *Chem. Soc. Rev*., 2014, **43**, 5982-5993.

10. (a) L. Zeng, X. Guo, C. He, C. Duan, *ACS Catal*., 2016, **6**, 7935-7947; (b) D. Farrusseng, S. Aguado, C. Pine, *Angew. Chem. Int. Ed*., 2009, **48**, 7502-7513; (c) L. Zhu, X. -Q. Liu, H. -L. Jiang, L. -B. Sun, *Chem. Rev*., 2017, **117**, 8129-8176.
11. (a) Z. Ju, S. Yan, D. Yuan, *Chem. Mater*., 2016, **28**, 2000-2010; (b) T. Sun, X. Ren, J. Hu, S. Wang, *J. Phys. Chem. C,* 2014, **118**, 15630-15639; (c) D. Jiang, A. Urakawa, M. Yulikov, T. Mallat, G. Jeschke, A. Baiker, *Chem. Eur. J*., 2009, **15**, 12255-12262; (d) S. Yuan, L. Zou, J. -S. Qin, J. Li, L. Huang, L. Feng, X. Wang, M. Bosch, A. Alsalme, T. Cagin, H. -C. Zhou, *Nature Commun*., 2017, **8**, 15356.
12. (a) D. Tanaka, K. Nakagawa, M. Higuchi, S. Horike, Y. Kubota, T. C. Kobayashi, M. Takata and S. Kitagawa, *Angew. Chem., Int. Ed*., 2008, **47**, 3914-3918; (b) H.-S. Choi and M. P. Suh, *Angew. Chem., Int. Ed*., 2009, **48**, 6865-6869.
13. M.J. Plater, M. R. S. J. Foreman, T. Gelbrich, M.B. Hursthouse, *Dalton Trans*., 2000, **13**, 1995-2000; (b) J. Y. Lee, S. J. Hong, C. Kim, *Inorg. Chem. Commun*., 2002, **8**, 692-696; (c) S. H. Choi, J. Y. Ryu, J.Y. Lee, *Appl. Organomet. Chem*., 2004, **18**, 369-379.
14. E. J. Gao, X. Y. Xu, M. C. Zhu, H. L. Yan, H. Fu, H. Wang, L. Zhan, Q. Yao, M. Y. Li, M. P. Jiang, *Russ. J. Coord. Chem*., 2014, **40**, 583-587.
15. (a) Q. Huang, J. -H. Huang, L. Gu, J. -X. Ruan, Y. -H. Yu, J. -S. Gao, RSC Adv., 2018, 8, 557-566; (b) F. -A. Li, W. -C. Yang, S. -Z. Bai, *Inorg. Chem. Commun*., 2014, 46, 65-68.
16. (a) A. Beziau, S. A. Baudron, G. Rogez, M. W. Hosseini, *Inorg. Chem*., 2015, **54**, 2032-2039; (b) J. J. Henkelis, M. J. Hardie, *Chem.Commun*., 2015, **51**, 11929-11943. (c) D. G. Kurth, *Sci. Technol. Adv. Mater*., 2008, **9**, 014103.
17. (a) K. Uemura, K. Saito, S. Kitagawa, H. Kita, *J. Am. Chem. Soc*., 2006, **128**, 16122-16130; (b) C. B. Aakeroy, A. M. Beatty, D. S. Leinen, *Angew. Chem. Int. Ed*., 1999, **38**, 1815-1819; (c) X. -Z. Luo, X. -J. Jia, J.-H. Deng, J. -L. Zhong, H. -J. Liu, K. -J. Wang, D. -C. Zhong, *J. Am. Chem. Soc*., 2013, **135**, 11684-11687; (d) T. K. Maji, S. Kitagawa, *Pure Appl. Chem*., 2007, **79**, 2155-2177.
18. (a) A. -X, Tian, J. Ying, J. Peng, J. -Q. Sha, H. -J. Pang, P. -P. Zhang, Y. Chen, M. Zhu, Z. -M. Su, *Cryst. Growth Des*., 2008, **8**, 3717-3724; (b) Pan, T. Frydel, M.B Sander, X. Huang, J. Li, *Inorg. Chem*., 2001, **40**, 1271-1283; (c) I. M. L. Rosa, M. C. S. Costa, B. S. Vitto, L. Amorim, C. C. Correa, C. B. Pinheiro, A. C. Doriguetto, *Cryst. Growth Des*., 2016, **16**, 1606-1616; (d) M. Mazaj, G. Mali, M. Rangus, E.

Zunkovic, V. Kaucic, N. Z. Logar, *J. Phys. Chem. C*, 2013, **117**, 7552-7564; (e) W. M. Singh, J. B. Baruah, *Inorg. Chim. Acta*, 2009, **362**, 4977-4984.

19. (a) M. Mazaj, T. B. Celic, G. Mali, M. Rangus, V. Kaucic, N. Z. Logar, *Cryst. Growth Des*., 2013, **13**, 3825-3834; (b) L. Li, S. Wang, T. Chen, Z. Sun, J. Luo, M. Hong, *Cryst. Growth Des*., 2012, **12**, 4109-4115; (c) F. F. B. J. Janssen, L. P. J. Veraart, J. M. M. Smits, R. de Gelder, A. E. Rowan, *Cryst. Growth Des*., 2011, **11**, 4313-4325; (d) J. Cepeda, S. Perez-Yanez, *Eur. J. Inorg. Chem*., 2014, **2014**, 3221-3234; (e) R. Sarma, J. B. Baruah, *Inorg. Chim. Acta*, 2009, **362**, 4977-4984; (f) W. M. Singh, J. B. Baruah, *Dalton Trans*., 2009, 2352-2358.
20. (a) Md. B. Zaman, K. Udachin, J. A. Ripmeester, *Inorg. Chem.*, 2005, **44**, 5047-5059; (b) E. -C. Yang, X. -J. Shi, Z. -J. Liu, X. -J. Zhao, *Inorg. Chem. Commun*., 2010, **13**, 733-736; (c) S. Wang, H. Xing, Y. Li, J. Bai, H. Xing, Y. Pan, X. You, *Eur. J. Inorg. Chem.*, 2006, **2006**, 3041-3053.
21. F. Makoto, A. Masaru, O. Katsuyuki, *Bull. Chem. Soc. Jpn.*, 1998, **71**, 1799-1804.
22. (a) M. A. Spackman, D. Jayatilaka, *CrystEngComm*, 2009, **11**, 19-32; (b) J. J. McKinnon, D. Jayatilaka, M. A. Spackman, *Chem. Commun*., 2007, 3814-3816.
23. N. Phukan, J. B. Baruah, *J. Mol. Struct.*, 2014, **1076**, 614-619.
24. (a) A. Taria, J. B. Baruah, *CrystEngComm* 2016, **18**, 9095-9102; (b) A. Taria, J. B. Baruah, *New J. Chem.*, 2017, **41**, 10750-10760.
25. (a) V. Y. Kukushkin, A. J. L. Pombeiro, *Coord. Chem. Rev.*, 1999, **181**, 147-175; (b) A. G. Smith, P. A. Tasker, D. J. White, *Coord. Chem. Rev*., 2003, **241**, 61-85.

Chapter 5

Supramoleular Aspects of Quinoline-4-carbaldoxime with Aliphatic Dicarboxylic or Mineral or Aromatic Carboxylic Acids

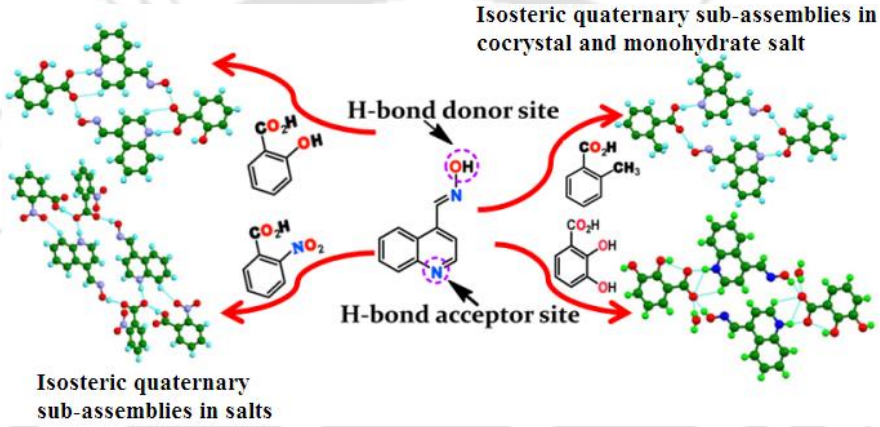

CrystEngComm, 2016, **18**, 298-308.
CrystEngComm, 2016, **18**, 9095-9102.

5.1: Introduction

Design and synthesis of non-covalently linked assemblies with desired chemical and physical properties are important in crystal engineering.[1] A cocrystal may be defined as a crystalline adduct composed of at least two components, where the components may be atoms, ions or molecules.[2] The physicochemical properties of a compound in the solid state can be modified by forming cocrystal with selective coformer molecule.[3] Because of directional properties of the weak interactions they are very useful to construct cocrystals.[4] Hydrogen bonds play a crucial role among other weak interactions in self-assemblies of cocrystals.[5] Supramolecular synthon approach in non-covalent synthesis and use of graph set notation in crystal engineering have offered excellent opportunities for pre-design non-covalent synthesis and to describe them elegantly.[6] Nature of architectures of supramolecular self-assemblies have extensive contributions from hydrogen bonds, types of supramolecular synthons, strength and directionality of hydrogen bonds to guide their structures.[7]

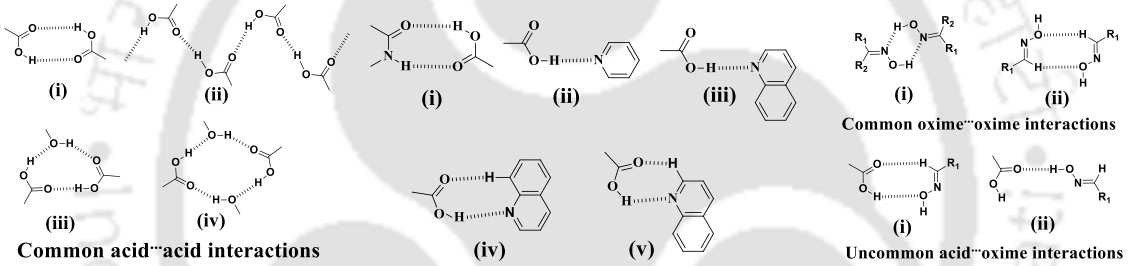

Figure 5.1: Common hydrogen bonds between (a) acid-acid and acid with alcohol, (b) acid-amide, acid-pyridine, acid-quinoline and (c) common oxime-oxime and uncommon acid-oxime interactions.

Advantages of weak interactions among various functional groups; that are capable of hydrogen bond formation in supramolecular chemistry are useful to design cocrystals. Among the functional groups hydroxy, carboxylic acid, amide and oxime are common functional groups to construct various self-assemblies of cocrystals.[8] Different types of hydrogen bonded motifs of carboxylic acids[9] are formed by intermolecular hydrogen bonds (**Fig. 5.1a-b)**. Centrosymmetric dimeric **(i)** assembly of carboxylic acids are well known. There are also examples of hydrogen bonded catemers or chain-like assemblies **(ii)** and single and double bridged assembly **(iii)** and **(iv)** incorporating one and two alcohol or water molecules as illustrated in **Fig. 5.1a**.[10] The carboxylic acids also interact with carboxamide or pyridine and related nitrogen containing heterocyclic compounds.[11] Some hydrogen bonded

motifs formed by interactions between carboxylic acid and carboxamide or pyridine and quinoline derivatives are shown in **Fig. 5.1b**.

Oxime is a typical organic functional group used in various organic reactions, oximes form different non-covalently linked dimers and catemers by interaction between two same kinds of oximes or two different oximes.[12] But, oxime has less affinity to form assemblies with carboxylic acids and phenols. So, there are limited literatures on the self-assemblies of oximes with carboxylic acids. Due to the limited study direct interactions between oximes and carboxylic acids; we explore interactions of quinoline based oxime quinoline-4-carbaldoxime (**5.1**) with different carboxylic acids. The compound **5.1** has sites to anchor carboxylic acid through quinoline part to form suitable cocrystal and in such cocrystals oxime-acid interactions should be possible (**Fig. 5.2**) as secondary interactions.

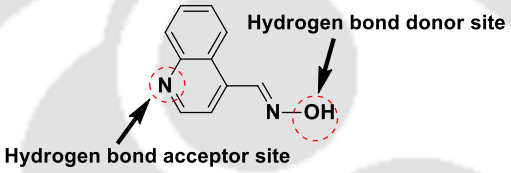

Figure 5.2: Amphoteric compound, quinoline 4-carbaldoxime (**5.1**)

Oxime **5.1** is chosen for such a study as it is an amphoteric compound, which has prospects to form self-assemblies with acidic and basic organic compounds. With such objectives we studied self-assemblies of various cocrystals and salts of oxime **5.1**. It is observed that oxime **5.1** forms cocrystals or crystalline salts with aliphatic-dicarboxylic or mineral or aromatic-carboxylic acids (**Fig. 5.3**).

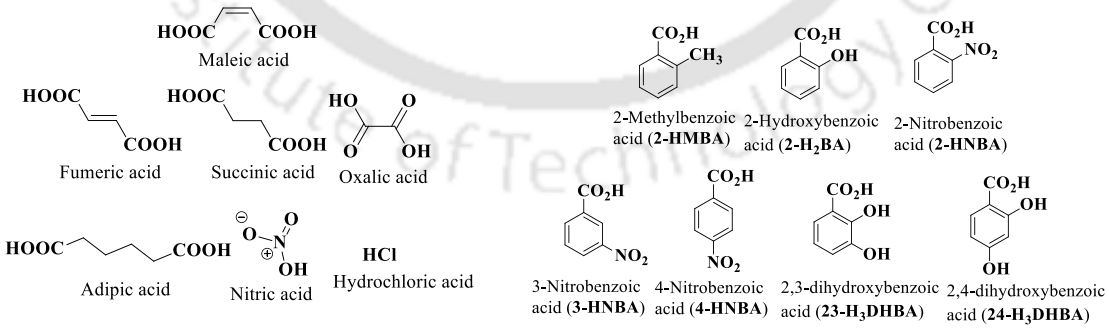

(a) (b)

Figure 5.3: (a) Aliphatic dicarboxylic acids, mineral acids and (b) aromatic carboxylic acids used as coformer for quinoline-4-carbaldoxime.

5.2: Synthesis of cocrystals and salts of quinoline-4-carbaldoxime (5.1)

Due to the two prominent sites for hydrogen bonds in oxime **5.1**, it can choose a partner molecule by one functional unit or by using both functional units to forming hydrogen bonds. Thus, there is a possibility for the quinoline moiety to interact with an acid or a base partner. Such interactions may cause through proton transfer to have electrostatic interactions or via hydrogen bond formation with a partner molecule. It is observed that oxime **5.1** easily forms cocrystals or crystalline salts with aliphatic dicarboxylic acids or mineral acids or aromatic carboxylic acids (listed in **Fig. 5.3**). It is found that oxime **5.1** forms cocrystals or salts with adipic (cocrystal **5.2**), succinic (cocrystal **5.3**), fumaric (cocrystal **5.4**), maleic (salt **5.5**), oxalic (salt **5.6**), hydrochloric (salt **5.7**), nitric (salt **5.8**), 2-methylbenzoic (cocrystal **5.9**), 2-hydroxybenzoic (salt **5.10**), 2-nitrobenzoic (salt **5.11**), 3-nitrobenzoic (salt **5.12**), 4-nitrobenzoic (salt **5.13**), 2,3-dihydroxybenzoic (salt **5.14**) and 2,4-dihydroxybenzoic (salt **5.15**) acids (**scheme 5.1**). But crystals either as cocrystals or salts of oxime **5.1** with nitrogen containing compounds such as imidazole, pyrazole, picoline and pyridine could not be prepared from solution of these compounds with oxime **5.1** in different solvents (methanol, DMF, THF, acetone etc).

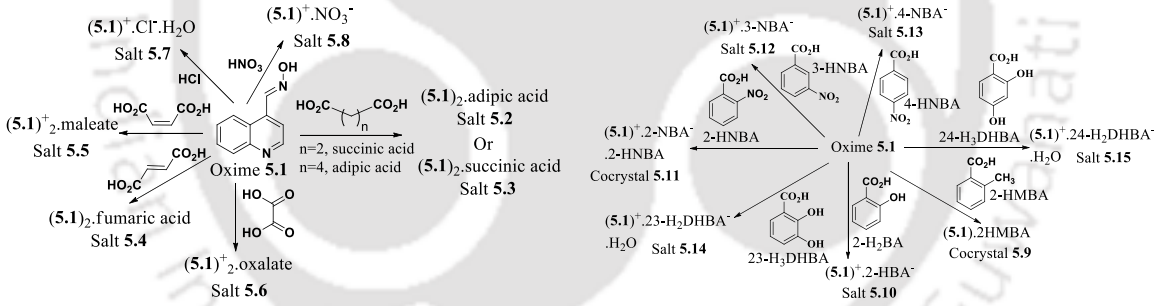

(a) (b)

Scheme 5.1: Synthesis of cocrystals and salts of quinoline-4-carbaldoxime with (a) aliphatic dicarboxylic or mineral and (b) aromatic carboxylic acids.

Cocrystals **5.2-5.4** of oxime **5.1** with aliphatic dicarboxylic acids have 2:1 molar ratio of oximes and carboxylic acid. Among the salts of carboxylic acids maleate salt **5.5** has 1:1 molar ratio between oxime **5.1** and maleate, whereas oxalate salt **5.6** has the ratio of oxime **5.1** to oxalate is 2:1. Upon reaction with mineral acids, oxime **5.1** forms corresponding salt, for example it forms 1:1 anhydrous salt **5.8** with nitric acid and 1:1 hydrated salt **5.7** with hydrochloric acid. But in the presence of aromatic carboxylic acids listed in **Fig. 5.3b**, 2-methylbenzoic acid forms 1:1 binary cocrystals **5.9** and 2-nitrobenzoic acid forms 1:1:1

ternary cocrystals **5.11** with oxime **5.1**, whereas, the rest of the aromatic carboxylic acids given in **Fig. 5.3b** form 1:1 salts on reaction with oxime **5.1**.

5.3: Structural description of oxime 5.1 and cocrystals or salts of oxime 5.1 with aliphatic dicarboxylic or mineral acids

The reported structure of oxime **5.1**[13] has hydrogen bonded $R_2^2(7)$ hetero-synthons formed by interaction of oxime nitrogen with *peri*-hydrogen atom of quinoline and a hydroxy-group interacting with nitrogen atom of a quinoline moiety through O-H···N hydrogen bond (**Fig. 5.4a**). The molecules are arranged as single chain-like structure. Upon interactions of oxime molecules with carboxylic acids such hetero-synthons may transform to other oxime synthons.

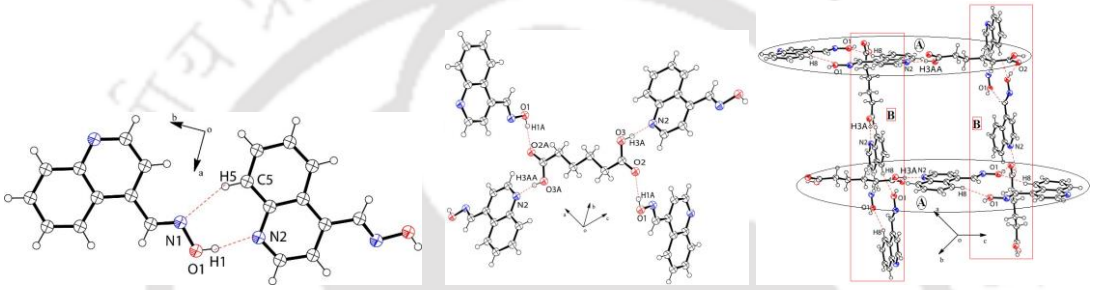

(a) (b) (c)

Figure 5.4: Hydrogen bonded self-assemblies of (a) oxime **5.1** and (b-c) cocrystal **5.2** (30% thermal ellipsoids in ORTEP diagram).

The hydrogen bonded self-assembly of cocrystals formed by interactions of the oxime **5.1** with adipic acid is shown in **Fig. 5.4b-c**. The self-assembly of this cocrystal **5.2** has O-H···N hydrogen bonds formed by the nitrogen atom of quinoline with the O-H groups of the adipic acid. The other prominent O-H···O hydrogen bonds in the lattice of this cocrystal **5.2** are formed between the carbonyl of the carboxylic acids and the O-H of neighbouring oxime molecules. These interactions help the partner molecules to self-assemble and generate cyclic sub-assemblies as a part of the self-assembly. The self-assemblies are constituted by the sub-assemblies; each comprising of a pair of oxime molecules with a dicarboxylic acid molecule designated as A in **Fig. 5.4c** held by another two pairs of two oxime molecules and a dicarboxylic acid designated as B in **Fig. 5.4c**.

The structures of the two cocrystals **5.3**-**5.4** formed by oxime **5.1** interacting with succinic acid and fumaric acid have close structural resemblances with that of the cocrystal **5.2**. The hydrogen bonded self-assemblies of cocrystals **5.3** and **5.4** are shown in **Fig. 5.5**. Self-assemblies of these cocrystals are guided by $R_2^2(14)$ oxime-oxime and $R_2^2(7)$ acid-quinoline synthons.

These cocrystals have $R_2^2(7)$ cyclic hydrogen bonded motifs in their lattice involving C-H···O interactions. The $R_2^2(7)$ motif is guided by C4-H4···O2 interactions. The H···O bonds distance of the C-H···O interactions are in the range of 2.62 to 2.78 Å with ∠D-H···A angles of 120.9°, 124.4° and 123.7° for the **5.2**, **5.3** and **5.4** cocrystals, respectively. From geometrical consideration, these interactions are very weak,[14] but the ∠D-H···A angles have an ascending trend with the increase in numbers of intervening methylene groups between the carboxylic acids.

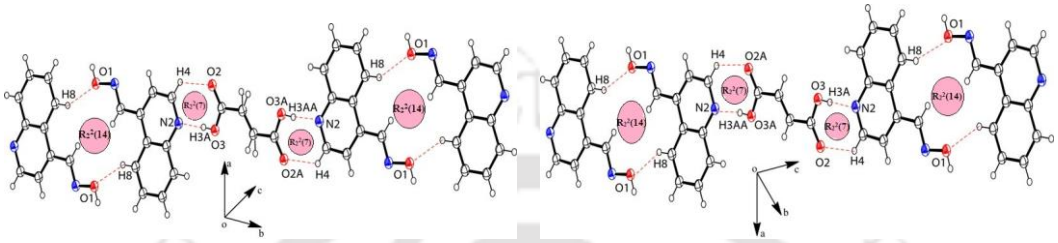

(a) (b)

Figure 5.5: Hydrogen bonded self-assemblies of cocrystals (a) **5.3** and (b) **5.4**.

As the flexibility of the tethers of the dicarboxylic acid molecules of these cocrystals increase, the relevance of such C-H···O bonds of the *peri*-hydrogen decreases. Generally, aldoximes form $R_2^2(8)$ type homo-synthons,[15] but such synthons are not observed in these cocrystals. The carboxylic acids disrupt the C-H···O bonded homo-synthons due to the hierarchy of O-H···N and O-H···O interactions between the carboxylic acids and oxime groups. The cocrystals of oxime **5.1** with aliphatic dicarboxylic acids are composed of uniformly distributed single phase as confirmed by the comparison of the powder XRD patterns of the bulk samples with the powder XRD pattern generated from the crystallographic information file of the single crystal data with the aid of Mercury software.

The oxime **5.1** reacted with maleic acid to form a salt having 1:1 molar ratio of cation and anion. The salt **5.5** has a mono-anion of maleic acid with a protonated oxime **5.1** molecule. Formation of mono-anion is attributed to high pKa_1 value of maleic acid. The mono dissociation of maleic acid with respect to di-dissociation arises due to stabilisation of mono-anion through intramolecular hydrogen bonds. Two maleate anions self-assembled by C-H···O and O-H···O interactions to form $R^2_2(8)$ type of homo-synthons (**Fig. 5.6a**). Such dimeric sub-assemblies are embedded by two oxime **5.1** cations through N-H···O and C-H···O interactions by to form $R^2_2(8)$ motifs. Such sub-assemblies are the basis of the repeated units; they are placed face-to-face in one direction to form chain-like arrangements. The C-H···O interactions between the C5-H5 bond of quinoline with oxygen atom of C=O of carboxylate and the O-H groups of oxime interacting with C=O of carboxylate of the

dicarboxylic acid at the other end are responsible to build chain-like architecture. The packing pattern of maleate salt is shown in **Fig. 5.6b**. Maleic acid and fumaric acids are two geometrical isomers and they form cocrystals in different proportions with partner molecules.[16] They are also adopt different hydrogen bonding patterns in respective packing pattern.

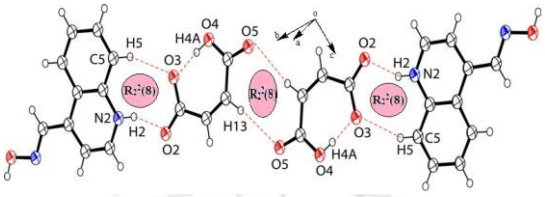

(a)

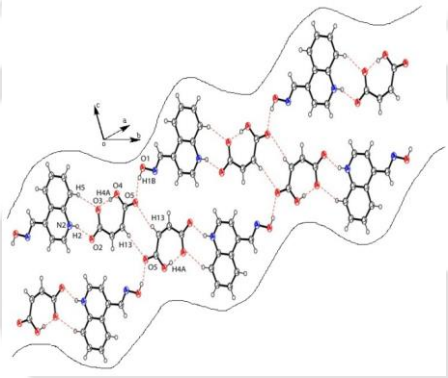

(b)

Figure 5.6: The self-assembly of (a) Maleate salt **5.5** and (b) Packing pattern of maleate salt **5.5** with oxime **5.1** (ORTEPs are with 30% thermal ellipsoids).

We observe oxime **5.1** forms cocrystal with fumaric acid whereas it forms salt with maleic acid. The result on formation of maleate salt **5.5** can be summarized by Etter's rule[17] as per this rule the six membered intramolecular hydrogen bonded motifs are more stable. Thus cyclic type structure is adopted by maleate anion and this participates in formation of hydrogen bonds with cationic counterpart. Accordingly, this cyclic intramolecular hydrogen bonded six member motif forms the hydrogen bonded homo and hetero-synthons.

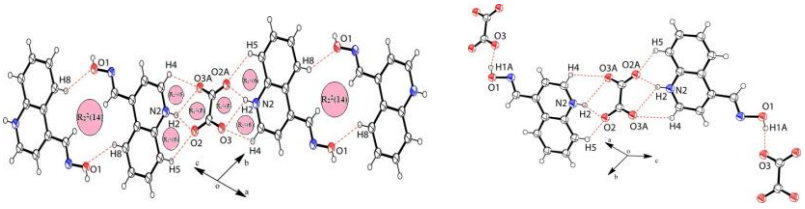

(a) (b)

Figure 5.7: Cyclic hydrogen motif in (a) Oxalate salt and (b) Hydrogen bonding between oxime OH and acidic partner in oxalate salt (30% thermal ellipsoids in ORTEP diagram).

However, a point to be noted in all these examples is that in each case all the good hydrogen bond donors and acceptors are utilized in formation of hydrogen bonds, other than the oxime nitrogen atom which does not participate in hydrogen bond scheme in any of these examples. Thus, these self-assemblies may be added as exceptions from conventional self-assemblies that utilizes all good hydrogen bond donors and acceptors. An oxalate salt **5.6** having a cation and anion in a ratio of 2:1 was obtained from the reaction of oxime **5.1** with oxalic acid. The oxalate ions are held between two oxime **5.1** cations (**Fig. 5.7a**) by hydrogen bonds. The packing is guided by bifurcated hydrogen bonds having C-H···O and $^{+}$N-H···O hydrogen bonds. The $^{+}$N-H···O interaction is ionic in nature; hence it contributes strongly to such an assembly. Oxalate di-anions makes this assembly different from the assemblies of the maleate salt **5.5** which has a mono anionic dicarboxylic acid. Hydrogen bond between oxime O-H and oxalate anion is shown in **Fig. 5.7b**. A comparison of hydrogen bonds and sort contacts parameters in the assemblies of the cocrystals and salts are given in **Table 5.1** and page 230 of appendix.

Table 5.1: Prominent hydrogen bond parameters of the cocrystals and salts of oxime **5.1**.

Cocrystal/Salt	D-H…A	d_{D-H} (Å)	$d_{H\cdots A}$ (Å)	$d_{D\cdots A}$ (Å)	∠D-H…A (°)
Cocrystal **5.2**	O(1)-H(1A)…O(2) [-1+x, -1+y, z]	0.82	1.89	2.702(19)	169
	O(3)-H(3A)…N(2) [1/2-x, -1/2+y, 1/2-z]	0.82	1.74	2.559(2)	171
	C(8)-H(8)…O(1) [-x, -y, 1-z]	0.93	2.52	3.426(3)	163
Cocrystal **5.3**	O(1)-H(1A)…O(2) [-1+x, 1+y, z]	0.82	1.84	2.655(19)	172
	O(3)-H(3A)…N(2) [1/2-x, 1/2+y, 1/2-z]	0.82	1.77	2.586(2)	173
	C(8)-H(8)…O(1) [-x, 2-y, 1-z]	0.93	2.44	3.284(2)	151
Cocrystal **5.4**	O(1)-H(1A)…O(2) [-1+x, -1+y, z]	0.82	1.83	2.655(2)	173
	O(3)-H(3A)…N(2) [1/2-x, -1/2+y, 1/2-z]	0.82	1.75	2.578(2)	176
	C(8)-H(8)…O(1) [-x, -y, -z]	0.93	2.44	3.273(2)	149
Salt **5.6**	O(1)-H(1A)…O(3) [1-x, 1-y, -z]	0.82	1.79	2.586(15)	163
	N(2)-H(2)…O(3) [1-x, 1-y, -z]	0.86	2.43	2.994(18)	124
	N(2)-H(2)…O(2) [-x, 1-y, 1-z]	0.86	1.85	2.665(18)	159
Salt **5.5**	O(1)-H(1B)…O(5) [2-x, 1-y, 1-z]	0.82	1.85	2.651(2)	166
	N(2)-H(2)…O(2) [-x, -y, 1-z]	0.86	1.87	2.681(2)	156
	C(5)-H(5)…O(3) [-x, -y, 1-z]	0.93	2.44	3.302(3)	154
	C(7)-H(7)…O(4) [x, y, -1+z]	0.93	2.41	3.263(3)	152
	C(13)-H(13)…O(5) [1-x, 1-y, 1-z]	0.93	2.51	3.437(3)	175
Salt **5.7**	O(1)-H(1)…O(2) [1/2-x, 1/2+y, 1/2-z]	0.82	1.82	2.600(8)	158
	O(2)-H(2A)…Cl(1)	1.05	2.20	3.117(8)	144(6)
	N(2)-H(2B)…Cl(1) [x, -1+y, z]	0.86	2.19	3.030(7)	166
	O(2)-H(3A)…Cl (1) [3/2-x, -1/2+y, 1/2-z]	0.97	2.19	3.094(10)	156(6)
	C(1)-H(1A)…O(1) [-x, 1-y, -z]	0.93	2.59	3.436(9)	152
Salt **5.8**	O(1)-H(1)…O(4) [-1+x, y, z]	0.82	1.92	2.717(19)	164
	N(2)-H(2)…O(2) [x, -1+y, 1+z]	0.86	2.50	3.091(18)	127
	N(2)-H(2)…O(4) [x, -1+y, 1+z]	0.86	1.92	2.778(17)	173

Since the self-assemblies of the salts and cocrystals are guided by proton transfer or hydrogen bonds with the carboxylic acids; the ^{1}H NOESY spectra of representative salt (**Fig. 5.8a**) and cocrystal (**Fig. 5.8b**) were recorded. The oxime hydroxyl-group interacts with the residual water molecules in DMSO-d_6 solvent. This is reflected in the correlation peak appearing at

12.00 ppm and peak at 3.35 ppm. ^{1}H NOESY experiments are based on double quantum coherence and relates directly to the spin-lattice relaxation.

The correlation peak obtained from the salt is broader than the cocrystal, which is suggested that in the salt the proton transfer is slow. The relatively slower exchange of the proton in the case of the salt is attributed to the stronger interactions of the hydrogen atom to nitrogen atom in the salt. This reduced the exchange of oxime O-H with the $^{+}$N-H group. This is also revealed in the proton NMR spectrum of the salt with oxalic acid where it shows a broad O-H peak. In both the cases the carboxylic acid O-H or $^{+}$N-H signals of quinoline merges with the signal from residual water molecules that are present with the deuterated solvent.

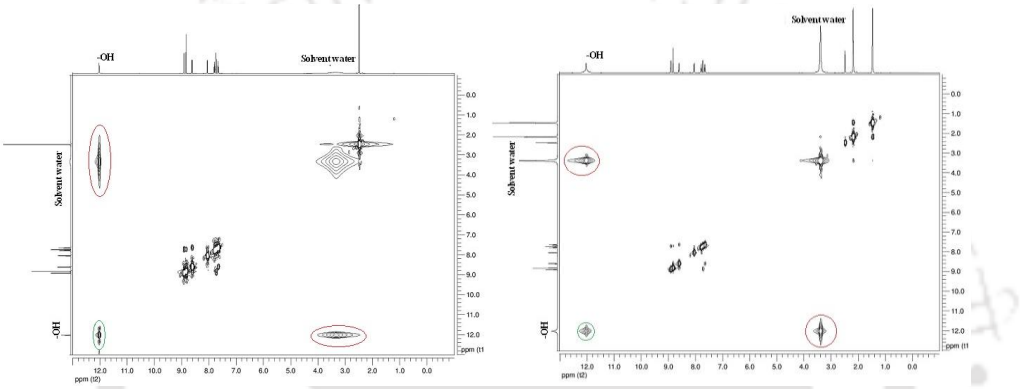

(a) (b)

Figure 5.8: ^{1}H-NOESY spectra (600MHz, DMSO-d_6) of (a) Oxalate salt **5.6** and (b) Cocrystals **5.2** of oxime **5.1** (encircled ones are the cross peaks showing NOE effect).

Both the salts are anhydrous and no hydrated crystals were found, the bulk sample as revealed in the powder XRD patterns of the salts. Maleic acid salt of quinoline derivative was suggested to be coloured, whereas same quinolone derivative was found to form cocrystal with fumaric acid which was colourless.[18] In the present examples also the salts are yellowish whereas the cocrystals are colourless.

To compare the self-assemblies of salts of **5.1** with inorganic acids with the carboxylate salts, the structures of the chloride and the nitrate salt have been studied. The self-assembly of the chloride salt **5.7** is guided by three strong hydrogen bonds to maintain a distorted tetrahedral hydrogen bonded geometry around each chloride ion (**Fig. 5.9a**). T-shaped hydrogen bond environment was observed in chloride ion assisted hydrogen bonded self-assemblies.[19] In the present example chloride ions interacts with water molecules and results in the formation of chloride water chains (inset of **Fig. 5.9b**). The self-assembly of the chloride salt **5.7** is comprised of protonated oxime **5.1** molecules held on the channel by strong $^{+}$N-H···Cl interactions.

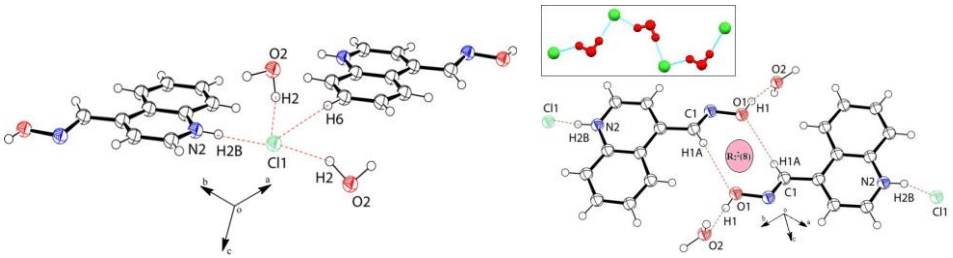

(a) (b)

Figure 5.9: (a) Hydrogen bonded geometry of chloride in chloride salt **5.7** and (b) Two interacting units of oximes in the self-assembly of **5.7**. In the inset is the chloride water chain in the chloride salt (Water molecules and chloride ions are label by red and green colour).

Due to such arrangements the quinoline rings are not available for formation of the $R^2_2(14)$ type homosynthons that are conventionally observed in the salts and cocrystals. But it forms $R^2_2(8)$ type homosynthons involving the aldehydic C-H interacting with the oxygen atom of the oxime. This synthon is routinely observed in assemblies of aldoximes.[15] To reduce repulsions between similar ions in the lattice and to involve the hydrogen bond donor O-H of oxime **5.1** in the scheme of hydrogen bonds, the O-H of the oxime **5.1** group forms hydrogen-bonds with water molecules. Thus, the water molecules also act as bridging molecules to anchor the chloride ions together with another oxime molecule of the assembly forming a spiral chain-like structure along the crystallographic b-axis. Hence, due to formation of chain-like structures having $^{+}$N-H···Cl interactions and also to adopt a distorted tetrahedral hydrogen bonded geometry around the chloride ions, the water molecules interacting with chloride are embedded in the lattice as filler molecules. Hydrated chloride[20] ions have relevance in natural environments as chloride ions are abundant in sea water or as sea-salt aerosols. Trapping of different forms of water chloride aggregates in various crystals has revealed their existence in different forms such as clusters, one or two dimensional hydrogen bonded networks.[19] Hexameric hybrid water-chloride-ethanol octamers are stabilized by quinolone-containing cobalt complexes, and the present water clusters are composed of one-dimensional chain-like structures with alternating water molecules and chloride ions.

Thermo-gravimetric analysis (TGA) of monohydrated chloride salt 5.7 (**Fig. 5.39**) showed weight loss in the region of 100-110°C due to evaporation of one water molecules. The weight loss corresponded to loss of one water molecule per salt molecule, which left no ambiguity that only the monohydrate was formed.

The nitrate salt **5.8** of oxime **5.1** has the nitrate ions assisting in the formation of hydrogen bonded cyclic sub-assemblies. The nitrate ions occur as pairs and such arrangements are formed by bifurcated hydrogen bonds between $^{+}$N-H and two oxygen atoms of the nitrate.

The sub-assemblies are held together by C4-H···O4 interactions as shown in **Fig. 5.10a**. These dimeric motifs are held by two O-H···O interactions between the oxime O-H bond and oxygen (O4) atoms of the nitrate. In general, nitrate ions are planar and form complementary hydrogen bonds with host molecules or they get encapsulated in assemblies formed by host molecules.[21]

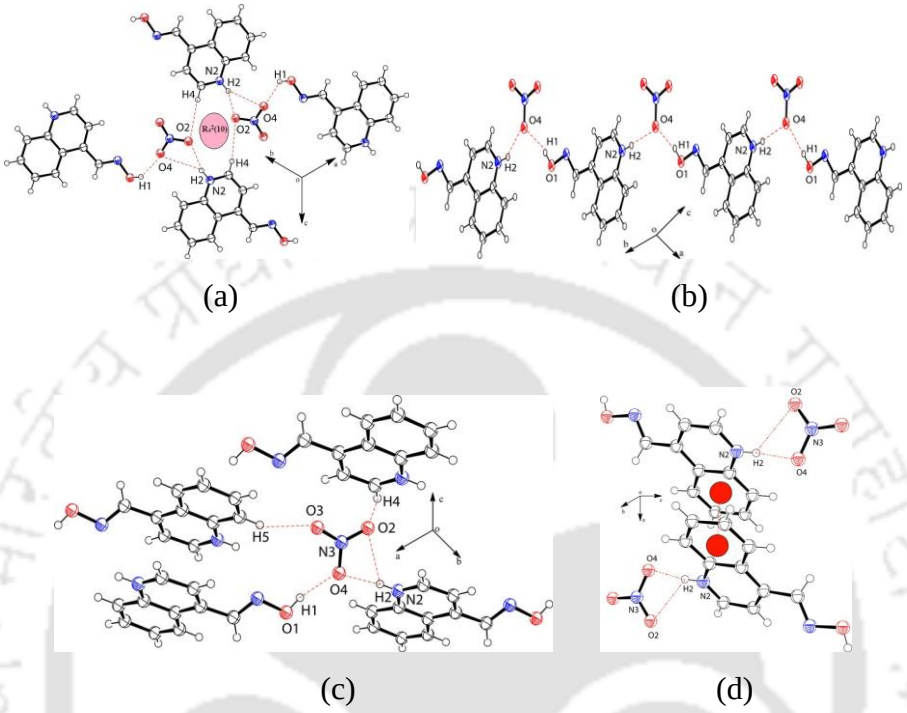

Figure 5.10: (a) Cyclic type hydrogen bond motifs of nitrate ions in lattice of the nitrate salt **5.8**, (b) Bifurcated hydrogen bonds in nitrate salt **5.8**, (c) One nitrate ion interacts with four protonated oxime **5.1** molecules and (d) π-π interaction between two protonated oxime **5.1** molecules in nitrate salt **5.8** (30% thermal ellipsoids in ORTEP diagram).

In the present case the nitrate ions form two-dimensional non-planar sheets in which the nitrate ions are slightly oblique in orientations with respect to the plane of oxime **5.1** molecules. There is also $R_2^2(14)$ type homo-synthons similar to the one observed in the self-assembly of salts exception being the chloride salt **5.7**. Different types of hydrogen bonds between nitrate anion and cationic oxime **5.1** molecules are observed in the nitrate salt are shown in **Fig. 5.10b-d**. The difference in having completely different synthons in the chloride salt **5.7** is due to presence of hydrate anions; in all other cases the anhydrous salts are observed.

This structural study with oxime salts or cocrystals of aliphatic carboxylic and mineral acids have revealed several types of synthons contributing to those assemblies. The prominent hydrogen bonds interactions contributing to these self-assemblies are shown in **Fig. 5.11**. The oxime O-H forms strong hydrogen bonds with the corresponding acid partner.

Oxime generally prefers to form cocrystals with basic compounds[12] and quinoline attached to oxime **5.1** forms O-H···N hydrogen bonds with oxime. The nitrogen atom of the quinoline prefers to bind with O-H of a carboxylic acid. Such interactions are found in pyridine-carboxylic acid or quinoline-carboxylic acid systems.[11b] The interactions between quinoline and carboxylic acid facilitates the other site (the carbonyl oxygen) of a dicarboxylic acid to bind to the O-H of the oxime group as shown in **Fig. 5.11a**. The $O_{(carboxyl)}$-H···$N_{(pyridine)}$ and $C_{(pyridine)}$-H···$O_{(carbonyl)}$ hydrogen bonds control the self-assembly of pyridine-carboxylic acid.[10a] In the present example, there are synergistic contributions from the $O_{(carboxyl)}$-H···$N_{(quinoline)}$ and $O_{(oxime)}$-H···$O_{(carbonyl)}$ in the self-assemblies guiding the self-assembly of the cocrystals.

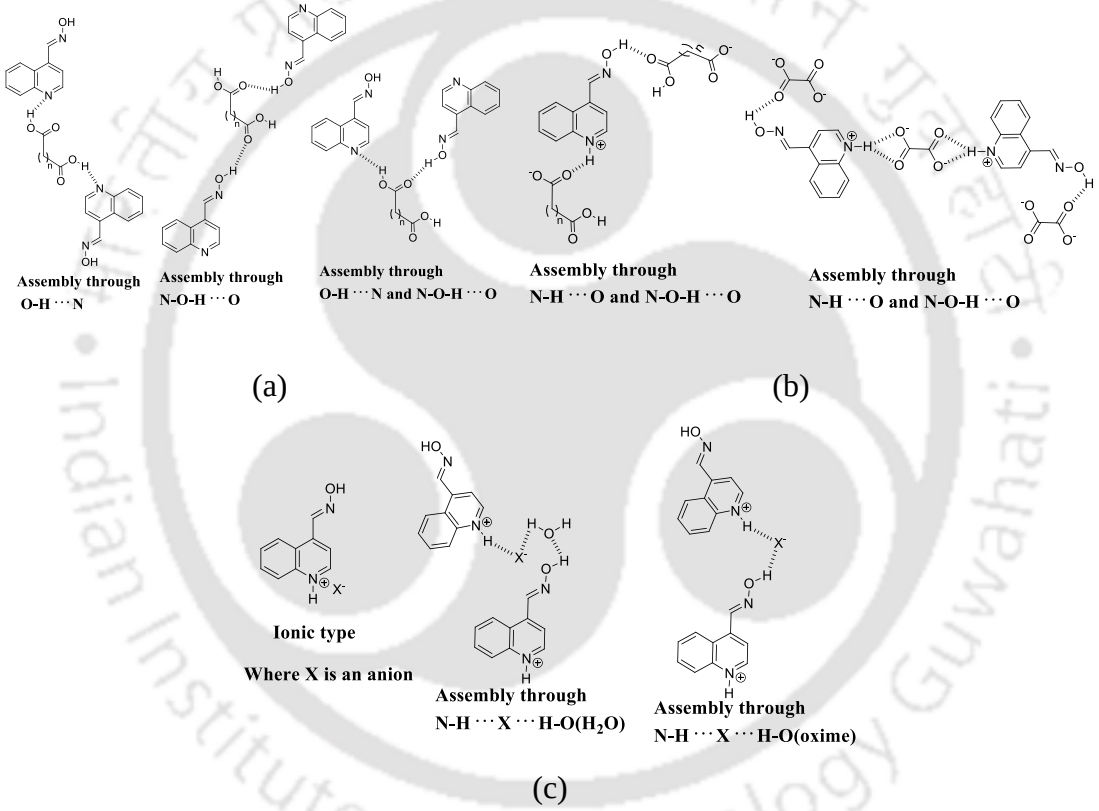

Figure 5.11: Observed hydrogen bonded motifs contributing to the assemblies of oxime **5.1** with acid partners in the (a) Cocrystals and (b-c) Salts.

Thus, such self-assemblies are guided by O-H···O and N-H···O synthons. This may be also one of the reasons that carboxylic acid-oxime interactions are observed in the salts. In the self-assemblies of the cocrystals, carboxylic acids contribute in a dual manner; they form the cocrystals by interacting with the oxime and they also provide extension to the hydrogen bonded assembly by acting as bridges. On the other hand, the inherent directional properties of anions guide the packing pattern of the respective salts or cocrystals.

5.4: Structural studies of cocrystal or salts of oxime 5.1 with aromatic carboxylic acids

A cocrystal and a series of salts of oxime **5.1** with different aromatic carboxylic acids listed in **Scheme 5.1** are characterized by determining crystal structures and through other spectroscopic analysis. The self-assembly in each case is comprised of isosteric quaternary sub-assemblies. Isosteric assemblies in supramolecular chemistry mean two different assemblies having same number of molecules or components. Isostructural (structurally similar) have importance in crystal engineering to design new non-covalent assemblies with interesting properties.[22] Isostructural cocrystals provides scope to correlate properties among them.[23] Isostructural quaternary cocrystals of olanzapine[24] and isostructural solvates are reported in literature.[25] Structural aspects of oximes are extensively studied,[26] but their cocrystals with aromatic carboxylic acids are less studied. Due to poor affinity of carboxylic acids or phenols to bind oximes supporting interactions within various self-assemblies are needed to examine the interactions between oximes with phenols and carboxylic acids.[27] In this part of this chapter we discussed the utility of oxime **5.1** to form isosteric hydrogen bonded cyclic quaternary sub-assemblies of systems represented in **Fig. 5.12** is explored. In such assemblies oxime **5.1** (regions A and B) have possibilities to adopt different orientations of the planar part and also to have conformational adjustments in regions C and D. The distance between regions A and B as well as between regions C and D may also vary and decide their stabilities. It is found that the substituted benzoic acids listed in **Fig. 5.3b** form quaternary sub-assemblies and we take advantage of such assemblies to examine several aspects: (a) the validity of the pKa relationship to guide the formation of salts or cocrystals and (b) the consequence of different substituents at two remote sides of a quaternary cyclic sub-assembly (**Fig. 5.12**); (c) the possible expansion of a quaternary assembly; (d) the size of quaternary sub-assemblies.

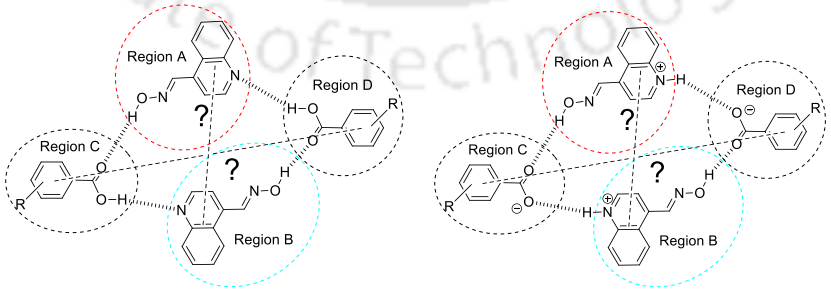

(a) (b)

Figure 5.12: Isosteric quaternary sub-assemblies of oxime **5.1** with aromatic carboxylic acids in (a) cocrystal and (b) salts.

The differences of pK_a of oxime **5.1** with the aromatic carboxylic acids listed in **Table 5.2**, except 2-methylbenzoic acid listed in **Fig. 5.3b** are in between 1.11 and 2.39. Whereas, in the case of oxime **5.1** and 2-methylbenzoic acid, this difference is 0.67. The literature suggests that the differences in pK_a of the partner molecules falling between 1 and 4 indicate the formation of either cocrystals or salts.[28] Thus the combinations chosen here except one have differences of pK_a values greater than 1 and less than 2.5.

Table 5.2: pK_a and pK_b value of different coformers and oxime **5.1**.

Compound	pK_a	pK_b- pK_a
2-Methylbenzoic acid	3.91	0.67
2-Hydroxybenzoic acid	2.97	1.61
2-Nitrobenzoic acid	2.19	2.39
3-Nitrobenzoic acid	3.47	1.11
4-Nitrobenzoic acid	3.41	1.17
2,3-Dihydroxybenzoic acid	2.96	1.62
2,4-Dihydroxybenzoic acid	3.32	1.26
*pKb value of oxime **5.1** is 4.58		

In such a situation, the number of hydrogen bonds between the partner molecules influences the formation of salts or cocrystals.[28a] In the present combinations, there is scope to have a minimum two hydrogen bonds between oxime **5.1** and the carboxylic acids to form quaternary sub-assemblies. Hence, the formation of salts should be favoured in such situations. From crystallographic study it is found that among the acids listed in **Fig. 5.3b**, 2-methylbenzoic acid forms binary cocrystal **5.9** and 2-nitrobenzoic acid forms ternary cocrystals **5.13**, whereas, the rest of the carboxylic acids given in **Fig. 5.3b** form salts. Thus, these salts are formed as per the guidelines provided for differences in pK_a.[28a] In the case of 2-methylbenzoic acid, it has comparable pK_a with oxime **5.1**, hence forms cocrystal. Oxime **5.1** with 2-methylbenzoic acid forms a 1:1 cocrystal **5.9**. 2-Nitrobenzoic acid (2-HNBA) formed a ternary cocrystal **5.11**; whereas 2-hydroxybenzoic acid, 3-nitrobenzoic acid, 4-nitrobenzoic acid, 2,3-dihydroxybenzoic acid or 2,4-dihydroxybenzoic acid formed their respective salt, abbreviated as salts **5.10**, **5.12**, **5.13**, **5.14** and **5.15** (**Scheme 5.1**) respectively. Self-assembly of the cocrystal **5.9** of oxime **5.1** with 2-HMBA is composed of quaternary sub-assemblies formed by O-H···N and O-H···O hydrogen bonds (**Fig. 5.13a**). The host oxime **5.1** behaves as a hydrogen bond donor and acceptor, the quinoline part acts as hydrogen bond acceptor to form conventional quinoline···carboxylic acid synthon[27] and the oxime part acts as a hydrogen bond donor. In this cocrystal, two oxime **5.1** molecules are held by two 2-HMBA molecules forming a quaternary sub-assemblies which contributes to the overall packing pattern (**Fig. 5.13a**)

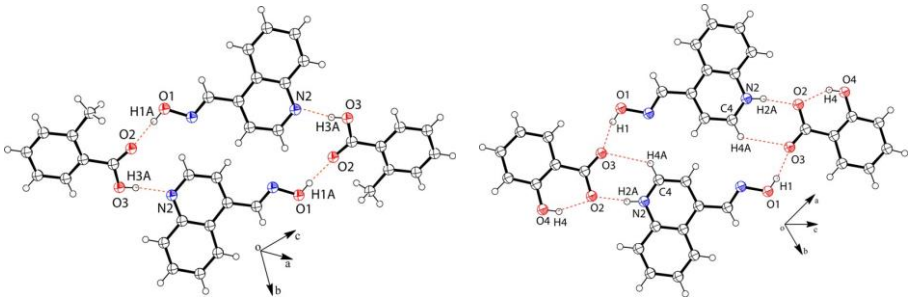

(a) (b)

Figure 5.13: Isosteric quaternary sub-assemblies of (a) cocrystal **5.9** and (b) salt **5.10** of oxime **5.1** with 2-HMBA and 2-H_2BA molecules respectively (30% thermal ellipsoids).

The salt **5.10** of oxime **5.1** with 2-H_2BA has a free hydroxy-group involved in formation of intramolecular hydrogen bonds. An interesting aspect of this assembly is that each quaternary sub-assembly lies in one plane. In this salt, protonated oxime **5.1** acts as a hydrogen bond donor (**Fig. 5.13b**), whereas in the cocrystal **5.9** with 2-HMBA, quinoline is hydrogen bond acceptor.

Crystallisation of a solution of oxime **5.1** and 2-HNBA yielded a ternary cocrystal **5.11** which has one protonated oxime **5.1**, an anionic 2-NBA and a neutral 2-HNBA molecule. The composition of this cocrystals has an exception as it has two molecules of 2-nitrobenzoic acid per molecule of oxime **5.1**, which is not the case with the other homologues. The nitro-group of 2-nitrophenyl carboxylic acid is perpendicular to the aromatic plane and has attracted considerable interest in crystal engineering.[29] The nitro groups on 2-nitrophenyl carboxylates in the sub-assemblies in present example are perpendicular to the plane of the quinoline rings. The quinoline rings within the quaternary sub-assemblies are almost parallel to each other lying in the same plane. Same is the case of the phenyl planes of the 2-nitrophenyl rings (**Fig. 5.14a**). Out of plane orientations of the nitro groups of phenyl carboxylates help in generating a puckered quaternary sub-assembly. Thus, the overall assembly constructed from such sub-assemblies has suitable spaces to accommodate neutral 2-HNBA molecules. Alternatively, the repeat sub-assemblies of this cocrystal may be suggested to be composed of sub-assemblies of six molecules, namely, two protonated oxime **5.1** and two 2-HNBA molecules and two 2-NBA ions. The 2-HNBA molecules in the self-assembly interact with the 2-NBA anions by O-H···O and C-H···π interactions as shown in **Fig. 5.14b**. For hydrogen bonds and short contacts parameters of cocrystal and salts please see **Table 5.3** and page 230-231 of appendix.

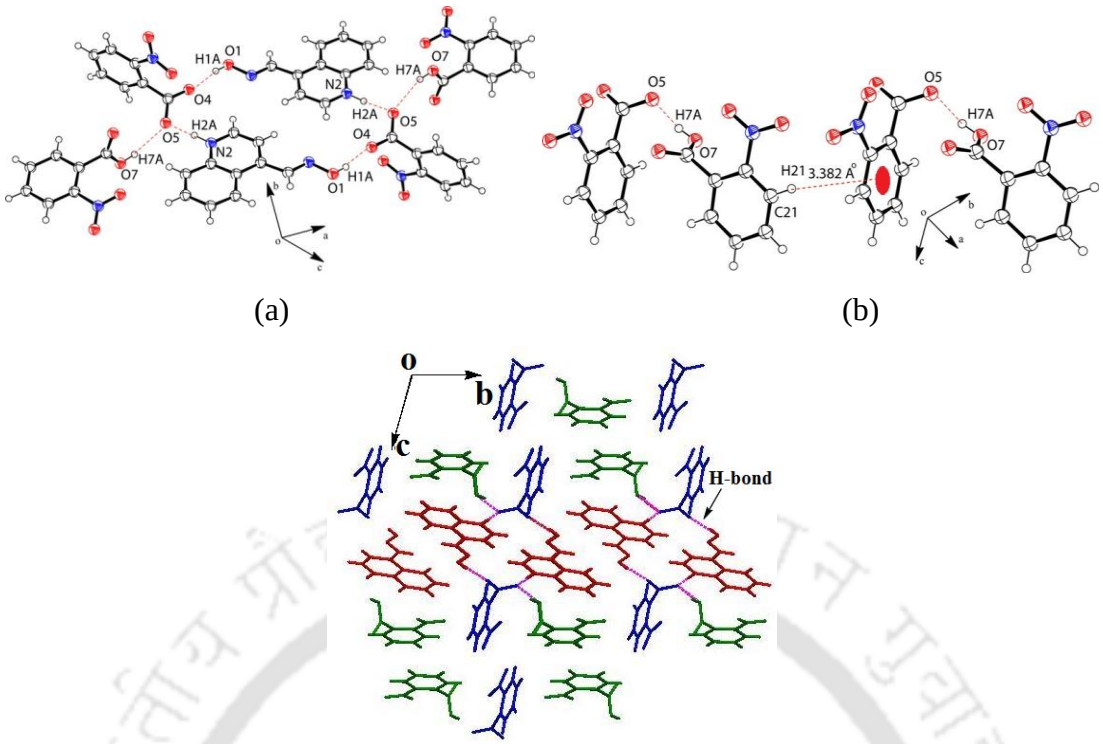

(a) (b)

(c)

Figure 5.14: (a) Hydrogen bonded senary sub-assemblies of cocrystal **5.11**, (b) Interaction of 2-HNBA and 2-NBA in this cocrystal and (c) Packing diagram of cocrystal **5.11**; protonated oxime **5.1** (red), anionic 2-HNBA (blue) and a neutral 2-HNBA (green) molecule (30% thermal ellipsoids in ORTEP diagram).

The packing diagram generated by interactions between protonated oxime **5.1** (red), 2-NBA (blue) and 2-HNBA (green) molecules is shown in **Fig. 5.14c**. Though this salt has isosteric quaternary sub-assemblies found in the analogous salts, such sub-assemblies are modified to behave as hexa-molecular senary sub-assemblies. Due to the non-planar nature of 2-nitrobenzoate, the quaternary sub-assemblies of conjugate acid-base pairs lack co-planarity. However, the sub-assemblies of conjugate acid-base pairs of other homologous acids are co-planar. Due to non-planar arrangements of the sub-assemblies formed from conjugate acid-base pairs between oxime **5.1** and 2-nitrobenzoic acid, spaces are present in the lattice to accommodate additional 2-nitrobenzoic acid molecules. Such neutral 2-nitrobenzoic acid molecules get anchored to quaternary sub-assemblies to extend the quaternary sub-assemblies to senary sub-assemblies and generate a tight packed structure (**Fig. 5.14c**). Each senary sub-assembly has oxime···carboxylic acid, quinoline···carboxylic acid and acid···acid synthons, whereas the quaternary sub-assemblies are guided by oxime···carboxylic acid and quinoline···carboxylic acid synthons.

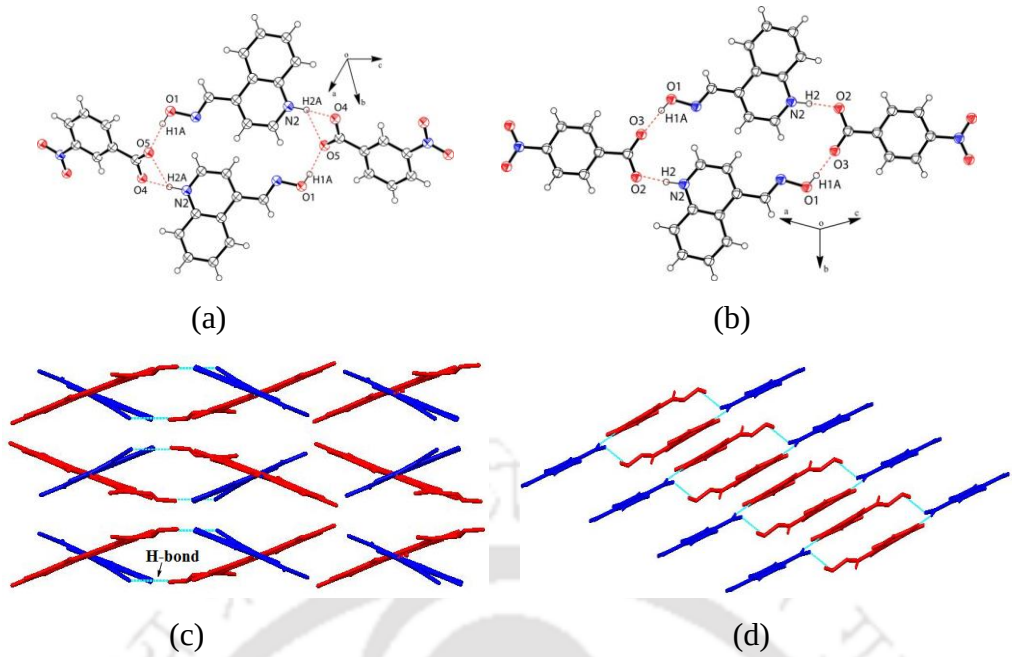

Figure 5.15: Isosteric quaternary sub-assemblies of salts (a) **5.12** and (b) **5.13**. Packing diagrams of salts (c**) 5.12** and (d) **5.13** (30% thermal ellipsoids in ORTEP diagram).

The above explanation is supported by the structures of quaternary sub-assemblies found in the salt **5.12-5.13** of 3-HNBA or 4-HNBA (**Fig. 5.15a-b**). Packing in these examples is guided by quaternary sub-assemblies which have 3- or 4-nitrophenyl carboxylate ions that lie parallel to the aromatic ring of oxime **5.1**. However, the hydrogen bonds of the two carboxylic acids in the respective sub-assembly have differences. One has a bifurcated hydrogen bond and the other does not have such type of hydrogen bonds. This differences change the respective packing pattern (**Fig. 5.15c-d**). One has a criss-cross arrangement, whereas the other has a planar arrangement. Among the three isomeric nitrobenzoic acids, there are considerable conformational changes during formation of salts or cocrystals which are reflected in the torsion angles listed in **Table 5.4**. The conformational changes in anionic form or neutral 2-nitrobenzoic acid are similar, both carboxylic and nitro groups change their orientations. This change provides non-planar arrangement between the quinoline ring and the respective phenyl rings. 4-nitrobenzoate salt has the nitro group on the plane of the phenyl ring but the carboxylate group undergoes conformational adjustments. Whereas in the 3-nitrobenzoate salt, the carboxylate group is in plane with respect to the phenyl ring also keeps the original orientation of the nitro-group intact. These make each packing pattern different from each other.

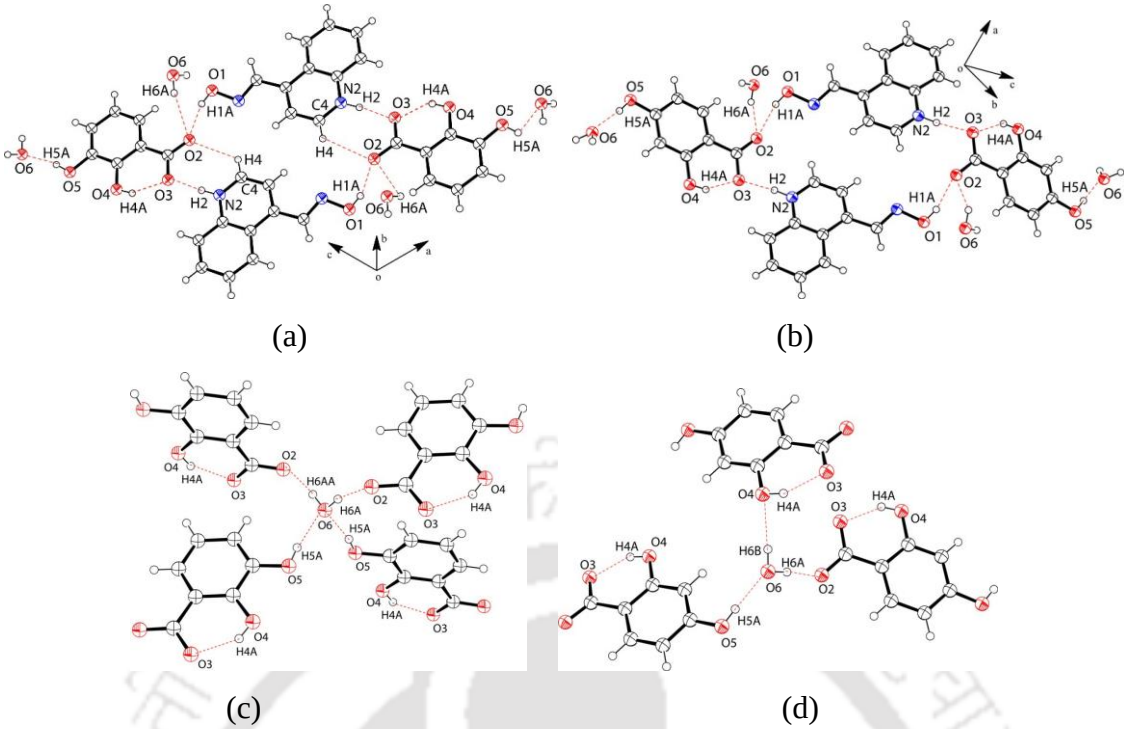

Figure 5.16: Hydrogen bonded senary sub-assemblies of salts (a) **5.14** and (b) **5.15**; water assisted self-assembly of salts (a) **5.14** and (b) **5.15** (30% thermal ellipsoids).

Salts **5.14**-**5.15** of oxime **5.1** with 2,3-H_3DHBA and 2,4-H_3DHBA are obtained as the corresponding monohydrate salts. These salts also possess quaternary sub-assemblies similar to the other salts (**Fig. 5.16a-b**). One water molecule occupies the hydrophilic spaces in the connecting junction between the oxime and carboxylic acid groups. In the packing patterns, these water molecules form hydrogen bonds with the hydroxy groups of neighbouring sub-assemblies to act as fillers and guide the overall packing pattern. Comparisons of sub-assemblies of the anhydrous salt **5.10** with hydrated salts shows that the free hydroxy-group at the 3- or 4-position of the respective phenyl ring of 2,3-H_3DHBA and 2,4-H_3DHBA forms phenol···water synthon.[30] The hydrogen bonds of lattice water molecules are directional hydrogen bonds, which guide the positions and orientations of the quaternary sub-assemblies. Thus, such sub-assemblies can be considered as senary sub-assemblies. Senary sub-assemblies in these cases are formed from quaternary sub-assemblies holding water molecules by hydrogen bonds (**Fig. 5.16a-b**). The water molecules fill up the spaces at the hydrophilic sites formed by hydrogen bonds among three hydrophilic sites of functional groups namely oxime, carboxylate and hydroxy-groups. The water molecules also act as linkages to inter connect the senary sub-assemblies by hydrogen bonding with the free hydroxyl group at the 3 or 4-positions of the respective carboxylate. Thus, the sub-assemblies of hydrated salts of dihydroxybenzoate have similarity to senary subassemblies found in the

ternary cocrystal **5.11** of 2-nitrobenzoic acid. Packing patterns of salt **5.14** showed herringbone packing where protonated oxime **5.1** and 23-H_2DHBA anions have C-H···π interactions ($d_{C\text{-}H\cdots\pi}$ = 2.98 Å). But the salt **5.14** has columnar packing where the 24-H_2DHBA anions are π-stacked. The distance between π-clouds of two neighbouring anions in parallel positions is 3.459 Å (**Fig. 5.17**).

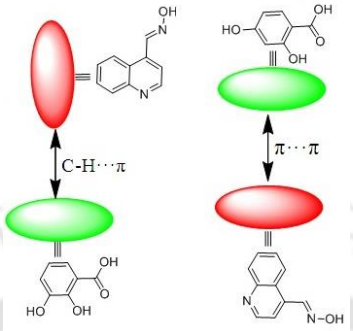

Figure 5.17: (a) Herringbone stacking in salt **5.14** and (b) Columnar stacking in salt **5.15**.

The nitrogen atom of oxime generally acts as a hydrogen bond acceptor but in these examples they remain free. This is against Etter's rule.[17a] This is due to a lack of an adequate partner in the vicinity of the sp^2-hybridized nitrogen atom of the oxime with appropriate orientation for hydrogen bonding.

Torsion angles associated with the orientations of the oxime group across the quinolinium cation in different salts are listed in Table 5.5. These angles are comparable, except in the case of the 2-nitrobenzoate salt with oxime **5.1**, where conformational adjustment is large in comparison to the others. In the self-assembly of cocrystals **5.9** of 2-methylbenzoic acid, regions A, B, C and D are planar. Based on the centroid to centroid distance of the aryl groups across the quaternary sub-assemblies, the distances between the two ends of the quaternary sub-assemblies are in the range 1.3 nm to 1.7 nm (**Table 5.6).** This suggests that these sub-assemblies provide scope to understand the variation of packing patterns[31] in the assemblies guided by a change of the substituent of the partner moleculeas conjugate acid-base pairs for preparation of cocrystals with enhanced solid-state properties.[32]

Table 5.3: Prominent hydrogen bond parameters of cocrystals and salts of oxime **5.1** with aromatic carboxylic acids.

Cocrystal/Salt	D-H···A	$d_{D\text{-}H}$ (Å)	$d_{H\cdots A}$ (Å)	$d_{D\cdots A}$ (Å)	∠D-H···A (°)
Cocrystal **5.9**	O(1)-H(1A)…O(2) [-1+x,y,-1+z]	0.92	1.88	2.694(5)	172
	O(3)-H(3A)…N(2) [2-x,1-y,1-z]	0.82	1.84	2.653(5)	170
Salt **5.10**	O(1)-H(1)…O(3) [-1+x,1/2-y,-1/2+z]	0.82	1.83	2.642(8)	169
	N(2)-H(2A)…O(2) [1-x,-1/2+y,1/2-z]	0.87(6)	1.79(6)	2.649(9)	169(7)
	C(4)-H(4A)…O(3) [1-x,-1/2+y,1/2-z]	0.93	2.54	3.184(9)	127

Salt **5.14**	O(1)-H(1A)…O(2) [-x,y,1/2-z]	0.82	1.91	2.703(3)	161
	N(2)-H(2)…O(3) [x,-y,-1/2+z]	0.90(3)	1.64	2.674(3)	174(3)
	O(5)-H(5A)…O(6) [1/2+x,1/2+y,z]	0.93	1.93	2.735(3)	169
	O(6)-H(6A)…O(2) [x, y, z]	0.84(3)	1.92	2.765(3)	163(3)
	C(3)-H(3)…O(4) [-1/2+x,1/2-y,-1/2+z]	0.93	2.58	3.371(3)	143
Salt **5.15**	O(1)-H(1A)…O(2) [1-x,2-y,1-z]	0.82	1.87	2.672(3)	165
	N(2)-H(2)…O(3) [x,y,-1+z]	0.91(2)	1.76(2)	2.671(3)	174(3)
	O(5)-H(5A)…O(6) [1/2-x,1/2+y,1/2-z]	0.82	1.86	2.680(3)	175
	O(6)-H(6A)…O (2) [1-x,1-y,1-z]	0.87(3)	1.88(3)	2.741(3)	171(3)
	O(6)-H(6B)…O(4) [/2+x,3/2-y,-1/2+z]	0.85(3)	2.07	2.916(3)	174(3)
Salt **5.11**	O(1)-H(1A)…O(4) [2-x,1-y,1-z]	0.82	1.87	2.681(3)	173
	N(3)-H(2A)…O(5) [-1+x,y,z]	0.98(4)	1.67(4)	2.654(4)	178(3)
	O(3)-H(7A)…O(5) [x, y, z]	0.82	1.80	2.599(4)	164
Salt **5.12**	O(1)-H(1A)…O(5) [1-x,1/2+y,1/2-z]	0.82	1.85	2.665(2)	172
	N(2)-H(2A)…O(4) [x,3/2-y,1/2+z]	0.98(2)	1.60(19)	2.571(2)	173(3)
	N(2)-H(2A)…O(5) [x,3/2-y,-1/2+z]	0.98(2)	2.56(2)	3.157(2)	119(2)
Salt **5.13**	O(1)-H(1A)…O(3) [2-x,1-y,-z]	0.82	1.89	166	166
	N(2)-H(2)…O(2) [-1+x,y,z]	0.95(2)	1.61(2)	177(3)	177(3)

We observed ternary cocrystals in the case of 2-nitrobenzoic acid, but binary salts with other nitrobenzoic acids as well as with salicylic acid. Salicylic acid form ternary cocrystals with other carboxylic acids.[33] But we could not obtain cocrystals with our oxime. Thus the powder XRD of the crude solid mass after evaporating a solution of a 1:2 mole ratio of oxime oxime **5.1** and salicylic acid. The resultant solid had powder XRD peaks of the 1:1 salt and free carboxylic acid (**Fig. 5.36a**). Similarly, the powder XRD pattern of the solid mass obtained by evaporating a solution of a 1:2 (mole ratio) mixture of oxime **5.1** and 2-nitrobenzoic acid shows peaks of the 1:2 cocrystal (**Fig. 5.36b**) along with some other peaks from free acid and oxime. On the other hand, a solution of an equimolar mixture of oxime **5.1** and 2-nitrobenzoic acid in acetone/methanol (equal volume) solvent, upon slow evaporation, resulted in crystallisation of the 1:2 cocrystal of conjugate acid-base pairs. These results along with the conformational adjustments observed in the cocrystal of the conjugate acid-base pair 2-nitrobenzoic acid suggest that expansion of quaternary to senary assemblies is due to a packing requirement guided by the interplay of weak interactions.

The UV-visible spectra of a solid-sample of oxime **5.1** has a broad absorption at 350 nm, whereas the aromatic carboxylic acids under consideration do not show significantly distinct absorption in the UV-visible region in the solid state above 300 nm. Each salt of oxime **5.1** with different nitrobenzoic acids shows broad absorption in the region 375-400 nm (**Fig. 5.37a**). Other than very small differences in the intensity of absorption, the shapes and positions of absorptions are not distinguishable for these salts. The 2-hydroxybenzoate salt **5.10** of oxime **5.1** showed a broad absorption at the same wavelength as that of oxime **5.1**. Whereas, the 2,3-dihydroxybenzoate and 2,4-dihydroxybenzoate salts **5.14**-**5.15** of oxime **5.1** showed distinguishable absorptions. In these cases, the absorptions are at 410 nm to 450 nm (**Fig. 5.37b**), respectively, and the relative absorption intensity of the 2,3-dihydroxybenzoate

salt **5.14** is higher than that of the 2,4-dihydroxybenzoate salt **5.15**. Since π-interactions control solid state optical properties,[34] the observed differences are attributed to differences in packing patterns; if the sole contribution would have been from resonance effect involving the 4-hydroxy group, it should have shown absorption of the 2,4-dihydroxybenzoate salt **5.15** at higher wavelength than that of the 2,3-dihydroxybenzoate salt **5.14**. π-Stacking[35] of 2,4-dihydroxybenzoate salt **5.15** in the packing of the salt causes a reduction of intensity and shows absorption at lower wavelength than that of the 2,3-dihydroxybenzoate salt **5.14** as the latter does not have such an interaction. It is also noted that the solution of each salt in dimethylformamide shows absorption spectra resembling the spectra of the parent oxime. This suggests that the components of the salts fall apart in solution and behave independently like single species (**Fig. 5.38**)

5.5: Conclusions

Various cocrystals of oxime **5.1** with aliphatic dicarboxylic or mineral or aromatic carboxylic acids suggests that knowledge on the structures can help in indemnifications of synthons and make a systematic predesign synthesis by closely characteristic supramolecular features of series of compounds. The systematic observation to obtain similar sub-assemblies from three cocrystals closely related dicarboxylic acids has made it possible to use the synthons for non-covalent synthesis in predictive manner from understanding of one analogue. The packing patters of the salts of dicarboxylic acids are guided by extent of deprotonation while forming anion.

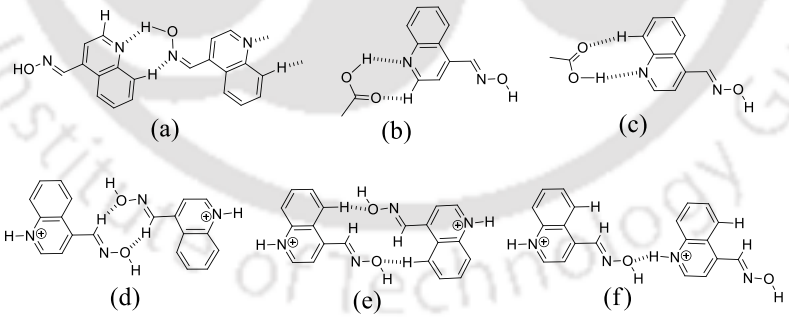

Figure 5.18: (a) The self-assembly of oxime **5.1**; (b-c) Some probable hydrogen bonded motifs in cocrystals of oxime **5.1** with carboxylic acids and in (d-f) salts of oxime **5.1**.

In the case of mono maleate anion a cyclic motif is formed through intramolecular hydrogen bond, which is the characteristic signature of a mono maleate anion and found in the salt. The hydrated chloride salt has oxime-oxime interactions through $R^2_2(8)$ type homo-synthons. Homo-synthons formed between protonated oxime molecules in the respective self-assemblies of the salts are influenced by anions. From this analysis it may be suggested that

the extent of deprotonation of a dicarboxylic acid and proton sharing play important roles which are to be considered for a predesigned building of such soft materials. But the self-assembled binary cocrystals and salts between aromatic carboxylic acids and oxime **5.1** are composed of quaternary sub-assemblies, whereas the ternary cocrystals or hydrated salts have senary sub-assemblies as constituents. Senary sub-assemblies are built from quaternary sub-assemblies to meet the orderly packing requirements. There are large differences in packing patterns arising due to the synergistic effects of weak interactions providing variations in the arrangements of the sub-assemblies. This study has showed an approach to list the basic sub-assemblies of different packing patterns generated from different combinations to understand the effect of substituents of a hydrogen bonded substrate in terms of those sub-assemblies.

5.6: Experimental section

Synthesis and characterization of cocrystals and salts of oxime 5.1:

Synthesis of quinoline-4-carbaldoxime was obtained by reported procedure.[13] Cocrystals and salts were obtained by slow evaporation of a solution of the quinoline-4-carbaldehyde oxime and the guest molecules in methanol-acetone mixture with their respective molar ratio.

Cocrystal of quinoline-4-carbaldoxime with adipic acid (**5.2)**: Isolated yield: 74 %. ^{1}H NMR (400 MHz, DMSO-d_6): 12.03 (s, 1H), 8.93 (d, J = 4.4 Hz, 1H), 8.85 (s, 1H), 8.64 (d, J = 8.4 Hz, 1H), 8.06 (d, J = 8.4 Hz, 1H), 7.82 (t, J = 6.8 Hz, 1H), 7.75 (d, J = 4.4 Hz, 1H), 7.68 (t, J = 8.4, 1H), 2.20 (m, 4H), 1.49 (m, 4H). IR (KBr, cm^{-1}): 3045 (br, m), 2962 (w), 1695 (s), 1583 (s), 1517 (m), 1488 (m), 1462 (s), 1428 (m), 1408 (m), 1358 (m), 1328 (w), 1279 (s), 1247 (w), 1193 (s), 1142 (w), 1042 (s), 927 (s), 856 (m), 818 (m), 756 (s), 735 (s), 688 (m), 612 (w), 512 (s). ESI mass: calcd. 173.0715 [M + H^{+}]; found 173.0710 [M + H^{+}].

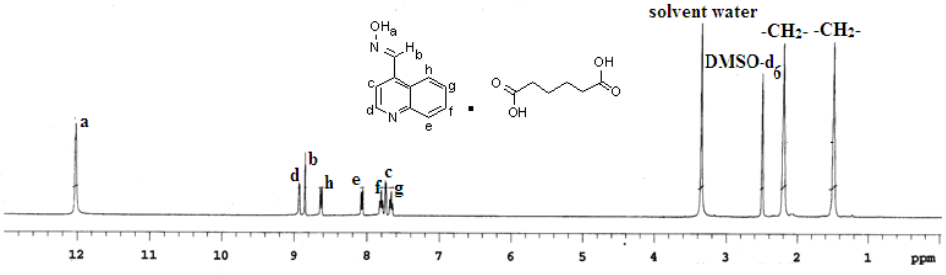

Figure 5.19: ^{1}H NMR (400 MHz, DMSO-d_6) of cocrystal **5.2**.

Cocrystal of quinoline-4-carbaldoxime with succinic acid (**5.3)**: Isolated yield: 71 %. ^{1}H-NMR (400 MHz, DMSO-d_6): 12.03 (s, 1H), 8.93 (d, J = 4.4 Hz, 1H), 8.85 (s, 1H), 8.64 (d, J = 8.4 Hz, 1H), 8.08 (d, J = 8.4 Hz, 1H), 7.80 (m, 1H), 7.75 (d, J = 4.4 Hz, 1H), 7.67 (m, 1H), 2.41 (m, 2H), 2.08 (m, 2H). IR (KBr, cm^{-1}): 3050 (br, m), 2989 (w), 1680 (m), 1583 (s), 1517 (s), 1486 (s), 1458 (m), 1421 (w), 1372 (w), 1330 (s), 1295 (m), 1243 (s), 1178 (s),

1143 (m), 1047 (s), 1022 (w), 993 (m), 923 (s), 857 (s), 817 (s), 802 (m), 786 (m), 765 (s), 661 (s), 603 (m), 554 (s), 537 (m), 516 (s).

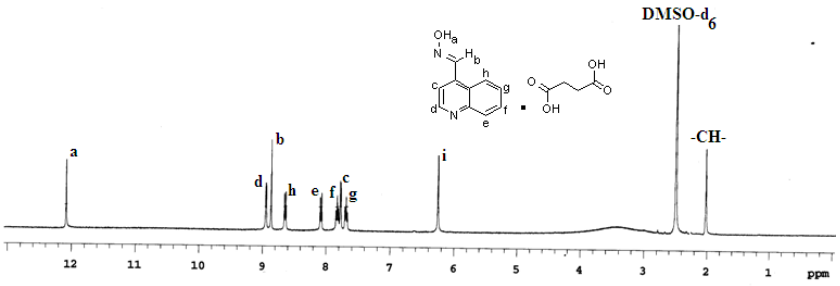

Figure 5.20: ^{1}H NMR (400 MHz, DMSO-d_6) of cocrystal **5.3**.

Cocrystal of quinoline-4-carbaldoxime with fumaric acid (**5.4)**: Isolated yield: 75 %. ^{1}H NMR (400 MHz, DMSO-d_6): 12.03 (s, 1H), 8.93 (d, J = 4.4 Hz, 1H), 8.85 (s, 1H), 8.64 (d, J = 8.4 Hz, 1H), 8.08 (d, J = 8.4 Hz, 1H), 7.80 (t, J = 6.8, 1H), 7.75 (d, J = 4 Hz, 1H), 7.67 (t, J = 8, 1H), 2.41 (s, 1H), 2.08 (s, 1H). IR (KBr, cm^{-1}): 3137 (br, m), 2989 (w), 1679 (m), 1585 (s), 1517 (s), 1486 (s), 1459 (m), 1373 (w), 1331 (s), 1296 (m), 1244 (s), 1208 (m), 1181 (s), 1145 (m), 1048 (s), 1023 (w), 987 (m), 970 (m), 924 (s), 857 (s), 818 (s), 792 (s), 765 (s), 668 (s), 602 (m), 559 (s), 536 (m), 516 (s).

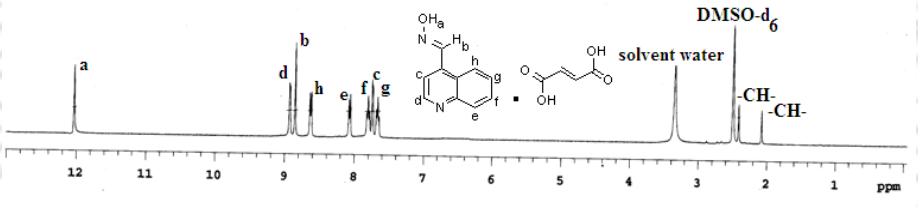

Figure 5.21: ^{1}H NMR (400 MHz, DMSO-d_6) of cocrystal **5.4**.

Maleate salt of quinoline-4-carbaldoxime (**5.5):** Isolated yield: 81 %. ^{1}H NMR (400 MHz, DMSO-d_6): 12.08 (s, 1H), 8.95 (d, J = 4.4 Hz, 1H), 8.86 (s, 1H), 8.65 (d, J = 8.8 Hz, 1H), 8.09 (d, J = 8.4 Hz, 1H), 7.83 (t, J = 6.8 Hz, 1H), 7.78 (d, J = 4 Hz, 1H), 7.69 (t, J = 8, 1H), 6.25 (s, 1H), 2.03 (s, 2H). IR (KBr, cm^{-1}): 3066 (br, m), 2923 (w), 1693 (w), 1633 (m), 1592 (m), 1490 (w), 1448 (s), 1349 (s), 1271 (m), 1235 (w), 1216 (m), 1055 (m), 994 (s), 865 (s), 784 (m), 766 (m), 737 (m), 658 (s), 573 (s), 527 (s).

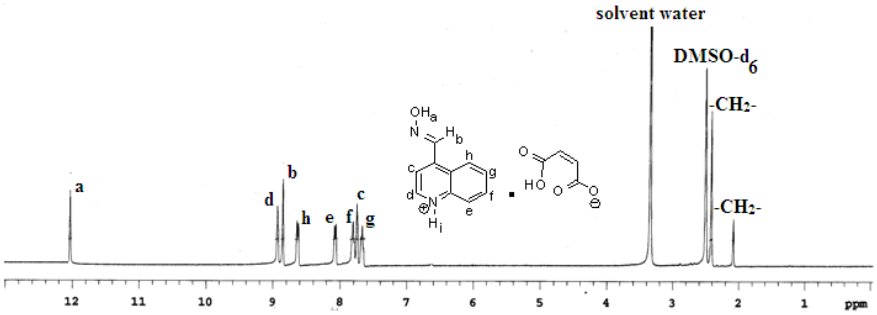

Figure 5.22: ^{1}H NMR (400 MHz, DMSO-d_6) of salt **5.5**.

Oxalate salt of quinoline-4-carbaldoxime (**5.6):** Isolated yield: 78 %. ^{1}H NMR (400 MHz, DMSO-d_6): 12.07 (s, 1H), 8.94 (d, J = 4.4 Hz, 1H), 8.85 (s, 1H), 8.64 (d, J = 8.8 Hz, 1H), 8.08 (d, J = 8 Hz, 1H), 7.83 (t, J = 6.8 Hz, 1H), 7.76 (d, J = 4.8 Hz, 1H), 7.69 (t, J = 8, 1H). IR (KBr, cm^{-1}): 3329 (br, m), 3048 (w), 2946 (w), 1634 (s), 1578 (s), 1498 (m), 1460 (m), 1409 (w), 1375 (m), 1325 (w), 1306 (m), 1281 (w), 1238 (w), 1127 (m), 1056 (s), 1025 (s), 997 (s), 919 (s), 846 (s), 808 (m), 760 (s), 658 (m) 648 (s), 528 (s).

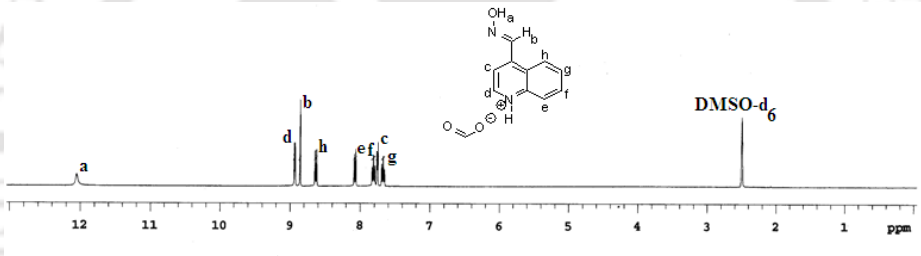

Figure 5.23: ^{1}H NMR (400 MHz, DMSO-d_6) of salt **5.6**.

Chloride salt of quinoline-4-carbaldoxime (**5.7)**: Isolated yield: 73 %. ^{1}H NMR (400 MHz, DMSO-d_6): 12.89 (s, 1H), 9.17 (d, J = 5.5 Hz, 1H), 9.07 (s, 1H), 8.82 (d, J = 8.8 Hz, 1H), 8.34 (d, J = 8.4 Hz, 1H), 8.15 (d, J = 5.6 Hz, 1H), 8.08 (t, J = 6.8 Hz, 1H), 7.91 (t, J = 7.2, 1H). IR (KBr, cm^{-1}): 3229 (br, m), 3058 (w), 2956 (w), 1627 (s), 1558 (s), 1530 (m), 1448 (m), 1381 (m), 1362 (m), 1323 (m), 1274 (s), 1237 (s), 1143 (s), 1043 (s), 991 (s), 888 (m), 840 (s), 759 (s), 534 (s).

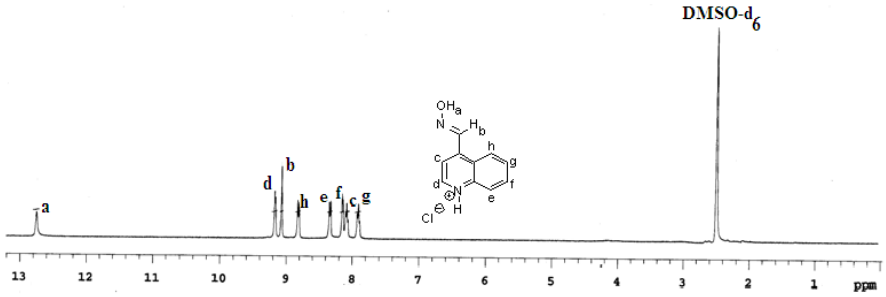

Figure 5.24: ^{1}H NMR (400 MHz, DMSO-d_6) of salt **5.7**.

Nitrate salt of quinoline-4-carbaldoxime (**5.8)**: Isolated yield: 75 %. ^{1}H NMR (400 MHz, DMSO-d_6): 12.88 (s, 1H), 9.21 (d, J = 5.2 Hz, 1H), 9.09 (s, 1H), 8.84 (d, J = 8 Hz, 1H), 8.23 (d, J = 8.8 Hz, 1H), 8.19 (d, J = 5.6 Hz, 1H), 8.10 (t, J = 6.8 Hz, 1H), 7.93 (t, J = 7.2, 1H). IR (KBr, cm^{-1}): 3223 (br, m), 3096 (w), 2956 (w), 1637 (s), 1594 (s), 1540 (m), 1460 (s), 1383 (s), 1321 (s), 1292 (m), 1274 (m), 1221 (s), 1152 (w), 1104 (s), 1049 (s), 1029 (s), 989 (s), 927 (s), 885 (s), 854 (s), 817 (w), 770 (s), 720 (s), 655 (s), 630 (w), 533 (s).

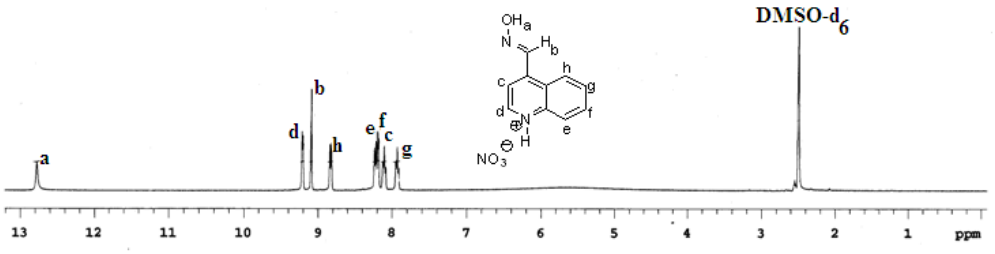

Figure 5.25: ^{1}H NMR (400 MHz, DMSO-d_6) of salt **5.8**.

Cocrystal of quinoline-4-carbaldoxime with o-Toluic acid (**5.9):** Isolated yield: 78 %. ^{1}H NMR (400 MHz, DMSO-d_6): 12.81 (s, 1H), 12.04 (s, 1H), 8.92 (d, J = 4 Hz, 1H), 8.84 (s, 1H), 8.63 (d, J = 4 Hz, 1H), 8.07 (d, J = 4 Hz, 1H), 7.81 (d, J = 8 Hz, 1H), 7.74 (d, J = 4 Hz, 1H), 7.64 (t, J = 8 Hz, 1H), 7.44 (t, J = 8 Hz, 1H), 7.29 (t, J = 8 Hz, 1H) . IR (KBr, cm^{-1}): 3334 (br, s), 3060 (w), 2968 (w), 1685 (s), 1602 (w), 1587 (s), 1577 (s), 1513 (s), 1492 (s), 1464 (m), 1447 (s), 1428 (s), 1379 (s), 1364 (s), 1317 (s), 1294 (w), 1277 (m), 1244 (w), 1199 (m), 1173 (m), 1147 (m), 1089 (s), 1021 (s), 987 (s), 949 (m), 919 (s), 855 (s), 831 (s), 812 (s), 789 (s), 769 (m), 751 (s), 728 (s), 688 (s), 649 (s), 560 (m), 544 (s).

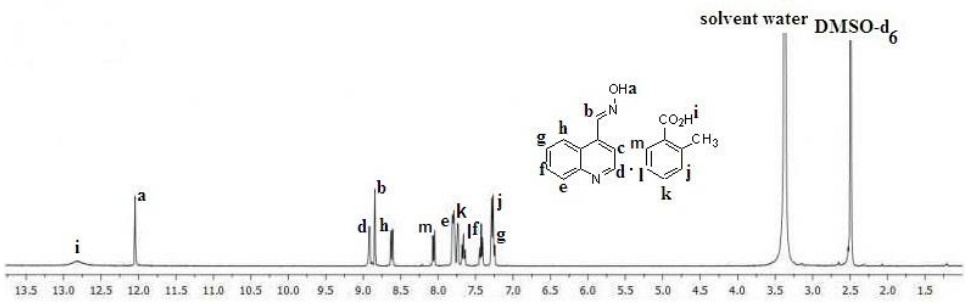

Figure 5.26: ^{1}H NMR (400 MHz, DMSO-d_6) of cocrystal **5.9**.

Salt of quinoline-4-carbaldoxime with salicylic acid (**5.10)**: Isolated yield: 77 %. ^{1}H NMR (400 MHz, DMSO-d_6): 12.88 (s, 1H), 9.21 (d, J = 5.2 Hz, 1H), 9.09 (s, 1H), 8.84 (d, J = 8 Hz, 1H), 8.23 (d, J = 8.8 Hz, 1H), 8.19 (d, J = 5.6 Hz, 1H), 8.10 (t, J = 6.8 Hz, 1H), 7.93 (t, J = 7.2, 1H). IR (KBr, cm^{-1}): 3322 (br, s), 3069 (w), 2896 (w), 2773 (w), 1656 (s), 1586 (s), 1508 (m), 1485 (s), 1462 (s), 1425 (m), 1376 (w), 1344 (m), 1293 (s), 1253 (s), 1227 (s), 1150 (s),

1106 (s), 1065 (w), 1050 (w), 1030 (w), 993 (w), 981 (s), 948 (m), 860 (m), 848 (w), 796 (w), 755 (w), 747 (w), 700 (s), 667 (s), 631 (w), 581 (w), 533 (s).

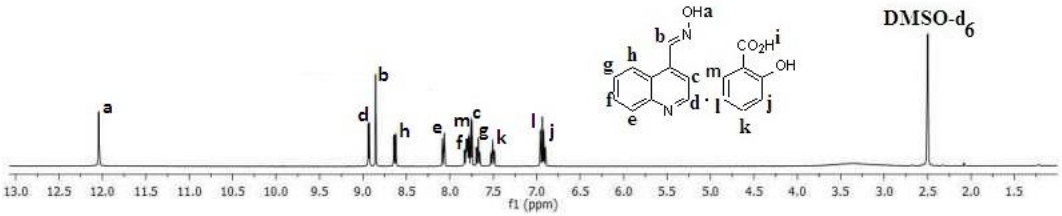

Figure 5.27: ^{1}H NMR (400 MHz, DMSO-d_6) of salt **5.10**.

Salt of quinoline-4-carbaldoxime with 2-Nitrobenzoic acid (**5.11):** Isolated yield: 75 %. ^{1}H NMR (400 MHz, DMSO-d_6): 12.06 (s, 1H), 8.93 (d, J = 4 Hz, 1H), 8.85 (s, 1H), 8.63 (d, J = 4 Hz, 1H), 8.07 (d, J = 4 Hz, 1H), 7.98 (t, J = 8 Hz, 1H), 7.86 (t, J = 4 Hz, 1H), 7.84 (t, J = 4 Hz, 1H), 7.82 (t, J = 4 Hz, 1H), 7.81 (t, J = 4 Hz, 1H), 7.79 (d, J = 4 Hz, 1H), 7.77 (d, J = 4 Hz, 1H), 7.76 (d, J = 4 Hz, 1H), 7.75 (d, J = 8 Hz, 1H). IR (KBr, cm^{-1}): 3179 (br, s), 2860 (w), 2765 (w), 1720 (s), 1648 (w), 1617 (m), 1582 (s), 1522 (s), 1474 (s), 1455 (w), 1371 (s), 1346 (s), 1281 (s), 1247 (s), 1260 (w), 1166 (m), 1149 (s), 1131 (s), 1109 (s), 1072 (s), 1049 (s), 1022 (s), 1000 (s), 968 (w), 921 (s), 874 (s), 860 (s), 841 (s), 812 (s), 790 (s), 763 (s), 698 (s), 682 (s), 650 (s), 638 (s), 570 (s), 532 (s).

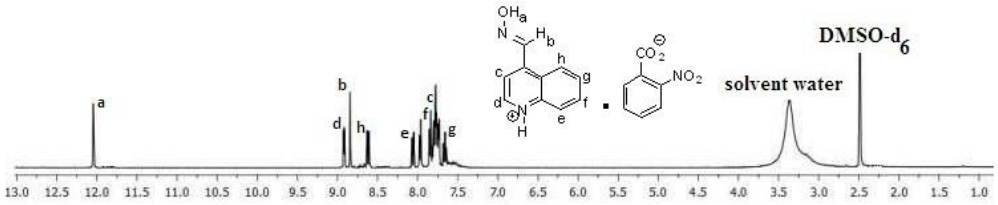

Figure 5.28: ^{1}H NMR (400 MHz, DMSO-d_6) of salt **5.11**.

Salt of quinoline-4-carbaldoxime with 3-Nitro benzoic acid (**5.12):** Isolated yield: 73 %. ^{1}H-NMR (400 MHz, DMSO-d_6): 12.04 (s, 1H), 8.92 (d, J = 4 Hz, 1H), 8.84 (s, 1H), 8.63 (s, 1H), 8.61 (d, J = 4 Hz, 1H), 8.47 (d, J = 8 Hz, 1H), 8.35 (d, J = 4 Hz, 1H), 8.07 (d, J = 4 Hz, 1H), 7.82 (t, J = 4 Hz, 1H), 7.74 (d, J = 4 Hz, 1H), 7.68 (t, J = 4 Hz, 1H). IR (KBr, cm^{-1}): 3209 (br, s), 3108 (w), 2994 (w), 1655 (m), 1614 (s), 1591 (s), 1575 (m), 1534 (s), 1480 (s), 1458 (s), 1344 (s), 1321 (s), 1297 (m), 1252 (s), 1176 (s), 1151 (s), 1097 (w), 1068 (m), 1046 (s), 1021 (s), 990 (s), 925 (m), 901 (m), 867 (s), 837 (s), 817 (s), 793 (m), 782 (s), 763 (s), 719 (s), 668 (w), 652 (m), 578 (w), 537 (w).

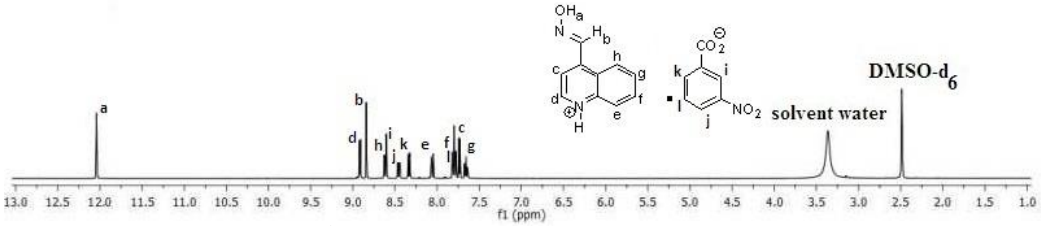

Figure 5.29: ^{1}H NMR (400 MHz, DMSO-d_6) of salt **5.12**.

Salt of quinoline-4-carbaldoxime with 4-Nitro benzoic acid (**5.13):** Isolated yield: 76 %. ^{1}H-NMR (400 MHz, DMSO-d_6): 12.01 (s, 1H), 8.92 (d, J = 4 Hz, 1H), 8.83 (s, 1H), 8.62 (d, J = 8 Hz, 1H), 8.32 (d, J = 8 Hz, 2H), 8.17 (d, J = 8 Hz, 2H), 8.07 (d, J = 4 Hz, 1H), 7.81 (t, J = 4 Hz, 1H), 7.74 (d, J = 4 Hz, 1H), 7.68 (t, J = 4 Hz, 1H). IR (KBr, cm^{-1}): 3080 (br, s), 2838 (w), 2665 (w), 1694 (s), 1606 (s), 1542 (s), 1517 (s), 1492 (w), 1422 (s), 1350 (s), 1331 (w), 1318 (w), 1279 (m), 1245 (w), 1170 (m), 1150 (m), 1126 (m), 1107 (w), 1047 (s), 1012 (s), 990 (s), 919 (s), 879 (s), 859 (s), 817 (m), 798 (s), 766 (s), 719 (s), 643 (s), 610 (w), 558 (s), 534 (w), 515 (s).

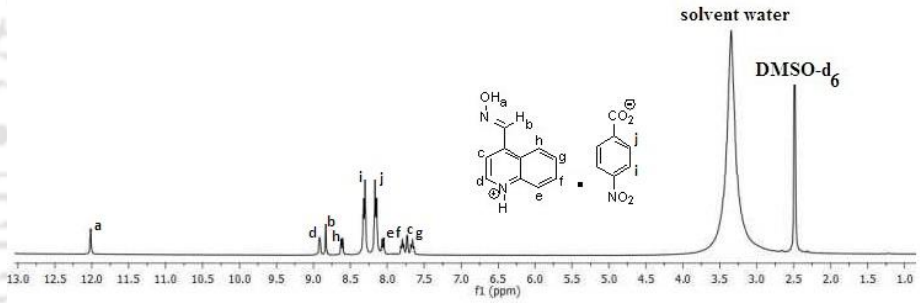

Figure 5.30: ^{1}H NMR (400 MHz, DMSO-d_6) of salt **5.13.**

Salt of quinoline-4-carbaldoxime with 2, 3-dihydroxy benzoic acid (**5.14)**: Isolated yield: 88 %. ^{1}H-NMR (400 MHz, DMSO-d_6): 12.06 (s, 1H), 9.32 (s, 1H), 8.93 (d, J = 4 Hz, 1H), 8.85 (d, J= 4 Hz, 1H), 8.63 (d, J = 4 Hz, 1H), 8.07 (d, J = 4 Hz, 1H), 7.82(t, J = 8 Hz, 1H), 7.75 (d, J = 4 Hz, 1H), 7.68 (t, J = 8 Hz, 1H), 7.23 (t, J = 8 Hz, 1H), 7.00 (t, J = 8 Hz, 1H), 6.72 (t, J = 8 Hz, 1H). IR (KBr, cm^{-1}): 3220 (br, s), 3048 (w), 2946 (w), 1655 (m), 1603 (w), 1544 (s), 1504 (m), 1472 (s), 1456 (s), 1396 (s), 1376 (s), 1338 (m), 1283 (m), 1259 (w), 1247 (w), 1223 (w), 1182 (w), 1152 (w), 1111 (s), 1077 (s), 991 (s), 975 (w), 954 (w), 919 (s), 878 (s), 869 (w), 856 (s), 840 (s), 783 (s), 759 (s), 735 (w), 642 (s), 533 (s).

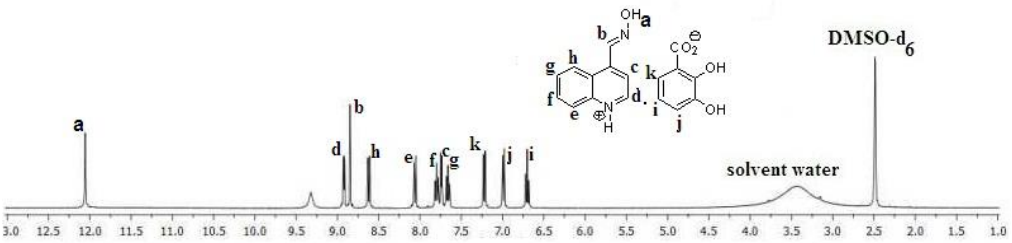

Figure 5.31: ^{1}H NMR (400 MHz, DMSO-d_6) of salt **5.14**.

Salt of quinoline-4-carbaldoxime with 2, 4-dihydroxy benzoic acid (**5.15)**: Isolated yield: 87 %. ^{1}H NMR (400 MHz, DMSO-d_6): 12.04 (s, 1H), 11.43 (s, 1H), 10.38 (s, 1H), 8.92 (d, J = 4 Hz, 1H), 8.84 (s, 1H), 8.63 (d, J = 4 Hz, 1H), 8.07 (d, J = 4 Hz, 1H), 7.82 (t, J = 8 Hz, 1H), 7.74 (d, J = 4 Hz, 1H), 7.68 (t, J = 8 Hz, 1H), 7.61 (d, J = 8 Hz, 1H), 6.34 (d, J= 4 Hz,1H), 6.31 (s, 1H). IR (KBr, cm^{-1}): 3515 (br, s), 3163 (br, s), 2923 (w), 1656 (s), 1633 (w), 1609 (S), 1547 (s), 1519 (s), 1505 (w), 1478 (w), 1460 (s), 1406 (s), 1391 (s), 1375 (m), 1366 (w), 1336 (s), 1317 (s), 1250 (s), 1230 (w), 1220 (w), 1157 (w), 1150 (s), 1114 (s), 1098 (s), 1048 (s), 1020 (w), 993 (s), 974 (m), 922 (s), 889 (w), 879 (w), 857 (s), 840 (s), 812 (w), 754 (s), 699 (s), 649 (w), 631 (s), 608 (s), 534 (s).

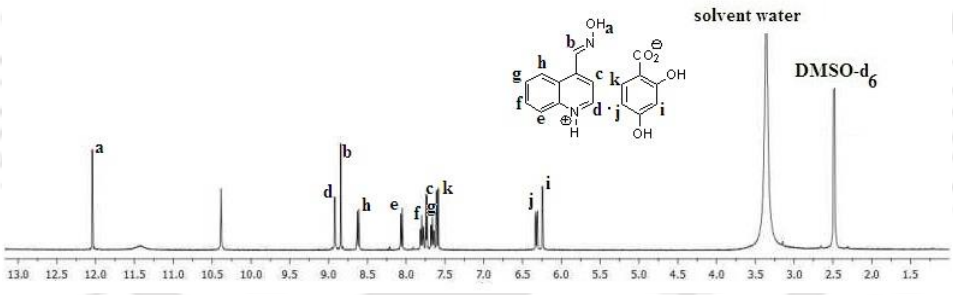

Figure 5.32: ^{1}H NMR (400 MHz, DMSO-d_6) of salt **5.15**.

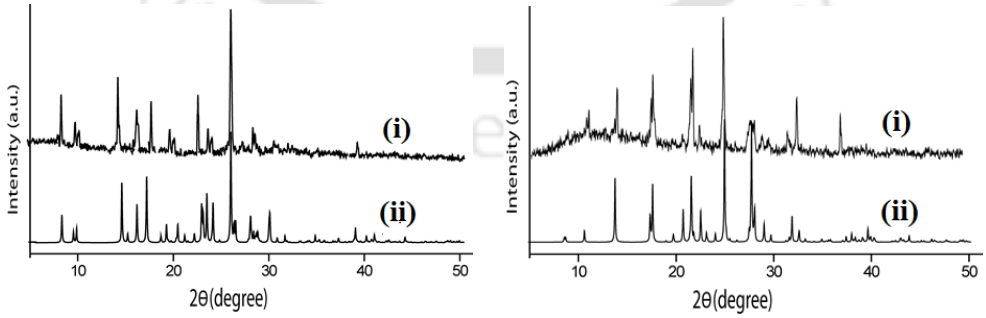

Figure 5.33: (i) Experimental and (ii) Simulated PXRD pattern of cocrystal (a) **5.2** and (b) **5.3**, Simulated PXRD pattern generated from cif file.

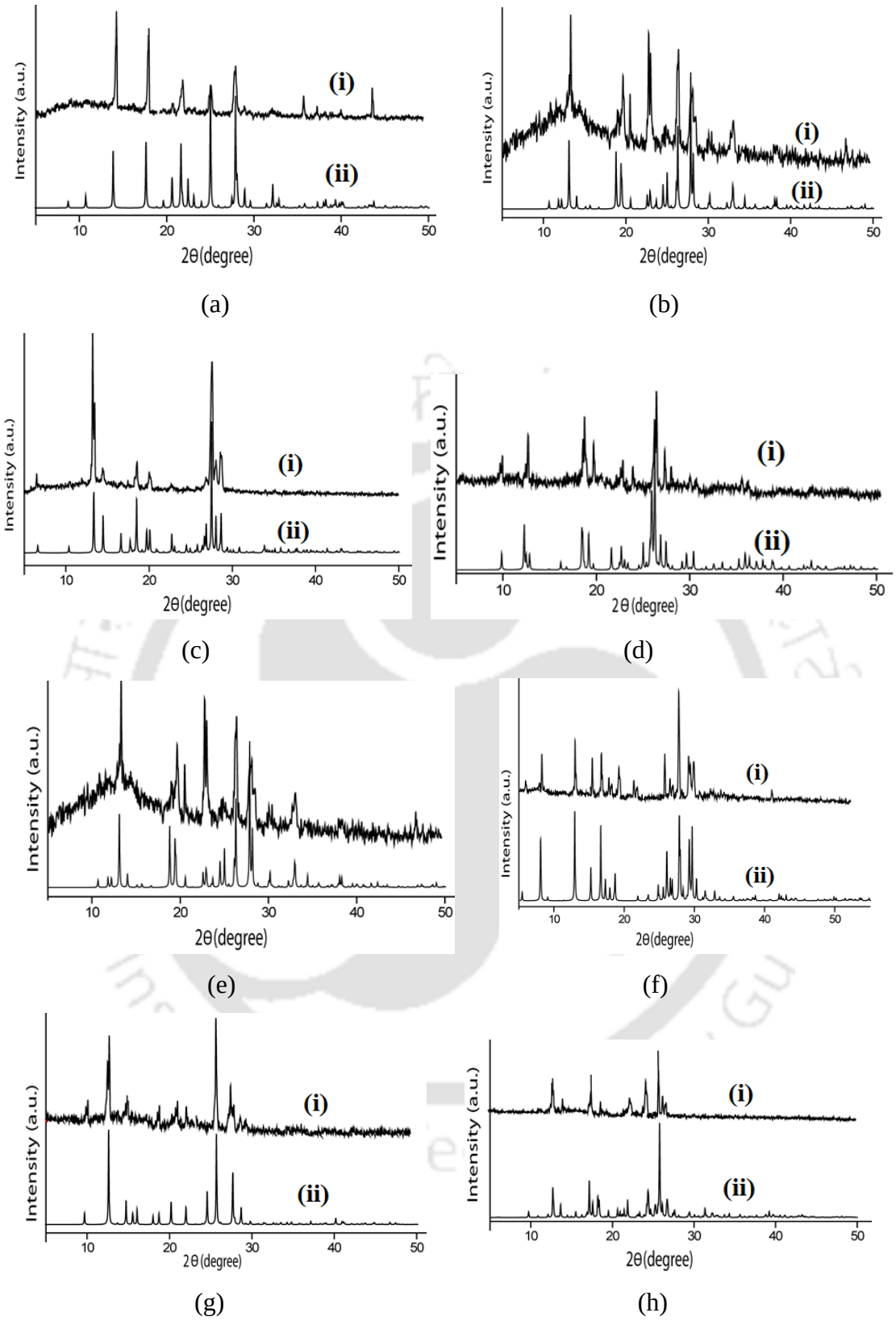

Figure 5.34: (i) Experimental and (ii) Simulated PXRD pattern of (a) cocrystal **5.4** and salt (b) **5.5**, (c) **5.6**, (d) **5.7**, (e) **5.8**, (f) cocrystal **5.9**, (g) salt **5.10** and (h) salt **5.11**, Simulated PXRD pattern generated from cif file.

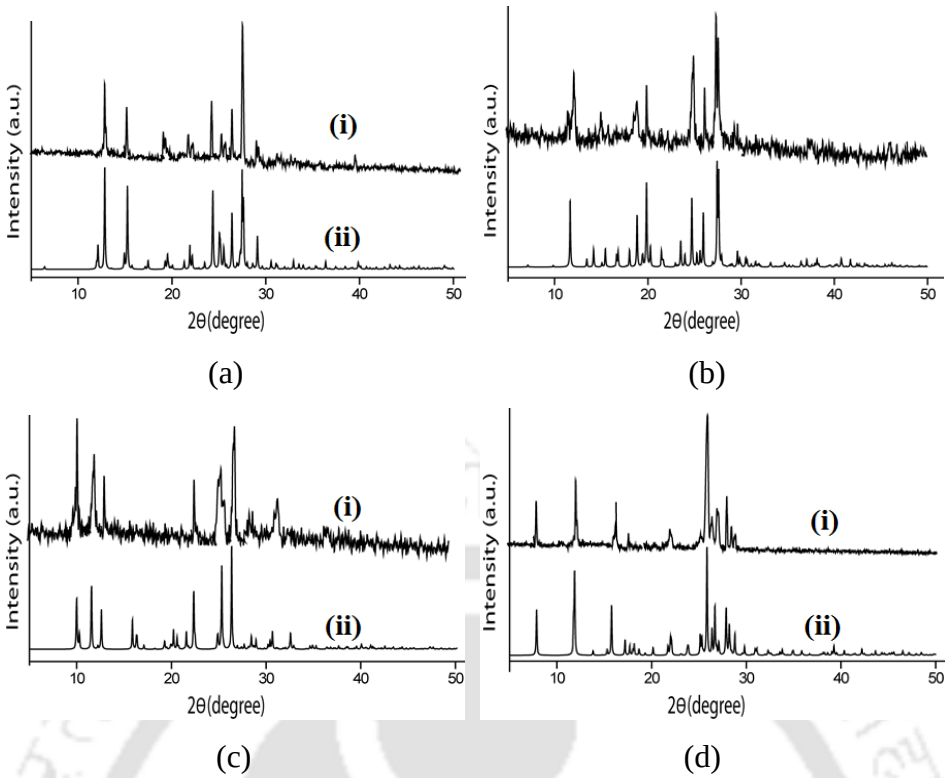

Figure 5.35: (i) Experimental and (ii) Simulated PXRD pattern of salt (a) **5.12**, (b) **5.13**, (c) **5.14** and (d) **5.15** Simulated PXRD pattern generated from cif file.

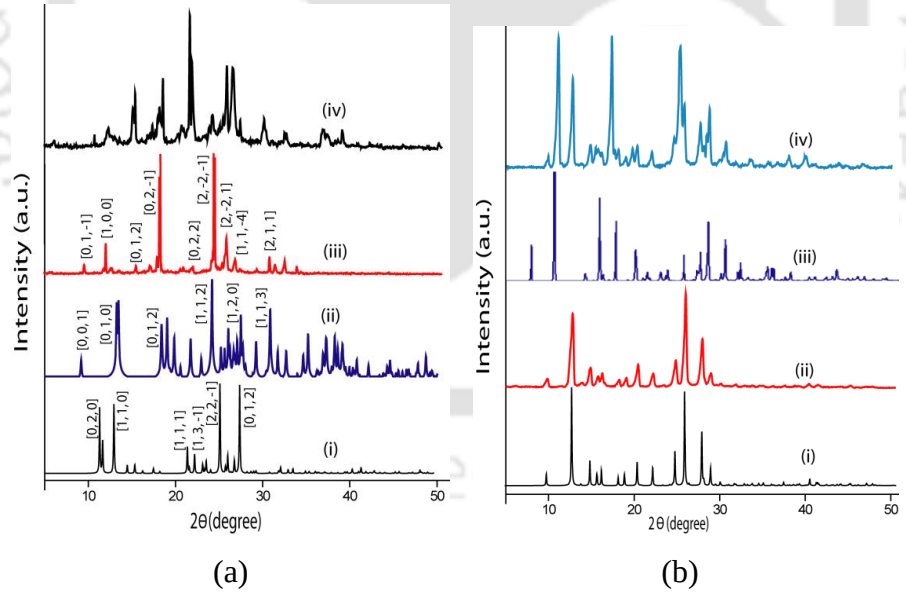

Figure 5.36: PXRD of (i) oxime **5.1**, (ii) 2-HNBA, (iii) cocrystal **5.11** and (iv) 1:2 ratio of oxime **5.11** and 2-HNBA in (a); and Simulated PXRD pattern of (i) salt **5.10**, (iii) 2-H_2BA and Experimental PXRD pattern of (ii) salt **5.10**, (iv) 1:2 ratio of oxime **5.1** and 2-H_2BA in (b). Simulated pattern generated from cif file.

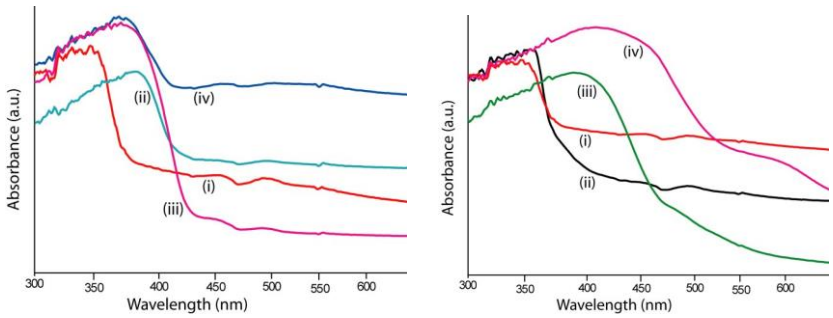

(a) (b)

Figure 5.37: Solid state UV-vis spectra of (i) oxime **5.1**, (ii) salt **5.13**, (iii) salt **5.14**, (iv) salt **5.15** in (a); UV-visible spectra of (i) cocrystal **5.9**, (ii) salt **5.10** , (iii) salt **5.12** and (iv) salt **5.11**.

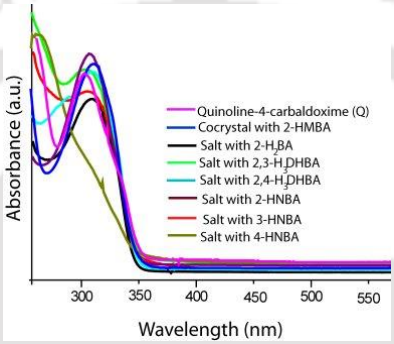

Figure 5.38: UV-vis spectra of oxime **5.1**, cocrystal and salts with different acids in dimethyl formamide solution.

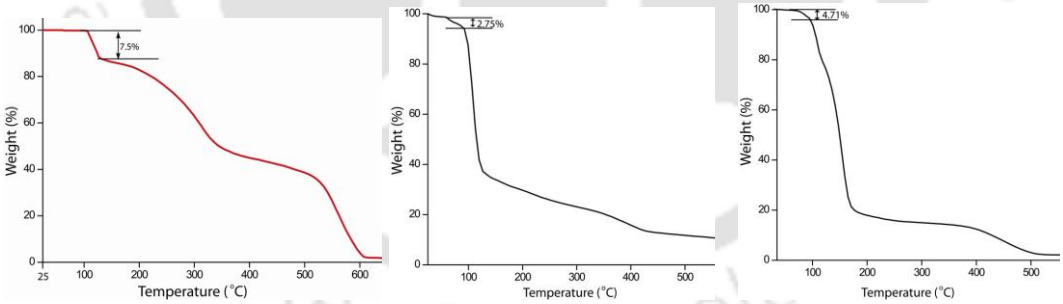

(a) (b) (c)

Figure 5.39: TGA diagram of salt (a) **5.7**, (b) **5.11** and (c) **5.12**.

Table 5.4: Torsion angles of nitrobenzoic acids in free state or in salts.

Atom numbering for torsion angles	Torsion angles	Torsion angles in free acid (°) (optimised by MM2 calculation)	Torsion angles in salts (°) Experimental
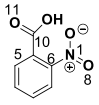	O11-C10-C5-C6 O8-N1-C6-C5	120.80 84.09	-84.99 (85.12*) 166.80 (166.10*) (* in guest carboxylic acid)

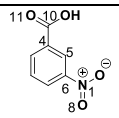	O11-C10-C4-C5 O8-N1-C6-C7	-119.00 -179.00	-171.31 -178.81
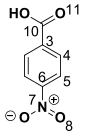	O11-C10-C3-C4 O9-N7-C6-C5	-179.00 46.20	-179.08 176.40

Table 5.5: Torsion angles in cocrystal and salts of oxime **5.1**.

Atom numbering for torsion angles	Torsion angle (°)	Cocrystal	Salts of oxime **5.1** with				
		2-HMBA	2-H_2BA	23-H_3DHBA	24-H_3DHBA	2-HNBA	3-HNBA	4-HNBA
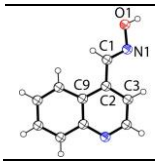	O1-N1-C1-C2	179.23	178.84	-177.78	177.33	-178.82	-179.13	-177.97
	N1-C1-C2-C3	18.26	22.75	24.41	-19.82	-3.06	17.25	19.60
	N1-C1-C2-C9	-161.62	-153.62	-157.63	160.47	177.06	-162.70	-161.68

Table 5.6: Core distances between two acid molecules and two oxime **5.1** molecules in quaternary sub-assemblies.

Molecules	Core distance (Å)						
	Cocrystal	Salts					
	5.9	**5.10**	**5.11**	**5.12**	**5.13**	**5.14**	**5.15**
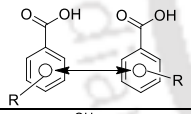	17.377	16.573	16.870	16.334	17.210	16.810	16.378
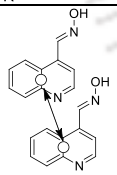	8.228	8.219	8.593	8.264	8.077	8.245	8.145

5.7: References

1. (a) G. R. Desiraju, *Angew. Chem., Int. Ed. Engl*., **1995, 34**, 2311-2327; (b) S. Basavoju, D. Boström, S. P. Velaga, *Cryst. Growth Des*., 2006, **6**, 2699-2708; (c) N. Schultheiss, A. Newman, *Cryst. Growth Des*., 2009, **9**, 2950-2967; (d) R. Thakuria, A. Delori, W. Jones, M. P. Lipert, L. Roy, N. Rodríguez-Hornedo, *Int. J. Pharm*., 2013, **453**, 101-12; (e) M. D. Eddleston, W. Jones, *Cryst. Growth Des*., 2010, **10**, 365-370.
2. G. P. Stahly, *Cryst. Growth Des*., 2009, **9**, 4212-4229.

3. (a) A. Nayak, V. R. Pedireddi, *Cryst. Growth Des*., 2016, **16**, 5966-5975; (b) R. Liu, H. Wang, W. J. Jin, *Cryst. Growth Des*., 2017, **17**, 3331-3337; (c) H. Sun, J. Peng, K. Zhao, R. Usman, A. Khan, M. Wang, *Cryst. Growth Des*., 2017, **17**, 6684-6691; (d) E. Sangtani, S. K. Mandal, A. S. Sreelakshmi, P. Munshi, R. G. Gonnade, *Cryst. Growth Des*., 2017, **17**, 3071-3087.
4. (a) W. Yang, A. Greenaway, X. Lin, R. Matsuda, A. J. Blake, C. Wilson, W. Lewis, P. Hubberstey, S. Kitagawa, N. R. Champness, M. Schroder, *J. Am. Chem. Soc*., 2010, **132**, 14457-14469; (b) D. GonzalezRodriguez, A. P. H. Schenning, *J. Chem. Mater*., 2011, **23**, 310-325; (c) M. Klaus, V. Vasylyeva, *CrystEngComm*, 2010, **12**, 3989-4002; (d) G. R. Desiraju, *Chem. Commun*., 1997, 1475-1482; (e) D. S. Reddy, D. C. Craig, G. R. Desiraju, *J. Am. Chem. Soc*., 1996, **118**, 4090-4093.
5. (a) K. N. Jarzembska, A. A. Hoser, S. Varughese, R. Kaminski, M. Malinska, M. Stachowicz, V. R. Pedireddi, K. Wozniak, *Cryst. Growth Des*., 2017, **17**, 4918-4931; (b) P. K. Goswami, R. Thaimattam, A. Ramanan, *Cryst. Growth Des*., 2016, **16**, 1268-1281; (c) M. Oruganti, S. K. Nechipadappu, P. A. Khade, D. R. Trivedi, *ACS Omega*, 2017, **2**, 7146-7162.
6. (a) G. R. Desiraju, Crystal Engineering: The Design of Organic Solids; Elsevier: Amsterdam, 1989; (b) G. R. Desiraju, *Angew. Chem., Int. Ed. Engl*., 1995, **34**, 2311-2327; (c) F. Grepioni, D. Braga, Making Crystals by Design: From Molecules to Molecular Materials, Methods, Techniques, Applications; *Eds.; Wiley-VCH: Weinheim, Germany*, 2007, 209-240.
7. (a) E. R. T. Tiekink, J. J. Vittal, Frontiers in Crystal Engineering, *Eds.; Wiley: West Sussex, England*, 2006; (b) C. B. Aakeröy, A. M. Beatty, B. A. Helfrich, *Angew. Chem., Int. Ed*., 2001, **40**, 3240-3242; (c) T. Steiner, *Angew. Chem., Int. Ed*., 2002, **41**, 48-76; (d) J. D. Dunitz, *Chem. Commun*., 2003, 545-548; (e) J. D. Wuest, *Chem. Commun*., 2005, 5830-5837; (f) G. R, Desiraju, *Angew. Chem., Int. Ed. Engl*., 2007, **46**, 8342-8356; (g) A. B. Joanna, P. Vishweshwar, D. Weyna, M. J. Zaworotko, *Mol. Pharm*., 2007, **4**, 401-416.
8. (a) T. J. M. Luo, G. T. R. Palmore, *Cryst. Growth Des*., 2002, **2**, 337-350; (b) B. Sarma, S. Roy, A. Nangia, *Chem. Commun*., 2006, 4918-4920; (c) S. Roy, P. M. Bhatt, A. Nangia, G. J. Kruger, *Cryst. Growth Des*. 2007, **7**, 476-480; (d) G. S. McGrady, M. Odlyha, P. D. Prince, J. W. Steed, *CrystEngComm*, 2002, **4**, 271-276; (e) S. Aitipamula, A. B. H. Wong, P. S. Chowa, R. B. H. Tan, *CrystEngComm*, 2012,

14, 8515-8524; (f) C. B. Aakeröy, A. M. Beatty, D. S. Leinen, *CrystEngComm*, 2002, **4**, 310-314.

9. (a) L. Leiserowitz, *Acta Crystallogr.*, 1976, **B32**, 775; (b) J. Bernstein, M. C. Etter, L. Leiserowitz, In *Structure Correlation*; H.-B. Burgi, J. D. Dunitz, Eds.; V C H: Weinheim, 1994; Vol. 2; (c) S. V. Kolotuchin, E. E. Fenlon, S. R. Wilson, C. J. Loweth, S. C. Zimmerman, *Angew. Chem., Int. Ed. Engl.*, 1995, **34**, 2654-2657.
10. (a) P. Vishweshwar, A. Nangia, V. M. Lynch, *J. Org. Chem.*, 2002, **67**, 556-565; (b) S. Roy, K. Biradha, *Cryst. Growth Des*., 2013, **13**, 3232-3241; (c) S. Tothadi, G. R. Desiraju, *Cryst. Growth Des*., 2012, **12**, 6188-6198.
11. (a) S. Cherukuvada, R. Kaur, T. N. Guru Row, *CrystEngComm*, 2016, **18**, 8528-8555; (b) D. Singh, P. K. Bhattacharyya, J. B. Baruah, *Cryst. Growth Des*., 2010, **10**, 348-356; (c) B. R. Bhogala, A. Nangia, *Cryst. Growth Des*., 2003, **3**, 547-554; (d) S. Mohamed, D. A. Tocher, M. Vickers, P. G. Karamertzanis, S. L. Price, *Cryst. Growth Des*., 2009, **9**, 2881-2889.
12. (a) E. A. Bruton, L. Brammer, F. C. Pigge, C. B. Aakeröy, D. S. Leinen, *New J. Chem.*, 2003, **27**, 1084-1094; (b) C. B. Aakeröy, K. N. Epa, S. Forbes, J. Desper, *CrystEngComm*, 2013, **15**, 5946-5949; (c) C. B. Aakeröy, M. M. Smith, J. Desper, *CrystEngComm*, 2012, **14**, 71-74.
13. F. -H. Zhou, H. -B. Zhao, X. -D. Gu, Z. -G. Li, J. -W. Xu, *Acta Crystallogr.*, 2007, **E63**, o329-o330
14. (a) G. R. Desiraju, *Chem. Commun*., 1997, 1475-1482; (b) T. Steiner, *New J. Chem*., 1998, **22**, 1099-1103; (c) C. R. Jones, P. K. Baruah, A. L. Thompson, S. Scheiner, M. D. Smith, *J. Am. Chem. Soc*., 2012, **134**, 12064-12071.
15. A. S. Sinha, K. N. Epa, P. D. Chopade, M. M. Smith, J. Desper, C. B. Aakeroy, *Cryst. Growth Des*., 2013, **13,** 2687-2695.
16. (a) A. Mukherjee, G. R. Desiraju, *Chem. Commun.*, 2011, **47**, 4090-4092; (b) J. C. Espinosa-Lara, D. Guzman-Villanueva, J. I. Arenas-García, D. Herrera-Ruiz, J. Rivera-Islas, P. Roman-Bravo, H. Morales-Rojas, H. Hopfl, *Cryst. Growth Des*., 2013, **13**, 169-185; (c) D. Kalita, H. Deka, S. S. Samanta, S. Guchait, J. B. Baruah, *J. Mol. Struct.*, 2011, **990**, 183-196.
17. (a) M. C. Etter, *Acc. Chem. Res.*, 1990, **23,** 120-126; (b) M. C. Etter, J. C. McDonald, J. Bernstein, *Acta Crystallogr.* 1990, **B46,** 256-262.
18. D. Kalita, J. B. Baruah, *J. Mol. Struct*., 2010, **969**, 75-82.

19. C. Tamuly, R. J. Sarma, A. S. Batsanov, A. E. Goeta, J. B. Baruah, *Acta Crystallogr.*, 2005 **61C**, o324-o327.
20. (a) R. Custelcean, M. G. Gorbunova, *J. Am. Chem. Soc*., 2005, **127**, 16362-16363; (b) J. R. Butchard, O. J. Curnow, D. J. Garrett, R. G. A. R. Maclagan, *Angew. Chem., Int. Ed*., 2006, **45**, 7550-7553; (c) D. L. Reger, R. F. Semeniuc, C. Pettinari, F. Luna-Giles, M. D. Smith, *Cryst. Growth. Des*., 2006, **6**, 1068-1070; (d) V. Gorteau, G. Bollot, J. Mareda, A. Perz-velasco, S. Matile, *J. Am. Chem. Soc*., 2006, **128**, 14788-14789; (e) J. K. Nath, J. B. Baruah, *New J. Chem.*, 2013, **37**, 1509-1519. (f) S.Q. Bai, G. Y. H. Quek, L. L. Koh, T. S. A. Hor, *CrystEngComm*, 2010, **12,** 226-233; (g) D. A. Safin, P. M. J. Szell, A. Keller, I. Korobkov, D. L. Bryce, M. Murugesu, *New J. Chem.*, 2015, **39**, 7147-7152; (h) P. S. Lakshminarayanan, E. Suresh, P. Ghosh, *Angew. Chem., Int. Ed*., 2006, **45**, 3807-3811; (i) M. S. Deshpande, A. S. Kumbhar, V. G.; Puranik, K. Selvaraj, *Cryst. Growth Des*., 2006, **6**, 743-748; (j) R. R. Fernandes, A. M. Kirillov, M. Fátima C. G. da Silva, Z. Ma, J. A. L. da Silva, J. J. R. Frausto da Silva, A. J. L. Pombeiro, *Cryst. Growth Des.*, 2008, **8,** 782-785.
21. (a) K. Bouchouit, N. Benali-Cherif, L. Benguedouar, L. Bendheif, H. Merazig, *Acta Crystallogr.*, 2002, **58E**, o1397-1399; (b) H. Casellas, C. Massera, F. Buda, P. Gamez, J. Reedjik, *New. J. Chem*., 2006, **30,** 1561-1566; (c) D. -X. Wang, M. -X. Wang, *J. Am. Chem. Soc.*, 2013, 135, 892-897; (d) L .Valencia, R. Bastda, E. Gracia-Espana, J. V. de Julian-Ortiz, J. M. Llinares, A. Macias, P. P. Lourido, *Cryst. Growth and Des*., 2011, 10, 3418-3423; (e) P. Khakhlary, J. B. Baruah, *J. Chem. Sci.*, 2015, **127**, 95-102.
22. (a) C. B. Aakeroy, N. R. Champness, C. Janiak, *CrystEngComm*, 2010, **12**, 22-43; (b) E. F. Paulus, F. J. J. Leusen, M. U. Schmidt, *CrystEngComm*, 2007, **9**, 131-143; (c) P.A. Wood, M. A. Oliveira, A. Zink, M. B. Hickey, *CrystEngComm*, 2012, **14**, 2413-2421; (d) K. Durka, K. Gontarczyk, S. Lulinski, J. Serwatowski, K. Wozniak, *Cryst. Growth Des*., 2016, **16**, 4292-4308.
23. A. J. C. Cabeza, G. M. Day, W. D. S. Motherwell, W. Jones, J. Am. Chem. Soc., 2006, **128**, 14466-14467.
24. H. D. Clarke, M. B. Hickey, B. Moulton, J. A. Perman, M. L. Peterson, L. Wojtas, O. Almarsson, M. J. Zaworotko, *Cryst. Growth Des*., 2012, **12**, 4194-4201.
25. R. Thakuria, A. Nangia, *Cryst. Growth Des*., 2013, **13**, 3672-3680.
26. (a) J. N. Low, L. M. N. B. F. Santos, C. F. R. A. C. Lima, *Eur. J. Chem*., 2001, **1**, 61-66; (b) C. B. Aakeroy, A. M. Beattyand D. S. Leinen, *Cryst. Growth Des*., 2001, **1**,

47-52; (c) C. B. Aakeroy, A. M. Beatty, D. S. Leinen, *CrystEngComm*, 2002, **4**, 310-314; (d) E. A. Bruton, L. Brammer, F. C. Pigge, C. B. Aakeroy, D. S. Leinen, *New J. Chem*., 2003, **27**, 1084-1094; (e) C. B. Aakeroy, K. N. Epa, S. Forbes, J. Desper, *CrystEngComm*, 2013, **15**, 5946-5949; (f) A. S. Sinha, K. N. Epa, P. D. Chopade, M. M. Smith, J. Desper, C. B. Aakeroy, *Cryst. Growth Des*., 2013, **13**, 2687-2695.

27. A. Tarai, J. B. Baruah, *CrystEngComm*, 2016, **18**, 298-308.
28. (a) A. J. Cruz-Cabeza, *CrystEngComm*, 2012, **14**, 6362-6365; (b) L. Johnson, K. A. Rumon, *J. Phys. Chem*., 1965, **69**, 74-86; (c) S. L. Childs, G. P. Stahly, A. Park, *Mol. Pharmaceutics*, 2007, **4**, 323-338; (d) B. R. Bhogala, S. Basavoju, A. Nangia, *CrystEngComm*, 2005, **7**, 55-562; (e) C. C. Seaton, K. Chadwick, G. Sadiq, K. Guo, R. G. Davey, *Cryst. Growth Des*., 2010, **10**, 726-733.
29. V. V. Zhurov, A. A. Pinkerton, *J. Phys. Chem. A,* 2015, **119**, 13092-13100.
30. N. K. Duggirala, G. P. F. Wood, A. Fischer, L. Wojtas, M. L. Perry, M. J. Zaworotko, *Cryst. Growth Des*., 2015, **15**, 4341-4354.
31. E. Busseron, Y. Ruff, E. Moulin, N. Giuseppone, *Nanoscale*, 2013, **5**, 7098-7140.
32. (a) S. R. Perumalla and C. C. Sun, *CrystEngComm*, 2012, **14**, 3851-3853; (b) S. R. Perumalla, C. C. Sun, *CrystEngComm*, 2013, **15**, 5756-5759.
33. B. Lou, S. R. Perumalla, C. C. Sun, *Cryst. Growth Des*., 2015, **15**, 24-28.
34. (a) B. Kupcewicz and M. Malecka, *Cryst. Growth Des*., 2015, **15**, 3893-3904; (b) F. C. Spano, *Acc. Chem. Res*., 2010, **43**, 429-439.
35. P. S. Salini, S. K. Rajagopal, M. Hariharan, *Cryst. Growth Des.*, 2016, **16**, 5822-5830; (b) S. K. Rajagopal, P. S. Salini, M. Hariharan, *Cryst. Growth Des.*, 2016, **16**, 4567-4573.

Chapter 6

Self-assemblies, Absorption and Emission Properties of Picrate Salts of Aromatic Amine or Heterocycle Linked Oxime Derivatives

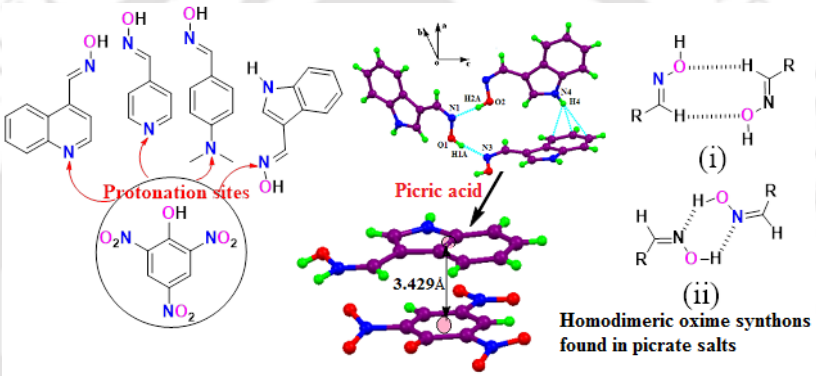

New J. Chem., 2018, **42**, 4757-4765.

6.1: Introduction

Supramolecular self-assembly, confinement and molecular recognition are important core aspects of crystal engineering. These aspects have received significant attention from researchers over the years and have provided insight and control over constructions of new -assemblies.[1] Weak interactions present in a self-assembly and molecular recognition property associated with such assembly are extensively studied with the aid of crystallography. Among the weak interactions electrostatic forces, hydrogen bonds, cation···π interactions, C-H···π and π···π interactions, are constantly studied as key factors to stability of a non-covalently linked self-assembly.[2] Multiple numbers of hydrogen bonds are observed widely among interacting molecules in crystal engineering and advantage of such bonds have been utilized to design the self-assembled structures. Some of such assemblies are capable of molecular encapsulation.[3] Molecular recognition is an important property commonly encountered in biological processes, such as in enzymatic activity, allosteric regulation, molecular transport, genetic information, protein assembly, sensing and separation.[4] On the other hand physical properties of an organic compound in solid or in solution are influenced by the constituent of self-assemblies.[5] The physical properties change from parent components of organic compounds upon combination with another substrate forming cocrystal or salt.[6]

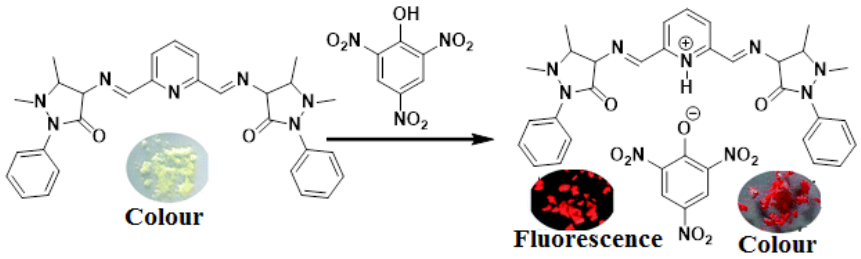

Figure 6.1: Recognition of picric acid through colorimetric and fluorometric changes.

There is an interest for selective and rational design of host molecules for particular guest molecules or ions because of their vital importance in the fields of biological and environmental sciences.[7] Among the widely recognized territory of guests, nitro-aromatics occupy a special position due their utility in military actions and environmental concerns. Nitro group substituted molecules are generally explosive compounds,[8] for example 2,4,6-trinitrophenol (commonly known as picric acid) is a widely used explosive component; it is used in battle fields.[8] Picric acid has applications in dyes, pharmaceutical industries and chemical laboratories.[9] It can also cause irritation and can damage certain human organs.[10] It is a strong organic acid with pKa = 0.38; thus it easily get contaminated in water; and such dissolution may cause epidemics.[11]

Due to such advantages and disadvantages there is necessity to detect their presence in selectively through sensitive recognition of a molecular receptor. Environmental pollution caused by picric acid are well known, so it is an important field of research well sought after in recent years.[12] Optical[13] and electrochemical[14] methods are extensively used to detect trace amount of picric acid from aqueous medium. Among the optical methods fluorescence based sensors are popular due to their short response time, real-time usage, low cost with high sensitivity, high selectivity, simple and portable to on-site for detection.[15] There are many fluorescence-based organic small molecules,[16] inorganic and organic-inorganic hybrid materials such as pyrene,[17] anthracene,[18] boron compounds,[19] luminescent gels,[20] dendrimers,[21] carbazole derivatives,[22] fluoranthene,[23] nano-particales,[24] polyhedral oligomeric-silsesquioxane,[25] metal-organic cages,[26] metal-organic frame works,[27] covalent organic frameworks,[28] covalent organic polymers[29] arte used for the detection of trace amounts of picric acid. However, majority of such receptors detect picric acid through fluorescence "turn off" mechanism. There are only few examples of receptors that detect picric acid through fluorescence "turn on" mechanism.[30] A crab claw shaped 2,6-pyridine bi(iminoantipyrine) ligand (**Fig. 6.1**) having multiple non-covalent binding sites for guest molecules, showed selective recognition of picric acid (PA) through supramolecular interactions. It leads to an intermolecular charge transfer induced naked-eye colour and fluorescence turn-on detection of picric acid in solution and solid state.[31]

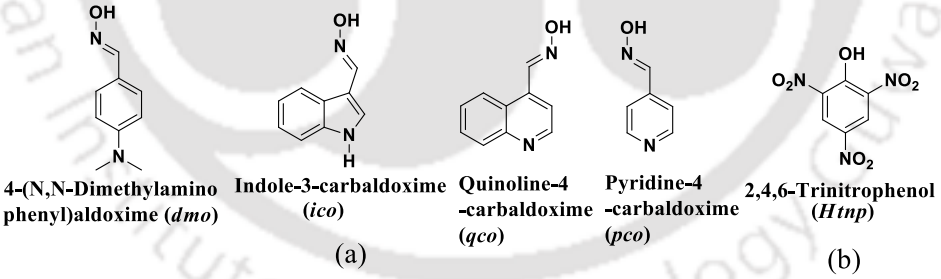

Figure 6.2: (a) Different oximes and (b) 2,4,6-trinitrophenol (picric acid).

There are also large numbers of studies devoted towards developing sensors for nitrophenols.[32] In such detection fluorescence technique is used where the proton transfer at ground or excited state are of general concern. Thus, understanding the effect of proton accepting behavior of a fluorescent oxime from picric acid or nitrophenolic compounds is important. Study on protonation of oximes listed in **Fig. 6.2** by picric acid to form corresponding salt would provide the basis to understand the interplay of weak interactions among various functional groups in those salts. In these salts there will be competitions among non-covalent interactions such as oxime-amine,[33] phenol-amine,[34] phenol-oxime,[35]

and oxime-oxime[36] interactions. Furthermore, non-pyridinium oximes[37] causes catalytic detoxification of nerve agent. This is a biological process so interaction of non-pyridinium oximes with picric acid a compound with medicinal[38] and toxic activities[39] is important. The chosen oximes have some other important issues that can influence formation of self-assemblies. For example different kinetic factors such as protonation at nitrogen atom (a) of **Fig. 6.3** of an oxime by kinetic control process transforming to thermodynamically favorable species (b) of **Fig. 6.3** may be decisive in guiding self-assemblies.[40] Thus the supramolecular synthons[41] in self-assemblies of these molecules will vary and there is need to understand feasibility of isolating un-common protonated species contributing to self-assembly formation.

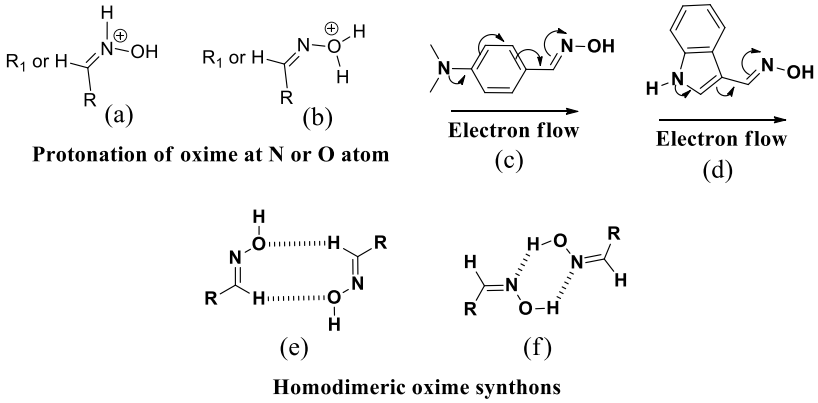

Figure 6.3: Protonated species of aldoxime (a) and (b); (c) and (d) are two examples where extended conjugation may help in changing electron density at oxime nitrogen atom. (e) and (f) are two different synthons in oxime homodimers.

We also felt that oximes such as 4-(N,N-dimethylaminophenyl)aldoxime or indole-3-carbaldoxime (c) and (d) of **Fig. 6.3** has nitrogen atom present at a remote site from the oxime has the lone-pair of electrons on conjugated with the oxime group through intervening carbons. Such delocalization of electrons would allow more flow of electrons to the oxime nitrogen atom to facilitate protonation on the nitrogen atom of the oxime functional group. Among these two examples, the indole unit has an extra ability to form charge-transfer complex with electron deficient molecules such as 2,4,6-trinitrophenol (picric acid).[42]

Thus, such a difference would influence weak interaction schemes of non-covalent linked assemblies[43] comprising of binary or multi-components systems. Due to this a clear difference in physical properties[44] is expected in the salt of picric acid with indole derivative from other salts. Furthermore, varieties of synthons are found in self-assemblies of different oximes derivatives (e) and (f) of **Fig. 6.3**. These arrangements are sensitive to environment.[36,45] Domain expansion of conventional synthons in oximes happens on

interacting with carboxylic acids[46] and interactions of tetrabutylammonium salts with oximes generates interesting self-assemblies.[47] Hence, supramolecular environment created in salts of oxime shown in **Fig. 6.2** will differ case by case; and their self-assemblies will not be as simple as that of a conventional aldoxime. Hence, we describe here a study on picrate salts of four oximes listed in **Fig. 6.2** to find out the descriptor sub-assemblies, also to look the at the possibility to stabilize unusual protonated oxime species and understand optical properties.

6.2: Synthesis of picrate salts 6.1-6.4

Four different picrate salts **6.1-6.4** of aromatic amine or heterocycle linked oxime derivatives were synthesized and characterized by various spectroscopic and X-ray diffraction techniques. Picric acid forms 1:1 anhydrous salts **6.1** and **6.4** with 4-(N,N-dimethylaminophenyl)aldoxime (*dmo*) or pyridine-4-carbaloxime (*pco*) oxime derivatives; whereas the similar 1:1 picrate salts **6.2** and **6.3** with indole-3-carbaldoxime (*ico*) or quinoline-4-carbaldoxime (*qco*) were obtained as monohydrate.

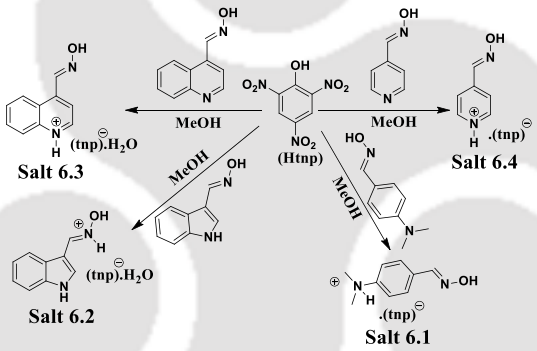

Scheme 6.1: Synthesis of different picrate salts of oxime derivatives with different protonation sites.

But in the case of pyridine-4-carbaloxime or quinoline-4-carbaldoxime derivatives protonation takes place at the nitrogen atom of the ring, whereas in 4-(N,N-dimethylaminophenyl)aldoxime or indole-3-carbaldoxime derivatives protonation take place at 4-(N,N-dimethylaminophenyl) group and at oxime nitrogen atom respectively (**Scheme 6.1**).

6.3: Structural descriptions of picrate salts 6.1-6.4 and oxime derivatives

The picrate salts **6.1** or **6.4** of 4-(N,N-dimethylaminophenyl)aldoxime and pyridine-4-carbaloxime are obtained 1:1 salt; whereas similar 1:1 salt of indole-3-carbaldoxime or quinoline-4-carbaldoxime are obtained as monohydrate. Picrate salt **6.1** of 4-(N,N-dimethylaminophenyl)aldoxime is formed by protonation at the N,N-dimethylaminophenyl

group. To have a protonation at the nitrogen atom of oxime, it would require a partial loss of aromaticity by pumping electron from the -NMe_2 group; which is the possible reason to protonation at nitrogen atom of the -NMe_2 group as such a protonation retains the conjugation of oxime group with the aromatic ring and more importantly the -NMe_2 group has sp^3 type nitrogen atom having more p-character on the orbital occupying lone pair of electrons.

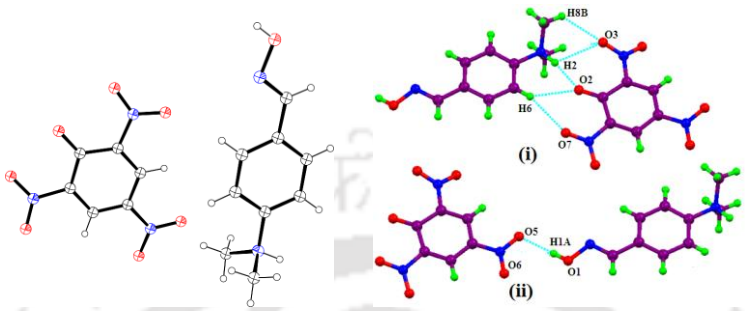

(a) (b)

Figure 6.4: (a) ORTEP diagram of picrate salt **6.1** (with 30% thermal ellipsoids) and (b) Interaction among oxime and picrate ion in salt **6.1**.

It has $^{+}N\text{-}H_{(amine)}\cdots O_{(phenolate)}$ hydrogen bonds between phenolate oxygen of picrate and $^{+}$N-H bond of N,N-dimethylphenylammonium cation. A hydrogen atom of methyl groups of the N,N-dimethylphenylammonium cation part forms supplementary weak C-H···O bonds (i of **Fig. 6.4b)**.The O-H group of oxime form $O\text{-}H_{(oxime)}\cdots O_{(nitro)}$ hydrogen bond with a nitro-group of picrate (ii of **Fig. 6.4b**). An ionic hydrogen bond formed through proton transfer,[48a] provides higher stability to the respective self-assembly.

The picrate salt **6.2** of indole-3-carbaldoxime is obtained as monohydrate. The crystal structure of this salt shows that protonation of indole-3-carbaldoxime at oxime nitrogen atom. Protonation at oxime nitrogen is reflected in C=N bond distance 1.294(6) Å found in this salt, whereas C=N bond distances in neutral benzaldoxime derivatives is 1.266 Å -1.2749 Å,[48b] this distance is slightly higher as compared to C=N bond distance 1.276(4) Å observed in indole-3-carbaldoxime (**Table-6.1**). The $^{+}$N-H forms hydrogen bond with phenolate oxygen of picrate as depicted in **Fig. 6.5a**. On the other hand, $N\text{-}H_{(indole)}\cdots O_{(nitro)}$ hydrogen bonds provide interactions between the ion pairs. The aromatic rings of picrates are located parallel over indole rings in the packing pattern of this salt. The centroid to centroid distance between such aromatic rings is 3.429 Å (iii of Fig. **6.5a**). A centroid to centroid distance between parallel π-aromatic rings falling within 3.5 Å is generally conducive for π-interactions.[49] These results on the schemes of hydrogen bonds have made it clear that principal supramolecular oxime synthons in the salts **6.1** and **6.2** are different. The water molecule of picrate salt **6.2** of indole-3-carbaldoxime has crystallographic disorder. The protonation of

oxime observed was unusual, so it was necessary to optimize the structure of hydrated picrate salt **6.2** of indole-3-carbaldoxime was theoretically.

Table 6.1: Selected bond lengths in the structure of picrate salts and indole-3-carbaldoxime.

Oxime/Picrate salts	C=N (oxime)	Length (Å)	N-O (oxime)	Length (Å)
Indole-3-carbaldoxime	C10-N3	1.276(4)	N3-O2	1.396(3)
Salt **6.2**	C8-N1	**1.294(6)**	N1-O1	**1.357(5)**
Salt **6.3**	C1-N1	1.277(4)	N1-O1	1.374(3)
Salt **6.4**	C1-N1	1.274(6)	N1-O1	1.391(5)
Salt **6.1**	C1-N1	1.270(2)	N1-O1	1.394(2)

The optimized structure by gas-phase density functional theory using B3LYP functional and 6-31++G (d,p) as basis set have revealed that (optimized structure shown in **Fig. 6.5b**) experimentally observed protonation is possible. It also have suggested that the stable form of optimized structure in unusual protonated state has the hydrogen bond donors and acceptors in different orientations with reference to the structure determined by single crystal X-ray diffraction technique. Structure of salt **6.2** is shown in **Fig. 6.5c** by ORTEP.

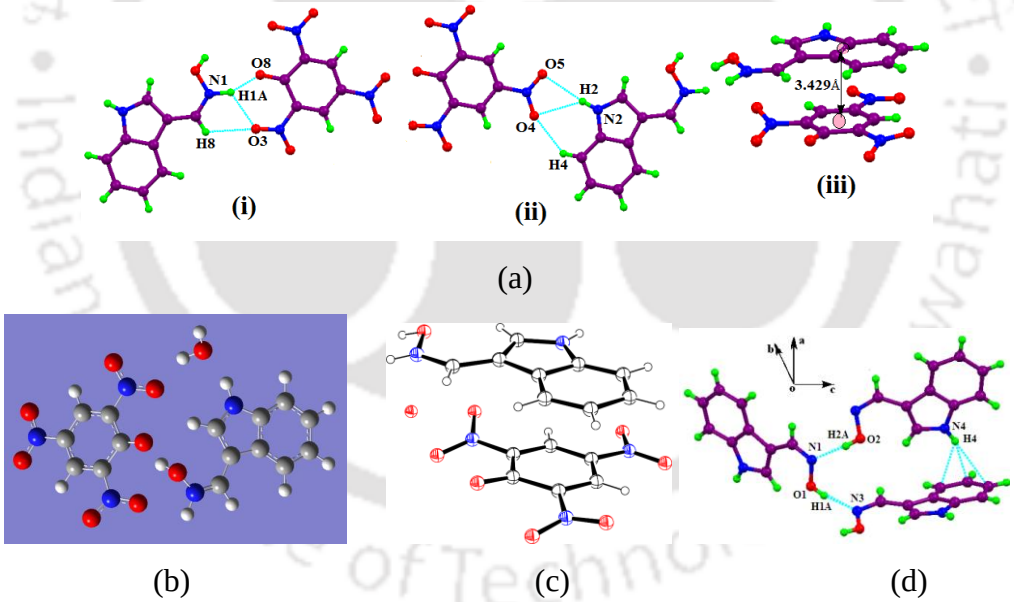

Figure 6.5: (a) Weak interactions in the hydrated picrate salt **6.2** of indole-3-carbaldoxime and charge-transfer interaction in this salt, (b) Optimized structure of the hydrated picrate salt **6.2** by DFT using B3LYP function at 6-31+G (d,p) level, (c) ORTEP diagram of picrate salt **6.2** (30% thermal ellipsoids) and (d) Trimeric sub-assemblies of indole-3-carbaldoxime.

For the comparison purpose crystal structure of indole-3-carbaldoxime was determined. The structure and the packing patterns of indole-3-carbaldoxime though is not an exceptional, but it has certain interesting features. The structure of indole-3-carbaldoxime shown in **Fig. 6.5d** has trimeric sub-assemblies formed by O-$H_{(oxime)}$···$N_{(oxime)}$ and N-H···π interactions. The N-

H···π interactions are often observed in self-assemblies of indole derivatives.[50] Comparison of the structure of the parent compound *ico* with protonated indole-3-carbaldoxime of hydrated picrate salt **6.2** showed a major difference in weak interaction schemes. In the latter case there are no oxime···oxime and N-H···π interactions. This could be attributed to strong electrostatically guided hydrogen bonds are influencing the packing patterns and disaffiliating the homeric interactions between oxime groups.

The other two picrate salts namely picrate salt **6.3** of quinoline-4-carbaloxime and picrate salt **6.4** of pyridine 4-carbaloxime; each gets protonation at nitrogen atom of the respective heterocycle. The picrate salt **6.3** of quinoline-4-carbaldoxime is a salt in hydrated form. In this particular case the self-assembly can be represented by two alternative ways. To describe the repeat sub-assemblies of hydrated picrate salt **6.3** of quinoline-4-carbaloxime one may focus the homodimeric parts in the either starting from the oxime or picrate units.

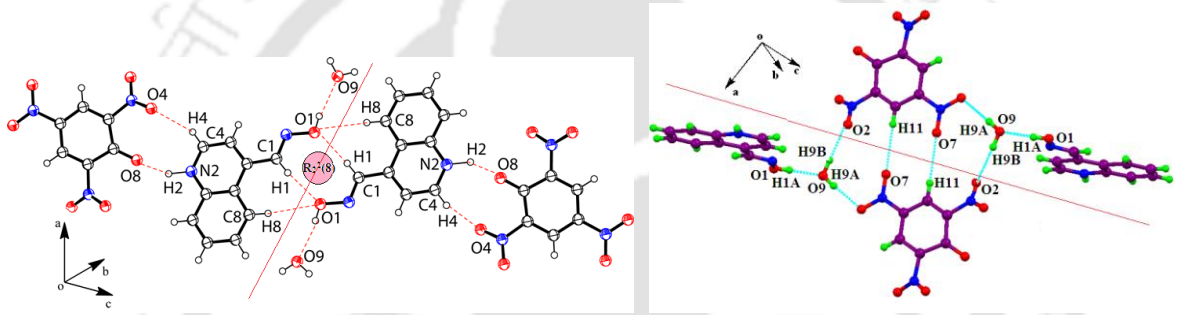

(a) (b)

Figure 6.6: Two different representations of the packing pattern of hydrated picrate salt **6.3** of quinoline-4-carbaloximeby domain expanded sub-assemblies built on homodimers of (a) oximes and (b) picrate (red line showing two symmetric halves).

Thus focusing on the oxime part, the packing pattern of picrate salt **6.3** may be described as built with hydrogen bonded homodimers of oxime with $R_2^2(8)$ graph set description. In such description each dimer holds two anions at two ends (**Fig. 6.6a**). Such sub-assemblies are formed through C-H···O hydrogen bonds (**Fig. 6.6a**). Overall the homodimers of oxime are also held by $^{+}$N-H···$O_{(phenolate)}$ and C-H···$O_{(nitro)}$ hydrogen bonds with two picrate anions located at two sides. The same self-assembly may be alternatively described as build-up of homodimers of picrates anion each holding two water molecules at two sides and which are also further linked two oxime molecules as illustrated in **Fig. 6.6b**. This is a case of domain expansion of the homodimers formed by interactions of picrates through water and oxime molecules.[44] Hence, both these descriptions as replica of self-assembly are possible. But, a mirror plane bisecting the three components of these assemblies as shown by red lines in the **Fig. 6.6** suggest that the primary interactions between the three components are different in

each case, former description has ionic hydrogen bonds which have higher strengths over the other hydrogen bonds, hence the sub-assembly based on oxime homodimers should be more appropriate to describe. Structure of salt **6.4** is shown in **Fig. 6.7a** by ORTEP diagram. Self-assembly of picrate salt **6.4** of pyridine-4-carbaldoxime has also oxime homodimers but these homodimers are different from those observed in the similar picrate salt **6.3** of quinoline-4-carbaldoxime. The homodimers of picrate salt **6.4** of pyridine-4-carbaloxime are formed by O-H···N hydrogen bonds (**Fig. 6.7b**) whereas the homodimers of oximes in picrate salt **6.3** of quinoline-4-carbaloxime are formed by C-H···O bonds.

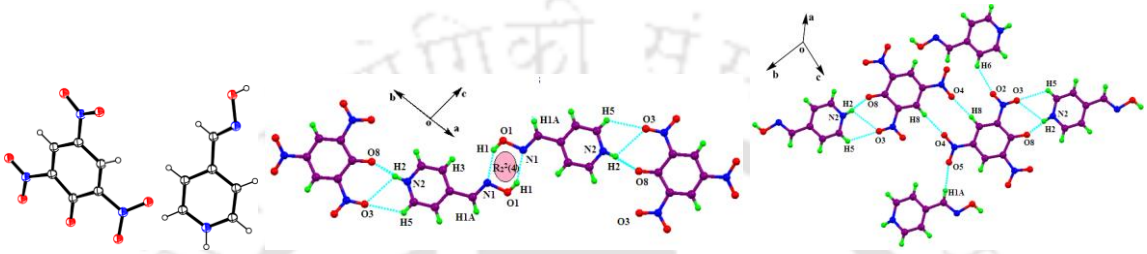

(a) (b) (c)

Figure 6.7: (a) ORTEP diagram of picrate salt **6.4** (with 30% thermal ellipsoids), (b) Homodimer of oximes pyridinium-4-carbaloxime holding two picrate anions by N-H···O interactions and (c) Homodimers of picrates that are flanked by four pyridinium-4-carbaloxime in picrate salt **6.4** of pyridine 4-carbaloxime.

Alternative description of this self-assembly can be presented as a sub-assembly comprising of picrate homodimers attached to four neighbouring pyridine-4-carbaloxime cations (**Fig. 6.7c**). The homodimers of these oximes of this salt have N-H···O interactions but there are also C-H···O interactions in picrate salt **6.3** of quinoline-4-carbaloxime. Thus a description based on homodimers of oximes in the case of picrate salt **6.4** of pyridine-4-carbaloxime is more appropriate. Though, these two salts are guided by ionic $^{+}$N-H···O bond, the $d_{N^{+}\cdots O}$ distances are 2.718(3) Å and 2.630(6) Å with respective ∠D-H···A are 170(3)° and 172(10)° respectively (**Table-6.2**). For hydrogen bonds and short contacts parameters of salts **6.1-6.4** and indole-3-carbaloxime please see **Table 6.2** and page 231-232 of appendix. Literature suggest that the N-H···O bonds having mean $d_{N^{+}\cdots O}$ distance 2.74(4) Å with ∠D-H···A up to 179° belong to category of strong hydrogen bonds.[51a] Pyridoxal oxime derivatives has shown interesting supramolecular architecture in their self-assemblies.[51b] The self-assemblies of pyridoxal oxime derivative 1,2-diaryl(3-pyridyl)ethanone has revealed chain and layer like structures.[51c] These results not only establish that changing pyridine unit by quinoline as substituent of the oxime, the oxime synthon adopts a suitable complementing hydrogen bonded synthon from two possibilities illustrated in **Fig. 6.3** (e and f).

The filler water molecules are present in the hydrophobic pockets of picrate salt **6.3.** These water molecules form hydrogen bonds with hydroxy-group of the oximes. Hence, this self-assembly of the salt adopts a homodimer different than the one in the picrate salt **6.4** of pyridine-oxime case.

Table 6.2: Prominent hydrogen bond parameters of salts **6.1-6.4** and indole-3-carbaldoxime

Salts/oxime	D-H…A	d_{D-H} (Å)	$d_{H...A}$ (Å)	$d_{D...A}$ (Å)	∠D-H…A (°)
Salt **6.3**	O(1)-H(1A)…O(9) [-x,-y,-z]	0.82(4)	1.81(3)	2.632(4)	176(4)
	N(2)-H(2)…O(4) [1/2-x,1/2+y,1/2-z]	0.90(3)	2.50(4)	2.962(4)	113(3)
	N(2)-H(2)…O(8) [1/2-x,1/2+y,1/2-z]	0.90(3)	1.83(3)	2.718(3)	170(3)
	O(9)-H(9A) … O(6) [1-x,2-y,-z]	0.87(5)	2.06(5)	2.923(4)	176(3)
	O(9)-H(9B)…O(2) [x,-1+y,z]	0.86(3)	2.01(3)	2.858(4)	172(3)
Salt **6.4**	O(1)-H(1)…N(1) [1-x,2-y,-z]	0.82(6)	2.12(4)	2.843(6)	146(6)
	N(2)-H(2)…O(3) [1+x,y,z]	0.87(7)	2.57(9)	3.020(6)	114(7)
	N(2)-H(2)…O(8) [1+x,y,z]	0.87(7)	1.77(7)	2.630(6)	172(10)
Salt **6.1**	O(1)-H(1A)…O(5) [2-x,-y,1-z]	0.82(3)	2.08(4)	2.896(2)	171(4)
	N(2)-H(2)…O(2) [1-x,1-y,-z]	0.94(2)	1.82(2)	2.738(2)	165(2)
	N(2)-H(2)…O(3) [1-x,1-y,-z]	0.94(2)	2.55(2)	3.066(3)	114(15)
Indole-3-carbaldoxime	O(1)-H(1A)…N(3) [1-x,1-y,1/2+z]	0.82(4)	2.02(4)	2.824(2)	166(5)
	N(2)-H(2)…O(2) [1+x,y,z]	0.88(2)	2.39(2)	3.227(3)	159.(19)
	O(2)-H(2A)…N(1) [1/2-x,-1/2+y,-1/2+z]	0.82(2)	1.94(4)	2.759(2)	172(4)
Salt **6.2**	N(1)-H(1A)…O(3) [1-x,1-y,-z]	0.94(6)	2.24(7)	2.888(5)	125(5)
	N(1)-H(1A)…O(8) [1-x,1-y,-z]	0.94(6)	1.83(6)	2.705(6)	153(6)

These structural analysis have suggested the following points: (a) The nitrogen atom acting as donor or acceptor for hydrogen atom makes difference in self-assembly which in conjunction with electron delocalisation can enforce stabilisation of species protonated at nitrogen atom of the oxime functional group. (b) The homodimeric assembly of oximes of closely related systems vary due to the filler water molecules which hydrogen bonds to oxime. (c) The oximes having quinoline and pyridine unit are good examples to illustrate need of alternative sub-assemblies within their respective self-assemblies. The self-assemblies may be either described to be constructed as built up on picrate homodimers that are connected to oximes or oxime homodimers connected to picrates. (d) Domain expansion observed in these examples is conceptually very important as repeat sub-assemblies are the final replica to decide any solid state or solution properties involving aggregates.

6.4: FT-IR, Thermal and Hirschfeld surface analysis on picrate salts 6.1-6.4 and oxime derivatives

FT-IR spectra of 4-(N,N-dimethylaminophenyl)aldoxime has characteristic C=N bond stretching at 1608 cm^{-1} which is shifted to 1631 cm^{-1} in the picrate salt **6.1**. This shift to higher side by 13 cm^{-1} between the two forms is due to loss of conjugation of the oxime group upon protonation of the dimethylphenylamine group. On protonation the lone pair on the nitrogen of the -NMe_2 group is not available to be in conjugation with the π-electrons of

the ring. On the other hand, in the indole-3-carbaldoxime the C=N stretching is observed at 1684 cm^{-1}, but in the picrate salt **6.2** this stretching is observed to 1640 cm^{-1}. This suggests that the double bond character is less in this salt than the parent compound. All the picrate salts show stretching in the region of 1342-1280 cm^{-1} due to -NO_2 groups (**Fig. 6.18**). Raman spectra of oximes (**Fig. 6.19**) and picrate salts have bands in the regions 3085-3061 cm^{-1} and 1325-1200 cm^{-1} due to O-H and -NO_2 groups. The assignments are based on comparison of Raman spectra of oxime derivatives[52] and picrate salt of L-nitroarginine[52d] that was earlier used to assign structures.

Thermal properties of picrate salts **6.1-6.4** and oxime derivatives were carried out by differential scanning calorimetry (DSC) studies. As we known that nitroaromatics are high-energy molecules and their explosive properties are modified through adduct formation.[43] DSC plots for two oximes, their corresponding picrate salts and picric acid are shown in **Fig. 6.8** and melting points of the picrate salts and parent compounds are listed in **Table 6.3**. Quinoline-4-carbaldoxime, 4-(N,N-dimethylaminophenyl)aldoxime and picric acid show sharp endothermic peaks at 180 ºC, 147 ºC and 122 ºC respectively due to melting. Hydrated picrate salt **6.3** of quinoline-4-carbaloxime showed endothermic peaks at 82-123 ºC and 199 ºC. These peaks are followed by a broad exothermic peak at 220 °C. This peak is due to exothermic degradation of the compound; in second cycle of heating no such peak is observed; neither cooling in first or second cycle has shown recrystallization. Broad endothermic peak in observed first cycle of heating at 82-123 ºC is due to dehydration. Sharp peak at 199 ºC corresponds to melting followed by decomposition (ii of **Fig. 6.8a**).

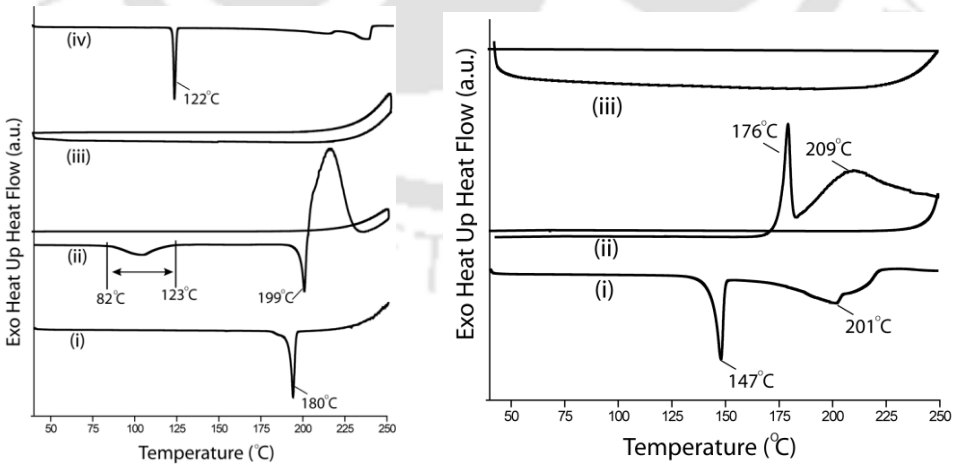

(a) (b)

Figure 6.8: DSC plots of (i) Quinoline-4-carbaldoxime, (ii) hydrated picrate salt **6.3** of quinoline-4-carbaloxime, (iii) second cycle of heating of this salt and (iv) Picric acid in (a); and (i) 4-(N,N-dimethylaminophenyl)aldoxime, (ii) picrate salt **6.1** of 4-(N,N-dimethylaminophenyl)aldoxime and (iii) second cycle of heating of this salt in (b).

Due to exothermic process relates explosive nature and hence due care must be taken while dealing with such substance such salt while heating. Similar DSC plot was observed for picrate salt **6.4** of pyridine-4-carbaloxime (**Fig. 6.20**) and hydrated picrate salt **6.2** of indole-3-carbaldoxime (**Fig. 6.21**). But in the case of picrate salt **6.1** of 4-(N,N-dimethylaminophenyl)aldoxime two broad exothermic peaks at 176 ºC and 209 ºC were observed (ii of **Fig. 6.8b**). Two broad exothermic peaks are assigned to melt extrusion. DSC plots in all the cases except salt **6.3** of quinoline-4-carbaldoxime showed exothermic processes while melting. Exothermic peaks of picrate salt **6.3** of quinoline-4-carbaldoxime at two temperatures are attributed to phase change followed by exothermic decomposition. However, due to exothermic nature we have not done extensive variations in heating conditions and the explanation is qualitative.

Table 6.3: Melting and decomposition temperature of the oximes and picrate salts **6.1-6.4**.

Compound	*qco*	*pco*	*dmo*	*ico*	Picric acid	Picrate salts			
						6.3	**6.4**	**6.1**	**6.2**
Melting point (°C)	180	134	147	192	122	199	125	176	147
Decomposition Temperature (°C)	>250	207	201	>250	>250	>225	208	209	> 250

Melting points of cocrystals of 4-nitrophenol with aza-compounds depend on packing efficiency, crystal density, number of strong hydrogen bonds.[53] Hirshfeld surface[54] analysis of different picrate salts (**Fig. 6.22**) has showed that O···H interactions predominates in all the salts (**Table 6.4** and **Fig. 6.9**). Hirsfeld analysis on extent of different weak interactions have suggested that two hydrated salts; hydrated picrate salt **6.3** of quinoline-4-carbaloxime and hydrated picrate salt **6.2** of indole-3-carbaldoxime have comparable percentages of interactions involving O-H (38.1% and 39.9%),

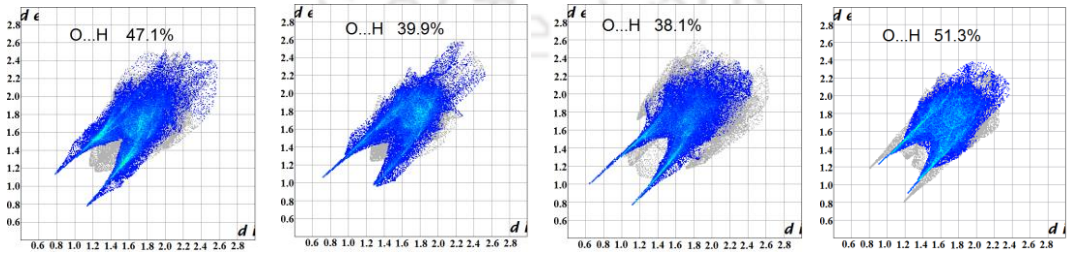

(a) (b) (c) (d)

Figure 6.9: Fingerprint plots for picrate salts (a) **6.1**, (b) **6.2**, (c) **6.3** and (e) **6.4** with O···H interactions highlighted in colour.

which are relatively less than the percentages O-H interaction in picrate salt **6.4** of pyridine-4-carbaloxime (51.3%) and picrate salt **6.1** of 4-(N,N-dimethylaminophenyl) aldoxime (47.1%). Nevertheless, these interactions predominate in the respective self-assembly and causing melting temperature to deviate from the parent oxime. In the three cases where heterocycles were protonated had melting points at higher temperature than the parent compound, but due to unusual protonation of oxime in indole-3-carbaldoxime, corresponding picrate salt melted at 147 ºC has lower melting than the parent oxime at 192ºC.

6.5: Solid state UV-visible, Fluorescence and ^{1}H NMR studies

Weak interactions contribute to various optical and electrical properties like aggregation induced emission,[54] proton conductivities.[55] We also examined optical properties of the picrate salts **6.1-6.4**. Solid samples of the three picrate salts **6.1**, **6.3** and **6.4** are light yellow (inset i-iii of **Fig. 6.10**) absorbs in the region 381-468 nm and the absorptions are due to picrate anion (**Fig. 6.10**).

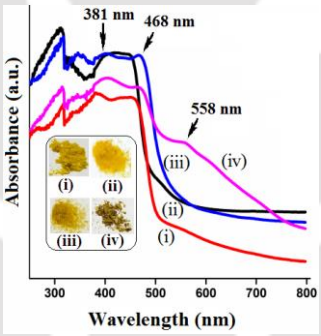

Figure 6.10: Solid-state UV-visible spectra of picrate salts (i) **6.3**, (ii) **6.4**, (iii) **6.1** and (iv) **6.2**. Colour of corresponding picrate salts are shown in inset.

Exceptionally, a brownish-yellow coloured (inset iv of **Fig. 6.10**) salt hydrated picrate salt **6.2** of indole-3-carbaldoxime has a new peak at 558 nm in addition to the picrate peaks. This new absorption is due to strong charge-transfer interactions. Solid-state UV-visible spectra of oxime derivatives and picric acid are shown in **Fig. 6.23**. The absorptions of the picrate salts are independent of the absorptions of the parent components.

Solid powdered samples of the picrate salts show insignificant fluorescence emissions. However, picric acid is well known to cause fluorescence quenching of fluorophores.[32] Fluorescence emission of *qco*, *pco*, *dmo* and *ico* in acetonitrile were observed at 408 nm, 384 nm, 380 nm and 383 nm on excitation at 347 nm, 312 nm, 349 nm and 324 nm respectively (Fluorescence excitation spectra's are given in **Fig. 6.24**). These fluorescence emissions peaks are quenched upon addition of picric acid. Similar results were found upon addition of 2,4-dinitrophenol or 4-nitrophenol (**Fig. 6.25-6.28**). Fluorescence emission of pyridine-4-

carbaldoxime is plotted against concentrations of different nitro compounds (**Fig. 6.11a**). Percentages of quenching are shown in bar graph in **Fig. 6.11b**. It shows that picric acid cause highest quenching among the others.

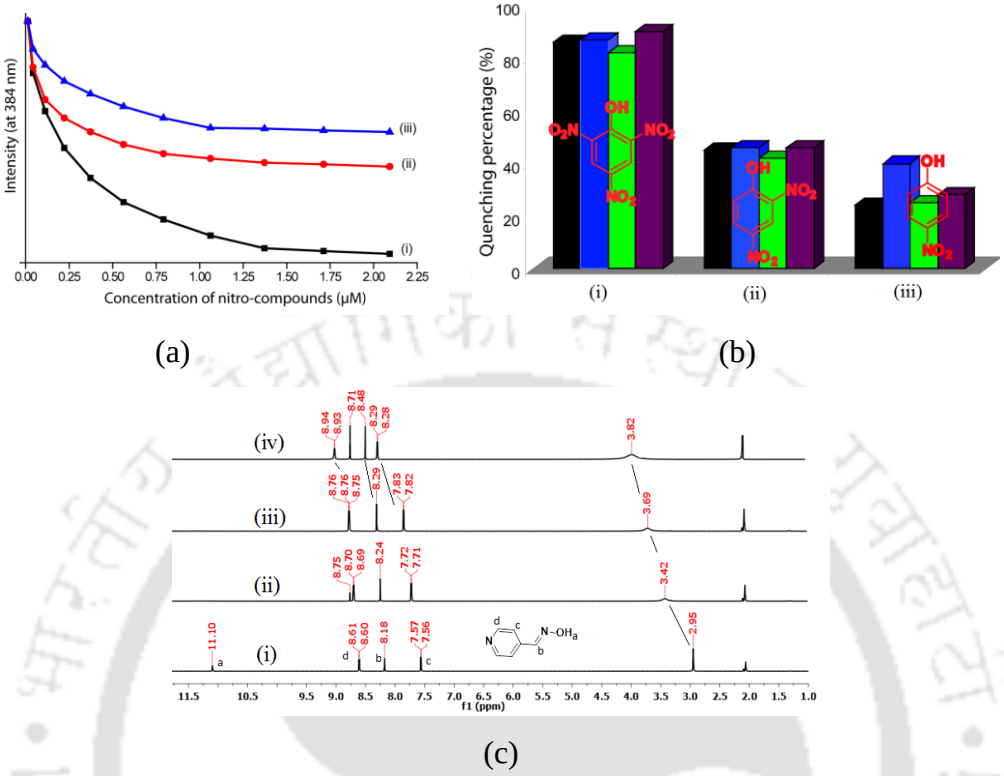

Figure 6.11: (a) Plots of changes fluorescence intensity at 384 nm of pyridine-4-carbaldoxime at different concentrations of different nitro compounds; (b) Relative fluorescence quenching of indole-3-carbaldoxime (black bar), quinoline-4-carbaldoxime (blue bar), pyridine-4-carbaldoxime (green bar) and 4-(N,N-dimethylaminophenyl)aldoxime (brown bar) with (i) picric acid, (ii) 2,4-dinitrophenol and (iii) 4-nitrophenol. (c) ^{1}H NMR (600 MHz, Acetone-d_6) titration of pyridine-4-carbaldoxime with (i) 0, (ii) 0.25, (iii) 0.50 and (iv) 1 mole equivalent of picric acid.

Generally for an electron transfer from the excited state to electron deficient picric acid molecule causes fluorescence quenching.[57] Density functional theory with B3LYP functionals 6-31++G (d,p) level in gas-phase of oxime derivatives and picric acid showed that LUMO energy of all oxime derivatives are in the range -2.351 eV to -1.035 eV (**Fig. 6.29**). These energy values are much higher compared to energy of HOMO of picric acid (-4.52 eV). Hence, picrate causes fluorescence quenching due to efficient protonation of the nitrogen at remote site of oximes. Relative charge-transfer at excited state is dependent on electron accepting ability of nitro-phenols and this is in fact reflected in quenching ability of the nitro-phenols in solution picric acid > 2,4-dintrophenol > 4-nitrophenol.

^{1}H NMR titration of pyridine-4-carbaldoxime with picric acid below stoichiomentric amount of picric acid showed gradual shift in the proton labeled as *c* towards low-field and it shifts from 7.56 ppm to 8.28 ppm (**Fig. 6.11c**). Similarly the peak *d* observed for the oxime at 8.60 ppm also shifts to 8.93 ppm. Chemical shit position of the =CH proton is not affected in lower concentrations of picric acid but gets de-shielded by shifting from 8.18 ppm as found in picric acid to 8.48 ppm when picric acid is in equivalent amount with respect to the oxime. The O-H peak at 2.95 ppm moves downfield to show higher chemical shift value and it gets broadened. The broadening is due to rapid exchange of it with proton of picric acid in solution. These solution studies indicate that intrinsic acidity of nitro-phenols to generate protonated species which inhibits the excited state proton transfer from oxime to heterocyclic fluorophore. Unavailability of suitable site for intermolecular proton transfer to heterocycle from oxime excited sate proton transfer that were seen with parent oxime is hindered, hence the quenching takes place upon interaction with nitrophenols.[58]

6.6: Conclusions

This study has established (a) an example of a stable protonated oxime species, (b) different substrate homodimers of oximes causing synthon variations, (c) charge-transfer interactions and (d) domain expansion of synthons forming new sub-assemblies in different picrate salts of heterocycle based oximes. The difference in oxime synthons in the salts of pyridine oxime and quinoline oxime suggests that the role of aquation in a compound has to be accounted for while predicting synthons. Hence, a prior knowledge of the structure and composition is essential. Charge-transfer π-stacks have a nominal role in the self-assemblies of these salts other than the salt of indole containing oxime. π-Type charge-transfer interactions of the salt of indole-3-carbaldoxime with picric acid provide distinct visible absorption. Fluorescence quenching of these oxime derivatives is caused by picric acid due to the protonation of the good hydrogen bond acceptors at the remote site linked to the fluorophore. The magnitude of fluorescence quenching by nitro-phenols differs due to the intrinsic acidity associated with them. The melting points of the picrate salts, where the nitrogen heterocycles are proton acceptors, were higher than those of the parent oxime, whereas in the case of the picrate salt of indole-3-carbaldoxime, it melted at a much lower temperature than the parent oxime. The exothermic changes observed in these salts near the melting temperature suggest the high energy transformation above the melting points of the salts. Finally, we make a general summary from these results that (a) synthon prediction for supramolecular assemblies requires extensive knowledge of synthon competition but such information may also not be

enough. Hydration or kinetic product formation may not involve an ordinarily predictable synthon. We have provided examples of changes in the oxime synthon by moving from the picrate salt of pyridine oxime to the quinoline oxime. (b) The domain expansion of sub-assemblies requires attention, as the domains of repeat sub-assemblies are the deciding factors to understand the ultimate properties of a self-assembly. (c) The contribution from the ground state in fluorescence emission quenching does not implicate a real picture when there is scope to modify the excited states with partner molecules/ions.

6.7: Experimental section

Note of caution: Nitrophenols and their cocrystals and salts are potentially explosive; hence experiments performed in the solid state must be done under a hood or with a minimum quantity in a hood covered with an explosive damage preventive cover so as to avoid any hazard.

Synthesis and characterization of oxime derivatives and picrate salts 6.1-6.4:

Quinoline-4-carbaldoxime, pyridine-4-carbaldoxime, indole-3-carbaldoxime and 4-(N,N-dimethylaminophenyl)aldoxime were prepared by reacting hydroxylamine hydrochloride with respective oxime in a procedure followed earlier.[46] Salts of oximes with picric acid were prepared by equimolar amount of corresponding (1mmol) oximes with picric acid (1.1mmol) in methanol (25 ml). Such solutions on slow evaporation yielded the respective salt.

Indole-3-carbaldoxime (*ico*): Isolated yield: 83%.^{1}H NMR (600 MHz, Acetone-d_6): 10.77 (s, -OH), 10.41 (s, -NH), 8.37 (s, 1H), 7.86 (d, J = 6 Hz, 1H), 7.76 (s, 1H), 7.49 (d, J = 6 Hz, 1H), 7.20 (t, J = 6 Hz, 1H), 7.15 (t, J = 6 Hz, 1H). IR (KBr, cm^{-1}): 3387 (br, s), 3156 (w), 3013 (w), 1679 (w), 1640 (s), 1612 (w), 1521 (s), 1489 (m), 1458 (s), 1414 (s), 1340 (s), 1234 (s), 1130 (m), 1098 (s), 1048 (w), 1008 (w), 930 (s), 905 (m), 866 (m), 840 (m), 747 (s), 659 (m), 612 (w), 588 (m) 551 (s). ESI mass: calcd. 161.0715 [M + H^{+}]; found 161.0712 [M + H^{+}].

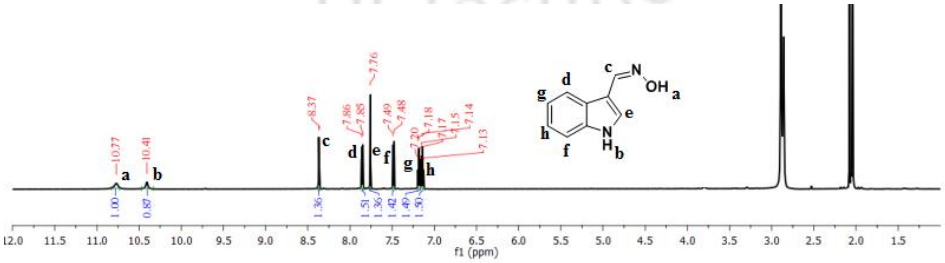

Figure 6.12: ^{1}H NMR (600 MHz, Acetone-d_6) spectra of indole-3-carbaldoxime.

4-(N,N-dimethylaminophenyl)aldoxime (*dmo*): Isolated yield: 80%.^{1}H NMR (600 MHz, Acetone-d_6): 9.84 (s, 1H), 7.97 (s, 1H), 7.43 (d, J = 6 Hz, 2H), 6.72 (d, J = 8 Hz, 2H), 2.09 (-CH_3). IR (KBr, cm^{-1}): 3243 (br, w), 2914 (w), 1608 (s), 1556 (s), 1526 (s), 1565 (w), 1477 (w), 1444 (w), 1427 (w), 1361 (s), 1301 (s), 1224 (s), 1185 (m), 1169 (m), 1126 (s), 1065 (m), 1002 (m), 956 (s), 867 (s), 812 (s), 734 (s), 635 (w), 570 (s), 528 (s). ESI mass: calcd. 165.1028 [M + H^+]; found 165.1020 [M + H^+].

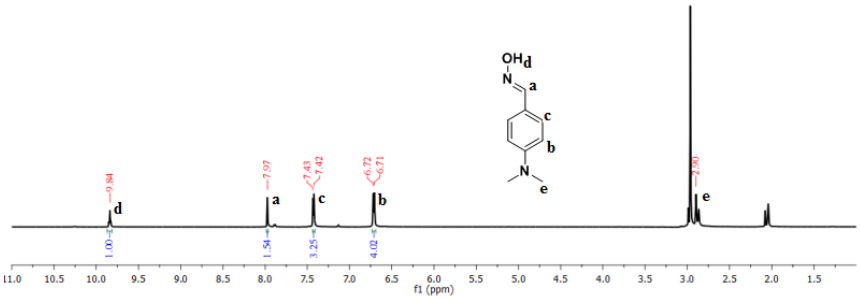

Figure 6.13: ^{1}H NMR (600 MHz, Acetone-d_6) spectra of 4-(N,N-dimethylaminophenyl) aldoxime.

Picrate salt **6.1** of 4-(N,N-dimethylaminophenyl)aldoxime**:** Isolated yield: 52%. ^{1}H NMR (600 MHz, Acetone-d_6): 8.89 (s, 2H), 8.05 (s, 1H), 7.57 (d, J = 12 Hz, 2H), 7.12 (d, J = 6 Hz, 2H), 3.14 (s, 6H). IR (KBr, cm^{-1}): 3416 (br, s), 3088 (w), 2987 (w), 1631 (s), 1591 (w), 1564 (s), 1514 (w), 1480 (m), 1462 (m), 1435 (s), 1365 (s), 1335 (s), 1313 (w), 1280 (s), 1194 (m), 1184 (w), 1162 (s), 1127 (s), 1077 (s), 1057 (w), 988 (w), 968 (s), 947(w), 922 (m), 875 (w), 851 (s), 788 (s), 745 (s), 711 (s), 635 (w), 595 (w).

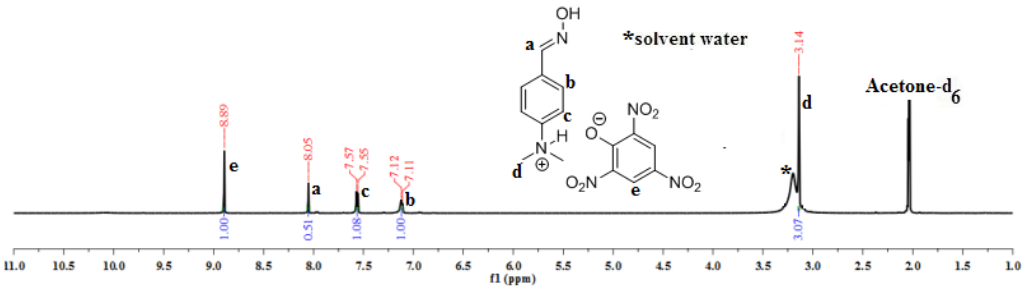

Figure 6.14: ^{1}H NMR (600 MHz, Acetone-d_6) spectra of picrate salt **6.1**.

Hydrated picrate salt **6.2** of indole-3-carbaldoxime: Isolated yield: 53%.^{1}H NMR (600 MHz, Acetone-d_6): 11.03 (s, -OH), 10.54 (s, -NH), 9.11 (s, 4H), 8.47 (s, 1H), 8.31 (s, 1H), 8.10 (d, J = 12 Hz, 1H), 7.99 (s, 1H), 7.90 (d, J = 6 Hz, 1H), 7.60 (s, 1H), 7.53 (d, J = 6Hz, 1H), 7.44 (d, J = 12 Hz, 1H), 7.24 (t, J = 6Hz, 1H), 7.20 (m, 2H), 7.10 (t, J = 6 Hz, 1H). IR (KBr, cm^{-1}): 3338 (br, s), 3149 (m), 3081 (w), 1684 (m), 1631 (w), 1610 (w), 1565 (w), 1521 (w), 1492

(w), 1459 (w), 1419 (s), 1362 (s), 1337 (w), 1315 (w), 1270 (m), 1240 (w), 1159 (w), 1138 (w), 1079 (s), 1006 (w), 910 (m), 788 (m), 749 (s), 713 (s), 669 (w), 612 (s), 558 (w).

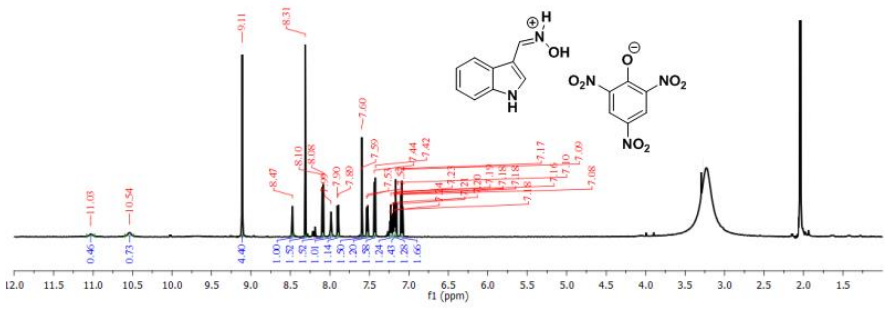

Figure 6.15: ^{1}H NMR (600 MHz, Acetone-d_6) spectra of picrate salt **6.2**.

Hydrated picrate salt **6.3** of quinoline-4-carbaldoxime**:** Isolated yield: 64%. ^{1}H NMR (400 MHz, DMSO-d_6): 12.61 (s, 1H), 9.15 (d, J = 4 Hz, 1H), 9.04 (s, 1H), 8.80 (d, J = 8 Hz, 1H), 8.58 (s, 2H), 8.21 (d, J = 12 Hz, 1H), 8.10 (d, J = 4 Hz, 1H), 8.06 (t, J = 8 Hz, 1H), 7.90 (t, J = 8 Hz, 1H). IR (KBr, cm^{-1}): 3494 (br, s), 3112 (w), 1634 (m), 1613 (s), 1566 (S), 1549 (s), 1485 (s), 1454 (m), 1429 (s), 1366 (s), 1343 (m), 1323 (s), 1277 (s), 1226 (w), 1165 (s), 1114 (s), 1084 (s), 1055 (s), 1022 (w), 1006 (s), 940 (w), 917 (m), 891 (w), 786 (s), 766 (s), 744 (s), 725 (s), 712 (s), 677 (w), 544 (w), 532 (s).

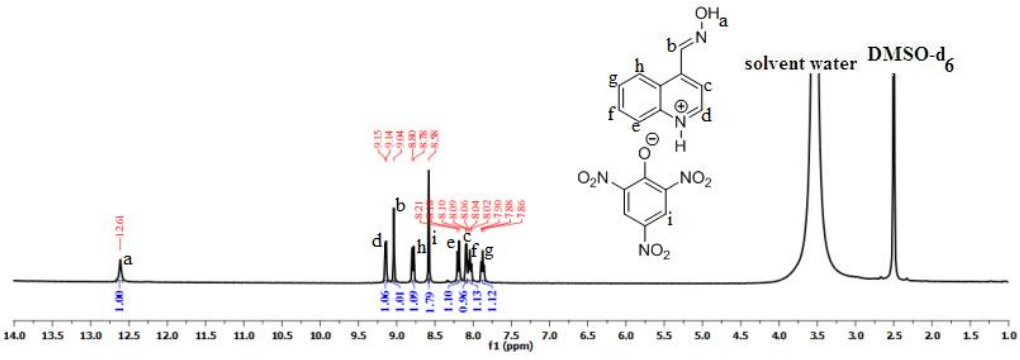

Figure 6.16: ^{1}H NMR (600 MHz, DMSO-d_6) spectra of salt (Hqco).(tnp).H_2O.

Picrate salt **6.4** of pyridine-4-carbaldoxime: Isolated yield: 55%.^{1}H NMR (600 MHz, Acetone-d_6): 11.90 (s, 1H), 8.98 (d, J = 6 Hz, 2H), 8.76 (s, 2H), 8.46 (s, 1H), 8.27 (d, J = 6 Hz, 2H). IR (KBr, cm^{-1}): 3317 (br, m), 3076 (w), 1634 (s), 1604 (w), 1558 (s), 1505 (w), 1485 (w), 1459 (w), 1429 (s), 1369 (s), 1342 (m), 1321 (w), 1276 (s), 1201 (s), 1160 (s), 1084 (s), 988 (s), 957 (w), 907 (m), 884 (s), 817 (s), 786 (m), 745 (m), 708 (s), 528 (m).

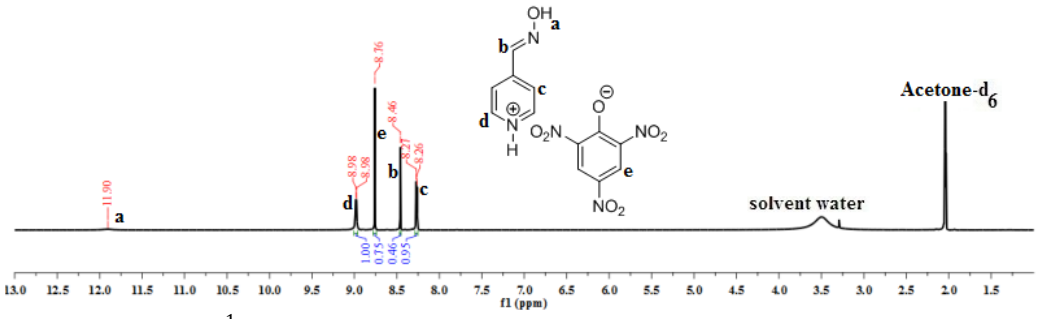

Figure 6.17: ^{1}H NMR (600 MHz, Acetone-d_6) spectra of picrate salt **6.4**.

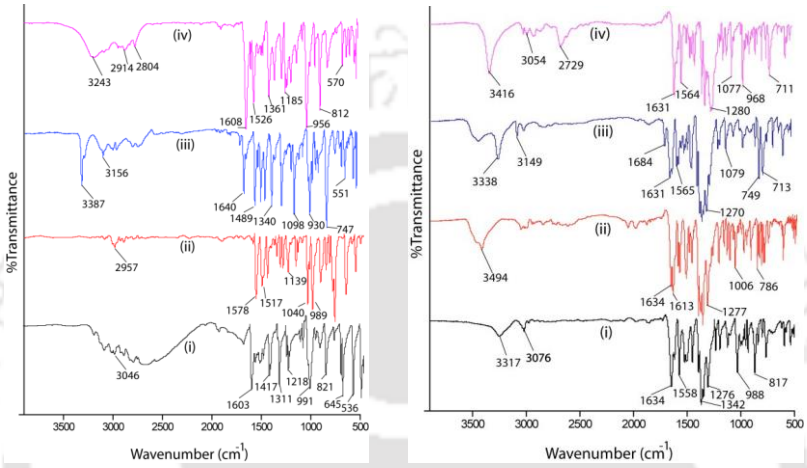

(a) (b)

Figure 6.18: FT-IR spectra of (i) pyridine-4-carbaldoxime, (ii) quinoline-4-carbaldoxime, (iii) indole-3-carbaldoxime, (iv) 4-(N,N-dimethylaminophenyl)aldoxime in (a) and picrate salts (i) **6.4**, (ii) **6.3**, (iii) **6.2** and (iv) **6.1** in (b).

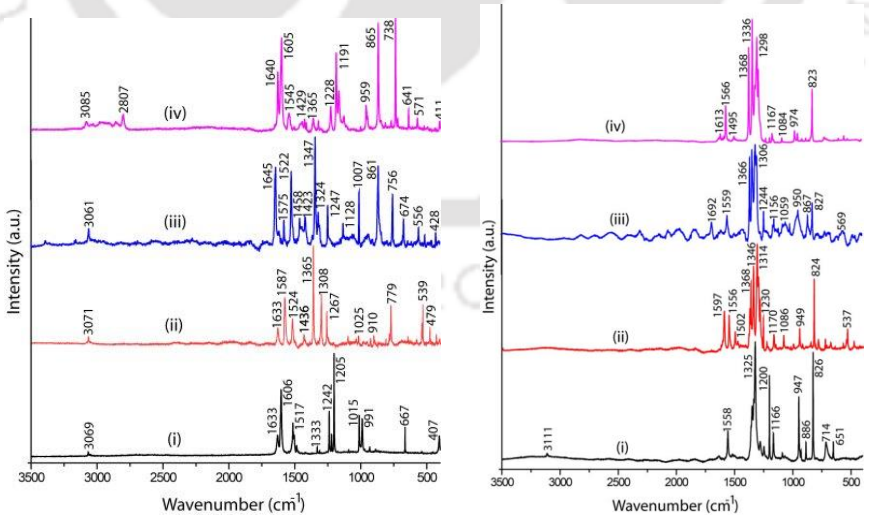

(a) (b)

Figure 6.19: Raman spectra of (i) pyridine-4-carbaldoxime, (ii) quinoline-4-carbaldoxime, (iii) indole-3-carbaldoxime, (iv) 4-(N,N-dimethylaminophenyl)aldoxime in (a) and picrate salts (i) **6.4**, (ii) **6.3**, (iii) **6.2** and (iv) **6.1** in (b).

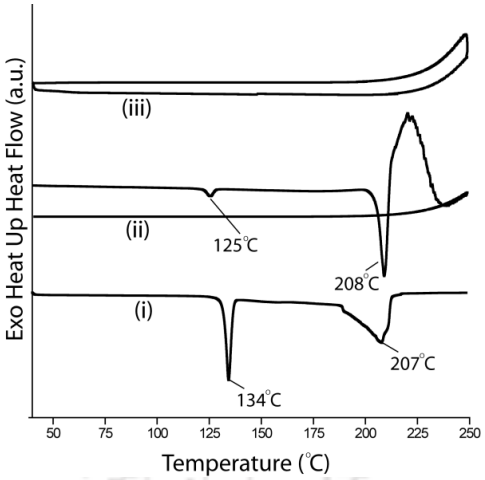

Figure 6.20: DSC plots of (i) Pyridine-4-carbaldoxime and picrate salt **6.4** with (ii) 1st cycle heating and (iii) 2nd cycle heating.

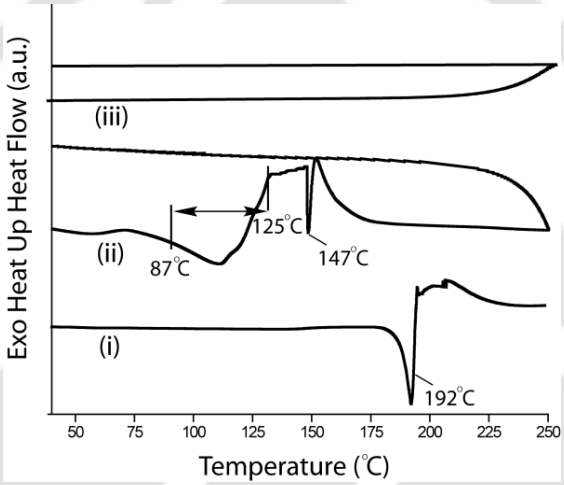

Figure 6.21: DSC plots of (i) Indole-3-carbaldoxime and hydrated picrate salt **6.2** with (ii) 1st cycle heating and (iii) 2nd cycle heating.

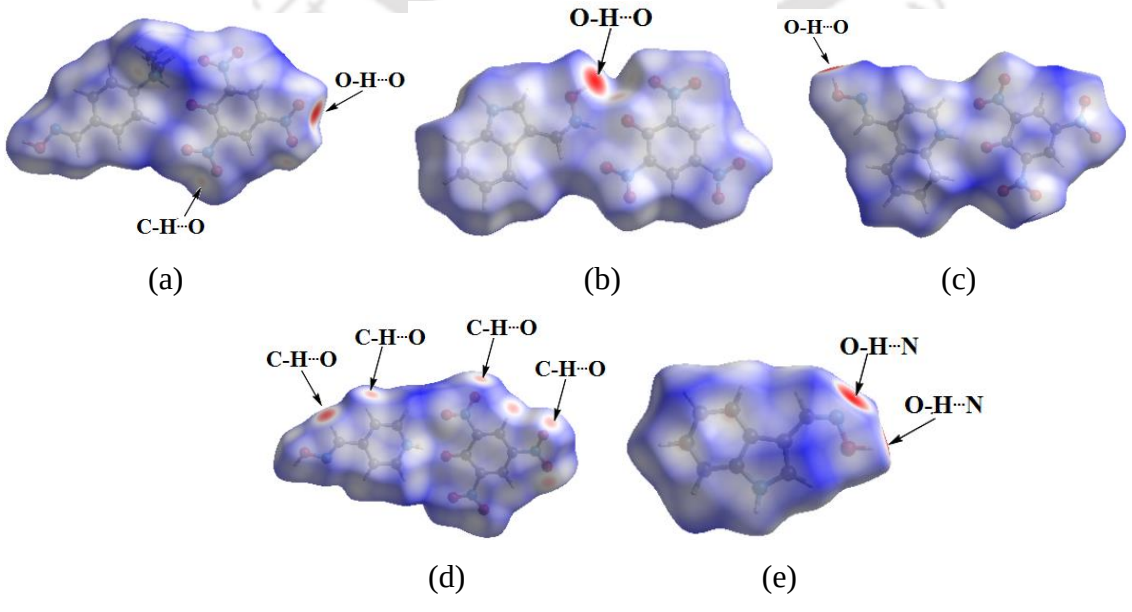

Figure 6.22: Hirshfeld surface of picrate salts (a) **6.1**, (b) **6.2**, (c) **6.3**, (d) **6.4** and (e) Indole-3-carbaldoxime.

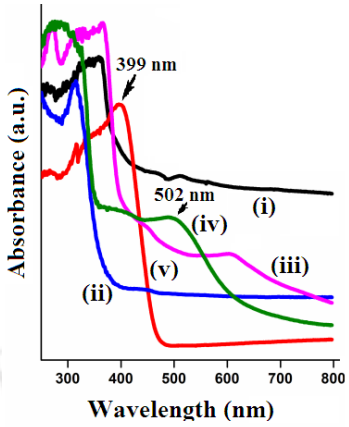

Figure 6.23: Solid-state UV-visible spectra of (i) quinoline-4-carbaldoxime, (ii) pyridine-4-carbaldoxime (iii) 4-(N,N-dimethylaminophenyl)aldoxime, (iv) indole-3-carbaldoxime and (v) picric acid.

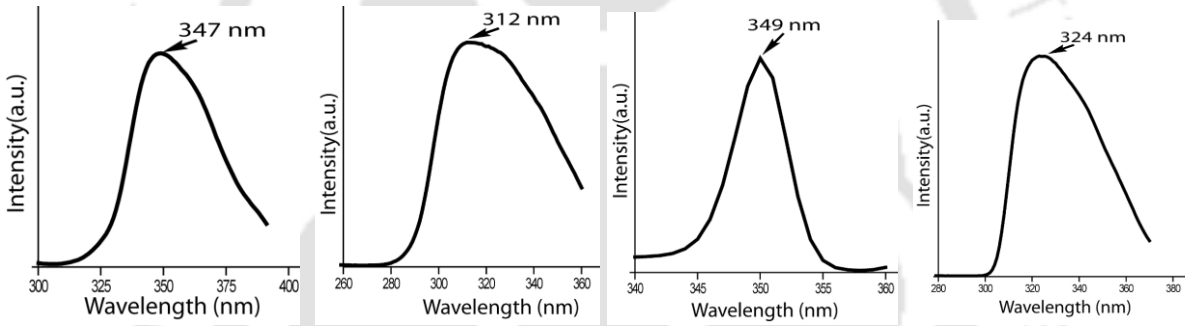

(a) (b) (c) (d)

Figure 6.24: Fluorescence excitation spectra of (a) quinoline-4-carbaldoxime, (b) pyridine-4-carbaldoxime, (c) 4-(N,N-dimethylamino)benzaldoxime and (d) Indole-4-carbaldoxime.

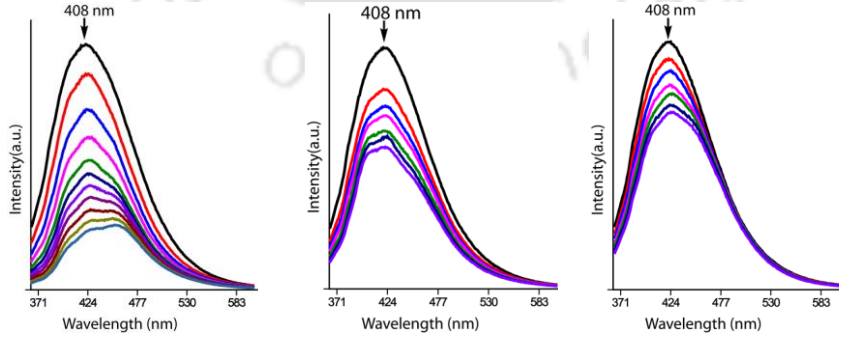

(a) (b) (c)

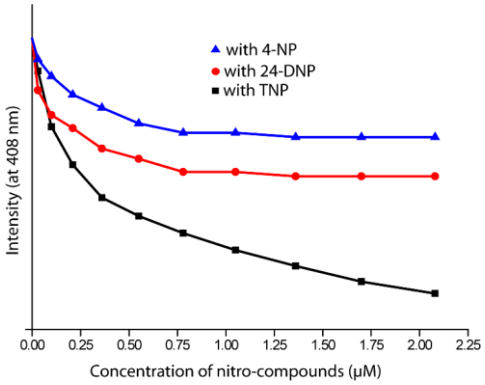

(d)

Figure 6.25: Changes in fluorescence emission of quinoline-4-carbaldoxime (10^{-4} M in acetonitrile) at 420 nm (excitation at 347 nm) upon addition (a) picric acid, (b) 2,4-dinitrophenol and (c) 4-nitrophenol (10 μl aliquots 10^{-5} M in acetonitrile in each case); (d) Plots of fluorescence intensity vs concentration with different nitro-compounds.

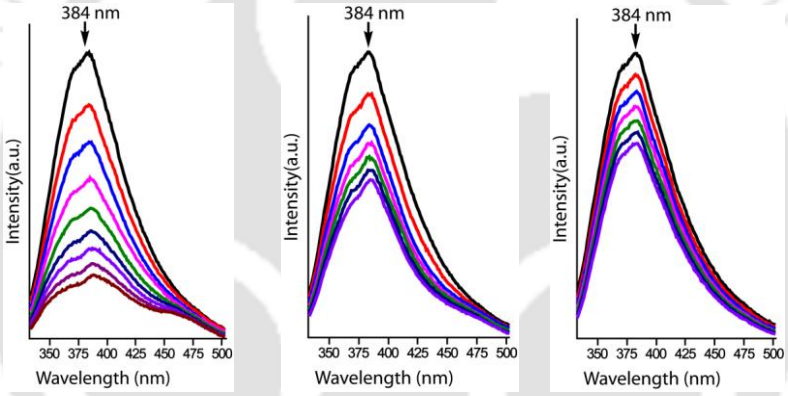

(a) (b) (c)

Figure 6.26: Changes in fluorescence emission of pyridine-4-carbaldoxime (10^{-4} M in acetonitrile) at 384 nm (λ_{em} at 312 nm) upon addition of different aliquots of (a) picric acid, (b) 2,4-dinitrophenol and (c) 4-nitrophenol (10 μl aliquots 10^{-5} M in acetonitrile in each case).

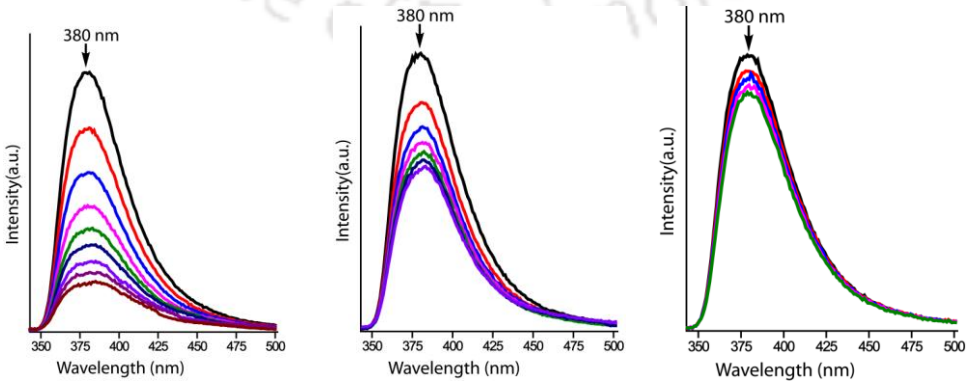

(a) (b) (c)

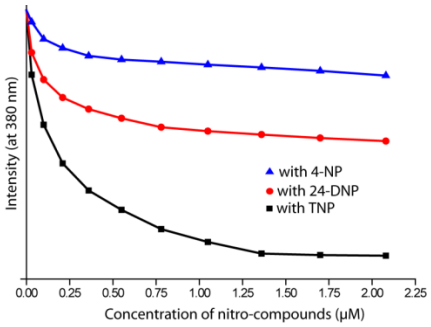

(d)

Figure 6.27: Changes in intensity of fluorescence emission at 380 nm of 4-(dimethylamino)benzaldehyde oxime (10^{-4} M in acetonitrile) (excitation at 349 nm) upon addition (a) picric acid, (b) 2,4-dinitrophenol and (c) 4-nitrophenol (10 μl aliquots 10^{-5} M in acetonitrile in each case); (d) Plots of fluorescence intensity vs concentration with different nitro-compounds.

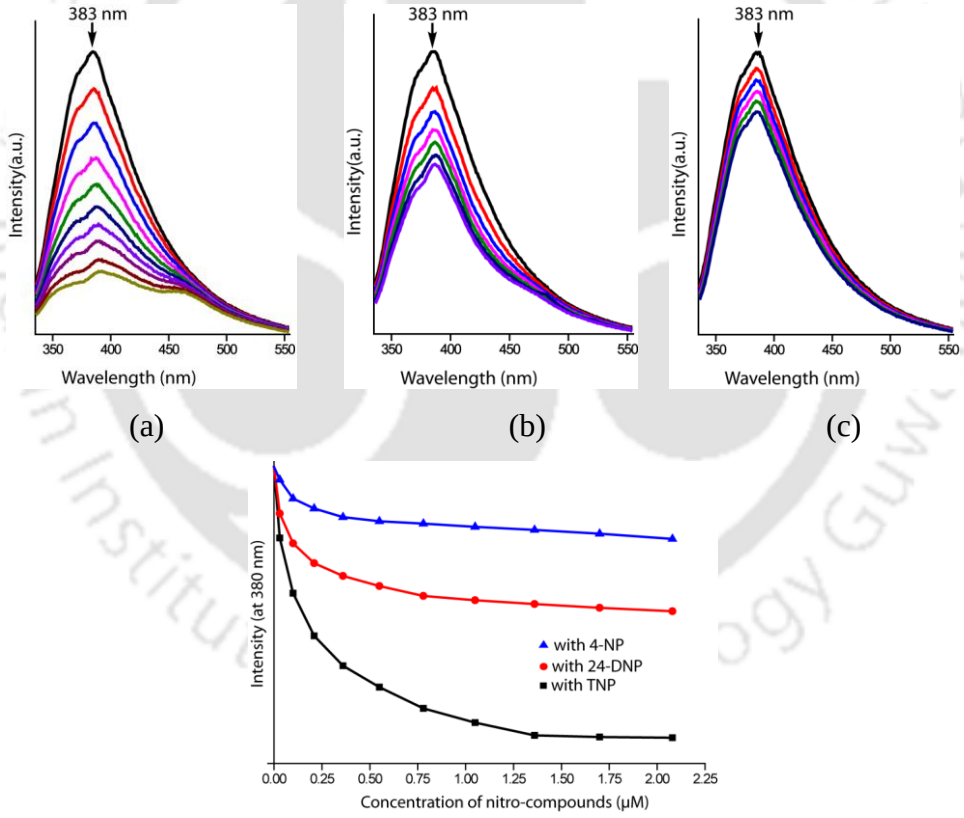

(d)

Figure 6.28: Changes in fluorescence emission of indole-3-carbaldoxime (10^{-4} M in acetonitrile) at 383 nm (excitation at 324 nm) upon addition (a) picric acid, (b) 2,4-dinitrophenol and (c) 4-nitrophenol (10 μl aliquots 10^{-5} M in acetonitrile in each case); (d) Plots of fluorescence intensity vs concentration at different nitro-compounds.

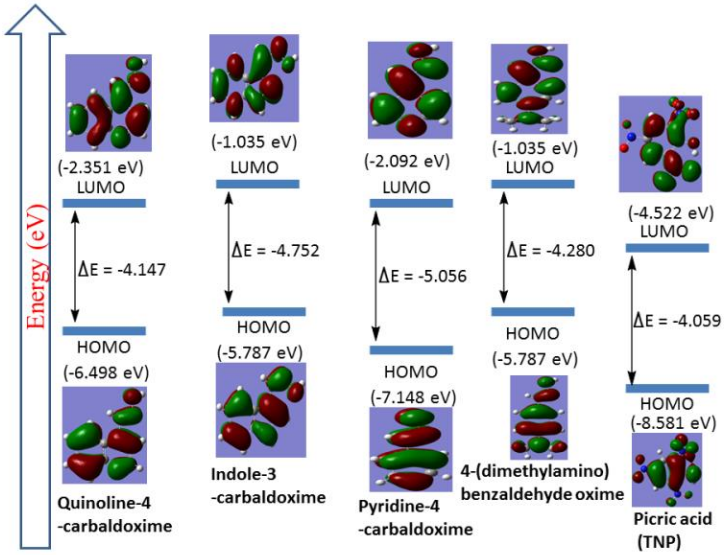

Figure 6.29: HOMO-LUMO of oxime derivatives and picric acid calculated by DFT using B3LYP/6-31+G (d,p) as a function.

Table 6.4: Relative contributions from various interactions from Hirshfeld analysis of structures in chapter 6.

Close contacts	**6.3**	**6.4**	**6.1**	**6.2**	ico
O···O	5.4	6.4	3.7	11.9	0.0
N···O	5.3	6.2	2.0	2.8	0.0
C···O	8.5	4.1	4.0	3.6	0.6
H···O	38.1	51.3	47.1	39.9	9.4
C···N	3.6	2.5	4.6	4.6	0.8
N···H	2.5	6.2	3.2	2.8	14.2
C···H	17.3	8.9	7.9	3.8	35.9
C···C	3.2	8.1	5.7	12.4	0.0
H···H	15.8	6.3	20.9	18.1	39.0

6.8: References

1. X. Sun, Y. Wang, Y. Lei, *Chem. Soc. Rev*., 2015, **44**, 8019-8061.
2. (a) T. Steiner, *Angew. Chem., Int. Ed*., 2002, **41**, 48-76; (b) J. C. Ma, D. A. Dougherty, *Chem. Rev*., 1997, **97**, 1303-1324; (c) M. Nishio, *CrystEngComm*, 2004, **6** , 130-158; (d) C. G. Claessens, J. F. Stoddart, *J. Phys. Org. Chem*., 1997, **10**, 254-272; (e) E. A. Meyer, R. K. Castellano, F. Diederich, *Angew. Chem., Int. Ed*., 2003, **42**, 1210-1250; (f) G. R. Desiraju, *Angew. Chem., Int. Ed*., 1995, **34**, 2311-2327.

3. (a) J. L. Atwood, G. A. Koutsantonis, C. L. Raston, *Nature*, 1994, **368**, 229-231; (b) G. W. Orr, L. J. Barbour, J. L. Atwood, *Science*, 1999, **285**, 1049-1052; (c) J. L. Atwood, L. J. Barbour, A. Jerga, *Science*, 2002, **296**, 2367-2369.
4. (a) P. A. Gale, *Acc. Chem. Res*., 2011, **44**, 216-226; (b) M. Cacciarini, V. A. Azov, P. Seiler and F. Diederich, *Chem. Commun*., 2005, 5269-5271; (c) M. M. Safont-Sempere, G. Fernandez, F. Wurthner, *Chem. Rev*., 2011, **111**, 5784-5814.
5. (a) J. -M. Lehn, *Proc. Nat. Acad. Sci. USA* 2002, **99**, 4763-4768; (b) G. M. Whitesides, M. Boncheva, *Proc. Nat. Acad. Sci. USA* 2002, **99,** 4769-4774; (c) L. R. Nassimbeni, *Acc. Chem. Res.* 2003, **36,** 631-637; (d) G. M. Whitesides, J. P. Mathias, C. T. Seto, *Science*, 1991, **254,** 1312-1319.
6. (a) D. P. Yan, A. Delori, G. O. Lloyd, B. Patel, T. Friscic, G. M. Day, D. K. Bucar, W. Jones, J. Lu, M. Wei, D. G. Evans, X. Duan, *CrystEngComm*, 2012, **14,** 5121-5123; (b) D. Yan, A. Delori, G. O. Lloyd, T. Friscic, G. M. Day, W. Jones, J. Lu, M. Wei, D. G. Evans, X. Duan, *Angew. Chem., Int. Ed.*, 2011, **50,** 12483-12486; (c) A. Tarai, J. B. Baruah, *ChemistrySelect*, 2017, **2**, 10101-10106.
7. (a) B. W. Xu, X. F. Wu, H. B. Li, *Macromolecules*, 2011, **44**, 5089-5092; (b) F. Zhang, L. Luo, Y. Sun, *Tetrahedron*, 2013, **69**, 9886-9889.
8. (a) Y. Salinas, R. M. Manez, M. D. Marcos, F. Sancenon, A. M. Costero, M. Parra, S. Gil, *Chem. Soc. Rev*., 2012, **41**, 1261-1296; (b) D. T. McQuade, A. E. Pullen, T. M. Swager, *Chem. Soc. Rev*., 2000, **100**, 2537-2574; (c) M. E. Germain, M. J. Knapp, *Chem. Soc. Rev.*, 2009, **38**, 2543-2555.
9. (a) D. T. Meredith, C. O. Lee, *J. Am. Pharm. Assoc*. 1939, **28**, 369-373; (b) E. H. Volwiler, *Ind. Eng. Chem*., 1926, **18**,1336-1337.
10. (a) V. Pimienta, R. Etchenique, T. Buhse, *J. Phys. Chem. A*, 2001, **105**, 10037-10044; (b) J. Y. Shen, J. F. Zhang and Y. Zuo, *J. Hazard. Mater*., 2009, **163**, 1199-1206.
11. (a) J. F. Wyman, M. P. Serve, D. W. Hobson, *J. Toxicol. Environ. Health, Part A*, 1992, **37**, 313-327; (b) G. Anderson, J. D. Lamar, P. T. Charles, *Environ. Sci. Technol*., 2007, **41**, 2888-2893.
12. (a) H. Sohn, M. J. Sailor, D. Magde, W. C. Trogler, *J. Am. Chem. Soc*., 2003, **125**, 3821-3830; (b) J. I. Steinfeld, J. Wormhoudt, *Annu. Rev. Phys. Chem*., 1998, **49**, 203-232.
13. (a) J. M. Sylvia, J. A. Janni, J. D. Klein, K. M. Spencer, *Anal. Chem*., 2000, **72**, 5834-5840; (b) K. Hakansson, R. V. Coorey, R. Zubarev, V. L. Talrose, P. Hakansson, *J. Mass Spectrom*., 2000, **35**, 337-346.

14. J. R. C. Junqueira, W. R. deAraujo, M. O. Salles, T. R. L. C. Paixao, *Talanta*, 2013, **104**, 162-168.
15. (a) J. -S. Li, Y. -J. Tang, S. -L. Li, S. -R. Zhang, Z. -H. Dai, L. Si, Y. -Q. Lan, *CrystEngComm*, 2015, **17**, 1080-1085; (b) W. Xie, S. -R. Zhang, D. -Y. Du, J. -S. Qin, S. -J. Bao, J. Li, Z. -M. Su, W. -W. He, Q. Fu, Y. -Q. Lan, *Inorg. Chem*., 2015, **54**, 3290-3296; (c) A. K. Bandela, S. Bandaru, C. P. Rao, *Chem. Eur. J*., 2015, **21**, 13364-13374; (d) N. Venkatramaiah, S. Kumar, S. Patil, *Chem. Commun*., 2012, **48**, 5007-5009.
16. (a) S. Shanmugaraju, P. S. Mukherjee, *Chem. Eur. J*., 2015, **21**, 6656-6666; (b) M. Alfonso, A. Espinosa, A. Tarraga, P. Molina, *Chemistry Open*, 2014, **3**, 242-249; (c) D. S. Kim, V. M. Lynch, K. A. Nielsen, C. Johnsen, J. O. Jeppesen, J. L. Sessler, *Anal. Bioanal. Chem*., 2009, **395**, 393-400; (d) J. Pan, F. Tang, A. Ding, L. Kong, L. Yang, X. Tao, Y. Tiana, J. Yang, *RSC Adv*., 2015, **5**, 191-195.
17. (a) R. Chopra, P. Kaur, K. Singh, *Anal. Chim. Acta*, 2015, **864**, 55-63; (b) D. Udhayakumari, S. Velmathi, P. Venkatesan, S. -P. Wu, *Anal. Methods*, 2015, **7**, 1161-1166; (c) S. K. Gupta, D. Kaleeswaran, S. Nandi, R. Vaidhyanathan, R. Murugavel, *ACS Omega*, 2017, **2**, 3572-3582.
18. K. Durga Prasad, T. N. Guru Row, *RSC Adv*., 2014, **4**, 45306-45310.
19. K. K. Neena, P. Thilagar, *J. Mater. Chem. C*, 2016, **4**, 11465-11473.
20. K. K. Kartha, A. Sandeep, V. K. Praveen, A. Ajayaghosh, *Chem. Rec*., 2015, **15**, 252-265
21. P. E. Shaw, S. S. Chen, X. Wang, P. L. Burn, P. Meredith, *J. Phys. Chem. C*, 2013, **117**, 5328-5337.
22. G. Hong, J. Sun, C. Qian, P. Xue, P. Gong, Z. Zhang, R. Lu, *J. Mater. Chem. C*, 2015, **3**, 2371-2379.
23. S. Shanmugaraju, P. S. Mukherjee, *Chem. Commun*., 2015, **51**, 16014-16032.
24. S. Xu, H. Lu, *Chem. Commun*., 2015, **51**, 3200-3203.
25. X. Ma, F. Tao, Y. Zhang, T. Li, M. F. Raymo, Y. Cui, *J. Mater. Chem. A*, 2017, **5**, 14343-14354.
26. (a) A. Chowdhury, P. Howlader, P. S. Mukherjee, *Chem. Eur. J*., 2016, **22**, 7468-7478; (b) S. Sandhu, R. Kumar, P. Singh, S. Kumar, *J. Mater. Chem. C*, 2016, **4**, 3209-3216.
27. (a) H. Xu, F. Liu, Y. Cui, B. Chen, G. Qian, *Chem. Commun*., 2011, **47**, 3153-3155; (b) B. Gole, A. K. Bar, P. S. Mukherjee, *Chem. Commun*., 2011, **47**, 12137-12139; (c) D. Samanta, P. S. Mukherjee, *Dalton. Trans*., 2013, **42**, 16784-16795; (d) V.

Vajpayee, H. Kim, A. Mishra, P. S. Mukherjee, P. J. Stang, M. Lee, H. K. Kim, K. W. Chi, *Dalton Trans*., 2011, **40**, 3112-3115; (e) S. Ghosh, P. S. Mukherjee, *Organometallics*, 2008, **27**, 316-319; (f) S. Shanmugaraju, H. Jadav, P. Y. Patil, P. S. Mukherjee, *Inorg. Chem*., 2012, **51**, 13072-13074; (g) S. Shanmugaraju, S. A. Joshi, P. S. Mukherjee, *Inorg. Chem*., 2011, **50**, 11736-11745; (h) S. S. Nagarkar, B. Joarder, A. K. Chaudhari, S. Mukherjee, S. K. Ghosh, *Angew. Chem., Int. Ed*., 2013, **52**, 2881-2885.

28. (a) G. Das, B. P. Biswal, S. Kandambeth, V. Venkatesh, G. Kaur, M. Addicoat, T. Heine, S. Verma, R. Banerjee, *Chem. Sci*., 2015, **6**, 3931-3939; (b) S. Dalapati, S. Jin, J. Gao, Y. Xu, A. Nagai, D. Jiang, *J. Am. Chem. Soc*., 2013, **135**, 17310-17313.
29. L. Guo, D. Cao, *J. Mater. Chem. C*, 2015, **3**, 8490-8494.
30. (a) Y. Erande, S. Chemate, A. More, N. Sekar, *RSC Adv*., 2015, 5, 89482-89487; (b) G. Sivaraman, B. Vidya and D. Chellappa, *RSC Adv*., 2014, **4**, 30828-30831; (c) B. Gogoi, N. S. Sarma, *ACS Appl. Mater. Interfaces*, 2015, **7**, 11195-11202; (d) R. Mitra, A. Saha, ACS Sustainable Chem. Eng., 2017, 5, 604-615.
31. J. Pitchaimani, A. Kundu, S. Karthikeyan, S. P. Anthony, D. Moon, V. Madhu, *CrystEngComm*, 2017, **19**, 3557-3561.
32. (a) N. Dey, S. K. Samanta, S. Bhattacharya, *ACS Appl. Mater. Interfaces*, 2013, **5,** 8394-8400; (b) V. Bhalla, A. Gupta, M. Kumar, *Org. Lett.*, 2012, **14,** 3112-3115; (c) M. Kumar, S. I. Reja, V. Bhalla, *Org. Lett.*, 2012, **14,** 6084-6087; (d) G. He, H. N. Peng, T. H. Liu, M. N. Yang, Y. Zhang, Y. Fang, *J. Mater. Chem*., 2009, **19,** 7347-7353; (e) V. Bhalla, A. Gupta, M. Kumar, D. S. Rao, S. K. Prasad, *ACS Appl. Mater. Interfaces*, 2013, **5,** 672-679; (f) B. W. Xu, X. F. Wu, H. B. Li, H. Tong, L. X. Wang, *Macromolecules*, 2011, **44,** 5089-5092; (g) Y. Y. Long, H. B. Chen, H. M. Wang, Z. Peng, Y. F. Yang, G. Q. Zhang, N. Li, F. Liu, J. Pei, *Anal. Chim. Acta*, 2012, **744,** 82-91.
33. (a) F. H. Allen, V. J. Hoy, J. A. K. Howard, V. R. Thalladi, G. R. Desiraju, C. C. Wilson, G. J. McIntyre, *J. Am. Chem. Soc*., 1997, **119**, 3477-3480; (b) F. H. Allen, W. D. S. Motherwell, P. R. Raithby, G. P. Shields, R. Taylor, *New J. Chem*., 1999, **23**, 25-33.
34. G. Wojcik, J. Holband, J. J. Szymczak, S. Roszak, J. Leszczynsk, *Cryst. Growth Des*., 2006, **6**, 274-284.
35. A. Tarai, J. B. Baruah, *Cryst. Growth Des*., 2016, **16**, 126-135.

36. (a) C. B. Aakeroy, A. M. Beatty, D. S. Leinen, *Cryst. Growth Des*., 2001, **1**, 47-52; (b) C. B. Aakeroy, K. N. Epa, S. Forbes, J. Desper, *CrystEngComm*., 2013, **15**, 5946-5949; (c) C. B. Aakeroy, A. S. Sinha, K. N. Epa, P. D. Chopade, M. M. Smith, J. Desper, *Cryst. Growth Des*., 2013, **13**, 2687-2695; (d) E. A. Bruton, L. Brammer, F. C. Pigge, C. B. Aakeroy, D. S. Leinen, *New J. Chem*., 2003, **27**, 1084-1094; (e) A. Tarai, J. B. Baruah, *CrystEngComm*, 2016, **18**, 298-308.
37. Z. Radic, T. Dale, Z. Kovarik, S. Berend, E. Garcia, L. Zhang, G. Amitai, C. Green, B. Radic, B. M. Duggan, D. Ajami, J. Rebek, Jr., P. Taylor. *Biochem. J.* 2013, **450**, 231-242.
38. D. T. Meredith, C. O. Lee, *J. Am. Pharm. Assoc*., 1939, **28**, 369-373.
39. (a) J. F. Wyman, M. P. Serve, D. W. J. Hobson, *Toxicol. Environ. Health, Part A*, 1992, **37,** 313-327; (b) G. Anderson, J. D. Lamar, P. T. Charles, *Environ. Sci. Technol*., 2007, **41,** 2888-2893.
40. M. T. Nguyen, L. G. Vanquickenborne, *J. Chem. Soc., Perkin Trans.***,** 1993, **2**, 1969-1972.
41. G. R. Desiraju, *Angew. Chem. Int. Ed*., 1995, 34, 2311-2327.
42. (a) C. E. Bugg, U. Thewalt, *Science*, 1970, **170,** 852-854; (b) T. Ishida, H. Nagata, Y. In, M. Doi, M. Inoue, M.W. Extine, A. Wakahara, *Chem. Pharm. Bull*., 1993, **41**, 433-438.
43. K. B. Landenberger, A. J. Matzger, *Cryst. Growth Des*., 2010, **10,** 5341-5347.
44. A. Chandramohan, R. Bharathikannan, V. Kandhavelu, J. Chandrasekaran, M. A. Kandhaswamy, *Spectrochimica Acta Part A*, 2008, **71,** 755-759.
45. (a) C. B. Aakeroy, D. J. Salmon, M. M. Smith, J. Desper, *Cryst. Growth Des*., 2006, **4,** 1033-1042; (b) C. B. Aakeroy, J. Desper, M. M. Smith, *Chem. Commun*., 2007, 3936-3938; (c) C. B. Aakeroy, A. M. Beatty, D. S. Leinen, *Cryst. Growth Des*., 2001, **1,** 47-52.
46. A. Tarai, J. B. Baruah, *CrystEngComm*, 2016, **18**, 9095-9102.
47. A. Tarai, J. B. Baruah, *CrystEngComm*, 2015, **17**, 2301-2309.
48. (a) J. S. Stevens, S. J Byard, C. C. Seaton, G. Sadiq, R. J. Daveya, S. L. M. Schroeder, *Phys. Chem. Chem. Phys*., 2014, **16**, 1150-1160; (b) M. Kunduracı, E. Özkaramete, N. Yılmaz, S. Öz, I. Svoboda, E. K. İnal, O. Atakol, *J. Therm Anal. Calorim*., 2013, **112**, 1587-1599.
49. C. A. Hunter, J. K. M. Sanders, *J. Am. Chem. Soc.*, 1990, **112**, 5525-5534.

50. J. Braun, H. J. Neusser, P. Hobza, *J. Phys. Chem. A*, 2003, **107**, 3918-3924; (b) J. R. Kerr, L. Trembleau, J. M. D. Storey, J. L. Wardell, W. T. A. Harrison, *Acta Cryst.* 2016, **E72,** 699-703.
51. (a) I. Boldog, J. -C. Daran, A. N. Chernega, E. B. Rusanov, H. Krautscheid, K. V. Domasevitch, *Cryst. Growth Des.* 2009, **9**, 2895-2905; (b) M. Jukic, A. Hergold-Brundic, M. Cetina, A. Nagl, J. Vorkapic-Furac, *Struct. Chem.*, 2003**, 14**, 597-604; (c) E. Alcalde, N. Mesquida, C. Alvarez-Rúa, R. Cuberes, J. Frigola, S. García-Granda, *Molecules*, 2008, **13**, 301-318.
52. (a) S. Jeyavijayan, M. Arivazhagan, *Indian J. Pure Appl. Phys.*, 2012, **50,** 623-632; (b) T. Stepanenko, L. Lapinski, M. J. Nowak, L. Adamowicz, *Vibrational Spectrosc*., 2001, **26,** 65-82; (c) A. Tarai, J. B. Baruah, *CrystEngComm*, 2016, **18,** 5482-5491; (d) R. A. Apreyan, M. Fleck, A. K. Atanesyan, R. P. Sukiasyan, A. M. Petrosyan, *J. Mol. Struct*., 2015, **1101,** 236-242.
53. A. Nayak, V. R. Pedireddi, *Cryst. Growth Des.*, 2016, **16,** 5966-5975.
54. (a) M. A. Spackman and D. Jayatilaka, *CrystEngComm*, 2009, **11**, 19-32; (b) J. J. McKinnon, D. Jayatilaka, M. A. Spackman, *Chem. Commun*., 2007, 3814-3816.
55. (a) D. Ding, K. Li, B. Liu, B. Z. Tang, *Acc. Chem. Res*., 2013, **46,** 2441-2453; (b) Y. Hong, J. W. Y. Lam, B. Z. Tang, *Chem. Soc. Rev.*, 2011**, 40,** 5361-5388; (c) S. Li, S. M. Langenegger, R. Haner, *Chem. Commun.*, 2013, **49,** 5835-5837.
56. (a) X. -L. Sun, W. -H. Deng, H. Chen, H. -L. Han, J. M. Taylor, C. -Q. Wan, G. Xu, *Chem. Eur. J*., 2017, **23,** 1248-1252; (b) J. T. A. Jones, D. Holden, T. Mitra, T. Hasell, D. J. Adams, K. E. Jelfs, A. Trewin, D. J. Willock, G. M. Day, J. Bacsa, A. Steiner, A. I. Cooper, *Angew. Chem. Int. Ed*., 2011, **50**, 749-753.
57. (a) H. Gang, Y. Ni, Y. Jiayu, W. Hongyue, D. Liping, Y. Shiwei, F. Yu, *Macromolecules*, 2011, **44**, 4759-4766; (b) D. C. Santra, M. K. Bera, P. K. Sukul, S. Malik, *Chem. Eur. J*., 2016, **22**, 2012-2019; (c) Y. Salinas, R. M. Manez, M. D. Marcos, F. Sancenon, A. M. Costero, M. Parra, S. Gil, *Chem. Soc. Rev*., 2012, **41**, 1261-1296; (d) D. T. McQuade, A. E. Pullen, T. M. Swager, *Chem. Soc. Rev*., 2000, **100**, 2537-2574; (e) M. E. Germain, M. J. Knapp, *Chem. Soc. Rev*., 2009, **38**, 2543-2555.
58. I. S. K. Kerkines, I. D. Petsalakis, G. Theodorakopoulos, J. Rebek Jr., *J. Phys. Chem. A*, 2011, **115,** 834-840.

Thesis Conclusion

This thesis contains different self-assemblies of oxime derivatives, some of their cocrystals and ionic salts are studied through an approach of crystal engineering. Properties of oximes as well as their different adducts in solid state are compared with the properties observed in solution. The changes in non-covalent interactions in various adducts generally took place through conversions of conventional oxime-oxime homo-synthons to hetero-synthons with partner molecules. Different fluoride assisted assemblies of series of hydroxyaromatic aldoximes as ionic cocrystals with neutral tetrabutylammonium salt as partner molecule or salts of such oximes with or without fluoride ions have shown that the fluoride assisted assemblies are dictated by the intrinsic acidity associated with fluoride. It has been possible to construct fluoride guided assemblies forming grid like structures to encapsulate tetrabutylammonium cation. The differences in self-assemblies in solid state and solution were reflected in absorption and emission spectroscopies. These results have helped in modulating fluorescence emission spectra as well as absorption spectra enabling to distinguish fluoride ions from other ions. Majority of the anion assisted assemblies of hydroxyaromatic aldoximes have anion-hydroxy and anion-oxime interactions. The results obtained from polyhydroxyaromatic aldoximes suggest competition between the intramolecular hydrogen bonds and the intermolecular oxime-phenol interactions. The assemblies with or without fluoride ion adopt layer or grid-like structures to encapsulate cations.

The dialdoxime such as 1,3-benzenedialdoxime in presence of hydroxide, chloride and fluoride anions form varieties of self-assemblies where interesting conformations of oximes are observed. As a consequence of this and due to the electrostatic hydrogen bonds of the anions; dendrimer-like assemblies are observed in specific cases. Dendrimer-like assemblies formed in fluoride assisted assemblies are not observed in the chloride assisted assembly. The chloride assisted assembly has water molecules acting as filler to form a tight packed structure. This anion assisted study on dendrimer-like packing patterns has revealed the scopes of encapsulating neutral host molecules providing scope for multi-component cocrystals.

Aggregation induced emission (AIE) of 2-hydroxynapthaldoxime was observed on adding different amount of water to solution of the compound in organic solvents. It was found that aggregation induced emission of 2-hydroxynapthaldoxime is dependent on solvent. The intermolecular C-H$\cdots\pi$ interactions involving the C-H located at the *para* position with respect to oxime group of the naphthalene ring is suggested to be facilitate

formation of aggregate suitable to show AIE. In solution coformers cause quenching of fluorescence of 2,3-dihydroxyphenylaldoxime, suggesting that interactions of coformers with 2,3-dihydroxyphenylaldoxime involve the hydoxy-group at the 3- position. Π-stacking plays the decisive role to increase or decrease fluorescence intensity of 2-hydroxynapthaldoxime in the solid state. In solution no interactions between 2-hydroxynapthaldoxime with coformers were observed. By virtue of properties in solution and solid state, different oximes were distinguished by the fluorescence technique.

The roles of hydrogen bonds in the self-assemblies of the poly-hydroxyaromatic oxime metal complexes in different solvated formation were discerned. Interactions of fluoride ions with metal-oximate complexes of hydroxyaromatic alodoximes in solution clearly established that utility of divalent metal complexes of copper, nickel and zinc complexes can be used for detection of fluoride. In such complexes population of d-electron in the central metal ions in a delocalized chelate system plays a key role in shifting the emission or absorption spectra with respect to the parent ligand during the detection of fluoride ions. Fluorescence emission of the zinc complex can be a tool for the detection of fluoride ions despite the parent ligand is weakly fluorescent. It was found that the central metal ion or active hydrogen containing functional group of ligands controls the detection of fluoride ion in solution.

It was found that cadmium coordination polymers of 1,3-di(pyridin-4-yl)propane is capable to form guest encapsulated coordination polymer with 2,4-dihydroxybenzaldehyde and 2,4-dihydroxybenzaldoxime. The role of cadmium coordination polymer to facilitated the reaction of 2,4-dihydroxybenzaldehyde with hydroxylamine to form 2,4-dihydroxybenzaldoxime. This is attributed to lower binding ability of the coordination polymer to the aldehyde than that with the oxime.

The structures of various cocrystals or salts of quinolone-4-carbaldoxime with aliphatic dicarboxylic or mineral or aromatic carboxylic acids suggest that identification of synthons helps in predesign non-covalent synthesis. Three cocrystals of closely related dicarboxylic acids were utilized for predesign non-covalent synthesis. The exception in the sub-assemblies of designed synthesis is due to substituent nature and inherent properties of dicarboxylic acid were found out and these results were suggestive of emphasis on the domain of the different sub-assemblies.

The picrate salts of different oxime derivatives containing heterocycles have provided examples of (a) stable picrate salts of oximes, (b) different kinds of homodimers of oximes depending on the heterocyclic part causing synthon variations, (c) charge-transfer interactions

between the anionic and cationic parts in electrostatically guided assemblies and (d) domain expansion of synthons forming new sub-assemblies. Fluorescence quenching of these oxime derivatives is caused by picric acid due to the protonation of the good hydrogen bond acceptors at the remote site linked to the fluorophore. The magnitude of fluorescence quenching by nitro-phenols differs due to the intrinsic acidity associated with them.

To summarize, this thesis has delineated the scopes to utilize the weak interactions of oximes coupled with contribution from other weak interactions to generate new supramolecular assemblies with interesting optical properties in solid or solution state for molecular and ion recognitions.

Details of the analytical equipment

X-Ray Crystallography

The X-ray crystallographic data were collected at 296 K with Mo Kα radiation (λ = 0.71073 Å) using a Bruker Nonius SMART CCD diffractometer equipped with a fine focus 3.0 KW sealed tube. The SMART software (v 2.1.4) was used for data collection and also for indexing the reflections and determining the unit cell parameters; the collected data were integrated using SAINT software. The structures were solved by direct methods and refined by full-matrix least-square calculations using SHELXTL-14 and SHELXTL-97 software.[1] All the non-H atoms were refined in the anisotropic approximation against F^2 of all reflections. All the H atoms were refined in isotropic approximation and treated as 'riding' in calculated positions. The locations of the H atoms of the protonated organic molecules were justified by difference Fourier synthesis map. The H-atoms attached to water molecules were located in the difference Fourier synthesis maps, and refined with isotropic displacement coefficients. The hydrogen atoms attached to water molecules could not be located in few occasions. It was also necessary to apply restrains to optimize the distances of some hydrogen atoms of water molecules. The CIF of all the compounds characterized by single crystal X-ray structure are included in the soft copy.

Powder X-ray diffraction pattern were collected on a Bruker D2 Phaser diffractometer in Bragg-Brentano Θ-Θ geometry with Cu Kα radiation (λ = 1.5406 Å) equipped on a glass surface of air dried sample using a secondary curved graphite monochromator. Diffraction patterns were collected over a 2θ range of 5-45º at a step scan rate of 0.02º. ORTEP-3 for windows[2] version 2.0 was used for drawing the supramolecular assemblies of cocrystals, salts and oxime derivatives in the thesis. For molecular packing diagram we used mercury-3.7 software.[3]

FT-IR, Raman, UV-visible, Fluorescence, NMR and Mass spectroscopy

The FT-IR spectra were recorded with a Perkin Elmer Spectrum One spectrophotometer in the spectral region 4000-400 cm^{-1} using KBr pellets. Raman spectra were recorded by using LabRam HR800, Jobin Yvon with vertically polarized 488 nm Ar-ion laser beam with D1 filter. UV-visible absorption spectra were recorded using Perkin-Elmer Lambda 750 spectrophotometer equipped with double cell compartment. All the chemicals and solvents used were as obtained from the standard suppliers such as Sigma Aldrich, E. Merck, Ranbaxy etc. The solvents for spectroscopic were of HPLC grade (Aldrich or Merck) and used as such.

Fluorescence emissions were measured using Horiba Jobin Yvon Fluoromax-4 spectrofluorometer by taking definite amount of solutions and exciting at required wavelengths. ^{1}H-NMR was recorded on a Varian 400 MH_Z and BRUKER Ascend 600 MH_z NMR spectrometer using TMS as internal standard. Mass spectra were recorded on a micro mass Q-TOF (waters) mass spectrometer by using acetonitrile / formic acid matrix.

Thermal analyses (TGA and DSC), elemental analyses, ESR, DLS, ITC and Hirshfeld analyses

Thermogravimetric analysis (**TGA**) and Differential scanning calorimetry (**DSC**) were performed using thermal analyzer SDTQ600 simultaneous DTA/TGA systems, under nitrogen with a heating rate of 10°C/min.

Elemental analyses were performed with a Perkin-Elmer PE 2400 II CHNS micro analytical analyzer.

Electron Spin Resonance (**ESR**) spectra were recorded on a JES-FA200 ESR spectrometer at room temperature with microwave power of at 0.998 mW, microwave frequency of 9.14 GHz, and modulation amplitude of 2. EPR spectrum of all copper(II) complexes were recorded in solid state.

Dynamic light scattering (**DLS**) experiments was carried out on a Malvern Zetasizer Nano ZS instrument equipped with a 4.0 mW He-Ne laser operating at a wavelength of 633 nm. The samples and the background were measured at room temperature (25 °C) at a scattering angle of 173°.

Isothermal titration calorimetry (**ITC**) analysis was performed at 27 ºC with 25 injections at 90s time interval. After subtractions of control, the final fitting was obtained in single binding site model.

Hirshfeld analyses are done by using CrystalExploer 3.1 software.

References:

1. (a) G. M. Sheldrick, *Acta Cryst*., 2008, A**64**, 112-122; (b) G. M. Sheldrick, *Acta Cryst*., 2015, A**71**, 3-8.
2. L. J. Farrugia, *J. Appl. Cryst*., 1997, **30**, 565.
3. C. F. Macrae, P. R. Edgington, P. McCabe, E. Pidcock, G. P. Shields, R. Taylor, M. Towler, J. van de Streek, *J. Appl. Cryst*., 2006, **39**, 453-457

Crystallographic data and refinement parameters for compounds

Compound No.	Oxime **2.1.1**	Oxime **2.1.2**	Cocrystal **2.1.4**	Cocrystal **2.1.5**
Formulae	$C_{11}H_9NO_2$	$C_7H_7NO_3$	$C_{27}H_{45}FN_2O_2$	$C_{30}H_{50}FN_3O_6$
CCDC No.	**1003332**	**1417714**	**1003333**	**1012763**
Mol. wt.	187.19	153.14	448.65	567.73
Space group	$P2_1/c$	$P2_1/c$	$P2_1/c$	Pc
a /Å	14.856(2)	11.211(10)	10.1130 (6)	9.5189 (7)
b /Å	4.0568(6)	4.662(4)	17.5762 (10)	9.4321 (7)
c /Å	16.585(2)	14.146(12)	15.6751 (10)	18.7965 (14)
α/°	90.00	90.00	90.00	90.00
β/°	115.029(9)	111.793(17)	102.831 (6)	101.203 (4)
γ/°	90.00	90.00	90.00	90.00
V/ $Å^3$	905.6(2)	686.5(10)	2716.7 (3)	1655.5(2)
Density/g.cm^{-3}	1.373	1.482	1.097	1.139
Abs. Coeff. /mm^{-1}	0.096	0.118	0.073	0.082
F(000)	392	320	984	616
Total No. of reflections	1616	1173	4901	2989
Reflections, $I > 2\sigma(I)$	1147	599	2959	1766
Max. θ/°	25.24	25.25	25.25	25.24
Ranges (h, k, l)	−17 ≤ h ≤ 16 −4 ≤ k ≤ 4 −19 ≤ l ≤ 19	−12 ≤ h ≤ 11 −5 ≤ k ≤ 5 −12 ≤ l ≤ 16	-12 ≤ h ≤ 12 -16 ≤ k ≤ 21 -18 ≤ l ≤ 18	-9 ≤ h ≤ 10 -11 ≤ k ≤ 10 -22 ≤ l ≤ 22
Complete to 2θ (%)	98.70	93.70	99.80	99.00
Data/ Restraints/Parameters	1616/0/129	1173/0/103	4901/ 0/ 319	5031/3/374
Goof (F^2)	1.059	1.045	1.051	1.029
R indices [$I > 2\sigma(I)$]	0.0414	0.0721	0.0686	0.0383
wR_2 [$I > 2\sigma(I)$]	0.0661	0.1577	0.1729	0.0919
R indices (all data)	0.0623	0.1337	0.1120	0.0560
wR_2 (all data)	0.0718	0.1948	0.2015	0.1024

Compound No.	Salt **2.1.6**	Cocrystal **2.2.2**	Cocrystal **2.2.3**	Cocrystal **2.2.4**
Formulae	$C_{30}H_{49}N_3O_6$	$C_{32}H_{51}N_5O_4$	$C_{32}H_{52}N_5O_4F$	$C_{32}H_{54}N_5O_5Cl$
CCDC No.	**1012762**	**1452013**	**1452014**	**1452015**
Mol. wt.	547.72	569.78	589.79	624.25
Space group	*C2/c*	*P-1*	$P2_1/c$	$P2_1/c$
a /Å	16.2317(7)	8.3025(3)	20.7631(8)	19.3315(9)
b /Å	9.6547 (4)	13.6899(6)	8.2356(3)	8.5518(4)
c /Å	20.2299 (8)	15.9951(7)	21.9337(8)	22.8978(10)
α/°	90.00	90.908(3)	90.00	90.00
β/°	99.931 (3)	99.985(3)	107.378(2)	95.077(3)
γ/°	90.00	104.369(3)	90.00	90.00
V/ $Å^3$	3122.8 (2)	1731.16(12)	3579.4(2)	3770.6(3)
Density/g.cm^{-3}	1.165	1.093	1.094	1.100
Abs. Coeff. /mm^{-1}	0.081	0.073	0.076	0.142
F(000)	1192	620	1280	1352
Total No. of reflections	2711	6068	6383	6800
Reflections, $I > 2\sigma(I)$	1431	2993	3317	2100
Max. θ/°	24.99	25.25	25.25	25.25
Ranges (h, k, l)	$-19 \le h \le 18$ $-11 \le k \le 11$ $-23 \le l \le 23$	$-9 \le h \le 9$ $-16 \le k \le 16$ $-19 \le l \le 19$	$-23 \le h \le 24$ $-9 \le k \le 9$ $-25 \le l \le 26$	$-23 \le h \le 23$ $-9 \le k \le 9$ $-27 \le l \le 27$
Complete to 2θ (%)	98.50	97.10	98.70	99.50
Data/ Restraints/Parameters	2711/ 8/ 189	6068/ 2/ 377	6383/5/390	6800/ 7/ 404
Goof (F^2)	1.048	1.098	1.056	1.076
R indices [$I > 2\sigma(I)$]	0.0736	0.0839	0.0707	0.0688
wR_2 [$I > 2\sigma(I)$]	0.1531	0.1765	0.1388	0.1234
R indices (all data)	0.1135	0.1527	0.1286	0.2428
wR_2 (all data)	0.1636	0.2225	0.1613	0.1632

Cocrystal No.	Cocrystal **3.1**	Cocrystal **3.2**	Cocrystal **3.3**	Cocrystal **3.4**
Formulae	$C_{32}H_{26}N_4O_4$	$C_{14}H_{15}N_3O_2$	$C_{19}H_{19}N_5O_4$	$C_{14}H_{19}N_5O_7$
CCDC No.	**1417716**	**1417717**	**1417718**	**1417715**
Mol. wt.	530.57	257.29	381.39	369.34
Space group	$P2_1/c$	*Aba2*	$P2_1/c$	$P2_1/n$
a /Å	11.8301(5)	10.0199(5)	8.9467(9)	8.8538(8)
b /Å	14.4094(6)	27.8962(17)	25.487(3)	17.6944(15)
c /Å	23.9854(10)	9.1641(6)	8.8264(9)	10.7717(10)
α/°	90.00	90.00	90.00	90.00
β/°	96.922(3)	90.00	114.334(6)	90.464(5)
γ/°	90.00	90.00	90.00	90.00
V/ $Å^3$	4058.9(3)	2561.5(3)	1833.8(3)	1687.5(3)
Density/g.cm^{-3}	1.302	1.334	1.381	1.454
Abs. Coeff. /mm^{-1}	0.088	0.092	0.100	0.118
F(000)	1668	1088	800	776
Total No. of reflections	7344	2320	3335	3040
Reflections, $I > 2\sigma(I)$	3858	1948	2709	2308
Max. θ/°	25.25	25.24	25.25	25.24
Ranges (h, k, l)	−13 ≤ h ≤ 14 −17 ≤ k ≤ 16 −28 ≤ l ≤ 28	−7 ≤ h ≤ 7 −8 ≤ k ≤ 8 −15 ≤ l ≤ 15	−10 ≤ h ≤ 10 −24 ≤ k ≤ 30 −10 ≤ l ≤ 10	−10 ≤ h ≤ 10 −20 ≤ k ≤ 21 −12 ≤ l ≤ 12
Complete to 2θ (%)	99.90	100.00	100.00	99.60
Data/ Restraints/Parameters	7344/0/547	2320/1/175	3335/0/258	3040/4/256
Goof (F^2)	1.003	1.072	1.058	1.025
R indices [$I > 2\sigma(I)$]	0.0481	0.0384	0.0573	0.0428
wR_2 [$I > 2\sigma(I)$]	0.1046	0.1020	0.1794	0.1338
R indices (all data)	0.1119	0.0475	0.0704	0.0575
wR_2 (all data)	0.1317	0.1094	0.1957	0.1468

Complex No.	Complex **4.1.1**	Complex **4.1.2**	Complex **4.1.3**	Complex **4.1.4**
Formulae	$C_{20}H_{26}CuN_4O_8$	$C_{22}H_{30}CuN_4O_8$	$C_{16}H_{18}CuN_2O_7S$	$C_{24}H_{20}CuN_4O_6$
CCDC No.	**1402351**	**1402356**	**1402352**	**1402350**
Mol. wt.	514.00	542.05	445.93	523.99
Space group	*P-1*	*P21/n*	*P-1*	*P21*
a /Å	6.1974(7)	9.3108(3)	8.3981(7)	10.6759(6)
b /Å	7.3044(9)	7.1558(2)	9.6705(9)	7.0765(4)
c /Å	13.1416(16)	19.0122(6)	12.5186(9)	14.7557(9)
α/°	91.394(5)	90.00	73.944(7)	90.00
β/°	102.247(5)	94.749(2)	86.252(6)	96.369(4)
γ/°	101.071(5)	90.00	67.507(9)	90.00
V/ $Å^3$	569.23(12)	1262.36(7)	901.77(13)	1107.88(11)
Density/g.cm^{-3}	1.499	1.426	1.642	1.571
Abs. Coeff. /mm^{-1}	1.013	0.917	1.369	1.037
F(000)	267	566	458	538
Total No. of reflections	2040	2261	3252	3830
Reflections, $I > 2\sigma(I)$	1279	1830	2383	3231
Max. θ/°	25.24	25.24	25.25	25.24
Ranges (h, k, l)	$-7 \le h \le 7$ $-8 \le k \le 6$ $-10 \le l \le 14$	$-11 \le h \le 11$ $-8 \le k \le 8$ $-22 \le l \le 22$	$-10 \le h \le 9$ $-11 \le k \le 11$ $-15 \le l \le 13$	$-12 \le h \le 12$ $-8 \le k \le 8$ $-17 \le l \le 17$
Complete to 2θ (%)	98.70	98.90	99.80	99.50
Data/ Restraints/Parameters	2040/0/155	2261/0/165	3252/0/250	3830/1/321
Goof (F^2)	1.034	1.086	1.027	1.086
R indices [$I > 2\sigma(I)$]	0.0387	0.0526	0.0430	0.0367
wR_2 [$I > 2\sigma(I)$]	0.1184	0.1438	0.0734	0.0684
R indices (all data)	0.0407	0.0602	0.0651	0.0473
wR_2 (all data)	0.1222	0.1537	0.0852	0.0713

Complex No.	Complex **4.1.5**	Complex **4.1.6**	Complex **4.1.7**	Complex **4.2.1**
Formulae	$C_{20}H_{26}NiN_4O_8$	$C_{14}H_{12}N_2NiO_6$	$C_{40}H_{40}N_6O_6Zn$	$C_{13}H_{16}N_4O_7Cd$
CCDC No.	**1402354**	**1402353**	**1402355**	**1556234**
Mol. wt.	509.14	362.95	766.17	452.71
Space group	*P-1*	$P2_1/c$	*P-1*	*P-1*
a /Å	6.2331(6)	6.8784(8)	7.7539(6)	7.8485(6)
b /Å	7.2148(6)	7.0931(8)	9.7058(8)	10.3471(6)
c /Å	13.1150(12)	27.221(3)	13.6203(10)	11.9239(8)
α/°	90.288(5)	90.00	75.256(5)	100.594(4)
β/°	101.143(5)	90.610(3)	79.970(5)	103.197(4)
γ/°	100.988(5)	90.00	72.318(5)	104.459(3)
V/ $Å^3$	567.52(9)	1328.0(3)	939.22(13)	882.60(11)
Density/g.cm^{-3}	1.490	1.815	1.355	1.703
Abs. Coeff. /mm^{-1}	0.908	1.498	0.709	1.279
F(000)	266	744	400	452
Total No. of reflections	2044	2390	3398	3073
Reflections, $I > 2\sigma(I)$	1883	1239	2704	2846
Max. θ/°	25.00	25.24	25.25	25.05
Ranges (h, k, l)	$-7 \le h \le 7$ $-8 \le k \le 8$ $-15 \le l \le 15$	$-7 \le h \le 5$ $-4 \le k \le 7$ $-31 \le l \le 22$	$-9 \le h \le 9$ $-11 \le k \le 10$ $-16 \le l \le 15$	$-9 \le h \le 6$ $-12 \le k \le 12$ $-14 \le l \le 14$
Complete to 2θ (%)	99.90	99.30	99.40	98.20
Data/ Restraints/Parameters	2044/3/141	2390/0/209	3398/0/241	3073/ 0/ 234
Goof (F^2)	1.015	1.077	1.008	1.044
R indices [$I > 2\sigma(I)$]	0.0738	0.0658	0.0358	0.0255
wR_2 [$I > 2\sigma(I)$]	0.1888	0.1902	0.0818	0.0695
R indices (all data)	0.0754	0.0887	0.0491	0.0281
wR_2 (all data)	0.1880	0.2031	0.0882	0.0713

Compound No.	Complex **4.2.2**	Complex **4.2.3**	Cocrystal **5.2**	Cocrystal **5.3**
Formulae	$C_{40}H_{44}N_6O_{14}Cd$	$C_{40}H_{46}N_8O_{14}Cd$	$C_{13}H_{13}N_2O_3$	$C_{12}H_{11}N_2O_3$
CCDC No.	**1556235**	**1556236**	**1417579**	**1417580**
Mol. wt.	945.21	975.26	245.25	231.31
Space group	*P-1*	*P-1*	$P2_1/n$	$P2_1/n$
a /Å	9.5265(5)	9.7839(6)	12.7021(5)	12.7915(5)
b /Å	9.9800(6)	10.1048(7)	5.0401(2)	5.0009(2)
c /Å	12.0673(6)	11.9627(8)	19.1216(8)	16.4829(7)
α/°	75.012(4)	104.063(3)	90.00	90.00
β/°	68.870(4)	110.636(3)	98.951(3)	90.926(3)
γ/°	88.119(4)	90.303(3)	90.00	90.00
V/ $Å^3$	1031.42(10)	1068.23(12)	1209.25(9)	1054.26(7)
Density/g.cm^{-3}	1.522	1.516	1.347	1.457
Abs. Coeff. /mm^{-1}	0.605	0.588	0.097	0.107
F(000)	486	502	516	484
Total No. of reflections	3568	3634	2151	1843
Reflections, $I > 2\sigma(I)$	3224	3499	1488	1341
Max. θ/°	25.05	25.05	25.24	25.24
Ranges (h, k, l)	$-11 \le h \le 11$ $-11 \le k \le 9$ $-14 \le l \le 14$	$-11 \le h \le 11$ $-12 \le k \le 11$ $-14 \le l \le 14$	$-15 \le h \le 15$ $-5 \le k \le 5$ $-22 \le l \le 22$	$-15 \le h \le 15$ $-6 \le k \le 5$ $-19 \le l \le 19$
Complete to 2θ (%)	97.60	96.00	98.60	97.10
Data/ Restraints/Parameters	3568/0/287	3634/ 0/ 286	2150/0/163	1843/0/156
Goof (F^2)	1.002	1.017	1.026	1.034
R indices [$I > 2\sigma(I)$]	0.0403	0.0250	0.0447	0.0436
wR_2 [$I > 2\sigma(I)$]	0.0975	0.0775	0.1249	0.1260
R indices (all data)	0.0455	0.0263	0.0678	0.0654
wR_2 (all data)	0.1007	0.0784	0.1415	0.1408

Compound No.	Cocrystal **5.4**	Salt **5.5**	Salt **5.6**	Salt **5.7**
Formulae	$C_{12}H_{10}N_2O_3$	$C_{14}H_{12}N_2O_5$	$C_{11}H_9N_2O_3$	$C_{10}H_{11}N_2O_2Cl$
CCDC No.	**1417581**	**1417578**	**1417577**	**1417575**
Mol. wt.	230.20	288.26	217.20	226.66
Space group	*P2$_1$/n*	*P-1*	*P -1*	*P 21/n*
a /Å	12.6838(12)	5.3961(7)	4.9838(2)	7.650(9)
b /Å	5.0451(5)	9.4163(13)	9.8417(4)	7.943(8)
c /Å	16.3375(16)	13.6395(17)	10.3031(5)	18.15(2)
α/°	90.00	75.670(9)	100.059(3)	90.00
β/°	90.201(7)	89.392(9)	100.517(3)	92.26(2)
γ/°	90.00	80.448(8)	91.372(3)	90.00
V/ Å^3	1045.45(18)	661.83(15)	488.42(4)	1102(2)
Density/g.cm^{-3}	1.463	1.446	1.477	1.366
Abs. Coeff. /mm^{-1}	0.107	0.112	0.110	0.328
F(000)	480	300	226	472
Total No. of reflections	1892	2322	1706	1975
Reflections, $I > 2\sigma(I)$	1402	1591	1441	1250
Max. θ/°	25.24	25.25	25.25	25.24
Ranges (h, k, l)	$-15 \le h \le 15$ $-5 \le k \le 6$ $-19 \le l \le 19$	$-6 \le h \le 6$ $-10 \le k \le 11$ $-15 \le l \le 16$	$-5 \le h \le 5$ $-11 \le k \le 11$ $-12 \le l \le 11$	$-6 \le h \le 2$ $-8 \le k \le 1$ $-19 \le l \le 18$
Complete to 2θ (%)	100.00	96.70	96.90	99.40
Data/ Restraints/Parameters	1892/0/156	2322/0/192	1706/0/146	1975/0/144
Goof (F^2)	1.051	1.017	1.039	1.027
R indices [$I > 2\sigma(I)$]	0.0427	0.0488	0.0391	0.0414
wR$_2$ [$I > 2\sigma(I)$]	0.1191	0.1315	0.1339	0.0671
R indices (all data)	0.0618	0.0733	0.0459	0.1020
wR$_2$ (all data)	0.1314	0.1469	0.1255	0.0787

Compound No.	Salt **5.8**	Cocrystal **5.9**	Salt **5.10**	Salt **5.11**
Formulae	$C_{10}H_9N_3O_4$	$C_{18}H_{16}N_2O_3$	$C_{17}H_{14}N_2O_4$	$C_{24}H_{18}N_4O_9$
CCDC No.	**1417576**	**1481865**	**1481864**	**1468837**
Mol. wt.	235.20	308.33	310.30	506.42
Space group	*P-1*	*P-1*	$P2_1/c$	*P-1*
a /Å	7.9402(7)	3.9318(5)	9.0241(15)	7.3884(7)
b /Å	8.1717(8)	11.7049(15)	11.982(2)	11.2382(10)
c /Å	8.8975(8)	16.914(2)	14.549(2)	14.8080(13)
α/°	70.343(6)	99.084(8)	90.00	94.017(5)
β/°	89.333(6)	94.248(8)	107.874(19)	96.891(5)
γ/°	72.343(6)	94.176(8)	90.00	109.057(5)
V/ Å^3	515.42(8)	763.69(17)	1497.2(4)	1145.92(18)
Density/g.cm^{-3}	1.515	1.341	1.377	1.468
Abs. Coeff. /mm^{-1}	0.120	0.093	0.100	0.115
F(000)	244	324	1252	524
Total No. of reflections	1864	2760	2690	4150
Reflections, $I > 2\sigma(I)$	1097	1250	1114	2068
Max. θ/°	25.24	25.24	25.24	25.25
Ranges (h, k, l)	$-8 \le h \le 8$ $-8 \le k \le 8$ $-9 \le l \le 9$	$-4 \le h \le 4$ $-14 \le k \le 13$ $-19 \le l \le 20$	$-10 \le h \le 9$ $-14 \le k \le 5$ $-17 \le l \le 17$	$-8 \le h \le 7$ $-11 \le k \le 10$ $-17 \le l \le 17$
Complete to 2θ (%)	99.50	99.60	99.40	99.80
Data/ Restraints/Parameters	1864/0/155	2760/0/211	2690/1/214	4150/0/340
Goof (F^2)	0.870	1.022	1.063	1.000
R indices [$I > 2\sigma(I)$]	0.0324	0.0555	0.0928	0.0515
wR_2 [$I > 2\sigma(I)$]	0.1109	0.1151	0.1547	0.1042
R indices (all data)	0.0371	0.1602	0.1722	0.1260
wR_2 (all data)	0.1193	0.1705	0.1945	0.1284

Compound No.	Salt **5.12**	Salt **5.13**	Salt **5.14**	Salt **5.15**
Formulae	$C_{17}H_{13}N_3O_5$	$C_{17}H_{13}N_3O_5$	$C_{34}H_{30}N_4O_{11}$	$C_{17}H_{16}N_2O_6$
CCDC No.	**1468838**	**1468839**	**1481866**	**1481867**
Mol. wt.	339.30	339.30	670.62	344.32
Space group	*P* $2_1/c$	*P* $2_1/c$	*C* 2/*c*	*P* $2_1/n$
a /Å	14.4119(6)	6.5509(4)	16.7216(18)	14.9671(9)
b /Å	7.3071(3)	9.5558(7)	10.9118(11)	7.0737(4)
c /Å	15.2855(7)	24.5384(17)	18.807(2)	15.0978(9)
α/°	90.00	90.00	90.00	90.00
β/°	106.646(3)	91.662(4)	113.093(6)	96.540(4)
γ/°	90.00	90.00	90.00	90.00
V/ $Å^3$	1542.25(11)	1535.44(18)	3156.7(6)	1588.04(16)
Density/g.cm^{-3}	1.461	1.468	1.411	1.440
Abs. Coeff. /mm^{-1}	0.110	0.111	0.107	0.111
F(000)	704	704	1400	720
Total No. of reflections	2776	2697	2716	2847
Reflections, $I > 2\sigma(I)$	1884	1652	1665	1584
Max. θ/°	25.25	25.25	25.24	25.24
Ranges (h, k, l)	$-17 \le h \le 14$ $-8 \le k \le 8$ $-18 \le l \le 17$	$-7 \le h \le 7$ $-11 \le k \le 11$ $-29 \le l \le 28$	$-19 \le h \le 18$ $-13 \le k \le 13$ $-22 \le l \le 22$	$-16 \le h \le 17$ $-8 \le k \le 8$ $-18 \le l \le 17$
Complete to 2θ (%)	99.10	97.00	95.50	99.20
Data/ Restraints/Parameters	2690/1/214	2697/1/231	2716/1/233	2847/5/241
Goof (F^2)	1.031	1.013	1.045	1.027
R indices [$I > 2\sigma(I)$]	0.0438	0.0553	0.0557	0.0541
wR_2 [$I > 2\sigma(I)$]	0.1166	0.1441	0.1560	0.1265
R indices (all data)	0.0707	0.0960	0.0961	0.1155
wR_2 (all data)	0.1350	0.1713	0.1869	0.1535

Compound No.	Salt **6.1**	Salt **6.2**	Salt **6.3**	Salt **6.4**	Indole-3-carbaldoxime
Formulae	$C_{15}H_{15}N_5O_8$	$C_{15}H_{13}N_5O_9$	$C_{16}H_{13}N_5O_9$	$C_{12}H_9N_5O_8$	$C_9H_8N_2O$
CCDC No.	**1529111**	**1529110**	**1529114**	**1529113**	**1529109**
Mol. wt.	393.32	407.30	419.31	351.24	160.17
Space group	*P-1*	*P-1*	$P2_1/n$	*P-1*	$Pna2_1$
a /Å	7.2191(7)	6.7711(6)	17.0234(15)	3.8305(4)	8.6883(10)
b /Å	10.8361(8)	8.4733(11)	4.9886(5)	13.112(2)	11.8246(16)
c /Å	11.3880(9)	15.8026(17)	22.731(2)	14.5122(18)	15.412(3)
α/°	96.925(5)	78.747(10)	90.00	80.380(12)	90.00
β/°	100.591(5)	87.742(8)	109.651(5)	82.576(10)	90.00
γ/°	94.292(5)	75.439(10)	90.00	86.434(12)	90.00
V/ Å^3	864.98(13)	860.61(17)	1818.0(3)	711.98(17)	1583.3(4)
Density/g.cm^{-3}	1.510	1.572	1.532	1.638	1.344
Abs. Coeff. /mm^{-1}	0.125	0.133	0.128	0.141	0.091
F(000)	408	420	864	360	672
Total No. of reflections	3006	3037	3225	2443	2874
Reflections, $I > 2\sigma(I)$	2382	1932	1776	1720	2461
Max. θ/°	25.05	25.04	25.24	25.04	25.24
Ranges (h, k, l)	$-8 \le h \le 8$ $-12 \le k \le 12$ $-13 \le l \le 11$	$-8 \le h \le 8$ $-10 \le k \le 9$ $-18 \le l \le 15$	$-20 \le h \le 20$ $-5 \le k \le 5$ $-25 \le l \le 27$	$-4 \le h \le 4$ $-15 \le k \le 13$ $-16 \le l \le 17$	$-10 \le h \le 10$ $-13 \le k \le 14$ $-18 \le l \le 18$
Complete to 2θ (%)	98.10	99.90	98.50	96.00	99.90
Data/ Restraints/Parameters	3006/0/260	3037/1/270	3225/5/284	2443/1/231	2874/1/227
Goof (F^2)	1.031	1.004	1.006	1.066	1.057
R indices [$I > 2\sigma(I)$]	0.0452	0.0770	0.0534	0.0882	0.0360
wR_2 [$I > 2\sigma(I)$]	0.1094	0.1466	0.1259	0.1540	0.0845
R indices (all data)	0.0560	0.1126	0.1107	0.1148	0.0455
wR_2 (all data)	0.1165	0.1695	0.1572	0.1678	0.0899

Short contacts and hydrogen bond parameters of cocrystals **2.1.4**, **2.15** and salt **2.1.6** in chapter 2 (Part A).

Cocrystals/salt	D-H···A	d_{D-H}(Å)	$d_{H\cdots A}$ (Å)	$d_{D\cdots A}$(Å)	∠D−H···A (°)
2.1.4	C(12)-H(12A)···F(1) [x, 1/2-y, -1/2+z]	0.97	2.39	3.344	166
	O(2)-H(2)···F(1) [1-x, -1/2+y, 1/2-z]	0.82	1.61	2.421	169
	C(4)-H(4)···F(1) [x, y, z]	0.97	2.59	3.236	124
2.1.5	C(20)-H(20B)···O(1) [x, y, z]	0.97	2.64	3.438	140
	C(2)-H(2)···O(3) [x, y, z]	0.93	2.64	3.406	139
	C(24)-H(24A)···O(1) [x, y, z]	0.97	2.50	3.303	140
	O(4)-H(4A)···F(1) [x, y, z]	0.86	1.76	2.578	158
	C(10)-H(10)···O(6) [x, y, z]	0.92	2.64	3.445	145
	C(23)-H(23B)···C(15) [x, y, z]	0.96	2.89	3.813	162
	C(20)-H(20A)···O(4) [x, y, z]	0.97	2.66	3.499	145
	C(20)-H(20A)···O(5) [x, y, z]	0.97	2.62	3.443	142
2.1.6	C(11)-H(11B)···C(3) [x, y, z]	0.96	2.84	3.719	151
	C(11)-H(11B)···O(2) [x, y, z]	0.96	2.72	3.682	176
	C(14)-H(14B)···C(4) [x, y, z]	0.97	2.82	3.674	147
	C(12)-H(12A)···O(2) [x, y, z]	0.97	2.68	3.600	158
	O(3)-H(3A)···C(5) [x, y, z]	0.80	2.81	3.513	147

Short contacts and hydrogen bond parameters of cocrystals **2.2.2**-**2.2.4** in chapter 2 (Part B).

Cocrystals	D-H···A	d_{D-H} (Å)	$d_{H\cdots A}$ (Å)	$d_{D\cdots A}$ (Å)	∠D-H···A (°)
2.2.4	O(1)-H(1A)···Cl(1) [1-x, -y, -z]	0.82	2.22	3.039	172
	O(2)-H(2)···Cl(1)[1-x, 1/2+y, 1/2-z]	0.82	2.23	3.036	171
	O(3)-H(3A)···Cl(1) [-x, 1-y, -z]	0.82	2.28	3.078	166
	O(4)-H(4A)···O(5) [x, y, z]	0.82	1.87	2.681	176
	O(5)-H(5A)···N(1) [-x, 1/2+y, 1/2-z]	0.82	2.11	2.998	170
	O(5)-H(5B)···N(3) [-x, -1/2+y, 1/2-z]	0.85	2.25	3.146	171
	C(8)-H(8)···O(1) [x, y, z]	0.93	2.64	3.416	141
	C(1)-H(1)···O(4) [x, y, z]	0.93	2.38	3.279	162
	C(30)-H(30A)···O(2) [x, y, z]	0.97	2.71	3.607	153
	C(9)-H(9)···O(3) [x, y, z]	0.93	2.70	3.617	168
	C(17)-H(17B)···O(5) [x, y, z]	0.97	2.70	3.595	152
	C(28)-H(28A)···C(1) [x, y, z]	0.96	2.84	3.594	135
	C(5)-H(5B)···N(3) [x, y, z]	0.90	2.25	3.143	169
	C(21)-H(21B)···Cl(1) [x, y, z]	0.97	2.88	3.650	136
	C(29)-H(29B)···Cl(1) [x, y, z]	0.97	2.80	3.472	126
2.2.3	O(1)-H(1A)···F(1) [x, 1/2-y, -1/2+z]	0.89	1.69	2.545	176
	O(2)-H(2)···F(1) [x, y, z]	0.82	1.71	2.525	173
	O(3)-H(3A)···F(1) [-x, 1/2+y, 1/2-z]	0.82	1.64	2.460	177
	O(4)-H(4A)···O(3) [-x, 1-y, -z]	0.82	2.00	2.797	164
	C(13)-H(13)···O(2) [x, y, z]	0.93	2.64	3.530	159
	C(29)-H(29A)···O(3) [x, y, z]	0.97	2.71	3.525	142
	C(29)-H(29B)···O(1) [x, y, z]	0.97	2.66	3.606	164
	C(32)-H(32C)···C(8) [x, y, z]	0.96	2.76	3.651	154
	C(21)-H(21B)···N(3) [x, y, z]	0.97	2.73	3.648	158
2.2.2	O(1)-H(1A)···N(3) [x, -1+y, z]	0.82	2.03	2.807	159
	O(2)-H(2)···O(3) [1-x, 2-y, 1-z]	0.82	1.79	2.598	171
	O(4)-H(4A)···O(3) [-x, 2-y, -z]	0.82	1.75	2.567	165
	O(2)-H(2)···N(3) [x, y, z]	0.82	2.65	3.446	164
	C(21)-H(21B)···N(2) [x, y, z]	0.97	2.71	3.620	157
	C(21)-H(21A)···O(3) [x, y, z]	0.97	2.71	3.390	127
	C(29)-H(29B)···O(2) [x, y, z]	0.97	2.60	3.426	143
	C(9)-H(9)···N(4) [x, y, z]	0.93	2.65	3.468	146
	C(29)-H(29A)···N(3) [x, y, z]	0.97	2.56	3.439	150

Short contacts and hydrogen bond parameters of oxime **2.1.1**, **2.1.2** and cocrystals **3.1**-**3.4** in chapter 3.

Oximes/Cocrystals	D-H···A	d_{D-H} (Å)	$d_{H\cdots A}$ (Å)	$d_{D\cdots A}$ (Å)	∠D-H···A (°)
2.1.1	O(2)-H(2)···C(3) [x, y, z]	0.82	2.89	2.781	163
	C(9)-H(9)···O(2) [x, y, z]	0.93	2.63	3.483	153
	C(1)-H(1A)···O(2) [x, y, z]	0.93	2.67	3.542	156
2.1.2	O(1)-H(1)···O(1) [x, y, z]	0.82	2.60	3.014	112
	C(5)-H(5)···C(5) [x, y, z]	0.93	2.81	3.614	146
3.1	C(16)-H(16)···O(3) [x, y, z]	0.93	2.68	3.509	149
	C(20)-H(20)···O(1) [x, y, z]	0.93	2.63	3.311	130
	C(9)-H(9)···O(3) [x, y, z]	0.93	2.69	3.437	137
	C(18)-H(18)···O(2) [x, y, z]	0.93	2.70	3.540	150
	C(5)-H(5)···C(31) [x, y, z]	0.93	2.81	3.684	156
	C(5)-H(5)···C(32) [x, y, z]	0.93	2.86	3.561	133
	C(7)-H(7)···O(5) [x, y, z]	0.93	2.56	3.339	142
3.2	C(7)···C(1) [x, y, z]	----	----	3.270	----
	C(7)-H(7)···C(1) [x, y, z]	0.93	2.78	3.270	114
	C(6)···C(9) [x, y, z]	----	----	3.316	----
	C(1)-H(1A)···C(7) [x, y, z]	0.93	2.83	3.657	148
	C(9)-H(9)···C(6) [x, y, z]	0.93	2.79	3.672	158
3.3	C(5)-H(5)···C(10) [x, y, z]	0.93	2.71	3.575	155
	C(16)-H(16C)···O(3) [x, y, z]	0.96	2.70	3.548	148
	C(16)-H(16B)···O(1) [x, y, z]	0.96	2.62	3.499	152
	C(12)-H(12A)···O(1) [x, y, z]	0.96	2.71	3.574	150
3.4	O(3)-H(3)···O(7) [x, y, z]	0.82	1.99	2.756	155
	O(1)-H(1)···O(6) [x, y, z]	0.82	1.89	2.704	174
	C(13)-H(13A)···C(4) [x, y, z]	0.96	2.72	3.531	142
	O(2)-H(2)···O(5) [x, y, z]	0.82	2.69	3.071	110
	C(6)-H(6)···O(4) [x, y, z]	0.93	2.67	3.575	163
	C(5)···C(11) [x, y, z]	----	----	3.318	----
	O(6)-H(6A)···O(7) [x, y, z]	0.84	2.02	2.834	163
	O(7)-H(7B)···O(5) [x, y, z]	0.86	1.94	2.777	163
	O(6)-H(6B)···O(4) [x, y, z]	0.86	2.00	2.856	175

Short contacts and hydrogen bond parameters of complexes **4.1.1**-**4.1.7** in chapter 4 (Part A).

Complexes	D-H···A	d_{D-H} (Å)	$d_{H\cdots A}$ (Å)	$d_{D\cdots A}$ (Å)	∠D-H···A (°)
4.1.1	C(1)···C(7) [x, y, z]	----	----	3.326	----
	O(2)-H(2)···O(2) [x, y, z]	0.82	2.50	2.941	115
	O(3)-H(3)···O(4) [-x, 1-y, 1-z]	0.82	1.90	2.702	165
	C(10)-H(10)···C(6) [x, y, z]	0.93	2.80	3.715	161
4.1.2	O(2)-H(2)···O(2) [x, y, z]	0.82	2.71	3.078	109
	C(4)-H(4)···O(4) [x, y, z]	0.93	2.66	3.303	127
	O(3)-H(3A)···O(4) [x, y, z]	0.82	1.83	2.634	169
	C(10)-H(10A)···C(6) [x, y, z]	0.96	2.85	3.809	176
	C(10)-H(10A)···C(5) [x, y, z]	0.96	2.74	3.594	149
	C(11)-H(11B)···O(1) [x, y, z]	0.96	2.71	3.479	138

4.1.3	O(3)-H(3)···O(6) [x, y, z]	0.82	1.92	2.735	171
	C(3)···C(8) [x, y, z]	----	----	3.387	----
	C(10)···C(4) [x, y, z]	----	----	3.376	----
	O(6)-H(6)···O(7) [x, y, z]	0.82	1.79	2.611	177
	O(6)-H(6)···S(1) [x, y, z]	0.82	2.99	3.761	157
	C(11)-H(11)···O(7) [x, y, z]	0.93	2.60	3.254	128
	O(4)-H(4A)···S(1) [x, y, z]	0.82	2.98	3.352	111
	C(15)-H(15A)···O(7) [x, y, z]	0.96	2.66	3.543	153
4.1.4	C(7)···C(8) [x, y, z]	----	----	3.368	----
	C(8)-H(8)···C(2) [x, y, z]	0.93	2.89	3.713	148
	C(2)···C(3) [x, y, z]	----	----	3.399	----
	C(8)-H(8)···C(7) [x, y, z]	0.93	2.81	3.368	120
	C(3)-H(3A)···C(6) [x, y, z]	0.93	2.88	3.316	150
	C(3)-H(3A)···C(7) [x, y, z]	0.93	2.76	3.492	136
	O(6)-H(6)···N(4) [x, y, z]	0.82	1.89	2.699	166
	C(15)-H(15)···O(5) [x, y, z]	0.93	2.56	3.213	128
	C(22)-H(22)···O(6) [x, y, z]	0.93	2.67	3.377	134
	C(19)-H(19)···O(3) [x, y, z]	0.93	2.48	3.324	151
	C(23)-H(23)···O(4) [x, y, z]	0.93	2.72	3.518	145
	O(3)-H(3)···N(3) [x, y, z]	0.82	2.01	2.788	158
	O(3)-H(3)···C(22) [x, y, z]	0.82	2.82	3.590	156
4.1.5	O(2)-H(2)···O(2) [x, y, z]	0.82	2.51	2.978	117
	C(3)···C(1) [x, y, z]	----	----	3.356	----
	C(9)-H(9C)···O(3) [x, y, z]	0.96	2.65	3.389	134
	O(3)-H(3)···O(4) [x, y, z]	0.82	2.82	2.676	151
4.1.6	O(4)-H(4A)···O(5) [x, y, z]	0.82	2.58	2.968	111
	O(3)-H(3A)···O(4) [x, y, z]	0.82	1.98	2.793	173
	C(1)···C(7) [x, y, z]	----	----	3.262	----
	C(1)-H(1)···O(5) [x, y, z]	0.93	2.54	3.413	156
	O(6)-H(5A)···O(3) [x, y, z]	0.82	1.97	2.776	165
4.1.7	O(3)-H(3A)···N(3) [x, y, z]	0.82	1.93	2.737	169
	C(19)-H(19)···C(4) [x, y, z]	0.93	2.89	3.713	149
	C(19)-H(19)···C(5) [x, y, z]	0.93	2.86	3.531	130

Short contacts and hydrogen bond parameters of coordination polymers (CP) **4.2.2** and **4.2.3** in chapter 4 (Part B).

CP	D-H···A	d_{D-H} (Å)	$d_{H\cdots A}$ (Å)	$d_{D\cdots A}$ (Å)	∠D-H···A (°)
CP-**4.2.2**	C(7)-H(7)···C(16) [x, y, z]	0.93	2.84	3.567	136
	C(3)-H(3B)···O(3) [x, y, z]	0.97	2.67	3.588	159
	C(1)-H(1A)···C(18) [x, y, z]	0.97	2.79	3.731	165
	O(7)-H(7B)···O(5) [x, y, z]	0.82	2.69	3.213	123
	C(19)-H(19)···O(2) [x, y, z]	0.93	2.69	3.400	134
	O(3)-H(3)···O(4) [x, y, z]	0.82	2.65	3.323	140
CP-**4.2.3**	C(8)-H(8B)···O(5) [x, y, z]	0.97	2.48	3.235	135
	C(10)-H(10)···O(7) [x, y, z]	0.93	2.67	3.494	148
	C(1)-H(1)···C(20) [x, y, z]	0.93	2.77	3.487	134
	C(13)-H(13)···O(4) [x, y, z]	0.93	2.54	3.240	132
	C(5)-H(5)···O(4) [x, y, z]	0.93	2.72	3.615	163
	C(6)-H(6B)···O(2) [x, y, z]	0.97	2.68	3.456	137
	C(17)-H(17)···O(7) [x, y, z]	0.93	2.63	3.407	142

Short contacts and hydrogen bond parameters of cocrystals **5.2-5.4** and salts **5.5-5.8** in chapter 5.

Salts/Cocrystals	D-H···A	d_{D-H} (Å)	$d_{H\cdots A}$ (Å)	$d_{D\cdots A}$ (Å)	∠D-H···A (°)
5.2	C(4)-H(4)···N(1) [x, y, z]	0.93	2.73	3.579	152
	O(1)-H(1A)···O(2) [x, y, z]	0.82	1.89	2.702	169
	C(4)···C(11) [x, y, z]	----	----	3.308	----
	O(3)-H(3A)···N(2) [x, y, z]	0.82	1.75	2.559	171
5.3	C(1)···C(10) [x, y, z]	----	----	3.320	----
	C(4)···C(11) [x, y, z]	----	----	3.259	----
	C(4)-H(4)···N(1) [x, y, z]	0.93	2.66	3.346	143
	C(5)-H(5)···C(6) [x, y, z]	0.93	2.76	3.611	153
	C(4)-H(4)···O(2) [x, y, z]	0.93	2.62	3.238	124
5.4	C(10)···C(1) [x, y, z]	----	----	3.308	----
	C(5)-H(5)···C(6) [x, y, z]	0.93	2.74	3.609	155
	C(4)-H(4)···N(1) [x, y, z]	0.93	2.66	3.430	141
	C(4)-H(4)···O(2) [x, y, z]	0.93	2.63	3.237	124
	O(3A)-H(3A)···N(2) [x, y, z]	0.82	1.76	2.578	176
	C(4)···C(11) [x, y, z]	----	----	3.218	----
	O(1)-H(1A)···O(2) [x, y, z]	0.82	1.84	2.655	173
5.5	C(11)···C(14) [x, y, z]	----	----	3.334	----
	N(2)-H(2)···O(3) [x, y, z]	0.86	2.68	3.451	149
	C(11)···O(5) [x, y, z]	----	----	3.194	----
	C(14)···O(2) [x, y, z]	----	----	3.134	----
5.6	C(1)···C(10) [x, y, z]	----	----	3.268	----
	C(8)-H(8)···O(1) [x, y, z]	0.93	2.52	3.277	139
	C(6)-H(6)···O(2) [x, y, z]	0.93	2.59	3.504	167
	C(5)-H(5)···O(2) [x, y, z]	0.93	2.52	3.198	130
	C(4)-H(4)···O(3) [x, y, z]	0.93	2.52	3.062	117
5.7	C(4)-H(4)···N(1) [x, y, z]	0.93	2.67	3.575	164
	N(2)-H(2B)···Cl(1) [x, y, z]	0.86	2.19	3.030	166
	C(6)-H(6)···Cl(1) [x, y, z]	0.93	2.84	3.752	169
5.8	C(8)-H(8)···O(1) [x, y, z]	0.93	2.47	3.287	147
	C(7)-H(7)···O(4) [x, y, z]	0.93	2.70	3.426	136
	C(6)···C(10) [x, y, z]	----	----	3.381	----
	C(4)-H(4)···O(2) [x, y, z]	0.93	2.34	3.240	164
	C(5)-H(5)···O(3) [x, y, z]	0.93	2.44	3.259	147

Short contacts and hydrogen bond parameters of salts **5.10-5.15** in chapter 5.

Salts	D-H···A	d_{D-H} (Å)	$d_{H\cdots A}$ (Å)	$d_{D\cdots A}$ (Å)	∠D-H···A (°)
5.10	C(1)-H(1A)···O(4) [x, y, z]	0.93	2.47	3.387	168
	O(1)-H(1)···C(11) [x, y, z]	0.82	2.88	2.642	169
	C(5)-H(5)···O(1) [x, y, z]	0.93	2.71	3.332	125
5.11	C(2)···C(7) [x, y, z]	----	----	3.112	----
	C(5)-H(5)···O(8) [x, y, z]	0.93	2.72	3.312	123
	C(8)-H(8)···O(1) [x, y, z]	0.93	2.41	3.278	156
	C(16)-H(16)···O(6) [x, y, z]	0.93	2.57	3.413	151
	C(3)-H(3)···C(3) [x, y, z]	0.93	2.80	3.646	139
	C(24)-H(24)···O(2) [x, y, z]	0.93	2.66	3.393	137
	C(21)-H(21)···C(16) [x, y, z]	0.93	2.77	3.647	158
	C(23)-H(23)···O(6) [x, y, z]	0.93	2.69	3.493	145

5.12	C(2)···C(13) [x, y, z]	----	----	3.391	----
	C(4)-H(4)···O(1) [x, y, z]	0.93	2.57	3.390	147
	C(8)-H(8)···O(2) [x, y, z]	0.93	2.49	3.378	160
	C(6)-H(6)···O(2) [x, y, z]	0.93	2.65	3.508	153
	C(7)-H(7)···O(3) [x, y, z]	0.93	2.63	3.505	157
5.13	O(5)···C(12) [x, y, z]	----	----	3.214	----
	C(13)···C(10) [x, y, z]	----	----	3.389	----
	C(4)···O(1) [x, y, z]	----	----	3.162	----
5.14	C(5)-H(5)···O(1) [x, y, z]	0.93	2.63	3.241	124
	C(4)-H(4)···O(2) [x, y, z]	0.93	2.66	3.304	127
	N(2)-H(2)···O(2) [x, y, z]	1.03	2.68	3.327	121
	C(15)-H(15)···C(11) [x, y, z]	0.93	2.70	3.549	152
5.15	C(14)-H(14)···O(1) [x, y, z]	0.93	2.71	3.632	170
	C(8)-H(8)···O(5) [x, y, z]	0.93	2.55	3.459	168
	C(13)···C(5) [x, y, z]	----	----	3.370	----
	C(15)···C(9) [x, y, z]	----	----	3.364	----

Short contacts and hydrogen bond parameters of picrate salts **6.1-6.4** and indole-3-carbaldoxime in chapter 6.

Salts/Oxime	D-H···A	d_{D-H} (Å)	$d_{H\cdots A}$ (Å)	$d_{D\cdots A}$ (Å)	∠D-H···A (°)
6.1	C(4)-H(4)···O(6) [x, y, z]	0.93	2.62	3.473	153
	C(9)-H(9C)···O(6) [x, y, z]	0.96	2.43	3.329	155
	O(1)-H(1A)···O(6) [x, y, z]	0.82	2.60	3.183	129
	C(6)-H(6)···O(2) [x, y, z]	0.93	2.47	3.189	134
	C(6)-H(6)···O(7) [x, y, z]	0.93	2.64	3.536	162
	C(8)-H(8B)···O(3) [x, y, z]	0.96	2.38	3.040	126
	C(9)-H(9B)···O(3) [x, y, z]	0.96	2.69	3.292	121
	C(7)-H(7)···O(4) [x, y, z]	0.93	2.66	3.541	159
	C(7)···C(11) [x, y, z]	----	----	3.385	----
	C(9)-H(9B)···O(4) [x, y, z]	0.96	2.72	3.335	123
	C(8)-H(8B)···O(5) [x, y, z]	0.96	2.69	3.276	120
	C(8)-H(8C)···O(8) [x, y, z]	0.96	2.59	3.453	150
6.2	O(5)···O(6) [x, y, z]	----	----	3.009	----
	C(15)···C(6) [x, y, z]	----	----	3.356	----
	C(2)-H(2A)···O(2) [x, y, z]	0.93	2.71	3.394	131
	C(9)-H(9)···C(7) [x, y, z]	0.93	2.46	3.305	151
	C(3)-H(3)···O(5) [x, y, z]	0.93	2.62	3.263	127
	C(12)···C(5) [x, y, z]	----	----	3.385	----
	C(13)···C(4) [x, y, z]	----	----	3.395	----
	C(8)-H(8)···O(3) [x, y, z]	0.93	2.51	3.055	118
	N(1)-H(1A)···C(15) [x, y, z]	1.07	2.75	3.812	172
	N(2)-H(2)···O(5) [x, y, z]	0.86	2.42	3.269	171
	N(2)-H(2)···O(4) [x, y, z]	0.86	2.58	3.221	132
	C(4)-H(4)···O(4) [x, y, z]	0.93	2.37	3.134	140
	O(1)-H(1)···O(9) [x, y, z]	0.82	1.93	2.709	160
	O(7)···O(9) [x, y, z]	----	----	2.953	----

6.3	C(4)···C(13) [x, y, z]	----	----	3.365	----
	C(1)-H(1)···O(1) [x, y, z]	0.93	2.40	3.323	172
	C(8)-H(8)···O(1) [x, y, z]	0.93	2.66	3.584	172
	C(3)-H(3)···O(6) [x, y, z]	0.93	2.66	3.445	143
	C(4)-H(4)···O(5) [x, y, z]	0.93	2.47	3.252	141
	O(5)···O(4) [x, y, z]	----	----	2.973	----
	O(6)···O(2) [x, y, z]	----	----	3.007	----
	C(4)-H(4)···O(4) [x, y, z]	0.93	2.38	2.894	115
	C(11)-H(11)···O(7) [x, y, z]	0.93	2.61	3.542	178
6.4	O(4)···O(4) [x, y, z]	----	----	2.907	----
	C(8)-H(8)···O(4) [x, y, z]	0.93	2.52	3.337	147
	O(8)···N(2) [x, y, z]	----	----	3.008	----
	C(1)···O(5) [x, y, z]	----	----	3.210	----
	C(3)-H(3)···O(6) [x, y, z]	0.93	2.55	3.242	132
	C(6)-H(6)···O(2) [x, y, z]	0.93	2.50	3.227	137
	C(1)-H(1A)···O(5) [x, y, z]	0.93	2.29	3.210	169
	C(5)-H(5)···O(3) [x, y, z]	0.93	2.50	3.067	120
Indole-3-carbaldoxime	N(4)-H(4)···C(15) [x, y, z]	0.89	2.71	3.356	130
	N(4)-H(4)···C(16) [x, y, z]	0.89	2.61	3.455	159
	N(4)-H(4)···C(17) [x, y, z]	0.89	2.79	3.659	166
	O(1)-H(1A)···C(10) [x, y, z]	0.82	2.82	3.560	151
	C(3)-H(3)···C(14) [x, y, z]	0.93	2.78	3.593	146
	C(3)-H(3)···C(11) [x, y, z]	0.93	2.87	3.356	120
	C(10)-H(10)···C(8) [x, y, z]	0.93	2.85	3.736	160
	C(15)-H(15)···C(6) [x, y, z]	0.93	2.80	3.660	154
	O(2)-H(2A)···C(1) [x, y, z]	0.82	2.86	3.599	152
	C(18)-H(18)···C(7) [x, y, z]	0.93	2.83	3.471	127
	C(6)-H(6)···C(2) [x, y, z]	0.93	2.87	3.621	139

Curriculum Vitae

Name: Arup Tarai

Present address:
Department of Chemistry
Indian Institute of Technology Guwahati
Guwahati, Assam-781039
India.
Mob. No. +91 9085301502
Email: aruptarai@gmail.com
arup.tarai@iitg.ac.in

Permanent address:
S/o Mangobinda Tarai
AT- Bhamal, PO: Guruma-Bhamal
PS: Beliaberah, Dist.- Paschim Medinipur
West Bengal-721517, India.
Mob. No. +91 9635482741

Passport No.: M5178979 (India)
Skype Id: arup.tarai

Date of Birth: 06-04-1991
Sex: Male
Marital status: Married
Religion: Hinduism

Research Interest

My interests mostly focused on the synthesis and investigations of physicochemical properties of inorganic and organic as well as organometallic or Aggregation-Induced-Emission (AIE) active luminescent materials. Also, is to tune the physicochemical properties of these luminescent materials in solid state. Furthermore, my interest on the systematic investigations on ions or molecular recognition studies through coordination or supramolecular approach by small or big molecules (MOFs or COFs). Additionally, I am interested on the synthesis of metal complexes and study their application in various fields.

Educational Background

2013-Till date: **Doctor of Philosophy (Chemistry)**, **First class (CPI-8.75, out of 10.0)**, Indian Institute of Technology Guwahati, Guwahati, Assam, India.

2011-2013: **Master of Science (Chemistry)**, **First class (CGPI-7.67, out of 10.0)**, Indian Institute of Technology Kharagpur, Kharagpur, West Bengal, India.

2008-2011: **Bachelor of Science (Chemistry)**, **First class (63.25%)**, Midnapore college, Vidyasagar University, Midnapore, West Bengal, India.

2008: **10+2, First class (77.60%),** Kultikri SC high school, **WBCHSE** Board, West Bengal, India.

2006: **10th, First class (74.50%),** Guruma J.S. vidya pitch, **WBBSE** Board, West Bengal, India.

Achievements & Awards

2013 Qualified Graduate Aptitude Test for Engineering (**GATE**)
2012 Qualified National Eligibility Test (**NET**) for Junior Research Fellowship (JRF) by CSIR-UGC
2011 Awarded West Bengal Merit-Cum Means Scholarship **(WBMCM-2011)** in M.Sc
2011 Qualified Joint Admission Test for MSc (**IIT-JAM**)
2008 Awarded West Bengal Merit-Cum Means Scholarship **(WBMCM-2008)** in B.Sc

Teaching experience

2016-2017 Teaching Assistantship for MSc Laboratory Courses at IIT Guwahati, India.
2013-2014 Teaching Assistantship for MSc Laboratory Courses at IIT Guwahati, India.

Analytical Skills

Instruments Operate: Spectrofluorimeter, UV-Vis Spectrophotometer, Dynamic Light Scattering (DLS) based particle size analyzer, Field Emission Scanning Electron Microscope (FESEM), X-ray Diffractometer (SXRD or PXRD), FT-IR, TGA, DSC and ITC.

Softwares: Microsoft Office (Power Point, Excel and Word), Origin, Adobe Illustrator, Bruker Nonius SMART Apex 2, ORTEP, Mercury, RasMol, SHELX, ChemDraw, Gaussian 09W and Crystal Explorer etc.

Symposia Attended during PhD

2017 Chemical Research Society of India (CRSI-2016) organized by Guwahati University.

2017 Modern Trends in Inorganic Chemistry (MTIC-2017) organized by IISER Pune

2018 International Seminar on Emerging Trends in chemical science organized by Dibrugarh University

Publications

1. **A. Tarai**, J. B. Baruah*, A study on fluoride detection and assembly of hydroxyaromatic aldoximes caused by tetrabutylammonium fluoride, ***CrystEngComm***, 2015, **17**, 2301-2309.
2. **A. Tarai**, J. B. Baruah*, Study on divalent copper, nickel and zinc model complexes for fluoride ion detection, ***RSC Adv.***, 2015, **5**, 82144-82152.
3. **A. Tarai**, J. B. Baruah*, Solution and Solid State Study on the Recognition of Hydroxyaromatic Aldoximes by Nitrogen Containing Compounds, ***Cryst. Growth Des***., 2016, **16**, 126-135.
4. **A. Tarai**, J. B. Baruah*, Changing π-Interactions and Conformational Adjustments of N-(Isonicotinylhydrazide)-1,8-naphthalimide by Hydration and Complexation Affect Photophysical Properties, ***Cryst. Growth Des***., 2018, **18**, 456-465.
5. **A. Tarai**, J. B. Baruah*, Conformation and Visual Distinction between Urea and Thiourea Derivatives by an Acetate Ion and a Hexafluorosilicate Cocrystal of the Urea Derivative in the Detection of Water in Dimethylsulfoxide, ***ACS Omega***, 2017, **2**, 6991-7001.
6. **A. Tarai**, J. B. Baruah*, Oxime synthons in the salts and cocrystals of quinoline-4-carbaldoxime for non-covalent Synthesis, ***CrystEngComm***, 2016, **18**, 298-308.
7. **A. Tarai**, J. B. Baruah*, Anion assisted conformationally guided self-assemblies of multi-component cocrystals of dioxime, ***CrystEngComm***, 2016, **18**, 5482-5491.
8. **A. Tarai**, J. B. Baruah*, Competing phenol-imidazole and phenol-phenol interactions in the flexible supramolecular environment of *N*,*N*′-bis(3-imidazol-1-ylpropyl)naphthalenediimide causing domain expansion, ***New J. Chem.***, 2017, **41**, 10750-10760.
9. **A. Tarai**, J. B. Baruah*, Quaternary and senary sub-assemblies in cocrystals and salts of quinoline-4-carbaldoxime with aromatic carboxylic acids, ***CrystEngComm***, 2016, **18**, 9095-9102.
10. **A. Tarai**, J. B. Baruah*, Dimethylsulphoxide solvate of N, N'-dinaphthylthiourea and its selective interactions with fluoride and copper(II) ions, ***J. Mol. Struct***., 2015, **1091,** 147-151.
11. **A. Tarai**, T. Mondal, J. B. Baruah*, While deprotonating 1-(4-nitrophenyl)-3-{(pyridin-4-yl)methyl}thiourea by tetrabutylammonium fluoride it also provides a means for etching of glass, ***Inorg. Chim. Acta***, 2017, **464**, 108-113.
12. **A. Tarai**, J. B. Baruah*, Resonance energy transfer emission observed in cocrystal of N,N′-bis(3-imidazol-1-ylpropyl)naphthalenediimide with cinnamic acid, ***Chemistry Select***, 2017, **2**, 10101-10106.
13. **A. Tarai**, J. B. Baruah*, Inclusion of 2,4-Dihydroxybenzaldehyde and 2,4-Dihydroxybenzaldoxime in Cadmium Coordination Polymer and Conversion of Guest Aldehyde to Oxime, ***Chemistry Select***, 2017, **2**, 11482-11486.

14. **A. Tarai**, J. B. Baruah*, Different self-assemblies, absorption and emission properties of picrate salts of aromatic amine or heterocycle linked oximes, ***New J. Chem***., 2018, **42**, 4757-4765.

15. **A. Tarai**, J. B. Baruah*, Four Coordinated See-Saw N-(Aryl)-2-(propan-2-ylidene)hydrazinecarbothioamide Complexes of Nickel(II), Copper(II) and Zinc(II) and Propensity for Catalytic Cyclisation, ***Dalton Trans***., 2018, **47**, 4921-4930.

16. M. P. Singh, **A. Tarai**, J. B. Baruah*, Changes in Emission Properties by π-Stacking and Conformation Adjustment of an Imidazole-Tethered Naphthalimide Derivative, ***Chemistry Select***, 2018, **3**, 6364-6373.

Research Experience

PhD (July, 2013-till date, 2018): **Thesis Title-** Studies on Supramolecular Assemblies, Metal Complexes of Aromatic Oxime Derivatives for Molecular and Ions Recognition.

Supervisor-Prof. Jubaraj B. Baruah, Professor, Dept. of Chemistry, IIT Guwahati, Assam-781039, India.

During my PhD, I have worked on (i) supramolecular assemblies, (ii) solid-state emission, (iii) mechanochromic luminescence, (iv) fluorescent and chromogenic recognition of anions and Active Pharmaceutical Ingredients (API) and (v) Aggregation-Induced-Emission (AIE) of organic/inorganic fluorophoric materials. Also, I am familiar with the synthesis, structural, computational and physicochemical properties of oxime, urea, thiourea, naphthaliimide and naphthalenediimide based organic compounds. Physicochemical properties of these classes of compounds were tuned by cocrystal strategy in solution and solid state. Metal complexes of oxime based compounds were synthesized and the role of metal ion in the recognition of fluoride ion was studied. In addition, recognition of picric acids in solution and isolation of crystal structure of picrate salts of oxime based compounds were evaluated.

In addition, I have work on the following topics:

1. X-Ray Crystallographic studies (cocrystals or polymorphisms)
2. Coordination chemistry (synthesis of metal complexes and their applications)
3. Material chemistry (synthesis of light emitting organic materials)
4. Single-electron transfer process

MSc (July 2012-July 2013): **Thesis Title-** Preparation of Mixed Metal Oxides for the Photodegradation of 4-Nitrophenol under UV-Vis Light.

Supervisor-Dr. A. Rajakumar, Professor, Dept. of Chemistry, IIT Kharagpur, West Bengal-721302, India.

Various mixed metal oxides were prepared by co-precipitation method and evaluated for photocatalytic application. Photodegradation of 4-nitrophenol and common dye molecules (MO or MB) by mixed metal oxides were studied in presence of UV-Vis light irradiation. It was found that the rate of degradation is strongly dependent upon the initial concentration of dyes, catalytic dose, pH of the medium and presence of inorganic salts.

References

1. **Prof. Jubaraj B. Baruah** (PhD Supervisor), Department of Chemistry, Indian Institute of Technology Guwahati, Assam-781039, India, Phone No. +91-361-258-2311 (O) Email: juba@iitg.ac.in
2. **Dr. Debasis Manna**, Department of Chemistry, Indian Institute of Technology Guwahati, Assam-781039, India, Phone No. +91-361-258-2325 (O) Email: dmanna@iitg.ac.in